Self-healing coatings based on thiol-ene chemistry

Dissertation presented in partial fulfillment of the requirements for the degree of PhD in Polymer Science at the University of Stellenbosch

by

Eric T.A. van den Dungen

Supervisor: Prof Bert Klumperman

University of Stellenbosch - Faculty of Science

Department of Chemistry and Polymer Science

March 2009

DECLARATION

By submitting this dissertation electronically, I declare that the entirety of the work contained therein is my own, original work, that I am the owner of the copyright thereof (unless to the extent explicitly otherwise stated) and that I have not previously in its entirety or in part submitted it for obtaining any qualification.

Eric T.A. van den Dungen

Stellenbosch, February 2009

Abstract

The work presented in this dissertation describes the development of self-healing coatings based on thiol-ene chemistry. The approach was to synthesize capsules with thiol and ene compounds separately encapsulated. These capsules were embedded in various coating formulations and upon the formation of a crack with a razor blade, these capsules ruptured. This caused the healing agent to flow into the crack via capillary action and the thiol-ene healing mechanism was initiated. This resulted in recovery of the damaged coating and provided continued protection to the substrate.

Pentaerythritol tetrakis(3-mercaptopropionate) (TetraThiol), 1,6-hexanediol diacrylate (DiAcrylate) and 1,6-hexanediol di-(*endo, exo*-norborn-2-ene-5-carboxylate) (DiNorbornene) are the thiol and ene compounds used in this study. Kinetic experiments indicated that both TetraThiol-DiAcrylate and TetraThiol-DiNorbornene monomer pairs undergo rapid polymerization and form a network within minutes upon exposure to UV radiation and with the addition of a photoinitiator. The TetraThiol-DiNorbornene monomer pair also showed a high rate of polymerization without the addition of a photoinitiator and/or exposure to UV radiation. Styrene-maleic anhydride (SMA) copolymers and chain-extended block copolymers with styrene (P[(Sty-*alt*-MAh)-*b*-Sty]) were synthesized via Reversible Addition-Fragmentation chain Transfer (RAFT)-mediated polymerization. These copolymers were used as surfactant in miniemulsification for the synthesis of core-shell particles with TetraThiol as the core material. It appeared that P[(Sty-*alt*-MAh)-*b*-Sty] block copolymers, sterically stabilized via the addition of formaldehyde, provide optimal stability to the core-shell particles. DiNorbornene is encapsulated via miniemulsion homopolymerization of styrene and well-defined, stable nanocapsules were obtained. TetraThiol and DiAcrylate microcapsules were synthesized via *in-situ* polymerization of urea and formaldehyde. Microcapsules with a particle size of one to ten micrometers and with a very smooth surface were obtained. These microcapsules and nanocapsules were embedded in poly(methyl acrylate) (PMA), styrene-acrylate and pure acrylic films and the self-healing ability of these coatings, after introduction of a crack with a razor blade, was assessed.

The key question is whether the capsules do rupture upon the formation of a crack with a razor blade. A rhodamine-based fluorescent probe was used for this purpose. The probe itself does not show significant fluorescence emission but, after reaction with TetraThiol, rhodamine is formed, which does show intense fluorescence emission. TetraThiol microcapsules or TetraThiol nanocapsules were embedded in a PMA film, together with the rhodamine-based fluorescent probe. It was concluded that both TetraThiol microcapsules and TetraThiol nanocapsules do rupture upon formation of a crack with a razor blade in the PMA film, due to intense fluorescence emission observed under the fluorescence microscope. This means that the micro- and nanocapsules can potentially be used as a reservoir for healing agents for the development of self-healing coatings. Films that have been investigated for their self-healing ability contain either 5 wt% TetraThiol and 5 wt% DiAcrylate microcapsules or 10 wt% TetraThiol and 15 wt% DiNorbornene nanocapsules. A small quantity of photoinitiator is added and after introduction of a crack in the film with a razor blade, the film was exposed to UV radiation and analyzed with scanning electron microscopy (SEM). Visual observation with SEM indicated that the PMA film with microcapsules showed only partial recovery of the coating, due to the formation of large aggregates of (mainly) DiAcrylate microcapsules, which reduced the efficiency of self-healing. The PMA film with nanocapsules also showed partial recovery, albeit less pronounced than for the film with microcapsules. The main reason for this is the brittle nature of the film due to the DiNorbornene nanocapsules synthesized via miniemulsion polymerization of styrene. The incorporation of micro- and nanocapsules in commercial styrene-acrylate and pure acrylic coating formulations led to similar observations. The coatings with microcapsules showed only partial recovery, mainly due to the formation of large DiAcrylate microcapsule aggregates that reduced the self-healing efficiency of the coating. The self-healing effect of these coatings was less pronounced than that of the PMA film because of the inherently higher T_g of the commercial films. Due to the very brittle nature of the commercial films with nanocapsules, the recovery of these coatings was not very pronounced. This does however, not imply that coatings with nanocapsules do not have self-healing potential. The formation of a microcrack within the coating only requires the rupture of these well-defined nanocapsules. Overall, it was demonstrated that thiol-ene chemistry provides an

effective healing mechanism for the development of self-healing waterborne coatings based on either micro- or nanocapsules.

Opsomming

Die werk wat uiteengesit is in hierdie dissertasie, beskryf die ontwikkeling van self-herstellende deklae via tiol-één chemie. Die benadering was om kapsules te maak met tiol en één verbindings apart ge-inkapsuleer. Die kapsules was in verskillende bedekkingsformules ingevoeg en na die vorming van een kraak met 'n skeermessie, het die kapsules gebreek. Dit het daarvoor gesorg dat die herstellende verbinding deur kapillêre aksie in die kraak vloei en die tiol-één herstellende meganisme begin het. Dit het gelei tot die herstel van die beskadigde deklaag en het gesorg vir verlengde beskerming van die substraat.

Pentaerythritol tetrakis(3-merkaptopropionaat) (TetraTiol), 1,6-heksaandiol diakrilaat (DiAkrilaat) en 1,6-heksaandiol di-(*endo*, *exo*-norborn-2-een-5-karboxilaat) (DiNorborneen) is die tiol en één verbindings gebruik in hierdie studie. Kinetiese eksperimente het aangetoon dat TetraTiol-DiAkrilaat asook TetraTiol-DiNorborneen monomeerpare vinnige polimerisasie ondergaan en in enkele minute 'n netwerk vorm, na blootstelling aan UV straling en met die toevoeging van 'n fotoinisiator. Die TetraTiol-DiNorborneen monomeerpaar het ook vinnige polimerisasie getoon sonder die toevoeging van 'n fotoinisiator en/of blootstelling aan UV straling. Stireen-maleinesuuranhiedried (SMA) kopolimere en ketting-verlengde blok kopolimere met stireen (P[Sty-*alt*-MAh]-*b*-Sty) is gemaak via Omkeerbare Addisie-Fragmentasie ketting Oordrag-beheerde (*eng: RAFT-mediated*) polimerisasie. Die kopolimere is gebruik as seep in miniemulsiefikasie vir die sintese van kern-skil partikels met TetraTiol as kern materiaal. Dit het geblyk dat P[Sty-*alt*-MAh]-*b*-Sty blok kopolimere, steries gestabiliseer met die toevoeging van formaldehied, optimaal stabiliteit gegee het aan die kern-skil partikels. DiNorborneen is ge-inkapsuleer via miniemulsie polimerisasie van stireen, en goed definieerde, stabiele nanokapsules is verkry. TetraTiol en DiAkrilaat mikrokapsules is gemaak via *in-situ* polimerisasie van ureum en formaldehied. Mikrokapsules met 'n partikelgrootte van een tot tien mikrometer en met 'n baie gladde oppervlak is verkry. Hierdie mikrokapsules en nanokapsules is in poli(metielakrilaat) (PMA), stireen-akrilaat en suiwer akrilaat lae gemeng en die self-herstellende werking van die deklae is

vasgestel, na die vorming van 'n kraak met 'n skeermessie. Die belangrikste vraag is of die kapsules breek na die vorming van 'n kraak met 'n skeermessie. 'n Rhodamine gebaseerde fluoresente proob is gebruik vir hierdie doel. Die proob self toon nie benoeminswaardige fluoresente emissie nie, maar deur reaksie met TetraTiol word rhodamine gevorm, wat intense fluoresente emissie tot gevolg het. TetraTiol mikrokapsules of TetraTiol nanokapsules is in een PMA-laag gemeng, saam met die rhodamine gebaseerde fluoresente proob. Resultate toon aan dat TetraTiol mikrokapsules asook TetraTiol nanokapsules breek na die vorming van 'n kraak met 'n skeermessie in die PMA-laag, deur die waarneming van intense fluoresente emissie onder die fluoresente mikroskoop. Dit beteken dat die mikro- en nanokapsules die vermoë het om gebruik te word as houer vir herstellende verbindings vir die ontwikkeling van self-herstellende deklae. Lae wat ondersoek is vir hulle self-herstellende vermoë beskik oor of 5 gew% TetraTiol en 5 gew% DiAkrilaat mikrokapsules of 10 gew% TetraTiol en 15 gew% DiNorborneen nanokapsules. 'n Klein hoeveelheid fotoinisiator is bygevoeg en na die maak van 'n kraak met 'n skeermessie word die laag blootgestel aan UV straling en geanaliseer met skennende elektronenmikroskopie (SEM). Visuele waarneming met SEM het aangetoon dat die PMA-laag met mikrokapsules slegs gedeeltelike herstel van die deklaag getoon, as gevolg van die vorming van grote aggregate van (vernaamlik) DiAkrilaat mikrokapsules dat die effektiwiteit van die self-herstel verminder. Die PMA-laag met nanokapsules het ook gedeeltelik herstel getoon, maar nie so duidelik as vir die laag met mikrokapsules nie. Die belangrikste rede vir dit is die brosse natuur van die laag omdat DiNorborneen nanokapsules gemaak is via miniemulsie polimerisasie van stireen. Die invoeging van mikro- en nanokapsules in kommersiële stireen-akrilaat en suiwer akrilaat bedekkingsformules het gelei tot dieselfde waarnemings. Die deklae met mikrokapsules het slegs gedeeltelik herstel getoon, vernaamlik deur die vorming van grote aggregate van DiAkrilaat mikrokapsules en die self-herstellende effektiwiteit van die deklae het verminder. Die self-herstellende vermoë van hierdie deklae was nie so duidelik as die van die PMA-lae nie, deur die intrinsiek hoër T_g van die kommersiële lae. Deur die baie brosse natuur van die kommersiële lae met nanokapsules was die herstel van hierdie deklae nie baie groot nie. Dit beteken tog nie dat deklae met nanokapsules nie self-herstellend potensiaal het nie. Die vorming van een mikrokraak in die deklaag vereis

alleen dat die goed definieerde nanokapsules breek. In die algemeen is daar aangetoon dat tiol-één chemie 'n effektief herstellende meganisme verskaf vir die ontwikkeling van self-herstellende water gebaseerde deklae met mikro- of nanokapsules.

Samenvatting

Het werk dat wordt gepresenteerd in dit proefschrift beschrijft de ontwikkeling van zelf-herstellende coatings via thiol-één chemie. De aanpak was om capsules the maken met thiol en één verbindingen gescheiden geïnkapsuleerd. Deze capsules werden in verscheidene coating formuleringen toegepast en na de vorming van een kras met een scheermesje, braken deze capsules. Dit zorgde ervoor dat de herstellende verbinding via capillaire actie in de kras vloeit en het thiol-één herstellend mechanisme werd gestart. Dit resulteerde in herstel van de beschadigde coating en zorgde voor verlengde bescherming van het substraat.

Pentaerythritol tetrakis(3-mercaptopropionaat) (TetraThiol), 1,6-hexaandiol diacrylaat (DiAcrylaat) en 1,6-hexaandiol di-(*endo*, *exo*-norborn-2-een-5-carboxylaat) (DiNorborneen) zijn de thiol en één verbindingen gebruikt in deze studie. Kinetische experimenten toonden aan dat zowel TetraThiol-DiAcrylaat als TetraThiol-DiNorborneen monomere paren snelle polymerisatie ondergaan en binnen enkele minuten een netwerk vormen, na blootstelling aan UV straling en met de toevoeging van een fotoinitiator. Het TetraThiol-DiNorborneen monomere paar liet ook een snelle polymerisatie zien zonder toevoeging van fotoinitiator en/of blootstelling aan UV straling. Styreen-maleïnezuuranhydride (SMA) copolymeren en keten-verlengde blokcopolymeren met styreen (P[(Sty-*alt*-MAh)-*b*-Sty]) werden gemaakt via Reversibele Additie-Fragmentatie keten Overdracht-beheerde (*Eng: RAFT-mediated*) polymerisatie. Deze copolymeren werden gebruikt als surfactant in miniemulsificatie voor de synthese van kern-schil deeltjes met TetraThiol als kernmateriaal. Het bleek dat P[(Sty-*alt*-MAh)-*b*-Sty] blokcopolymeren, sterisch gestabiliseerd door toevoeging van formaldehyde, optimale stabiliteit geven aan de kern-schil deeltjes. DiNorborneen wordt geïnkapsuleerd via miniemulsie homopolymerisatie van styreen, en goed gedefinieerde, stabiele nanocapsules werden verkregen. TetraThiol en DiAcrylaat microcapsules werden gemaakt via *in-situ* polymerisatie van ureum en formaldehyde. Microcapsules met een deeltjesgrootte van één tot tien micrometer en met een heel glad oppervlak werden verkregen. Deze microcapsules en nanocapsules werden in poly(methylacrylaat) (PMA),

styreen-acrylaat en puur acrylaat lagen gemengd en de zelf-herstellende werking van deze coatings werd vastgesteld, na het aanbrengen van een kras met een scheermesje. De hamvraag is of de capsules breken na de vorming van een kras met een scheermesje. Een op rhodamine gebaseerde fluorescente probe werd gebruikt voor dit doel. De probe zelf toont geen significante fluorescente emissie, maar door reactie met TetraThiol wordt rhodamine gevormd, dat intense fluorescente emissie laat zien. TetraThiol microcapsules of TetraThiol nanocapsules werden in een PMA-laag gemengd, samen met de op rhodamine-gebaseerde fluorescente probe. Er werd geconcludeerd dat zowel TetraThiol microcapsules als TetraThiol nanocapsules breken na de vorming van een kras met een scheermesje in een PMA-laag, vanwege de intense fluorescente emissie die werd waargenomen onder de fluorescentie microscoop. Dit betekent dat de micro- en nanocapsules het vermogen hebben om gebruikt te worden als container voor herstellende verbindingen voor de ontwikkeling van zelf-herstellende coatings. Lagen die zijn onderzocht voor hun zelf-herstellende vermogen bevatten of 5 gew% TetraThiol en 5 gew% DiAcrylaat microcapsules of 10 gew% TetraThiol en 15 gew% DiNorborneen nanocapsules. Een kleine hoeveelheid fotoinitiator wordt toegevoegd en na het inbrengen van een kras met een scheermesje, wordt de laag blootgesteld aan UV straling en geanalyseerd met scanning elektronenmicroscopie (SEM). Visuele waarneming met SEM gaf aan dat de PMA-laag met microcapsules slechts gedeeltelijk herstel van de coating liet zien, wat komt door de vorming van grote aggregaten van (voornamelijk) DiAcrylaat microcapsules die de efficiëntie van het zelf-herstel verminderden. De PMA-laag met nanocapsules liet ook gedeeltelijk herstel zien, hoewel niet zo duidelijk als voor de laag met microcapsules. De belangrijkste reden voor dit is de brosse natuur van de laag doordat de DiNorborneen nanocapsules werden gemaakt via miniemulsie polymerisatie van styreen. Het inbrengen van micro- en nanocapsules in commerciële styreen-acrylaat en puur acrylaat coating formuleringen leidde tot vergelijkbare waarnemingen. De coatings met microcapsules liet slechts gedeeltelijk herstel zien, voornamelijk vanwege de vorming van grote aggregaten van DiAcrylaat microcapsules die de zelf-herstellende efficiëntie van de coatings verminderden. Het zelf-herstellende effect van deze coatings was minder duidelijk dan die van de PMA-lagen, vanwege de intrinsiek hogere T_g van de commerciële lagen. Door de hele brosse natuur van de commerciële lagen met

nanocapsules was het herstel van deze coatings niet heel groot. Dit betekent echter niet dat coatings met nanocapsules geen zelf-herstellend potentieel hebben. De vorming van een microkras binnen in de coating vereist alleen dat de goed gedefinieerde nanocapsules breken. Algemeen genomen, er werd aangetoond dat thiol-één chemie een effectief herstellend mechanisme verschaft voor de ontwikkeling van zelf-herstellende coatings op waterbasis met micro- of nanocapsules.

Table of contents

List of figures

Figure 3.5: Percentage of the RAFT-agent present as specific species vs. time for three RAFT-mediated MA polymerizations with target molecular weights of 11,000, 30,000 and 70,000 g/mol at 70 °C using CIPDB (AD) as the RAFT-agent (see Table 3.1, reactions 2, 4 and 5). The figure shows the conversion of the initial RAFT-agent into its first (AMD) and second (AM_2D) monomer adducts (AD represents the RAFT-endgroup and M one MA unit and M_2 two MA units).

Figure 3.6: $R^*R^*S^*$ stereoisomer of the second monomer adduct C-MAh-Sty-D showing selected NOE interactions that were detected via 1D NOE spectra.

Figure 3.7: ^{1}H-NMR spectra of a CIPDB-mediated styrene-maleic anhydride copolymerization at 70 °C, enlarged at the methyl region of the leaving group of the RAFT-agent (δ = 0.7–1.6 ppm). The spectra have been taken after 5, 15, 30, 45 and 60 minutes and shown are the leaving group CIP, $–C(CH_3)_2CN$, the MAh-derived first monoadduct, CIP-MAh-DB, the styrene-derived first monoadduct, CIP-Sty-DB and the second monomer adduct derived from one styrene unit and one maleic anhydride unit, CIP-Sty-MAh-DB.

Figure 3.8: ^{1}H-NMR spectra of a CDB-mediated styrene-maleic anhydride copolymerization at 60 °C, enlarged at the methyl region of the leaving group of the RAFT-agent (δ = 0.8–1.9 ppm). The spectra have been taken after 5, 10, 20, 30 and 40 minutes and shown are the leaving group C, $–C(CH_3)_2Ph$, the MAh-derived first monoadduct, C-MAh-DB and the second monomer adduct derived from one maleic anhydride unit and one styrene unit, C-MAh-Sty-DB.

List of schemes

List of tables

List of acronyms

AIBN	2,2'-Azobis(isobutyronitrile)
AMA	2-aminoethyl methacrylate hydrochloride
ATR	attenuated total reflectance
ATRP	atom transfer radical polymerization
BDB	benzyl dithiobenzoate
BHT	butylated hydroxytoluene
CCD	closed-circuit digital
CDB	cumyl dithiobenzoate
CIPDB	2-cyanoprop-2-yl dithiobenzoate
cmc	critical micelle concentration (chapters 2 and 4)
CMC	carboxymethyl cellulose (chapter 2)
COSY	correlation spectroscopy
CPDA	cumyl phenyl dithioacetate
CRP	controlled/living radical polymerization
CTAB	cetyltrimethylammonium bromide
CTC	charge-transfer-complex
DCM	dichloromethane
DDI	distilled deionized
DHBC	double hydrophilic block copolymer
DLS	dynamic light scattering
DMAEMA	(dimethylamino)ethyl methacrylate
DMF	*N*,*N*-dimethylformamide
DMPA	2,2-dimethoxy-2-phenylacetophenone
DNA	deoxyribonucleic acid
DSC	differential scanning calorimetry
EB	electron beam
EPHP	*N*-ethylpiperidine hypophosphite
ESR	electron spin resonance
FTIR	Fourier transform infrared

GC	gas chromatography
gHMBC	gradient-selective heteronuclear multiple bond correlation
gHSQC	gradient-selective heteronuclear single quantum coherence
HD	hexadecane
HEMA	2-hydroxyethyl methacrylate
HPLC	high-pressure liquid chromatography
IR	infrared
kCps	kilocounts per second
KPS	potassium persulfate
LC	liquid crystal
LCST	lower critical solution temperature
MA	methyl acrylate
MAh	maleic anhydride
MALDI-ToF-MS	matrix-assisted laser-desorption ionization time-of-flight mass spectrometry
MEK	methyl ethyl ketone
MEMA	*N*-(morpholino)ethyl methacrylate
MFFT	minimum film-forming temperature
MMA	methyl methacrylate
MW	molecular weight
NMP	nitroxide-mediated polymerization
NMR	nuclear magnetic resonance
NOE	nuclear Overhauser effect
P(DMA-*b*-[NIPAM-*co*-AzPAM])	poly[*N*,*N'*-dimethylacrylamide-*block*-(*N*-isopropyl-acrylamide-*co*-3-azidopropyl acryl-amide)]
P[(Sty-*alt*-MAh)-*b*-Sty]	poly[(styrene-*alt*-maleic anhydride)-*block*-styrene]
p-CIPDCA	p-(2-cyanoprop-2-yl dithiocarboxy) anisole
PCM	phase change material
PDI	polydispersity index

PEO-*b*-P(NIPAM-*co*-NAS)	poly[ethylene oxide-*block*-(*N*-isopropylacrylamide-*co*-*N*-acryloxysuccinimide)]
PMA	poly(methyl acrylate)
PMAC	polymeric micelle with aqueous core
POEGMA-*b*-PDMA-*b*-PDEA	poly[oligo(ethylene glycol)methyl ether methacrylate-*block*-2-(dimethylamino)ethyl methacrylate-*block*-2-(diethylamino)ethyl methacrylate]
POM	polyoxometalate
PSD	particle size distribution
PSMA	poly(styrene-maleic anhydride)
PU	penultimate unit
RAFT	reversible addition-fragmentation chain transfer
RI	refractive index
ROMP	ring-opening metathesis polymerization
RT	room temperature
SDS	sodium dodecylsulfate
SEC	size exclusion chromatography
SEC-ESI-MS	size exclusion chromatography-electrospray ionization-mass spectrometry
SEM	scanning electron microscopy
SMA	styrene-maleic anhydride alternating copolymer
SMA1000	commercial styrene-maleic anhydride alternating copolymer with a styrene to maleic anhydride ratio of one
SMA3000	commercial styrene-maleic anhydride alternating copolymer with a styrene to maleic anhydride ratio of three
SMI1000	styrene-maleimide alternating copolymer with a styrene to maleic anhydride ratio of one
Sty	styrene
Sty-MAh	styrene-maleic anhydride alternating copolymer

TEM	transmission electron microscopy
TGA	thermogravimetric analysis
THF	tetrahydrofuran
TOCSY	total correlation spectroscopy
UF	urea-formaldehyde
UV	ultraviolet
UV-Vis	ultraviolet-visible
VOC	volatile organic compounds

List of symbols

A	interfacial area (chapter 2)
A	pre-exponential factor (chapter 5)
d	fraction of chains that terminate via disproportionation
E_{act}	activation energy
f	initiator efficiency
f_{ene}	ene functionality
f_{thiol}	thiol functionality
G_s	surface free energy
H_R	total enthalpy of reaction
$H(t)$	enthalpy of reaction up to time t
$\Delta H_{reaction}$	enthalpy of reaction
$[I]_0$	initial initiator concentration
K	equilibrium constant
$K(T)$	temperature dependent rate constant
k_{-add}	fragmentation rate coefficient
k_{add}	addition rate coefficient
k_B	Boltzmann constant ($1.38\times10^{-23} J/K$)
k_{ct}	chain-transfer rate constant
k_d	rate of decomposition of the initiator
k_p	propagation rate constant of the monomer
$k_{p,I}$	addition rate constant of the leaving group radical to a monomer unit
ΔK_I	cyclic stress intensity
$[M]_0$	initial monomer concentration
M_n	number average molecular weight
$M_{n,target}$	target molecular weight

$M_{n,th}$	theoretical molecular weight
MW_M	molecular weight of the monomer
MW_{RAFT}	molecular weight of the RAFT-agent
n	reaction order
$P_{Laplace}$	Laplace pressure
R	leaving group (chapter 3)
R	radius of the droplet (chapter 2)
R	universal gas constant ($8.3145\ {}^{J}\!/_{mol \cdot K}$) (chapter 5)
r	copolymer reactivity ratio (chapter 3)
r	molar ratio of thiol and ene functional groups (chapter 5)
$[RAFT]_0$	initial RAFT-agent concentration
R_p	rate of polymerization
S	spreading coefficient
T	absolute temperature
t	polymerization time
T_g	glass transition temperature
T_p	peak temperature
x	monomer conversion
Z	activating group
Z_{avg}	Z-average particle size
$\alpha(t)$	degree of cure
$\frac{d\alpha}{dt}$	rate of reaction
β	(constant) heating rate
η	number of ultrahydrophobe molecules
$f(\alpha)$	reaction model
$\lambda_{em,\max}$	maximum wavelength of emission

λ_{exc}	excitation wavelength
$\Pi_{osmotic}$	osmotic pressure
σ	interfacial tension

Chapter 1: Prologue

1.1 Introduction to coatings[1-3]

1.1.1 General coating formulations

Paint is used to protect, preserve, decorate or add functionality to an object or substrate. This is achieved by covering the object or substrate with a (pigmented) coating. One of the most important applications of a coating is to provide protection of a metal substrate against oxidation (corrosion). Functionalities that can be added to the coating include modification of light reflection or heat radiation of a substrate or protection of the substrate against UV radiation.

A paint system consists of a series of coating layers (multicoat system), each with its specific function. A standard paint system consists of a primer, undercoat(s) and finishing/topcoat(s). In general, different types of paint are used for each function. However, there are also paint types that perform more than one function. The primer is a preparatory coating that is mainly added to ensure better adhesion of the paint to the substrate. In addition, the primer increases paint durability and provides additional protection of the material being painted. A primer is often used when porous materials such as wood are painted. Priming is mandatory if the substrate is not water resistant and the substrate will be exposed to water. The main ingredients of the various coating layers (primer, topcoat) are listed below:

- Binder
- Pigment/dye
- Solvent
- Additives

The most important component of a paint formulation is the binder or resin, which is the film-forming material and therefore the only component that must be present in the paint formulation. The other components are added optionally and (only) provide certain desired properties to the coating or are added to facilitate the application of the binder.

There are many different binders available, including acrylics, styrene-acrylates, polyurethanes, phenolics, (un)saturated polyesters, amino resins, epoxies and alkyds. The oldest available synthetic binders were phenolic resins, formed by the reaction between phenol and formaldehyde, introduced in the early 1920s. Alkyd resins followed soon after, in the 1930s. One way to classify a binder is according to its drying or curing mechanism. The most common drying/curing mechanisms are solvent evaporation, oxidative cross-linking, catalyzed polymerization and coalescence. Some of the most commonly used binders and their properties are the following:

- **Alkyds:** Alkyds form a very important class of binder in (conventional) solvent-based coatings as well as in waterborne coatings, and are referred to as a one-package coating formulation. They owe their importance to their universal applicability. Alkyds are formed by the reaction of a polyol (**alc**ohol) with an acid or anh**yd**ride. An unsaturated fatty acid (plant or vegetable oil) is always added to facilitate drying (curing) via reaction of oxygen from the air with the double bond of the unsaturated fatty acid to form a hard cross-linked network. Metal salts (such as octoate or naphthenate salts of cobalt and manganese) can be added to catalyze the cross-linking reaction. The resins are classified as short, medium or long oil alkyd resins, depending on the fatty acid content. Properties of alkyd resins can be modified by appropriate selection of vegetable oils and fats/fatty acids. Modification with urethanes, for example, leads to the formation of urethane-alkyd resins, which dry rapidly, have high hardness and good resistance to chemicals. These binders are used for interior and exterior coatings of wood, parquet floor seals and marine paints.
- **Acrylics:** Poly(meth)acrylates form another important class of binder in paints. They are used in solvent and waterborne coating formulations and also in powder coatings. Copolymers that consist entirely of (meth)acrylate monomers are termed pure acrylics. Easy access to copolymers allows for tuning of properties such as flexibility, adhesion, gloss, yellowing stability, etc. For application in a low-solvent high-solids system, oligomers are used, because high molecular weight (meth)acrylates result in high viscosity, which is not suitable for paint application.

Cross-linking after application increases the molecular weight and improves the mechanical properties. In this respect, acrylates are often cross-linked with isocyanates (polyurethane paint based on hydroxyl-containing acrylates), yielding coatings with superior properties, that are used in automotive finishes, for example. As dispersions (latexes) do not suffer from high viscosity, high molecular weight resins are used that are especially suited for physical drying (i.e. fast drying properties). Acrylic latexes are used in particular as (interior) decorative house paints.

- **Polyurethanes:** Polyurethanes refer to a class of polymers that are synthesized via the reaction of alcohols with isocyanates. This type of binder falls in the class of catalyzed polymerization. Polyurethanes are available in solvent-based, low-solvent high-solids and powder coating formulations. Although isocyanates do react with water, aqueous two-pack systems are also available. In this case low reactive aliphatic polyisocyanates (that may require an amine catalyst) are emulsified in the aqueous phase. Generally, high molecular weight polyurethanes are formed via cross-linking of polyisocyanates with polyols or via adducts that are cured via oxidation of conjugated double bonds. Polyurethanes are predominantly available as two-pack formulations, due to the high reactivity of (aromatic) isocyanates. One-pack coating formulations are also available, in which blocked isocyanates are used. The blocking agent can be eliminated by *e.g.* heat. Polyurethane coatings have outstanding mechanical and solvent resistance properties and a high gloss level. These properties can be optimally adjusted by proper combination and formulation of a wide range of monomers and adducts. Polyurethanes are used in many different areas: *e.g.* transportation (rail vehicles, aircraft, automobile finishes), the building sector (outdoor coatings, floor coatings) and the industrial sector (equipment, machinery and furniture).
- **Epoxies:** Epoxies also fall in the class of catalyzed polymerization. They consist of a two-pack coating formulation, where the binder and hardener cure after both components are mixed together. Most epoxy resins are condensation products of bisphenol A or bisphenol F with epichlorohydrin, and the most common curing agents are (aliphatic) polyamines, which allow for curing at room temperature.

> Epoxies are used in solvent-based, solvent-free, powder and waterborne coating formulations, and curing takes place at ambient temperature or at elevated temperature. Depending on the molecular weight of the epoxy resin, either solid or liquid epoxy resin is used as binder in the coating formulation. The low and medium molecular weight resins need a reaction partner to provide useful coatings. The high molecular weight coatings give useful, physical drying binders, mainly primers. Epoxy coatings provide strong adhesion, good flexibility, hardness, solvent resistance and corrosion protection.

Other ingredients that are added to a standard paint formulation are pigments, solvent and additives. Pigments provide color or toughness to the paint or simply reduce the cost of the paint. Some paints contain dyes instead of pigments, or a combination of a dye with a pigment. Dyes in this context refer to compounds that are dissolved in the solvent and form a solution or are a liquid themselves, whereas pigments are insoluble in the solvent and form suspensions. Other paints contain no pigment at all.

The function of a solvent in a paint formulation is to control and adjust the viscosity of the paint. The solvent functions as a carrier for the binder and is a volatile substance that serves as an aid in processing and to control and improve the quality of the coatings and their use. The solvent evaporates after application of the coating on the substrate and does not becomes part of the coating itself. Solvent-based coatings contain volatile organic solvents such as aliphatics, aromatics, ketones and alcohols (xylene, toluene, methyl ethyl ketone (MEK), turpentine, etc).

Besides the binder, pigment and solvent, a wide variety of additives are usually added to a paint formulation. They are added in very small quantities and yet can have a significant effect on the product. Examples of additives include thickeners, stabilizers, auxiliary solvents (cosolvents), wetting and dispersing agents, defoamers, dryers, emulsifiers, adhesion promoters, UV radiation stabilizers, film-forming agents and corrosion inhibitors.

1.1.2 Development of coatings with reduced solvent content

Mainly from a technical point of view, as the word ecology at that time was foreign and there was no environmental legislation, the first waterborne coatings were developed in the 1950s. The waterborne coatings formed the basis of the so-called electrodeposition paints that were introduced industrially in the early 1960s. The aim was to replace the common organic paint solvents with water, which has the obvious advantages of being cheap, non-combustible and non-toxic. With the introduction of more stringent environmental legislation on the emission of volatile organic compounds (VOCs) (especially effective since the beginning of the 1980s), together with the scarcity of raw material resources such as petroleum, waterborne coatings were developed on a broader scale from the early 1970s. The aim was to reduce the use of solvent-based coatings and to develop low-solvent (high-solids) coatings (60–80 wt% solid content) and solvent-free coatings (*e.g.* powder coatings). Among the solvent-based coatings, low-solvent high-solid coatings have enjoyed the largest growth rate. The following coating systems have been developed with the aim of reducing the solvent content of the formulation:[1]

- Waterborne coatings (1960)
  - Water soluble polymers
  - Polymer dispersions (latexes)
- Low-solvent high-solids coatings
- (Solvent-free) powder coatings (1952)
- Radiation curing coatings

In the architectural paint sector, conventional solvent-based coatings based on alkyd and other synthetic resins can largely be replaced by waterborne dispersions of acrylate polymers and copolymers, aqueous alkyd resin paints, and low-solvent high-solids paints. Over 90% of interior decorative paints are now water-based, but the move from solvent-based to water-based has been much slower in the exterior decorative and industrial paint sectors.[4] Modern low-solvent high-solids coating materials not only decrease environmental pollution, but also have improved paint quality (*e.g.* resistance to weathering). However, in some areas solvent-containing coatings are difficult to replace

without affecting quality. Among the coating systems that can be classified as environmentally friendly, waterborne coatings have the widest potential with respect to application, drying methods and industrial uses.[2] Waterborne coatings can be classified into four groups, depending on the nature of their stabilization in the aqueous phase:[1]

- True solution
- Colloidal solution (internally emulsified)
- Primary dispersion (latex)
- Secondary dispersion (externally emulsified)

The first class represents polymers that are synthesized in bulk and are completely water soluble or become water soluble after neutralization with an acid or base and/or with the aid of an auxiliary solvent. These are low molecular weight polymers (<10,000 g/mol, *e.g.* alkyds, epoxies, polyacrylates). The colloidal solutions also consist of polymers that are synthesized in an organic medium, and they are referred to as internally emulsified binders. They are dispersed in the aqueous phase with the aid of an auxiliary solvent and neutralization with a base. Primary dispersions are formed by polymerizing the monomer directly in the aqueous phase, *i.e.* via emulsion polymerization. These dispersions are referred to as waterborne latexes. They have a relatively high solid content (50–60 wt%) and low organic solvent content (<5 wt%). Many substrates can be coated with coating materials based on polymer dispersions, such as concrete, wood, plaster, wallpaper, etc. Dispersion paints now form the largest product group in the paint and coating industry worldwide.[2] The secondary dispersions, referred to as externally emulsified binders, are formed by dispersing the resin in the aqueous phase (emulsifying) and additional stabilization of these particles is achieved with the aid of a low or high molecular weight emulsifying agent (surfactant). The various methods that are available to dissolve or disperse polymer in the aqueous phase allows many of the solvent-based coating formulations to be transformed into waterborne coating formulations.

An important variable of waterborne coatings is the so-called minimum film-forming temperature (MFFT). The MFFT determines at what temperature film forming may still

be anticipated. The MFFT is closely related to the method of polymer synthesis and glass transition temperature (T_g). Waterborne coatings form a film based on a mechanism that is referred to as coalescence. The water evaporates and the polymer particles fuse together to form a film. Irreversible network structures are formed that are no longer dispersible in water. Generally, a coalescent (film-forming agent) is added to facilitate film formation. This coalescent lowers the T_g of the polymer and allows the particles to fuse together and form a film. The coalescent thus acts as a (temporary) plasticizer for the polymer. If film formation occurs below the MFFT, the emulsion paint forms a non-coherent, fissured, mechanically unstable film. After film formation, the film-forming agent leaves the film due to its volatility. Effective film-forming agents are *e.g.* ester-ketones, such as Texanol.

The technology of powder coatings was introduced in the early 1950s. This type of coating produces the least environmental pollution since it does not contain volatile organic solvents. There are two main application techniques, *i.e.* the fluidized bed process (1952) and the electrostatic powder coating technique (1965). Thermosetting as well as thermoplastic binders are used, but the majority of powder coatings constitute thermosetting binders. Thermoplastic binders are applied (mainly by fluidized bed) onto the (hot) substrate, causing the binder to melt and flow, and consequently adhere to the substrate. Thermosetting binders include a cross-linking agent in the coating formulation that provides curing of the binder upon application onto the (most often cold) substrate (mainly by electrostatic spraying). Powder coatings are used primarily in the construction and building industry, both for interior and exterior use. The coating of metallic as well as non-metallic (*e.g.* glass, ceramic) substrates are important areas of use for powder coatings.

Radiation-curing is another process in which no volatile organic solvents are used. It therefore has an ecological advantage. Curing of the coating formulation is achieved by exposing the coating to either UV radiation or to an electron beam (EB, accelerated electrons interact with the organic compounds). In this type of coating, the solvent is

replaced by a reactive diluent (monomer) that is incorporated in the network during curing. An important use of radiation-curing is for the coating of wood.

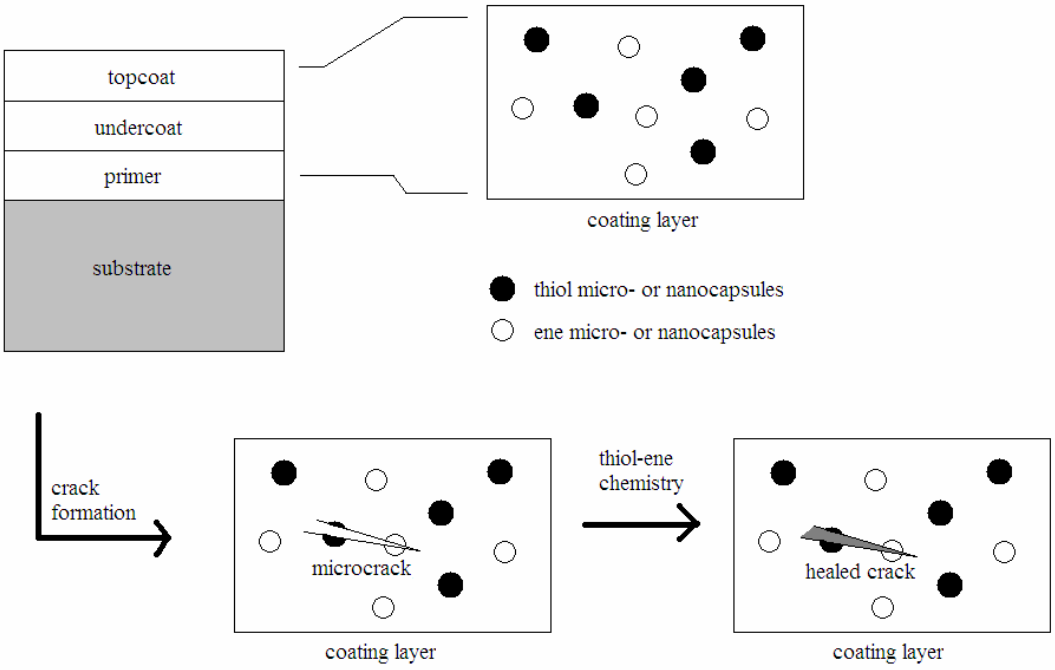

Scheme 1.1: Principle of the development of a self-healing coating as investigated and described in this dissertation.

1.2 Objectives and outline of dissertation

The present study focuses on waterborne coatings, and the overall aim is to introduce a *self-healing* functionality into the coating formulation. The process of self-healing that is anticipated is demonstrated in Scheme 1.1. Inspired by the work of White *et al.*[5], Yuan *et al.*[6] and Skipor *et al.*[7], capsules with a reactive load are embedded in a coating formulation. The capsules can be embedded in any of the various layers of a paint system, but embedding the capsules in the undercoat or primer provides advantages. The primer does not require gloss or any desired optical properties and therefore the effects of embedding capsules in this layer would be compensated for by the topcoat. Upon the formation of a microcrack within the coating, the capsules rupture and release their content, and the healing agent flows into the crack via capillary action. The healing reaction (curing) is then triggered upon contact with a catalyst embedded in the matrix

(one-component healing system) or upon contact between healing agent and hardener that are separately encapsulated (two-component healing system). The healing reaction repairs the microcrack and this prevents the coating from failing.

White *et al.*[5], Yuan *et al.*[6] and Skipor *et al.*[7] synthesized microcapsules via *in-situ* polymerization of urea and/or melamine with formaldehyde and obtained microcapsules with high strength and durability, and low permeability. They focused on the repair of mainly epoxy-type coating formulations.

In the present study, the feasibility of self-healing in a waterborne coating formulation (polymer dispersion, *i.e.* latex) will be investigated. As a self-healing mechanism, thiol-ene chemistry is examined, which is a robust technique and has many advantages over curing of conventional (meth)acrylates, such as reduced sensitivity to oxygen and network formation at high conversion.[8] Initially, microcapsules are synthesized via *in-situ* polymerization of urea and formaldehyde and embedded in a waterborne coating formulation. The coatings are tested for their self-healing ability after introduction of a crack with a razor blade. Nanocapsules are synthesized via both miniemulsification and miniemulsion polymerization. These nanocapsules are then dispersed in a waterborne coating formulation and tested for their self-healing ability.

Chapter 2 of this dissertation gives a detailed review on the theory of (mini)emulsion polymerization, encapsulation of various compounds via the formation of nanocapsules or amino-formaldehyde microcapsules, the introduction of a self-healing functionality in coatings, and thiol-ene chemistry.

Chapter 3 focuses on Reversible Addition-Fragmentation chain Transfer (RAFT)-mediated polymerization. It is shown that polymers with well-defined architecture are easily accessible via this technique. The main focus is on the kinetics of RAFT-mediated polymerizations at the early stages of the reaction, *i.e.* the so-called *initialization* period.[9]

Chapter 4 describes the synthesis of core-shell nanocapsules via miniemulsification. Styrene-maleic anhydride (SMA) alternating copolymers and chain-extended block copolymers with styrene (P[(Sty-*alt*-MAh)-*b*-Sty]) are synthesized via RAFT-mediated polymerization and used as surfactant for stabilization of the nanocapsules.

Chapter 5 first describes the synthesis of urea-formaldehyde microcapsules and the kinetics of thiol-ene chemistry for the thiol and ene compounds used in this study. Then, in combination with the use of a selective rhodamine-based fluorescent probe, the rupture of thiol containing microcapsules after crack formation with a razor blade is investigated. Finally, the self-healing ability is investigated by embedding these microcapsules in a waterborne poly(methyl acrylate) (PMA) film.

Chapter 6 first describes the synthesis of nanocapsules via miniemulsion polymerization. Then the nanocapsules synthesized as described in Chapter 4 via miniemulsification and the nanocapsules synthesized via miniemulsion polymerization are embedded in a waterborne PMA film. The rupture of the thiol containing nanocapsules is then investigated with the aid of a rhodamine-based fluorescent probe and the self-healing ability of the coating is determined. In addition, both microcapsules and nanocapsules are embedded in commercial styrene-acrylate and pure acrylic coating formulations. The coatings are tested for their self-healing ability.

Chapter 7 provides the general conclusions and mentions the extent to which the goals were reached. Finally, some recommendations are given on how to optimize the self-healing ability of the coatings, and to allow for their (industrial) application.

References

1. K. Dören, W. Freitag and D. Stoye, *Water-borne coatings: the environmentally-friendly alternative*, **1994**, ISBN: 1-56990-139-2
2. D. Stoye and W. Freitag, *Paints, coatings and solvents*, Second edition, **1998**, ISBN: 3-527-28863-5
3. R. Lambourne and T.A. Strivens, *Paint and surface coatings: theory and practice*, Second edition, **1999**, ISBN: 1 85573 348 X
4. European Chemical News, 15 April 2002, *76* (2001), 17-19
5. S.R. White, N.R. Sottos, P.H. Geubelle, J.S. Moore, M.R. Kessler, S.R. Sriram, E.N. Brown and S. Viswanathan, *Nature* **2001**, *409*, 794-797
6. Y.C. Yuan, M.Z. Rong, M.Q. Zhang, J. Chen, G.C. Yang and X.M. Li, *Macromolecules* **2008**, *41*, 5197-5202
7. A. Skipor, S. Scheifer and B. Olson, **2002**, *WO02/064653*
8. C.E. Hoyle, T.Y. Lee and T. Roper, *J. Polym. Sci., Part A: Polym. Chem.* **2004**, *42*, 5301-5338
9. J.B. McLeary, F.M. Calitz, J.M. McKenzie, M.P. Tonge, R.D. Sanderson and B. Klumperman, *Macromolecules* **2004**, *37*, 2383-2394

Chapter 2. Introduction and theory

2.1 Emulsion polymerization[1]

Emulsion polymerization is a widely applied technique via which polymer latexes can be obtained. An emulsion polymerization is a hetero-phase polymerization technique in which a monomer is dispersed in a continuous phase, usually water, and stabilized by surfactant molecules against coalescence. The monomer phase is dispersed in the continuous phase via mechanical agitation, and the size distribution of the monomer droplets is broad. Because the continuous phase is used as a heat sink, the removal of exothermic heat is facilitated and, as the particles are dispersed in the continuous phase, the viscosity of the medium is low, which makes stirring easy. Generally, particle sizes obtained via emulsion polymerization range from about 50 nanometers to a few microns.

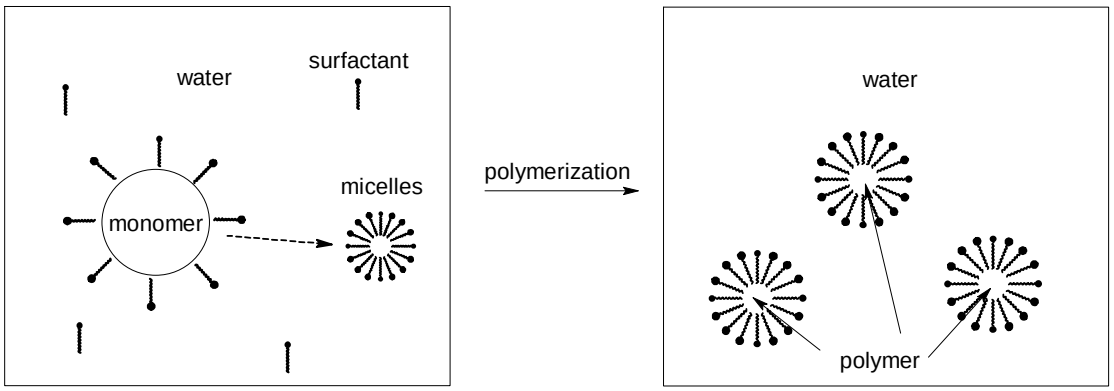

Scheme 2.1: Concept of emulsion polymerization.

In 1947 Harkins proposed a general theory for the mechanism of emulsion polymerization.[2] Although the theory is not in full accordance with current thinking, Harkins' theory gives valuable insight into the mechanistic aspects of the process and the theory is in fact perfectly well applicable to the batch polymerization of styrene (a rather water insoluble monomer). As shown in Scheme 2.1, the majority of monomer is present as big monomer droplets in the aqueous phase and they are stabilized by surfactant molecules. The majority of surfactant molecules are however present as aggregates, known as micelles, that are formed above a certain concentration (the critical micelle

concentration, cmc). These micelles contain a small amount of monomer (monomer swollen micelles) and a small fraction of the surfactant molecules exist as single molecules in the aqueous phase, the amount of which is dependent, for example, on the solubility, type of surfactant and the temperature. Finally, the aqueous phase contains an initiator, which initiates the polymerization. Usually additives like chain transfer agents are used in order to control the molecular weight. Initially, the radicals generated in the aqueous phase react with monomer units to form oligomeric radicals. The more hydrophobic monomers tend to polymerize in the micelles (particle nucleation), whereas the more hydrophilic monomers tend to form oligomers in the aqueous phase (homogeneous nucleation) before entering the micelles or precipitating in the aqueous phase and forming new particles stabilized by surfactant molecules. The concentration of monomer in the aqueous phase is very low, as most monomers are highly water insoluble (the solubility of styrene in the aqueous phase is about $2x10^{-3}$ M; butyl acrylate and methyl methacrylate have somewhat higher solubility in the aqueous phase). After the oligomeric radicals become water insoluble, the likelihood of them entering the monomer swollen micelles instead of the monomer droplets is much higher, because the surface area of the monomer swollen micelles is much higher than that of the monomer droplets. Because the concentration of monomer is high in the monomer swollen micelles, the rate of polymerization is high too. The monomer swollen micelles are turned into monomer swollen polymer particles (latex particles), and the large monomer droplets now act as a monomer reservoir. The monomer is transported by diffusion through the aqueous phase from the monomer droplets to the latex particles. In emulsion polymerization the monomer swollen micelle acts as an individual nanoreactor that grows and turns into a latex particle. Therefore, the rate of polymerization and the final molecular weight obtained are dependent on the number of particles and, as a consequence, both are inversely proportional to the particle size. The particles can at any instant contain zero or one radical, because the rate of termination is considered to be very much faster than the rate of radical entry. The polymer chain can thus grow until it is terminated by another radical, after which the particle will be dormant until another radical enters the particle. It must be pointed out however, that not all micelles are turned into latex particles. Because the size of the latex particles increases during the course of the polymerization, surfactant

molecules from the aqueous phase adsorb onto the surface of the latex particles. This disturbs the equilibrium between surfactant molecules in the aqueous phase and in the micelles, and this equilibrium is restored by the disappearance of micelles. Once all the micelles of the aqueous phase have been consumed, the number of latex particles remains constant (onset of Interval II).

More recently, Tauer and coworkers investigated the very early stages of a styrene emulsion polymerization and they focused on the nucleation mechanism by online monitoring of the transmission and the conductivity.[3-5] They examined surfactant-free emulsion systems as well as systems containing surfactant above and below the cmc. They extended their experiments with systems containing a certain volume of seed-latex. They concluded that at the very early stages of the reaction (conversions below 2% could be investigated) the nucleation takes place in the aqueous phase, forming oligomers, until they collapse and form particles (referred to as aggregative particle nucleation). Because they investigated the styrene emulsion polymerization for only a very limited conversion range, they could only conclude that at the very early stages the number of particles decreases, after which it remains constant, followed by an increase in the number of particles, indicating another particle nucleation step.

In emulsion polymerization usually three different intervals are distinguished, namely Interval I where the monomer is stored in large monomer droplets, in micelles, and in polymer particles, and where the number of particles is growing. This interval normally occurs at low conversions (<15%) and ends when all the micelles have been converted into latex particles or have disintegrated to stabilize growing particles. The rate of polymerization during this interval is vastly increasing. Interval II is characterized by a constant rate of polymerization and at this stage the number of particles is constant. During this interval all the monomer from the monomer droplets diffuses to the polymerization loci. During Interval II the conversion of monomer reaches about 35%, although this value may vary, depending on the monomer used. In Interval III, a constant number of particles is present and all monomer is present in the polymer particles. At this stage the rate of polymerization decreases and high conversions are obtained.

Although emulsion polymerization can easily be applied to the free-radical homopolymerization of certain highly water insoluble monomers, it has to be accepted that there are some disadvantages. The preparation of copolymers, for example, lacks homogeneity and there are restrictions in the accessible composition range. This is related to the polymerization mechanism in emulsion polymerization. Dependent on the monomer being polymerized, either homogeneous nucleation (aqueous phase nucleation) or micellar nucleation (nucleation in the monomer swollen micelles) will be the predominant mechanism. An industrially important procedure to carry out emulsion polymerization is via seeded emulsion polymerization. By employing a certain volume fraction of a seed latex, the nucleation of new particles is suppressed, and different morphologies such as a composite latex or core-shell particles can be obtained.[4,6] It remains a challenge though to accomplish the formation of well-defined copolymers with controlled composition, and the introduction of miniemulsion polymerization offered a new approach for the synthesis of such materials.

2.2 Miniemulsion polymerization[7]

In the previous section it was reported that in emulsion polymerization the locus of polymerization is mainly in the monomer swollen micelles or in the aqueous phase. This was attributed to the difference in size between the monomer droplets and monomer swollen micelles, leading to a difference in surface area. Because the total surface area of the monomer swollen micelles is much larger than that of the monomer droplets (the size of the monomer droplet is much larger, but the number of droplets is much lower) the competition for radicals between both nucleation loci favors the radicals to enter the monomer swollen micelles. In 1973 Ugelstad *et al.* were the first to publish on an emulsion polymerization process that was nucleated in the monomer droplets.[8] They reasoned that if the size of the monomer droplets could be reduced, the surface area of the monomer droplets would be increased, allowing them to compete for radical entry and thus monomer droplet nucleation. The latex obtained however, had a broad particle size distribution and consisted of rather large particles. This broad particle size distribution was a result of the method of dispersing the droplets in the aqueous phase, namely by simply stirring. Ultrasonication as a way to disperse the monomer in the aqueous phase,

to form a pre-emulsion, was only introduced in 1979 by Durbin *et al.*[9]. They obtained a bimodal particle size distribution however, resulting from nucleation in both monomer droplets and monomer swollen micelles. Later, in 1980, the term miniemulsion was given to this kind of emulsion polymerization processes, where the monomer droplets serve as a locus for polymerization.[10] Because nucleation predominantly occurs in the monomer droplets, miniemulsion polymerization is easily distinguishable from other heterogeneous polymerization systems, such as emulsion-, microemulsion- and suspension polymerization.

Although the concept of miniemulsion has existed for over 30 years now, and much research has been done in the field of miniemulsion polymerization, especially the last decade resulted in an increased understanding and new experimental developments, also in conjunction with the introduction of controlled/living radical polymerization techniques. This has increased the number of possibilities that can be achieved via miniemulsion polymerization enormously. This section further describes miniemulsion polymerization in great length and in Section 2.4 some of the achievements that can be obtained are described, such as the development of architectures that were initially not easily accessible, like polymer-polymer hybrids and inorganic-polymer hybrids. Furthermore, miniemulsion polymerization allows for the encapsulation of a number of compounds, such as Fe_3O_4 (magnetic nanoparticles), TiO_2, Y_2O_2S, and many more, forming so-called core-shell particles, with new and desired properties.

Over the last decade detailed reviews on miniemulsion polymerization have been reported by Antonietti and Landfester[7] and Asua.[11] Miniemulsion polymerization is a heterogeneous polymerization technique that yields small, stable polymer particles in a continuous phase (usually water) with a particle size in the range of 30 to 500 nanometers. Different from emulsion polymerization, in miniemulsion polymerization the monomer phase is dispersed in the aqueous phase via high shear (applied via *e.g.* a homogenizer or ultrasound) that breaks up the particles until a pseudo steady-state is reached. At this stage a uniform distribution in the monomer droplet size can be achieved (as long as the concentration of ultrahydrophobe, which suppresses the diffusion of

monomer out of the droplets (Section 2.2.1), is equal in all monomer droplets), and during polymerization these droplets are (ideally) copied into polymer particles while retaining their identity and keeping the number of particles constant (Scheme 2.2). This is also a consequence of the mechanism of miniemulsion polymerization, where the main nucleation mechanism is droplet nucleation. As long as homogeneous nucleation (nucleation in the aqueous phase) is prevented or suppressed, a one-to-one copy of monomer droplet to polymer particle can be achieved. However, for the monomer droplets to be copied into polymer particles a few requirements have to be fulfilled. First of all, the nucleation of all the droplets in the miniemulsion system must be very fast and the rate of polymerization must be much faster than the rate of mass transport of monomer among particles. Furthermore, droplet-droplet and droplet-particle coalescence and particle-particle coagulation have to be negligible. Although the predominant nucleation mechanism is droplet nucleation, both water- and oil-soluble initiators can be used in miniemulsion polymerization. The use of a water soluble initiator in the miniemulsion polymerization of styrene is successful, for example, but when more hydrophilic monomers are employed, such as methyl methacrylate, homogeneous nucleation will occur to a certain extent, broadening the particle size distribution and lowering the homogeneity of the miniemulsion. The use of an oil-soluble initiator has the disadvantage that radical recombination can occur within the particles. However, it has been shown that a substantial fraction of the radicals formed from the decomposition of an oil-soluble initiator desorb form the particles, and thus separation of the radicals occurs before they suffer from bimolecular termination.[12] Nevertheless, oil-soluble initiators, such as 2,2'-azobis(isobutyronitrile) (AIBN), are particularly useful for monomers with both relatively high water solubility and high water insolubility. In the former case homogeneous nucleation is prevented, whereas in the latter case polymerization is initiated in the droplets. The concentration of monomer in the aqueous phase would not be high enough to form oligoradicals that can enter the droplets if a water soluble initiator would have been employed.

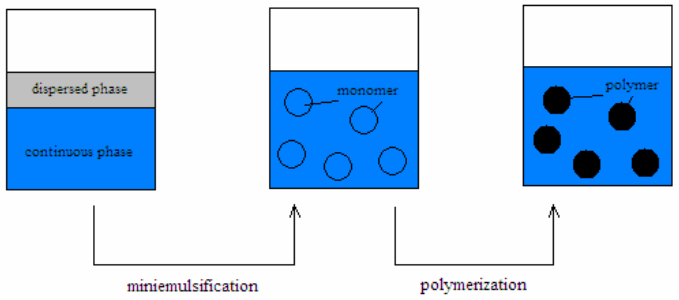

Scheme 2.2: Polymerization via miniemulsion.

To obtain a stable miniemulsion, the monomer droplets that are formed after dispersion in the aqueous phase need to be stabilized against coalescence/coagulation (droplet/particle fusion) and Ostwald ripening (molecular diffusion). Ostwald ripening is the diffusion of monomer from small particles to large particles, and coalescence and coagulation result from the collision between droplets and/or particles. In miniemulsion polymerization the addition of an ultrahydrophobe induces stability against Ostwald ripening, whereas the employment of a surfactant ensures stability against coalescence and coagulation.

2.2.1 Addition of an ultrahydrophobe

In 1981 Davis *et al.* showed that the stability against monomer diffusion from small to large droplets can be achieved via the addition of a third, non-volatile component that is miscible with the dispersed phase and not soluble in the aqueous phase.[13] Lifshitz and Slyozov (1961) were the first ones to provide a model for the growth of droplets (by other means than coagulation), and in the literature this process is often referred to as Lifshitz-Slyozov dynamics. Nowadays this process of droplet growth is more commonly known as Ostwald ripening. Webster and Cates thermodynamically described the growth rate of droplets by means of Lifshitz-Slyozov dynamics.[14] They considered an emulsion system and differentiated between systems with and without the addition of a third non-volatile component (trapped species). Via a description of the chemical potential of the dispersed phase they developed a growth rate which is dependent on the competition of the Laplace pressure of the droplets and the osmotic pressure of the trapped species. The Laplace pressure is given by:

$$P_{Laplace} = \frac{2\sigma_{ow}}{R} \qquad \textit{equation 2-1}$$

where σ_{ow} is the interfacial tension between the oil and water phases and R the radius of the droplet. The osmotic pressure is given by:

$$\Pi_{osmotic} = \frac{k_B T \eta}{(4\pi/3)R^3} \qquad \textit{equation 2-2}$$

where k_B and T are the Boltzmann constant ($1.38\times10^{-23} J/K$) and absolute temperature, respectively, η the number of ultrahydrophobe molecules, and R the radius of the droplet.

The driving force for Ostwald ripening is a difference in vapor pressure (solubility) between particles with different sizes. Providing the droplets are small (<1 µm) and have a finite solubility in the continuous phase, Ostwald ripening will occur, and this will be lower for uniform, small particles. Smaller particles have higher vapor pressure (solubility) than larger particles, and therefore diffusion from the smaller to the larger particles will take place. The addition of a third compound (ultrahydrophobe) that is less soluble in the continuous phase and soluble in the dispersed phase, and above all has a lower vapor pressure (higher boiling point) than the dispersed phase, will provide stability to the latex and prevent Ostwald ripening. Ostwald ripening results in the diffusion of oil from the small particles to the large particles and, as a consequence, the mole fraction of the oil decreases in the small droplets and the mole fraction of the ultrahydrophobe increases in the small droplets. On the other hand, the mole fraction of oil increases in the larger droplets and the mole fraction of the ultrahydrophobe decreases in the larger droplets. The oil and the ultrahydrophobe contribute to the total vapor pressure according to Raoult's law, leading eventually to an equilibrium and stability against Ostwald ripening. The extent of Ostwald ripening is, amongst other factors, dependent on the solubility of the dispersed phase in the aqueous phase, the concentration of surfactant,[15] the size and the polydispersity of the droplets formed. It must be pointed out however, that the addition of an ultrahydrophobe will never result in the complete

loss of small droplets by this process. It appears that when the hydrophobic chain length increases the stability of the miniemulsion also increases (the more hydrophobic the osmotic pressure agent the more effective it works against Ostwald ripening, and the more it increases the stability of the latex).[16]

The most common example in the literature of an ultrahydrophobe is hexadecane, and only a very small amount needs to be added to suppress Ostwald ripening. The amount of ultrahydrophobe added to the miniemulsion formulation only has a marginal effect on the particle size obtained,[17] although this behavior might be very system dependent.[16,18,19] Other examples of effective ultrahydrophobes are cetyl alcohol (which rather acts as a cosurfactant because of its presence at the oil–water interface),[20] dodecyl mercaptan (which acts as an ultrahydrophobe and simultaneously as a chain transfer agent, and also shows some cosurfactant-like behavior),[21] lauryl methacrylate (which acts as an ultrahydrophobe and simultaneously as a comonomer, and is incorporated in the polymer),[22] fluorinated alkanes,[23] silanes,[17] nematic liquid crystals (nematic LCs),[24] and many others. Polymer chains are also seen as effective ultrahydrophobes because they are insoluble in the aqueous phase and are compatible with the dispersed monomer phase.[19,25-27]

2.2.2 Employment of a surfactant

In miniemulsion polymerization colloidal stability is obtained by the addition of a surfactant, as is also the case in emulsion polymerization. Both systems employ the same type of surfactants, the most common of which is sodium dodecylsulfate (SDS), which is an anionic surfactant. It is also possible to form stable miniemulsions by using cationic surfactants, for example cetyltrimethylammonium bromide (CTAB). Even non-ionic surfactants such as poly(ethylene oxide) derivates are used to form stable latexes or amphiphilic block copolymers, where the polymer acts as a surfactant and simultaneously as a hydrophobe.[28,29] Non-ionic surfactants are less efficient surfactants however, because steric stabilization of surfactants is less efficient than electrostatic stabilization. Furthermore, polymerizations in the absence of surfactant (surfactant-free (mini)emulsion

polymerization) have been reported, and these polymerizations are more desirable for industrial application.[30-32]

As a general rule, the higher the concentration of surfactant added the smaller the particles become. For very high surfactant concentrations (up to 50 wt% relative to monomer) the particle size becomes very small, comparable to the sizes generally obtained in microemulsions (around 30 nm). In microemulsion the particles are formed spontaneously though, and much higher concentrations of surfactant are used, also leading to the presence of free micelles. In miniemulsion the concentration of surfactant can be high, so that small particles are obtained, but the free surfactant concentration is well below the cmc, so that no free micelles are present. In both cases the surface coverage of the particles by the surfactant is very high, so that the surface area per surfactant molecule is very small (about 0.4 nm^2). On the other boundary of the particle size, where rather low concentrations of surfactant are used (~0.3 wt% relative to monomer), the surface area per surfactant molecule is high and large particles need to be stabilized. At these low concentrations of surfactant the particles become colloidally unstable, and the region of clean miniemulsion is left.

The post-addition of surfactant (after mechanical homogenization) results in *thermodynamically* stable particles.[17,33,34] The number of particles does not change by this addition of extra surfactant, but the surface coverage of the droplets by the surfactant molecules decreases the surface tension between the oil and water phases, and thus also decreases the Laplace pressure ($P_{Laplace} \sim \sigma_{ow}$), where σ_{ow} represents the interfacial tension between the oil and water phases.

2.2.3 Preparation of a miniemulsion

For the preparation of a miniemulsion, the formulation has to be exposed to high shear that breaks up the monomer droplets. This increases the surface area of the monomer droplets and facilitates droplet nucleation. After the separate preparation of the oil and aqueous phases, the monomer is dispersed in the aqueous phase via simple stirring to form a pre-emulsion. This pre-emulsion has a broad size distribution and the particles are still large (a few microns). Further disruption of the particles is needed, which is done by subjecting the pre-emulsion to high shear until a pseudo steady-state is obtained. The application of high shear can be done via different methods, for example, with an ultraturrax, but nowadays the ultrasonicator is most widely used for small volume latexes. Initially the droplet size is a function of the amount of energy added to the miniemulsion. Once the pseudo steady-state is reached, further addition of energy to the miniemulsion does not result in smaller particles. Once this minimum amount of energy has been supplied to the miniemulsion, the fusion and fission processes are in equilibrium and the droplets are stable against Ostwald ripening. The pseudo steady-state obtained does not mean however that the droplet pressure (Laplace pressure) and the osmotic pressure generated by the ultrahydrophobe are in balance. Immediately after mechanical homogenization it appears that $P_{Laplace} - \Pi_{osmotic} \neq 0$ and that the droplets are in a pseudo steady-state. It must be noted though that the *difference* in Laplace pressure and osmotic pressure is constant for all droplets ($\Delta P > 0$), and therefore the droplets are in a pseudo steady-state (Scheme 2.3). In case $P_{Laplace} - \Pi_{osmotic} = 0$ would apply, the droplets would be in a thermodynamic steady-state. Because the Laplace pressure scales with R^{-1} and the osmotic pressure with R^{-3}, minor changes in size directly after mechanical homogenization have huge influences on this pressure balance. It is a common observation in miniemulsion polymerization that over long periods of time the particles grow in size. The growth in size continues until the Laplace pressure and the osmotic pressure balance each other. Thus, the constant (positive) pressure obtained in the droplets effectively stabilizes the droplets against mass exchange by diffusion (pseudo steady-state), but the growth of the droplets by all other means is not prevented.

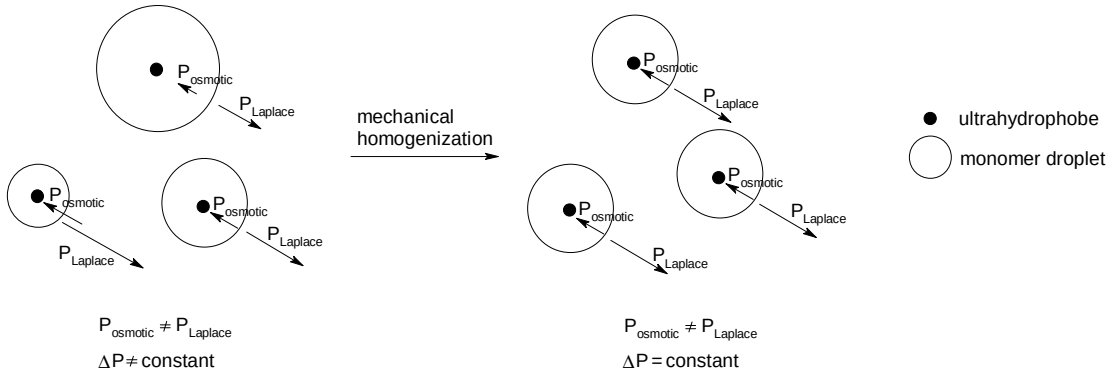

Scheme 2.3: Effect of ultrahydrophobe on droplet stability.

2.2.4 Kinetics in miniemulsion polymerization

Miniemulsion polymerization is characterized by a mechanism where the predominant nucleation takes place via monomer droplet nucleation. This also leads to the preservation of the number of particles that is formed after mechanical homogenization and each monomer droplet is (ideally) copied into a polymer particle while retaining its identity and size. In emulsion polymerization three different intervals are distinguished, each with its own characteristics regarding rate of polymerization and particle formation (see Section 2.1). In miniemulsion polymerization also three different intervals exist regarding rate of polymerization and number of radicals present in each particle. Compared to emulsion polymerization, Intervals I and III are present, but Interval II where the rate of polymerization is constant is not observed. There is an additional interval observed though, referred to as Interval IV. Interval I characterizes itself with an increase in the rate of polymerization, where the number of radicals within each droplet reaches an equilibrium radical concentration. This interval ends already at very low conversions (~10%). Interval III is known from emulsion polymerization to lead to a decrease in the rate of polymerization. That is exactly what is also observed in miniemulsion polymerization. The rate of polymerization decreases (exponentially) and the number of radicals is nicely kept constant at 0.5. This decrease in the rate of polymerization is a consequence of the consumption of monomer and thus the decrease in the monomer concentration in the particles. This also clearly indicates that the predominant nucleation mechanism is via droplet nucleation. The third interval

recognized in miniemulsion polymerization, and referred to as Interval IV, reflects a steep increase in the viscosity of the polymer particles. As a consequence, the number of radicals in the particles steadily increases because termination events are suppressed.

2.2.5 Applications of miniemulsion polymerization

Because in miniemulsion polymerization the predominant nucleation mechanism is monomer droplet nucleation, copolymers with more homogeneity in chemical composition throughout the particle size distribution can be obtained, which otherwise would be a challenging task. The introduction of living radical polymerization techniques in homogeneous radical polymerization has opened a way to synthesize latex particles consisting of homopolymers with predetermined molecular weight and narrow molecular weight distribution.[33,35] Also the formation of latexes consisting of well-defined block copolymers can be achieved.[36,37]

Although miniemulsion polymerization can be successfully applied to a wide range of monomers under a wide range of conditions (*e.g.* surfactant- and initiator concentration, composition), generally the miniemulsions prepared have a solid content of 10–20 wt% of monomer relative to water. This makes the miniemulsion process not very interesting for industrial applications, and a few groups have reported on the miniemulsion polymerization of high solid contents (up to about 70%).[38-41]

To summarize the main differences between emulsion- and miniemulsion polymerization:

- The predominant nucleation mechanism in emulsion polymerization is homogeneous or micellar nucleation, whereas the main nucleation mechanism in miniemulsion polymerization is droplet nucleation.
- In both systems colloidal stability is obtained by the addition of surfactant, but in miniemulsion polymerization a further stability against Ostwald ripening is obtained via the addition of an ultrahydrophobe (costabilizer).

- In emulsion polymerization the monomer is dispersed in the aqueous phase by simple stirring. In miniemulsion polymerization on the other hand, the monomer is generally dispersed via simple stirring, forming a pre-emulsion, after which the pre-emulsion is subjected to high shear that breaks up the droplets so that the droplets end up in a so-called pseudo steady-state, where they have a low polydispersity in droplet size.
- In miniemulsion polymerization the monomer droplets are transformed into polymer particles, whereas in emulsion polymerization the monomer swollen micelles or the oligoradicals formed in the aqueous are transformed into polymer particles and the monomer droplets act as a reservoir for the transport of monomer to the polymerization loci.
- In miniemulsion polymerization the number of particles formed at the onset of polymerization does (ideally) not change throughout the polymerization process. In emulsion polymerization new particles are formed during Interval I and the number of particles increases until no free micelles are present anymore (onset of Interval II).

2.3 Encapsulation via the formation of nanocapsules

In 1970 Torza and Mason published on the behavior of two immiscible liquid drops (phases 1 and 3) suspended in a third immiscible liquid (phase 2), based on thermodynamic considerations.[42] They could predict via calculations on the surface tensions among the phases (of equal density) what equilibrium morphology would be obtained, when the two drops are brought into contact via shear and electrical fields. Their calculations were solely based on the surface tensions between the different phases and the resulting spreading coefficients:

$$S_i = \sigma_{jk} - \left(\sigma_{ij} + \sigma_{ik}\right) \qquad \textit{equation 2-3}$$

These calculations yield the same results as would be obtained for minimizing the surface free energy $G_s = \sigma_{ij} \cdot A_{ij}$, where A_{ij} is the area of the interface between the two surfaces.

By designating phase 1 such that $\sigma_{12} > \sigma_{23}$, it follows from equation 2-3 that $S_1 < 0$. By examination of equation 2-3, it can be derived that only three possible sets of S_i exist, and each of these possibilities are related to a different equilibrium morphology (Figure 2.1), namely

- Complete engulfment
- Partial engulfment
- Non-engulfment

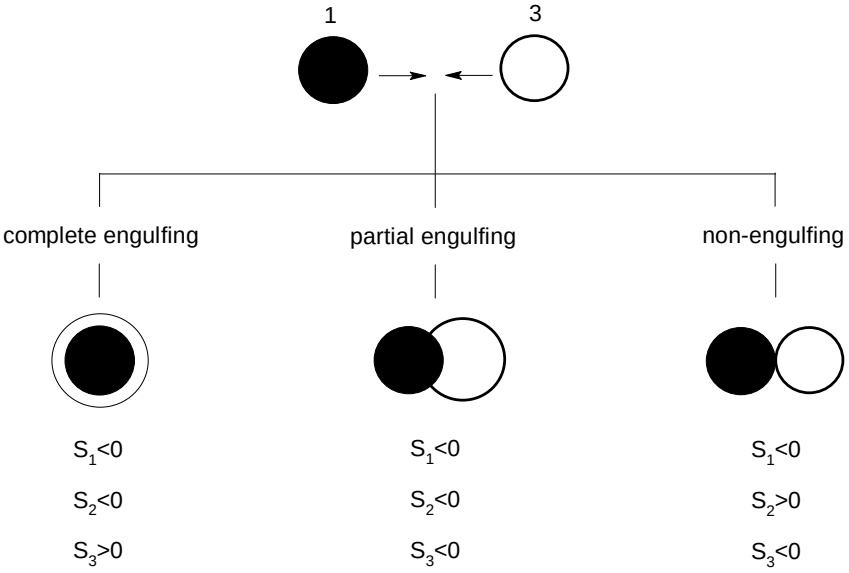

Figure 2.1: Possible equilibrium morphologies corresponding to the three sets of relations for S_i. The black drop is phase 1 and the medium is phase 2.

More recently, Waters extended the work of Torza and Mason to an emulsion system considering the thermodynamically favored morphology for composite latex particles.[43] On the basis of the particles minimizing their total interfacial energy and ensuring colloidal stability of the particles so that their identity is retained, he quantified the interfacial energy as a function of degree of engulfment for both a non-deforming sphere as well as a deforming sphere. Berg *et al.* correlated the particle morphology obtained

from the encapsulation of an oil (decane or hexadecane) with methyl methacrylate via emulsion polymerization to the type of surfactant and initiator used.[44] This was further investigated by Chen *et al.*, who demonstrated that the predicted morphology for composite latexes, derived from a seed latex and a second-stage polymerization, are in good agreement with experimental data. They showed that the morphology of the final composite latex is dependent on the type of initiator and surfactant used and that during the course of polymerization the morphology changes with conversion.[45,46]

2.3.1 Encapsulation via miniemulsion polymerization

Sections 2.1 and 2.2 introduced emulsion- and miniemulsion polymerization and there it was shown that both these heterogeneous polymerization techniques offer advantages over homogeneous polymerization, such as a lower rate of termination, low viscosity medium and the continuous phase serves as an effective heat sink. Miniemulsion polymerization in addition, offers great advantages over conventional emulsion polymerization, mainly resulting from the difference in nucleation mechanism. It was highlighted that the predominant nucleation mechanism in miniemulsion polymerization is via droplet nucleation, and this gives easier access to advanced structures with improved properties, such as core-shell particles where a core compound (hydrophilic or hydrophobic) is encapsulated with a shell that is formed during polymerization. This kind of structure shows high homogeneity in composition, because the material to be encapsulated does not have to diffuse through the continuous phase as it is already present at the locus of polymerization. The type of composite particles (hybrid particles) that can be synthesized via miniemulsion polymerization are for example polymer-polymer hybrids, core-shell particles where the core material can be chosen from a pigment, nematic liquid crystals (nematic LCs, where the core-material serves at the same time as the ultrahydrophobe),[24] drugs (potential for drug delivery),[47] inorganic particles such as Fe_3O_4 (magnetic nanoparticles),[32,48,49] yttrium oxysulphide (Y_2O_2S)[34] and TiO_2,[50] or a liquid, the last example also able to be transformed into nanocapsules by the evaporation of the liquid core after polymerization.[51-56] Crespy *et al.* recently reported on the synthesis of nanocapsules via interfacial polycondensation of an inverse miniemulsion and in this way prevented the use of a sacrificial core that otherwise would

have to be removed after polymerization to form hollow nanospheres.[57] They proved that this type of nanocapsules serve as a nanoreactor for the preparation of silver nanoparticles by reduction of silver nitrate solutions encapsulated during the polycondensation reaction.

The encapsulation of hydrophobic as well as hydrophilic compounds via miniemulsion polymerization is well documented in the literature. To achieve a successful encapsulation of such a compound via miniemulsion polymerization, two different interfaces, namely the core/polymer interface and the polymer/water interfaces have to be adjusted to obtain a state of lowest interfacial energy. This can be achieved via the appropriate use of two different surfactants, one surfactant stabilizing the core/polymer interface and the other surfactant stabilizing the polymer/water interface.[34,50] Prior to the miniemulsification process, the core component will be dispersed in the organic phase and stabilized with the aid of a surfactant, and then the organic phase is dispersed into the aqueous phase while being stabilized by a second surfactant. Generally, dependent on the size and the type of the compound to be encapsulated, low weight ratios of core-component (5–10% relative to monomer) can be encapsulated in a polymer particle.

The particle morphology is an interplay between thermodynamics, which determines the equilibrium particle morphology according to the minimum surface free energy, and kinetics that determines whether the equilibrium particle morphology can be obtained or the particles remain in a metastable (kinetically stable) morphology.[46,58,59] As the surface free energy is related to the surface tension between the phases, the chemical nature of the compounds has a big influence on the final particle morphology. The particle morphology of a three-phase system can be controlled by the addition of an appropriate compound (for example comonomer or a block copolymer) that reduces the interfacial tension between either the core/polymer interface or between the polymer/water interface.[59] An example is the encapsulation of hexadecane as a model compound with polystyrene. By the addition of methyl methacrylate or acrylic acid as a comonomer to the miniemulsion system, the interfacial tension between the polystyrene/water interface is drastically reduced and the particle morphology can be controlled.[52] Extra stability and

strength of miniemulsion particles can be accomplished by the introduction of inorganic nanoparticles. The extra stability provided by these inorganic nanoparticles, such as clay sheets, results from the fixation of the clay sheets onto the droplets (or particles) forming so-called 'armored latexes'.[60] The clay sheets are basically coated onto the surface of the droplets, applying high stability to the miniemulsion. Hollow shells can be obtained by removing the polymeric core of the particles after polymerization. The polymer itself thus actually serves as a template for the deposition and arrangement of the clay sheets. Because these inorganic-polymer hybrid particles provide high strength, this type of materials might be interesting for high performance applications, such as pressure sensitive adhesives.

2.3.2 Amphiphilic block copolymer micelles

Recently a renewed interest in precision polymer synthesis arose from the introduction of polymerization techniques via which the length and architecture can be controlled and via which amphiphilic block copolymers can be prepared that can self-assemble into block copolymer micelles in a selective solvent.[61,62] Among these techniques are the controlled radical polymerization techniques such as Nitroxide-Mediated Polymerization (NMP), Atom Transfer Radical Polymerization (ATRP) and Reversible Addition-Fragmentation chain Transfer (RAFT)-mediated polymerization and (catalytic) Ring-Opening Metathesis Polymerization (ROMP).[63-65] There is a great opportunity in terms of flexibility, diversity and functionality in the design of the polymeric building blocks.[66]

O'Reilly *et al.* wrote a brief review on block copolymers that spontaneously self-assemble into polymer micelles in a selective solvent.[67] This type of micelles forms an important class of materials, because a large variety of building blocks is at hand and the variety of functional groups present throughout the core and/or shell allows for stabilization via cross-linking chemistries. The additional covalent functionalization with compounds containing a wide range of functionalities leads to stabilized and selectively functionalized polymer micelles, tailoring these materials towards specific applications such as drug delivery vehicles.[68] They specifically dealt with the cross-linking and functionalization of either block and distinguished between:

- Shell cross-linking at the hydrophilic end
- Shell cross-linking along the hydrophilic polymer backbone
- Cross-linking at the hydrophilic-hydrophobic interface of the block copolymer
- Core cross-linking along the hydrophobic polymer backbone
- Core cross-linking at the hydrophobic end

Over the last decade numerous articles appeared on the synthesis of amphiphilic diblock copolymers via various (controlled) polymerization techniques. They either self-assemble into micelles upon dissolving in a selective solvent for one of the blocks or by incorporating thermo- or pH responsive blocks in the diblock copolymer and upon a variation in the pH or temperature self-assemble into micellar structures.[61,63,64,67,69-74] These micellar structures have shown to be preserved after cross-linking of either the core or the shell polymer via various chemistries. Bütün *et al.* reported on the synthesis of shell cross-linked block copolymer micelles with tunable hydrophilic/hydrophobic cores.[75] The core consisted of a temperature responsive *N*-(morpholino)ethyl methacrylate (MEMA) block that is hydrophilic at room temperature and hydrophobic above its lower critical solution temperature (LCST). By cross-linking of the (dimethylamino)ethyl methacrylate (DMAEMA) shell, the micellar structure is preserved upon cooling to room temperature. Apart from the temperature induced micelle formation, the block copolymer also shows electrolyte concentration dependent micelle formation. In the same fashion Liu *et al.* reported on the synthesis of thermoresponsive triblock copolymers that are cross-linked at the central block so that *inter*-micellar cross-linking was avoided and thus higher solid content could be used.[76] Qi *et al.* synthesized a poly(acrylic acid)-*b*-poly(methyl acrylate) block copolymer and used a biotin-functionalized ATRP-initiator.[77] Upon micelle formation and cross-linking of the shell, the biotin functionality was available at the surface of the shell cross-linked nanoparticles, albeit at a low concentration. A different approach involves the formation of shell cross-linked block copolymer micelles with the subsequent removal of a sacrificial block so that the micelles actually serve as a scaffold.[78] Another class of polymeric micelles is that of the polymeric micelles with aqueous core (PMACs) that basically comprises an inverse polymeric micelle containing a hydrophilic core and a

hydrophobic shell. It has been shown that in the aqueous core of these PMACs inorganic reactions are able to take place.[79]

2.3.3 Double Hydrophilic Block Copolymer micelles (DHBCs)

Recently the focus in the preparation of core- or shell cross-linked block copolymer micelles has shifted from amphiphilic di- or triblock copolymers to double hydrophilic block copolymers (DHBCs). The self-assembly of amphiphilic block copolymer micelles is usually accompanied with the introduction of a selective cosolvent to facilitate micelle formation. Also, the cross-linked core is water insoluble and in case the shell is being cross-linked, the necessary precautions have to be taken in order to prevent inter-micellar cross-linking. More importantly, the block copolymers do not show any stimuli responsiveness. Zhang *et al.* recently reported on the preparation of a stimuli-responsive, reversibly cross-linkable poly(ethylene oxide)-*b*-poly(*N*-isopropylacrylamide-*co*-*N*-acryloxysuccinimide) (PEO-*b*-P(NIPAM-*co*-NAS)) diblock copolymer employing RAFT polymerization as the living radical polymerization technique.[80] Starting from a PEO-based macro-chain transfer agent, they extended the PEO-based macroRAFT with a statistical copolymer containing the temperature responsive NIPAM and the cross-linkable NAS blocks. The reversible cross-linking of the NAS units was achieved by employing cystamine, which contains a primary amine functionality and a disulphide linkage which can easily be reduced to a thiol functionality. They showed that at room temperature the polymer is present as unimers in the aqueous phase and that upon heating above 40 °C the polymer self-assembles into micelles. By cross-linking the NAS units above the lower critical solution temperature (LCST) of the block copolymer, the micellar structure was preserved after cooling to room temperature. Swelling of the core was observed by cooling from above the LCST to room temperature and deswelling occurred by increasing the temperature again. The reversibility of the cross-linking was assessed via the reaction of the cystamine with dithiothreitol to disintegrate the micelles and subsequent reaction with cystamine restored the cross-linked micelles again. Jiang *et al.* used this same approach for the preparation of a diblock copolymer consisting of poly(*N*,*N'*-dimethylacrylamide)-*b*-poly(*N*-isopropylacrylamide-*co*-3-azidopropyl acryl-amide) (P(DMA-*b*-[NIPAM-*co*-AzPAM])), where the AzPAM represents a hydrophobic

monomer that contains an azide-functional group that can be cross-linked with a difunctional alkyne.[81] One of the main advantages of DHBCs over amphiphilic block copolymer micelles is that it contains a hydrophilic core, which makes these block copolymers suitable as potential containers in drug delivery applications. Liu *et al.* investigated the potential use of these DHBCs as containers for targeted drug delivery and controlled release by covalent binding of lysozyme to the DHBCs.[82] They employed ATRP with an initiator containing an aldehyde functionality and prepared a triblock copolymer consisting of oligo(ethylene glycol)methyl ether methacrylate, 2-(dimethylamino)ethyl methacrylate and 2-(diethylamino)ethyl methacrylate (POEGMA-*b*-PDMA-*b*-PDEA). The triblock copolymer is molecularly dissolved at acidic pH, but self-assembles into micelles at alkaline pH. By cross-linking the middle block at alkaline pH, they obtained shell cross-linked micelles which show reversible pH-responsive swelling/deswelling behavior. The surfaces of the micelles contain the aldehyde functionality from the ATRP-initiator, and they were able to form bioconjugates by covalently attaching lysozyme to the triblock copolymer. Narain and Armes synthesized various sugar containing methacrylate block copolymers (glycopolymers) via ATRP.[83] These di- and triblock copolymers showed either pH- or thermoresponsive behavior and well-defined micelles were formed. By the employment of an aldehyde-functional ATRP-initiator, they noted that by the availability of the aldehyde-functional group at the micelle periphery, these micelles should facilitate conjugation with biologically active motifs.

2.3.4 Encapsulation with styrene-maleic anhydride copolymers

Zhu *et al.* and Harrisson *et al.* both reported on the alternating copolymerization of styrene and maleic anhydride via RAFT-mediated polymerization.[84,85] They were able to prepare a block copolymer with one block consisting of alternating styrene and maleic anhydride copolymer and the other block of styrene homopolymer by just adding an excess of styrene monomer to the reaction formulation. Via hydrolysis of the maleic anhydride at high pH, these block copolymers self-assembled into uniform micelles with a diameter of 63 nm. Harrisson *et al.* additionally cross-linked the maleic anhydride units via amidation to retain the micellar morphology after lyophilization. Luo *et al.*

demonstrated the encapsulation of a highly hydrophobic material (that simultaneously acts as the ultrahydrophobe) via RAFT-mediated interfacial polymerization of styrene in miniemulsion.[55,56] They employed an oligomeric styrene-maleic anhydride RAFT-agent to circumvent the loss of control often observed in RAFT-mediated miniemulsion polymerization, which is believed to be mainly due to leaving group radical exit from the polymerization loci.[35,86] Furthermore, by converting the RAFT-agent into a macroRAFT-agent containing a styrene-maleic anhydride oligomer chain, they introduced amphiphilicity in the RAFT-agent that provides stability to the miniemulsion and thus acts as a surfactant and a controlling agent at the same time.

2.4 Encapsulation via the formation of microcapsules

One of the first polymers to be synthesized was a polymer known as bakelite, a highly cross-linked polymer that is formed by the reaction of formaldehyde and phenol, and the reaction is supposed to take place under acidic as well as basic conditions.[87]

Amino-aldehyde polymers are known as a class of materials with very good mechanical properties, and are therefore a material of choice for the micro-encapsulation of compounds that require impermeability and mechanical strength.[88] The *in-situ* polymerization of amino-formaldehyde proceeds via the formation of a pre-condensate, and the addition of modifiers that initially serve as emulsifier and later as initiator, enables the polymerization to develop at the surface of the emulsified oil droplet and not throughout the whole aqueous phase. Dietrich *et al.* gave a brief review on the use of amino resins as wall material for the production of microcapsules.[89] Amino resins were mentioned in the literature for the first time in 1908 and one of the most interesting developments is the utilization of amino resins as wall material for the micro-encapsulation of drugs, agrochemicals, adhesives and dyes. Generally a water soluble natural or synthetic polymer is added to the reaction formulation for the synthesis of microcapsules, and examples are styrene-maleic anhydride (SMA) copolymers, carboxy modified poly(vinyl alcohol), acrylic acid copolymers and carboxymethyl cellulose (CMC).[89] The functions of these water soluble polymers are:

- Emulsification of the hydrophobic material to be encapsulated
- Stabilizer for the emulsion
- Accelerator for the formation of the microcapsule walls
- Dispersing agent for the microcapsules

Xiao *et al.* reported on the formation of microcapsules induced via UV radiation.[90] They were able to encapsulate large amounts of core material (core content up to 71%) in microcapsules in the size range of 5–35 μm. The microcapsules are formed by solvent induced phase-separation of the wall-material, and the reaction was confined to the interface of the microcapsules.

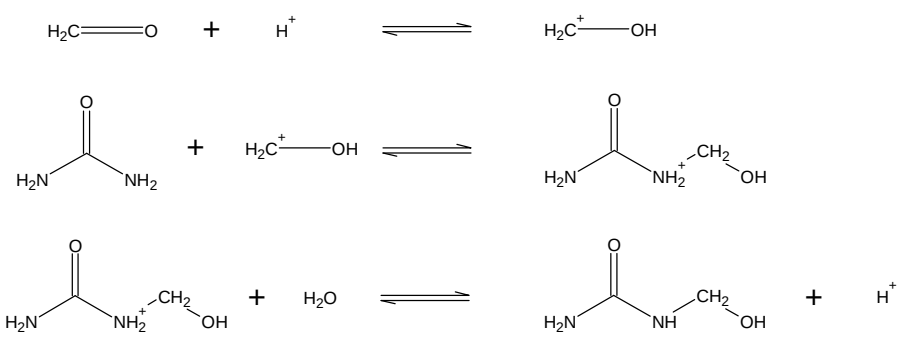

Urea-Formaldehyde reaction in acidic medium

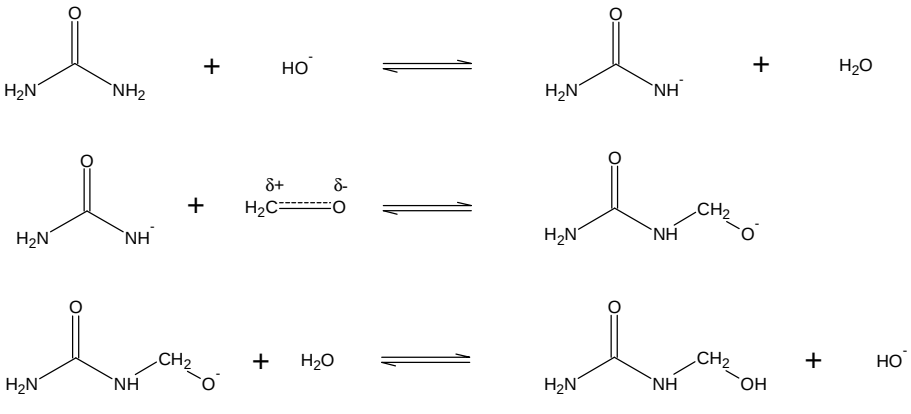

Urea-Formaldehyde reaction in alkaline medium

Scheme 2.4: The reaction of urea with formaldehyde to form monomethylol urea under either acidic or basic conditions.[89]

2.4.1 Urea-formaldehyde polymerization

The reaction between urea and formaldehyde is a two stage process. During the first step, which can take place under acidic as well as under basic conditions, urea reacts with formaldehyde which leads to the formation of a hydroxymethyl compound (Scheme 2.4).[91] Dependent on the molar ratio of urea and formaldehyde, up to three molecules of formaldehyde will be added to one molecule of urea (monomethylol, dimethylol and trimethylolurea).[92] The next step involves the polycondensation reactions between the various methylol species and urea to form low molecular weight urea-formaldehyde oligomers with the concomitant release of a molecule of water. At low pH the urea-formaldehyde oligomers link together to form an irreversible network consisting of methylene (-N-CH_2-N-) and dimethylene ether (-N-CH_2-O-CH_2-N-) linkages (Scheme 2.5).[92-94] The viscosity of the solution is related to the pH and increases sharply with decreasing pH.

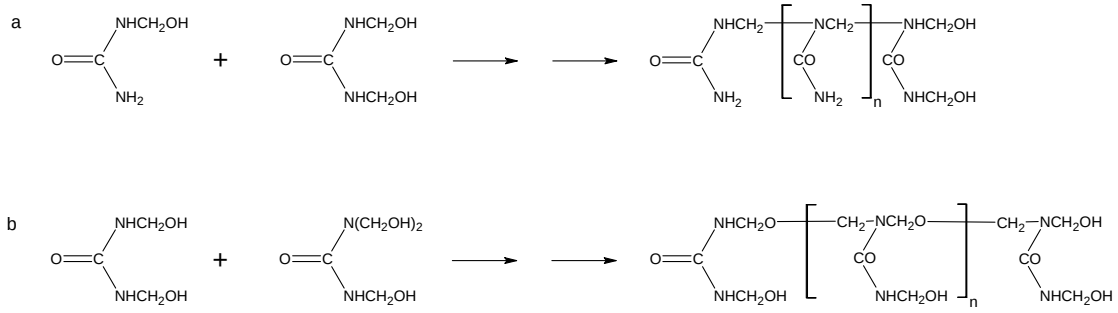

Scheme 2.5: The polycondensation reaction steps between urea and formaldehyde resulting in methylene linkages (a) and dimethylene ether linkages (b).

Brown *et al.* encapsulated dicyclopentadiene via *in-situ* polymerization of urea and formaldehyde.[95] They examined the surface morphology of the microcapsules and observed that a smooth inner membrane was formed with a thickness of 160–220 nm. During the course of the reaction urea-formaldehyde nanoparticles (~150 nm) deposit onto the microcapsule surface and this leads to a rough outer surface. The smooth inner membrane was composed of low molecular weight urea-formaldehyde pre-polymer that deposited onto the microcapsule surface while still being soluble. The nanocapsules were

composed of high molecular weight urea-formaldehyde particles formed in the aqueous phase that were not soluble anymore and consequently deposited and aggregated onto the microcapsule surface. The microcapsules that they prepared had a size range between 10 and 1000 μm, depending on the agitation rate. By controlling the pH during the reaction at a constant value and increasing the interfacial surface area between the core and aqueous phase by means of higher agitation rates and higher amounts of core-material, they were able to decrease the surface roughness of the microcapsules while maintaining high yield. Cosco *et al.* adopted the same procedure as described by Brown *et al.* to encapsulate an epoxy resin, a bisphenol-F-type epoxy resin in their case, via *in-situ* polymerization of urea and formaldehyde.[92,96] They specifically investigated the dependence of temperature and agitation rate on the size and morphology of the resultant microcapsules. They also found that at higher temperatures and agitation rate the microcapsules are composed of a smooth inner membrane with urea-formaldehyde nanoparticles deposited onto it. By decreasing the agitation rate and/or the temperature they obtained microcapsules characterized by a large amount of urea-formaldehyde nanoparticles. They believed that due to the lower agitation rate and temperature, the organic phase was not well dispersed in the aqueous medium and therefore the urea-formaldehyde polymerization took mainly place in the aqueous phase forming nanoparticles. The same results were obtained by Yuan *et al.*, who also investigated the influence of different reaction parameters on the formation of microcapsules via *in-situ* polymerization of urea and formaldehyde.[97]

2.5 Self-healing materials

The previous section dealt with the synthesis of microcapsules via urea-formaldehyde polymerization or interfacial polymerization induced via UV irradiation of epoxy, and a number of literature reports have been focusing on optimizing the structure and properties of the resulting microcapsules.[90,92,95-97] The microcapsules contained a reactive compound as the core material, either dicyclopentadiene or an epoxy resin, with the aim of introducing the microcapsules in an epoxy matrix which would serve then as an autonomic self-healing epoxy coating, without the need of external intervention to trigger the healing mechanism.[98] In order to develop an autonomic self-healing coating via the

introduction of microcapsules in a coating formulation, compatibility of the microcapsules with its environment has to be guaranteed. The microcapsules should be composed of a thin shell that does not rupture under processing conditions, so that the core component that provides the healing is not released prior to the formation of a crack. Only upon the formation of a propagating crack in the coating, the microcapsules have to rupture and release the core substance, applying stringent demands to the formulation of the wall material of the microcapsules. Another important aspect to consider is that while the crack is propagating through the material, the crack should be attracted to the microcapsules containing the self-healing agent, and not be deflected away from the microcapsules. White *et al.* developed microcapsules in the size range of 200 μm that consist of a urea-formaldehyde shell with dicyclopentadiene as the core material that acts as the self-healing agent, and embedded the microcapsules in an epoxy-coating.[99] As a healing mechanism they chose for the ring-opening metathesis polymerization (ROMP) of dicyclopentadiene, and to trigger the polymerization, they embedded a catalyst in the epoxy matrix. They found that upon the propagation of a crack through the epoxy matrix the microcapsules are ruptured and the healing reaction involving ROMP takes place. Fracture toughness experiments indicated that a 75% recovery of mechanical properties compared to the neat resin could be achieved, although optimizing the input variables (*i.e.* amount of catalyst and microcapsules, the size of the catalyst and microcapsules etc) could further improve the healing efficiency.[100] Yin *et al.* conducted the same approach as White *et al.* by encapsulating an epoxy via *in-situ* urea-formaldehyde polymerization and embedding a trigger (hardener) into the epoxy matrix.[101] It must be emphasized though, that Yin *et al.* needed to expose their samples to elevated temperatures for the curing of the released epoxy, which means that they needed external intervention to facilitate healing. Their results show good mechanical properties of the healed coating compared to the neat resin, and by employing a certain ratio of healing agent to hardener they even obtained a healing efficiency (based on the ratio of the fracture toughness of the original epoxy matrix to the fracture toughness of the healed epoxy matrix) of higher than 100%.

For the healing mechanism to be efficient and achievable, attention needs to be paid to the following points:

- The polymerization must be capable to proceed in an environment exposed to air/moisture
- The reactive components should be stored separately to avoid premature polymerization and also diffusion out of the capsules must be suppressed
- The viscosity of the reactants should be controlled to enable controlled diffusion to the reaction sites
- The polymerization should be rapid and able to take place at room temperature
- The network that is formed upon polymerization should induce low shrinkage so that the amount of stress build into the network is minimal

Kumar *et al.* employed various methods to apply microcapsules composed of a urea-formaldehyde shell and a corrosion inhibiting- or self-healing compound in a commercial coating formulation onto a substrate.[102] They found that the coating containing the microcapsules improved protection of the substrate at the scribe against environmental influences compared to the control experiments without added microcapsules. However, this improved performance regarding substrate protection was at the expense of a slight deterioration in substrate adhesion. Also it was suggested that the larger microcapsules (60–150 μm in diameter) would outperform the smaller microcapsules (<50 μm in diameter), which was assumed to be related to the number of microcapsules that is ruptured by a propagating crack and the volume of healing agent that is subsequently released per unit volume.

One of the most important reasons for the introduction of self-healing components in a coating is the inhibition of corrosion of a metal substrate. The applied coating should provide sufficient protection to the metal substrate, but in case the protecting coating is damaged, the metal substrate is exposed to environmental influences. So far, the most effective solution to protect metal substrates from corrosion was the introduction of a chromate-species in the coating.[103] However, as hexavalent chromium-species are toxic and known to be responsible for several diseases such as DNA-damage and cancer, anti-

corrosive coatings containing Cr^{6+}-species have been banned in Europe since 2007.[104,105] Alternatives that have been investigated as a substitute for chromates include the incorporation of inorganic (phosphates, vanadates, borates, cerium, molybdenum compounds) or organic (phenylphosphonic acid, mercaptobenzothiazole, mercaptobenzo-imidazole, triazole) species that act as inhibitors in sol-gel chemistry based coating systems.[106] Following this approach, Aramaki reported on the treatment of zinc surfaces with cerium (Ce^{3+}) and silicate ($Si_2O_5^{2-}$) compounds.[107] No corrosion on the zinc surface occurred after applying a scratch to the coating and exposing the surface in a sodium chloride solution. Shchukin *et al.* studied the effect of the incorporation of nanoreservoirs containing benzotriazole inhibitor in a hybrid epoxy-functionalized ZrO_2/SiO_2 sol-gel coating on self-healing upon the introduction of an artificial defect.[104] It was found that the nanoreservoirs incorporated in the composite coating release the inhibitor upon the formation of a crack to heal the defects in the coating and provide active corrosion protection.

The above examples examined the feasibility of sol-gel chemistry based coatings on corrosion inhibition of metal substrates. The sol-gel process is based on the evolution of inorganic or hybrid colloidal particles (sol) followed by its gelation to form a continuous polymer network (gel). Commonly, metal-alkoxides are employed as precursors that undergo hydrolysis and condensation reactions to form the polymer sol. The suspension of colloidal sol particles can be gelled through continued condensation. Zheludkevich *et al.* briefly reviewed the application of sol-gel coatings for corrosion protection of metals and they divided the type of protective sol-gel coating into four classes:[105]

- Inorganic sol-gel
- Hybrid sol-gel
- Nanostructured sol-gel
- Hybrid sol-gel with corrosion inhibitors

Although the sol-gel coatings provide a dense barrier for corrosive agents, the coating alone is not sufficient to protect the metal substrate from corrosion. Since a coating

contains micropores, cracks and areas of low cross-link density, they provide a path for diffusion of corrosive species such as water, oxygen and chloride ions to the coating/metal interface. The hybrid sol-gel with corrosion inhibitors, therefore, represents an important class, because by the introduction of inhibitors into the sol-gel films, the corrosion protection of the metal surface can be improved significantly. As mentioned above, a wide variety of organic and inorganic compounds can be used for this purpose, and some of the most effective and environmentally friendly inhibitors are derived from cerium salts.

Sugama and Gawlik adopted a different approach. They introduced calcium-aluminate fillers into a poly(phenylenesulfide) coating applied on steel substrates and studied the self-repairing effect of the coating upon the formation of a microcrack by exposing the coating to a 200 °C environment.[108] The rapid growth of crystals under these conditions led to densely filled and sealed cracks and provided a corrosion-preventing barrier. Another approach reported in the literature to prevent corrosion of substrates is the application and incorporation of an anion-exchanger that can exchange nitrate-ions with chloride ions.[109]

Caruso *et al.* recently reported on solvent induced autonomic healing properties in epoxy materials.[110] They found that the more polar aprotic solvents work well as healing agents, but because of difficulties in the encapsulation of more polar compounds via *in-situ* urea-formaldehyde polymerization, they chose chlorobenzene as material to be encapsulated. Although the mechanism of solvent-induced healing is not clearly understood yet, one of the suggestions is that the encapsulated solvent upon release plasticizes the epoxy matrix and allows for diffusional motion and unreacted groups to be cured and cause further cross-linking.

Numerous methods can be applied to introduce self-healing properties into a coating formulation. Dependent on the application of the coating and consequently the conditions to which the coating is exposed, a wide variety of compounds can be introduced in the coating formulation and serve as the healing agent. Whether the healing reaction takes

place via ring-opening metathesis polymerization, free-radical polymerization or oxidation reactions with corrosion inhibiting inorganic compounds, and whether the polymerization is triggered via a catalyst or UV radiation, is dependent on the healing compounds introduced and the specific application of the coating. Here we examine the feasibility of thiol-ene chemistry as healing mechanism and UV radiation as the initiating source. The next section provides an introduction into thiol-ene chemistry and shows the advantages of thiol-ene curing systems over conventional (meth)acrylate curing systems.

2.6 Thiol-ene chemistry

This section deals with thiol-ene chemistry and shows some of the advantages that are offered with this type of chemistry over conventional (meth)acrylates based cross-linking chemistry. The majority of cross-linked coating formulations nowadays are based on the photopolymerization of (meth)acrylates. However, as will be seen throughout this section, the photopolymerization of thiol and ene compounds offer significant advantages over conventional (meth)acrylate formulations, such as:

- Photopolymerization without the addition of an external initiator
- Thiol-ene photopolymerizations are not inhibited by the presence of oxygen
- Because thiol-ene chemistry proceeds via a step-growth mechanism, the gel-point is reached at high functional group conversions
- As a consequence, the networks formed are highly uniform and the stress-induced shrinkage is much lower than in conventional (meth)acrylate systems

In 2004 Hoyle *et al.* presented a detailed review on thiol-ene chemistry and highlighted the influence of the type of thiol and ene that can be used and the reaction conditions that can be employed (use of initiator, type of atmosphere) on the rate of the reaction.[111] Thiol-ene chemistry proceeds via a step-growth free-radical polymerization process and includes two main reactions, a propagation step and a chain transfer step, that are outlined in Scheme 2.6. It can be observed that by the employment of a difunctional ene and a difunctional thiol a linear polymer chain is obtained. By the employment of a thiol-ene pair with average functionality of greater than two, a polymer network is formed.

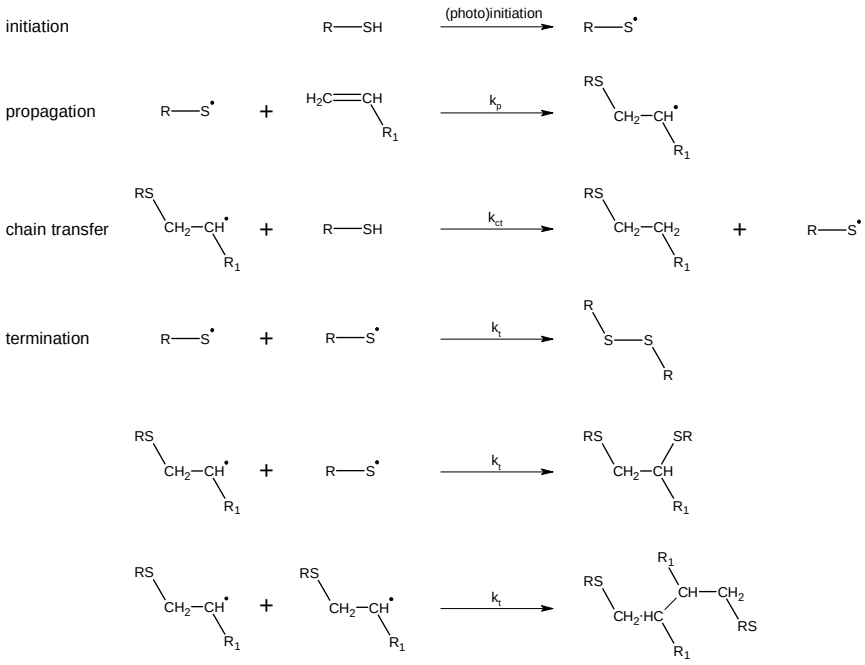

Scheme 2.6: The reactions involved in thiol-ene chemistry.

During the initiation step a proton is abstracted from a thiol-functional compound and creates a thiyl-radical. One of the advantages of thiol-ene chemistry is that the reaction can take place at room temperature under the influence of ultraviolet (UV) radiation. Initiation can then be accomplished via the addition of a photoinitiator; however, the addition of a photoinitiator is not a prerequisite, as the UV radiation is able to cleave the sulfur-hydrogen bond of the thiol. In case the thiol-ene reaction takes place at elevated temperatures, the addition of a thermal initiator will provide the generation of free radicals. The thiyl-radical thus formed reacts with the ene double-bond, the propagation step, and forms a carbon-centered radical. This carbon-centered radical abstracts a hydrogen atom from a thiol, the chain transfer step, with the subsequent formation of a thiyl-radical. Because thiol-ene chemistry involves a free-radical polymerization process, the species involved are capable of undergoing bimolecular termination reactions.[112] One important feature of thiol-ene chemistry is its significant insensitivity to the presence of oxygen.[111] Unlike conventional free-radical polymerization that is highly sensitive to oxygen and rates are drastically reduced in its presence, thiol-ene free-radical polymerization does not suffer from such a drawback. Scheme 2.7 shows the proposed

mechanism of oxygen incorporation into the thiol-ene network forming a peroxy-radical that after proton-abstraction from a thiol is transformed in a β-hydroperoxysulfide. This compound subsequently rearranges into a β-hydroxysulfoxide. Thiol-ene reactions can thus in principle be carried out in direct sunlight without the addition of a photoinitiator. Although the rates of reaction achieved are not as high as when carried out under a nitrogen atmosphere, acceptable rates are achieved. The rate of reaction can be adapted by the introduction of a photoinitiator or by the employment of an ene containing an electron-rich carbon-carbon double bond.

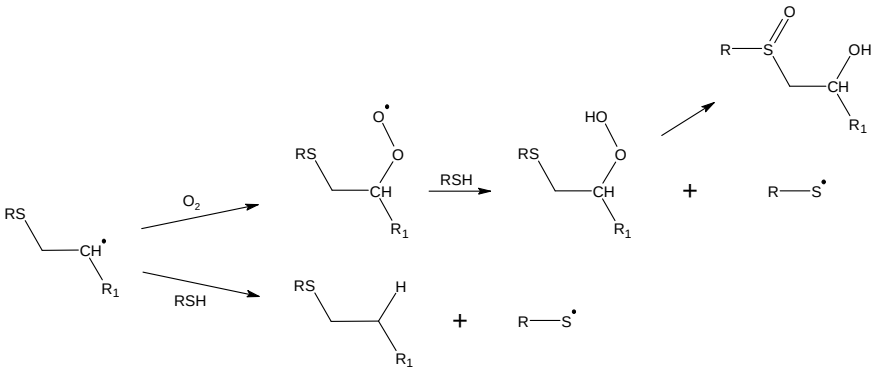

Scheme 2.7: Incorporation of oxygen into the thiol-ene network.

In classical thiol-ene chemistry vinyl monomers are employed that do not homopolymerize. However, if in a binary system an ene is adopted that does homopolymerize, an extra step is inserted in the thiol-ene mechanism depicted in Scheme 2.6 that accounts for the propagation step of the carbon-centered radical with a monomer unit.[113,114] Currently there is an increased interest in thiol-ene chemistry consisting of three compounds, a so-called ternary system.[115-118] In this case two types of ene-monomers are employed together with a thiol. One of the enes does not homopolymerize, whereas the other ene is susceptible to homopolymerization. Here, also the occurrence of cross-propagation and termination reactions between the vinyl monomers has to be taken into account. An interesting system in this regard is the thiol-ene radical polymerization of a multifunctional thiol with vinyl acrylate.[119] It is known that vinyl acrylate homopolymerizes through the acrylate double bond functionality and that the vinyl

double bond functionality is present as pendant side-groups on the acrylate backbone.[120] Only after most of the acrylate functionality has been consumed, is the vinyl functionality slowly consumed via homopolymerization. An additional point of interest is that vinyl acrylate readily polymerizes at room temperature via photoinitiation (without the addition of an external photoinitiator) in the presence of air, whereas the polymerization of common acrylates is inhibited by the presence of oxygen. The addition of a multifunctional thiol to vinyl acrylate drasically changes the kinetics of vinyl acrylate. It appears that two types of reactions take place simultaneously, *i.e.* the homopolymerization of the acrylate together with the copolymerization of the thiol and vinyl-functionalities. The type of reaction that has preference over the other reactions is strongly dependent on the type of enes employed and the concentration of the monomers. One must keep in mind that electron-poor carbon-carbon double bonds are not as reactive towards thiyl-radical addition as electron-rich carbon-carbon double bonds. Also the stability of the carbon-centered radical thus formed, has an influence on the progress of the reaction. The ratio of the propagating rate constant to the chain transfer rate constant ($\frac{k_p}{k_{ct}}$) is an important parameter to consider. The addition of a third component to a binary system in thiol-ene chemistry provides new ways to control the evolution of a cross-linked network and this leads to the formation of films with new and desired physical and mechanical properties.[118]

Generally there is no restriction in the choice of enes that can be employed in thiol-ene chemistry. Although electron-rich- as well as electron-poor carbon-carbon double bonds can be used in thiol-ene free-radical polymerization, the electron-rich carbon-carbon double bond shows higher reactivity towards radical addition. Usually three types of thiol-compounds are used in thiol-ene chemistry, namely alkyl 3-mercaptopropionates, alkyl thioglycolates and alkanethiols. Scheme 2.8 shows a variety of thiol and ene structures that are commonly employed in thiol-ene free-radical polymerization. The reactivity of the ene decreases in the order:

Norbornene > Vinyl ether > Alkene > Vinyl ester > Allyl ether > Acrylate > Methacrylate > Styrene > Conjugated diene

The reactivity of the thiol decreases in the order:

Alkyl (3-mercaptopropionate) > Alkyl thioglycolate > Alkanethiol

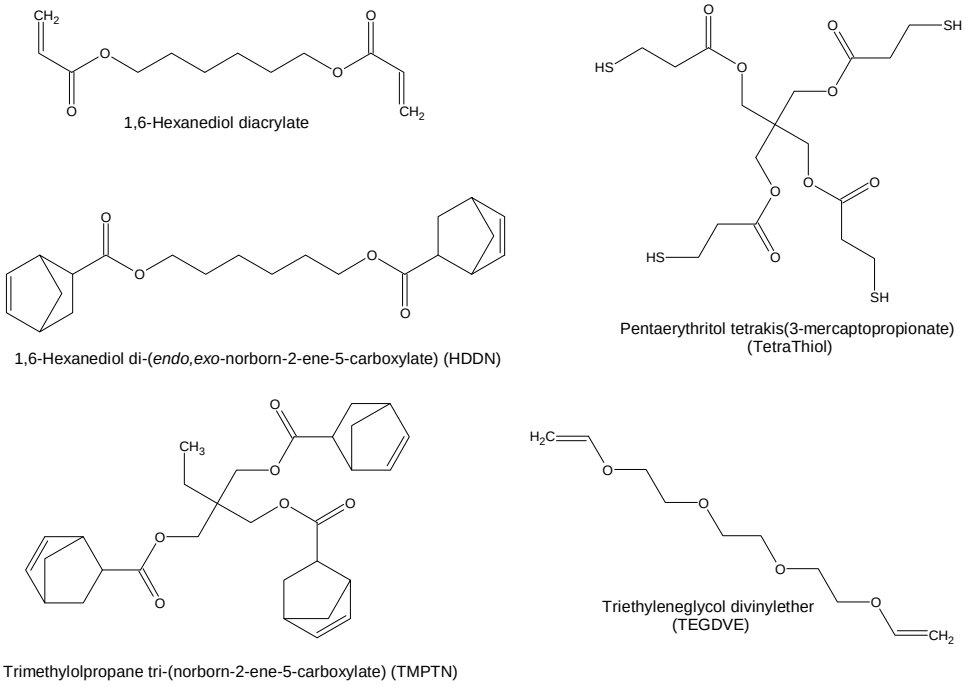

Scheme 2.8: Structures of various multifunctional thiol and ene compounds.

Roper *et al.* investigated the relationship between the structure of the alkene and the reactivity of the double bond.[121] Via model monofunctional alkene compounds they developed a theory for the reactivity of the carbon-carbon double bond and extended their results to multifunctional alkenes. They distinguished between a terminal and an internal double bond and concluded that the reactivity of the terminal double bond is much higher compared to the internal double bond. Also substituents on the carbon of a terminal alkene reduce the reactivity. Cyclic alkenes have been considered and the reactivity is determined by the ring-strain of the compound. Norbornene (bicyclo[2,2,1]hept-2-ene)

has received much attention in the literature because of its very high reactivity in thiol-ene chemistry. This high reactivity is a result from the release of ring-strain, the absence of any abstractable hydrogens and stereoelectronic affects. Furthermore, the ene-compounds containing an electron-rich carbon-carbon double bond are more reactive than the electron-poor carbon-carbon double bonds.[122] This is true for most of the enes available, but apart from norbornene, exceptions are methacrylate, styrene and conjugated dienes. Methacrylate, styrene and conjugated dienes form a rather stable carbon-centered radical upon the addition of a thiyl-radical, and it produces carbon-centered radicals that have low hydrogen-abstraction rate constants.

Because of the step-growth mechanism via which the thiol and ene react, during the initial stages of the polymerization only low molecular weight dimers, trimers, tetramers and so on are formed. This means that in thiol-ene polymerizations networks are formed at higher functional group conversions compared to conventional (multifunctional) acrylates and as a result there is a delayed onset of gel-formation, leading to less stress being built into the network. The thiol-ene network shows low shrinkage and forms a highly uniform cross-linked network and this results in excellent physical and mechanical properties. Because the variety in multifunctional thiol and ene compounds available is enormous, physical and mechanical properties can be tuned by the correct choice of network formers.[123] Also the inclusion of degradable sites in the network by the adoption of building blocks containing degradable functionalities allows the tailored design of the thiol-ene network with desired physical and mechanical properties.[123]

Recently Carioscia *et al.* investigated the influence of the norbornene backbone chemistry (aliphatic or aromatic) and functionality (di-, tri- or tetrafunctional) on the glass transition temperature (T_g) after photopolymerization with a tetrafunctional thiol at different conversions.[124] Norbornene monomers offer high rates of reaction and reach high conversion in thiol-ene polymerization, leading to high functional group conversion and a highly uniform cross-linked network. As the functional group conversion is high, leaching of unreacted monomer is limited and this also leads to improved mechanical properties. The uniformity of the cross-linked network is translated to the narrow T_g half-

height widths obtained from dynamic mechanical analysis. Li *et al.* also investigated the development of the glass transition temperature in thiol-ene chemistry.[125] They introduced thiourethane-based monomers for the photopolymerization with a trifunctional ene, and they developed films with high glass transition temperature. The high glass transition temperature was a result of the combination of the formation of hydrogen-bonds via the thiourethane groups and the rigidity of the trifunctional ene. Sangermano *et al.* introduced minimum amounts of a fluorinated allyl ether as a comonomer in the thiol-ene radical photopolymerization of multifunctional thiol and allyl ether to increase the hydrophobicity of the resulting network.[126]

Thiol-ene chemistry offers flexibility in terms of the variety of monomers available, reaction conditions that can be employed and properties of the resulting networks that can be attained. This makes thiol-ene chemistry an interesting candidate for utilization in advanced coating formulations that introduces apart from their protecting function an additional self-healing property. As described in Sections 2.3 and 2.4, several techniques are available via which well-defined, stable nano- and microcapsules can be synthesized. The separate encapsulation of thiol and ene compounds introduces a way to embed capsules containing a reactive load into an existing coating formulation. Ideally, upon the occurrence of a crack in the coating the capsules burst and release their monomers which subsequently react under the influence of UV radiation to restore the coating and protect the underlying substrate. Chapters 4 and 5 describe in detail the synthesis of such nano- and microcapsules respectively and in subsequent chapters attention will be paid to the incorporation of these capsules into an existing coating formulation.

References

1. A. Rudin, *The elements of polymer science and engineering*, Second edition, **1999**, ISBN 0-12-601685-2
2. W.D. Harkins, *J. Am. Chem. Soc.* **1947**, *69*, 1428-1444
3. I. Kühn and K. Tauer, *Macromolecules* **1995**, *28*, 8122-8128
4. P. Nazaran and K. Tauer, *Macromol. Symp.* **2007**, *259*, 264-273
5. K. Tauer, H.F. Hernández, S. Kozempel, O. Lazareva and P. Nazaran, *Macromol. Symp.* **2007**, *259*, 253-263
6. M.P. Merkel, V.L. Dimonie, M.S. El-Aasser and J.W. Vanderhoff, *J. Polym. Sci., Part A: Polym. Chem.* **1987**, *25*, 1219-1233
7. M. Antonietti and K. Landfester, *Prog. Polym. Sci.* **2002**, *27*, 689-757
8. J. Ugelstad, M.S. El-Aasser and J.W. Vanderhoff, *Polym. Lett. Ed.* **1973**, *11*, 503-513
9. D.P. Durbin, M.S. El-Aasser, G.W. Poehlein and J.W. Vanderhoff, *J. Appl. Polym. Sci.* **1979**, *24*, 703-707
10. Y.J. Chou, M.S. El-Aasser and J.W. Vanderhoff, *J. Dispersion Sci. Technol.* **1980**, *1*, (2), 129-150
11. J.M. Asua, *Prog. Polym. Sci.* **2002**, *27*, 1283-1346
12. C. Autran, J. de la Cal and J.M. Asua, *Macromolecules* **2007**, *40*, 6233-6238
13. S.S. Davis, H.P. Round and T.S. Purewal, *J. Colloid Interface Sci.* **1981**, *80*, 508-511
14. A.J. Webster and M.E. Cates, *Langmuir* **1998**, *14*, 2068-2079
15. J. Soma and K.D. Papadopoulos, *J. Colloid Interface Sci.* **1996**, *181*, 225-231
16. C.M. Miller, J. Venkatesan, C.A. Silebi, E.D. Sudol and M.S. El-Aasser, *J. Colloid Interface Sci.* **1994**, *162*, 11-18
17. K. Landfester, N. Bechthold, F. Tiarks and M. Antonietti, *Macromolecules* **1999**, *32*, 5222-5228
18. J. Jeng, C.-A. Dai, W.-Y. Chiu, C.-S. Chern, K.-F. Lin and P.-Y. Young, *J. Polym. Sci., Part A: Polym. Chem.* **2006**, *44*, 4603-4610
19. J.L. Reimers and F.J. Schork, *J. Appl. Polym. Sci.* **1996**, *60*, 251-262

20. C.C. Wang, N.S. Yu, C.Y. Chen and J.F. Kuo, *J. Appl. Polym. Sci.* **1996**, *60*, 493-501
21. D. Mouran, J. Reimers and F. Schork, *J. Polym. Sci., Part A: Polym. Chem.* **1996**, *34*, 1073-1081
22. G.R. Bardajee, C. Vancaeyzeele, J.C. Haley, A.Y. Li and M.A. Winnik, *Polymer* **2007**, *48*, 5839-5849
23. A.S. Kabalnov and E.D. Shchukin, *Adv. Colloid Interface Sci.* **1992**, *38*, 69-97
24. H.-D. Koh and J.-S. Lee, *Macromol. Rapid Commun.* **2007**, *28*, 315-321
25. J. Reimers and F.J. Schork, *J. Appl. Polym. Sci.* **1996**, *59*, 1833-1841
26. Z.-Q. Yu, D.-Y. Lee, I.-W. Cheong, J.-S. Shin, Y.-J. Park and J.-H. Kim, *J. Appl. Polym. Sci.* **2003**, *87*, 1933-1940
27. Z.-Q. Yu, D.-Y. Lee, I.-W. Cheong, J.-S. Shin, Y.-J. Park and J.-H. Kim, *J. Appl. Polym. Sci.* **2003**, *87*, 1941-1947
28. M.-S. Lim and H. Chen, *J. Polym. Sci., Part A: Polym. Chem.* **2000**, *38*, 1818-1827
29. P. Ni, M. Zhang, L. Ma and S. Fu, *Langmuir* **2006**, *22*, 6016-6023
30. Q. Meng, Z. Li, G. Li and X.X. Zhu, *Macromol. Rapid Commun.* **2007**, *28*, 1613-1618
31. S.B. Jhaveri, D. Koylu, D. Maschke and K.R. Carter, *J. Polym. Sci., Part A: Polym. Chem.* **2007**, *45*, 1575-1584
32. R. Faridi-Majidi, N. Sharifi-Sanjani and F. Agend, *Thin Solid Films* **2006**, *515*, 368-374
33. X. Huang, E.D. Sudol, V.L. Dimonie, C.D. Anderson and M.S. El-Aasser, *Macromolecules* **2006**, *39*, 6944-6950
34. H. Kim, E.S. Daniels, S. Li, V.K. Mokkapati and K. Kardos, *J. Polym. Sci., Part A: Polym. Chem.* **2007**, *45*, 1038-1054
35. M. Lansalot, T.P. Davis and J.P.A. Heuts, *Macromolecules* **2002**, *35*, 7582-7591
36. H. Matahwa, J.B. McLeary and R.D. Sanderson, *J. Polym. Sci., Part A: Polym. Chem.* **2006**, *44*, 427-442
37. A. Bowes, J.B. McLeary and R.D. Sanderson, *J. Polym. Sci., Part A: Polym. Chem.* **2007**, *45*, 588-604

38. R. Rodriguez, M.J. Barandiaran and J.M. Asua, *Macromolecules* **2007**, *40*, 5735-5742
39. S.J. Bohórquez and J.M. Asua, *J. Polym. Sci., Part A: Polym. Chem.* **2008**, *46*, 6407-6415
40. A. Guyot, F. Chu, M. Schneider, C. Graillat and T.F. McKenna, *Prog. Polym. Sci.* **2002**, *27*, 1573-1615
41. K. Ouzineb, C. Graillat and T.F. McKenna, *J. Appl. Polym. Sci.* **2005**, *97*, 745-752
42. S. Torza and S.G. Mason, *J. Colloid Interface Sci.* **1970**, *33*, 67-83
43. J.A. Waters, *Collloids Surf., A: Physiochem. Eng. Aspects* **1994**, *83*, 167-174
44. J. Berg, D. Sundberg and B. Kronberg, *J. Microencapsulation* **1989**, *6*, (3), 327-337
45. Y.-C. Chen, V. Dimonie and M.S. El-Aasser, *J. Appl. Polym. Sci.* **1991**, *42*, 1049-1063
46. Y.-C. Chen, V. Dimonie and M.S. El-Aasser, *J. Appl. Polym. Sci.* **1992**, *45*, 487-499
47. S.-J. Park and K.-S. Kim, *Colloids Surf., B: Biointerfaces* **2005**, *46*, 52-56
48. Y.-D. Luo, C.-A. Dai and W.-Y. Chiu, *J. Polym. Sci., Part A: Polym. Chem.* **2008**, *46*, 1014-1024
49. S. Yang, H. Liu and Z. Zhang, *J. Polym. Sci., Part A: Polym. Chem.* **2008**, *46*, 3900-3910
50. B. Erdem, E.D. Sudol, V.L. Dimonie and M.S. El-Aasser, *J. Polym. Sci., Part A: Polym. Chem.* **2000**, *38*, 4431-4440
51. Y. Chen, H. Liu, Z. Zhang and S. Wang, *Eur. Polym. J.* **2007**, *43*, 2848-2855
52. F. Tiarks, K. Landfester and M. Antonietti, *Langmuir* **2001**, *17*, 908-918
53. A.J.P. van Zyl, D. de Wet-Roos, R.D. Sanderson and B. Klumperman, *Eur. Polym. J.* **2004**, *40*, 2717-2725
54. C. Scott, D. Wu, C.-C. Ho and C.C. Co, *J. Am. Chem. Soc.* **2005**, *127*, 4160-4161
55. Y. Luo and H. Gu, *Macromol. Rapid Commun.* **2006**, *27*, 21-25
56. B. Klumperman, *Macromol. Chem. Phys.* **2006**, *207*, 861-863

57. D. Crespy, M. Stark, C. Hoffmann-Richter, U. Ziener and K. Landfester, *Macromolecules* **2007**, *40*, 3122-3135
58. V. Herrera, R. Pirri, J. R. Leiza and J.M. Asua, *Macromolecules* **2006**, *39*, 6969-6974
59. V. Herrera, R. Pirri, J.M. Asua and J.R. Leiza, *J. Polym. Sci., Part A: Polym. Chem.* **2007**, *45*, 2484-2493
60. B. zu Putlitz, K. Landfester, H. Fischer and M. Antonietti, *Adv. Mater.* **2001**, *13*, 500-503
61. S. Förster, V. Abetz and A.H.E. Müller, *Adv. Polym. Sci.* **2004**, *166*, 173-210
62. C.L. McCormick and A.B. Lowe, *Acc. Chem. Res.* **2004**, *37*, 312-325
63. L. He, E.S. Read, S.P. Armes and D.J. Adams, *Macromolecules* **2007**, *40*, 4429-4438
64. K. Stubenrauch, C. Moitzi, G. Fritz, O. Glatter, G. Trimmel and F. Stelzer, *Macromolecules* **2006**, *39*, 5865-5874
65. X. Tang, Y. Hu and C. Pan, *Polymer* **2007**, *48*, 6354-6365
66. C.J. Hawker and K.L. Wooley, *Science* **2005**, *309*, 1200-1205
67. R.K. O'Reilly, C.J. Hawker and K.L. Wooley, *Chem. Soc. Rev.* **2006**, *35*, 1068-1083
68. R.K. O'Reilly, M.J. Joralemon, C.J. Hawker and K.L. Wooley, *J. Polym. Sci., Part A: Polym. Chem.* **2006**, *44*, 5203-5217
69. C. Zheng, W.-D. He, W.-J. Liu, J. Li and J.-F. Li, *Macromol. Rapid Commun.* **2006**, *27*, 1229-1232
70. Y. Zhang, Z. Wang, Y. Wang, J. Zhao and C. Wu, *Polymer* **2007**, *48*, 5639-5645
71. V. Bütün, X.-S. Wang, M.V. de Paz Báñez, K.L. Robinson, N.C. Bilingham, S.P. Armes and Z. Tuzar, *Macromolecules* **2000**, *33*, 1-3
72. L. Houillot, C. Bui, M. Save, B. Charleux, C. Farcet, C. Moire, J.-A. Raust and I. Rodriguez, *Macromolecules* **2007**, *40*, 6500-6509
73. Y. Li, B.S. Lokitz and C.L. McCormick, *Macromolecules* **2006**, *39*, 81-89
74. D.S. Germack, S. Harrisson, G.O. Brown and K.L. Wooley, *J. Polym. Sci., Part A: Polym. Chem.* **2006**, *44*, 5218-5228

75. V. Bütün, N.C. Bilingham and S.P. Armes, *J. Am. Chem. Soc.* **1998**, *120*, 12135-12136
76. S. Liu and S.P. Armes, *J. Am. Chem. Soc.* **2001**, *123*, 9910-9911
77. K. Qi, Q. Ma, E.E. Remsen, C.G. Clark Jr. and K.L. Wooley, *J. Am. Chem. Soc.* **2004**, *126*, 6599-6607
78. C. Tang, K. Qi, K.L. Wooley, K. Matyjaszewski and T. Kowalewski, *Angew. Chem. Int. Ed.* **2004**, *43*, 2783-2787
79. F. Cheng, X. Yang, H. Peng, D. Chen and M. Jiang, *Macromolecules* **2007**, *40*, 8007-8014
80. J. Zhang, X. Jiang, Y. Zhang, Y. Li and S. Liu, *Macromolecules* **2007**, *40*, 9125-9132
81. X. Jiang, J. Zhang, Y. Zhou, J. Xu and S. Liu, *J. Polym. Sci., Part A: Polym. Chem.* **2008**, *46*, 860-871
82. H. Liu, X. Jiang, J. Fan, G. Wang and S. Liu, *Macromolecules* **2007**, *40*, 9074-9083
83. R. Narain and S.P. Armes, *Biomacromolecules* **2003**, *4*, 1746-1758
84. M.-Q. Zhu, L.-H. Wei, M. Li, L. Jiang, F.-S. Du, Z.-C. Li and F.-M. Li, *Chem. Commun.* **2001**, 365-366
85. S. Harrisson and K.L. Wooley, *Chem. Commun.* **2005**, 3259-3261
86. S.W. Prescott, M.J. Ballard, E. Rizzardo and R.G. Gilbert, *Macromolecules* **2002**, *35*, 5417-5425
87. T.W. Graham Solomons, *Organic chemistry*, sixth edition, **1996**, ISBN 0-471-01342-0
88. B. Boh, E. Knez and M. Staresinic, *J. Microencapsulation* **2005**, *22*, (7), 715-735
89. K. Dietrich, H. Herma, R. Nastke, E. Bonatz and W. Teige, *Acta Polym.* **1989**, *40*, (4), 243-251
90. D.S. Xiao, M.Z. Rong and M.Q. Zhang, *Polymer* **2007**, *48*, 4765-4776
91. B.R. Nair and D.J. Francis, *Polymer* **1983**, *24*, 626-630
92. S. Cosco, V. Ambrogi, P. Musto and C. Carfagna, *J. Appl. Polym. Sci.* **2007**, *105*, 1400-1411

93. Y.T. Wang, X.P. Zhao and D.W. Wang, *J. Microencapsulation* **2006**, *23*, (7), 762-768
94. S. Mehdiabadi, M.S. Nezhat and R. Bagheri, *J. Appl. Polym. Sci.* **1998**, *69*, 631-636
95. E.N. Brown, M.R. Kessler, N.R. Sottos and S.R. White, *J. Microencapsulation* **2003**, *20*, (6), 719-730
96. S. Cosco, V. Ambrogi, P. Musto and C. Carfagna, *Macromol. Symp.* **2006**, *234*, 184-192
97. L. Yuan, G. Liang, J. Xie, L. Li and J. Guo, *Polymer* **2006**, *47*, 5338-5349
98. C. Dry, *Composite Structures* **1996**, *35*, 263-269
99. S.R. White, N.R. Sottos, P.H. Geubelle, J.S. Moore, M.R. Kessler, S.R. Sriram, E.N. Brown and S. Viswanathan, *Nature* **2001**, *409*, 794-797
100. E.N. Brown, N.R. Sottos and S.R. White, *Exp. Mech.* **2002**, *42*, (4), 372-379
101. T. Yin, M.Z. Rong, M.Q. Zhang and G.C. Yang, *Compos. Sci. Tech.* **2007**, *67*, 201-212
102. A. Kumar, L.D. Stephenson and J.N. Murray, *Progr. Org. Coatings* **2006**, *55*, 244-253
103. J.H. Osborne, K.Y. Blohowiak, S.R Taylor, C. Hunter, G. Bierwagon, B. Carlson, D. Bernard and M.S. Donley, *Progr. Org. Coatings* **2001**, *41*, 217-225
104. D.G. Shchukin, M. Zheludkevich, K. Yasakau, S. Lamaka, M.G.S. Ferreira and H. Möhwald, *Adv. Mater.* **2006**, *18*, 1672-1678
105. M.L. Zheludkevich, I.M. Salvado and M.G.S. Ferreira, *J. Mater. Chem.* **2005**, *15*, 5099-5111
106. J.H. Osborne, *Progr. Org. Coatings* **2001**, *41*, 280-286
107. K. Aramaki, *Corros. Sci.* **2002**, *44*, 1375-1389
108. T. Sugama and K. Gawlik, *Mater. Lett.* **2003**, *57*, 4282-4290
109. H. Tatematsu and T. Sasaki, *Cem. Concr. Compos.* **2003**, *25*, 123-129
110. M.M. Caruso, D.A. Delafuente, V. Ho, N.R. Sottos, J.S. Moore and S.R. White, *Macromolecules* **2007**, *40*, 8830-8832
111. C.E. Hoyle, T.Y. Lee and T. Roper, *J. Polym. Sci., Part A: Polym. Chem.* **2004**, *42*, 5301-5338

112. S.K. Reddy, N.B. Cramer and C.N. Bowman, *Macromolecules* **2006**, *39*, 3673-3680

113. A.E. Rydholm, N.L. Held, C.N. Bowman and K.S. Anseth, *Macromolecules* **2006**, *39*, 7882-7888

114. N.B. Cramer and C.N. Bowman, *J. Polym. Sci., Part A: Polym. Chem.* **2001**, *39*, 3311-3319

115. T.Y. Lee, Z. Smith, S.K. Reddy, N.B. Cramer and C.N. Bowman, *Macromolecules* **2007**, *40*, 1466-1472

116. T.Y. Lee, J. Carioscia, Z. Smith and C.N. Bowman, *Macromolecules* **2007**, *40*, 1473-1479

117. S.K. Reddy, N.B. Cramer and C.N. Bowman, *Macromolecules* **2006**, *39*, 3681-3687

118. H. Wei, A.F. Senyurt, S. Jönsson and C.E. Hoyle, *J. Polym. Sci., Part A: Polym. Chem.* **2007**, *45*, 822-829

119. T.Y. Lee, T.M. Roper, E.S. Jönsson, C.A. Guymon and C.E. Hoyle, *Macromolecules* **2004**, *37*, 3606-3613

120. T.Y. Lee, T.M. Roper, E.S. Jönsson, I. Kudyakov, K. Viswanathan, C. Nason, C.A. Guymon and C.E. Hoyle, *Polymer* **2003**, *44*, 2859-2865

121. T.M. Roper, C.A. Guymon, E.S. Jönsson and C.E. Hoyle, *J. Polym. Sci., Part A: Polym. Chem.* **2004**, *42*, 6283-6298

122. N.B. Cramer, S.K. Reddy, A.K. O'Brien and C.N. Bowman, *Macromolecules* **2003**, *36*, 7964-7969

123. A.E. Rydholm, S.K. Reddy, K.S. Anseth and C.N. Bowman, *Polymer* **2007**, *48*, 4589-4600

124. J.A. Carioscia, L. Schneidewind, C. O'Brien, R. Ely, C. Feeser, N. Cramer and C.N. Bowman, *J. Polym. Sci., Part A: Polym. Chem.* **2007**, *45*, 5686-5696

125. Q. Li, H. Zhou, D.A. Wicks and C.E. Hoyle, *J. Polym. Sci., Part A: Polym. Chem.* **2007**, *45*, 5103-5111

126. M. Sangermano, R. Bongiovanni, G. Malucelli, A. Priola, A. Harden and N. Rehnberg, *J. Polym. Sci., Part A: Polym. Chem.* **2002**, *40*, 2583-2590

Chapter 3: Initialization behavior in RAFT-mediated (co)polymerization[a]

Abstract

This chapter gives an overview of the discussion that has arisen on induction and rate retardation phenomena often observed in Reversible Addition-Fragmentation chain Transfer (RAFT)-mediated polymerizations. These phenomena are particularly strong in dithiobenzoate-mediated (acrylate) polymerizations. Several plausible mechanisms have been suggested to explain these observations, such as the occurrence of an initialization period, reversible or irreversible termination of the RAFT intermediate radical, and slow fragmentation. This chapter gives further insight into the kinetics during the early stages of methyl acrylate (MA) polymerizations mediated by three different RAFT-agents (2-cyanoprop-2-yl dithiobenzoate (CIPDB), cumyl dithiobenzoate (CDB) and cumyl phenyl dithioacetate (CPDA)), and targeting three different molecular weights (11,000 g/mol, 30,000 g/mol and 70,000 g/mol). It appears that for each of these RAFT-mediated MA polymerizations an initialization period is observed during which the initial RAFT-agent is selectively converted into a first monomer adduct before further growth of the polymer chains takes place. In addition, two styrene-maleic anhydride (Sty-MAh) copolymerizations mediated by CIPDB and CDB were carried out via *in-situ* ^{1}H-NMR spectroscopy. A selective initialization period was observed during which one monomer unit was added to the initial RAFT-agent, before further growth of the polymer chains took place. Furthermore, the leaving group of the RAFT-agent preferentially added to one of the monomer units, which was governed by their electronic structure. The observation of a single monomer unit insertion into the polymer chain contradicts the charge-transfer-complex model (CTC) and is in favor of the penultimate unit (PU) model. The results reported in this chapter support the conclusion that the induction period observed in some RAFT-mediated polymerizations can be explained by the occurrence of an initialization period.

[a] This chapter is based on the publications:

- E.T.A. van den Dungen, H. Matahwa, J.B. McLeary, R.D. Sanderson and B. Klumperman, *J. Polym. Sci., Part A: Polym. Chem.* **2008**, *46*, 2500-2509
- E.T.A. van den Dungen, J. Rinquest, N.O. Pretorius, J.M. McKenzie, J.B. McLeary, R.D. Sanderson and B. Klumperman, *Aust. J. Chem.* **2006**, *59*, 742-748

3.1 RAFT-mediated polymerization[1-3]

The introduction of controlled/living radical polymerization (CRP) techniques over a decade ago has revolutionized the field of polymer chemistry. Among the CRP techniques available nowadays are Nitroxide-Mediated Polymerization (NMP),[4] Atom Transfer Radical Polymerization (ATRP)[5-9] and Reversible Addition-Fragmentation chain Transfer (RAFT)[10]-mediated polymerization. Among the CRP techniques that are available, RAFT-mediated polymerization has proven to be the most versatile one in terms of monomers to be polymerized and conditions employed.[11,12] A large number of monomers bearing various functional groups can be polymerized under a wide range of conditions, forming highly ordered and advanced architectures, such as di-, tri- or multiblock copolymers, star-shaped polymers, graft copolymers, etc.[13-21] RAFT-mediated polymerization shows compatibility with various solvents, but can also be conducted in aqueous[22] or heterogeneous media.[23-29] Furthermore, the polymerization can be carried out at ambient temperature via UV, solar or gamma radiation induced polymerization.[30-38] For the utilization of a successful RAFT-mediated polymerization the conditions under which the polymerization takes place must be correctly chosen and the RAFT-agent/monomer combination should be compatible under the given conditions (appropriate choice of R- and Z-groups).[39-41] It must be kept in mind that the RAFT-agent itself is susceptible to degradation via photolysis and in basic media to hydrolysis (and aminolysis).[22,31,42] The mechanism of RAFT-mediated polymerization is shown in Scheme 3.1. Apart from initiation, propagation and termination reactions, as encountered in conventional free-radical polymerization, RAFT-mediated polymerization includes two extra chain-transfer steps. These chain-transfer steps occur between an initiator derived radical or a propagating radical and the RAFT-agent during the pre-equilibrium (species 1 in Scheme 3.1). The RAFT-agent is a thiocarbonyl thio (Z-C(=S)-S-R) moiety that contains an activating group (Z) and a leaving group (R). The activating group should enhance the reactivity of the carbon–sulfur double bond towards radical addition of an incoming radical and the leaving group should readily fragment upon the formation of an intermediate radical (species 2 in Scheme 3.1) and reinitiate polymerization.[12] Radicals are generated in step 1 via the decomposition of an initiator, such as 2,2'-azobis(isobutyronitrile) (AIBN). Step 2 is the pre-equilibrium and represents a chain-

transfer step between a propagating radical and the initial RAFT-agent, and an intermediate radical is formed (species 2 in Scheme 3.1). The intermediate radical can fragment at either side, releasing either the incoming propagating radical or the leaving group radical. The leaving group is generally chosen to be a good homolytic fragmenting species with the capability of reinitiating the polymerization (step 3 in Scheme 3.1). During the pre-equilibrium, the initial RAFT-agent is thus converted into a macroRAFT-agent containing a dormant polymer chain (species 3 in Scheme 3.1). After fragmentation of the leaving group radical the active radical is capable of adding monomer units, and chain growth occurs. Step 4 in Scheme 3.1 is the main equilibrium of the RAFT process and involves the addition of a propagating chain to the macroRAFT-agent, forming an intermediate radical (species 4 in Scheme 3.1). This intermediate radical can fragment at either side, splitting off either the incoming propagating radical or a radical that was initially attached to the RAFT-agent (dormant chain). Because both polymer chains have equal chance of fragmentation, this equilibrium provides that all polymer chains have equal chance of growth and in this way polymer chains are formed with approximately the same size. As long as the addition rate constant of the propagating radical to the RAFT-agent is higher than the propagation rate constant of the monomer ($k_{add} > k_p$) control over the reaction will be achieved, resulting in a polymer with chains of approximately equal length, and thus a narrow molecular weight distribution is obtained. Because all polymer chains are initiated early in the reaction and grow throughout the reaction time, the molecular weight of the polymer increases linearly with conversion. In addition, by keeping the radical concentration low, that is, adopting a suitable RAFT-agent to initiator ratio, radical–radical termination is minimized and the fraction of 'dead' chains is reduced.

There are four common types of RAFT-agents and, dependent on the activating group, they are classified as follows:

- Dithioester, where Z is *e.g.* a phenyl or benzyl group (C_6H_5- or $C_6H_5CH_2$-)
- Trithiocarbonate, where Z is a thioalkoxy group (*e.g.* C_4H_9S- or $C_{12}H_{25}S$-)
- Xanthate, where Z is an alkoxy group (RO-)

- Carbamate, where Z is a tertiary amine group (R_1R_2N-)

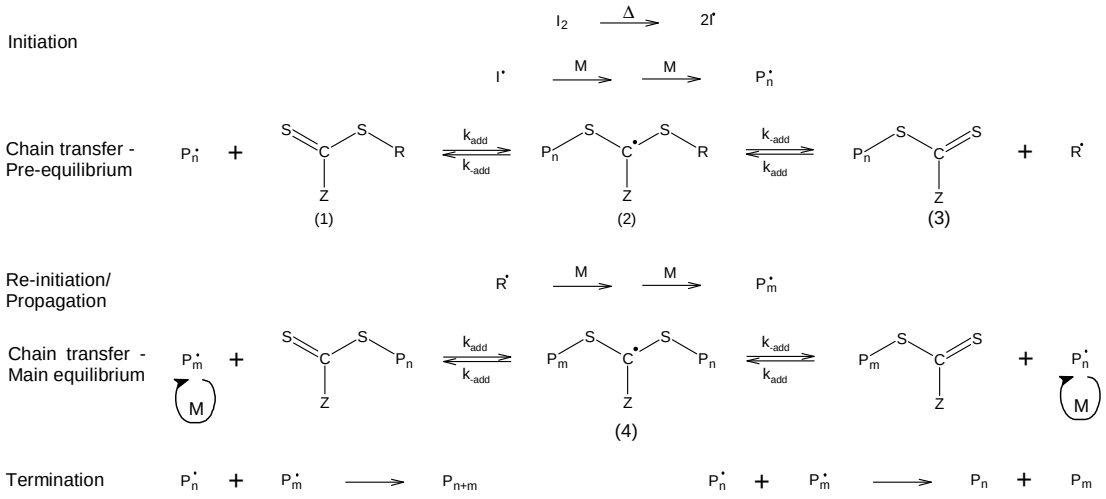

Scheme 3.1: The elementary steps in the RAFT process.

Common leaving groups employed in RAFT-mediated polymerization are cumyl, cyanoisopropyl, benzyl, 2-cyanopentanoic acid, etc, but the leaving group can be chosen from a much wider range of structures than the activating group, which allows for the incorporation of a number of different functional groups. As long as the fragmenting radical is a good homolytic leaving group and capable of reinitiating polymerization any structure can be adopted as the leaving group, provided that the functional groups are compatible with the polymerization conditions. The retention of the RAFT-agent on the majority of chains as an endgroup after polymerization allows for the synthesis of various advanced architectures, such as di- or triblock copolymers, graft copolymers and star-shaped polymers. Furthermore, if the RAFT-agent has a functional group incorporated in its structure, easy access to complex structures is achieved via post-polymerization (organic) reactions, such as telechelic polymers, polymer-bioconjugates, etc.[16,41,43-50]

Because (ideally) all the polymer chains contain one RAFT-moiety as an endgroup, the desired target molecular weight can be calculated using the following equation:

$$M_{n,th} = \frac{[M]_0 x}{[RAFT]_0 + (1+d) f [I]_0 (1-\exp[-k_d t])} \cdot MW_M + MW_{RAFT} \qquad \textit{equation 3-1}$$

where $M_{n,th}$ is the theoretical (target) molecular weight, $[M]_0$, $[RAFT]_0$ and $[I]_0$ are the initial monomer, RAFT-agent and initiator concentrations, respectively, x is the monomer conversion, d is the fraction of chains that terminate via disproportionation, f and k_d are the initiator efficiency and the rate of decomposition of the initiator, respectively, t is the polymerization time, and MW_M and MW_{RAFT} are the molecular weights of the monomer and RAFT-agent, respectively. Because RAFT-mediated polymerization generally provides good control over the reaction and the majority of chains contain the RAFT-agent as an endgroup, the number of chains that are formed via initiator-derived radicals is very low, and therefore the second term in the denominator of equation 3-1 is usually negligible.

It must be emphasized that in most cases the polymers synthesized via RAFT-mediated polymerization are intensely colored, and this might not be desirable from an industrial point of view. Moreover, volatile degradation products formed due to instability of the RAFT-endgroup are very odorous. Whatever reason one might have for doing so, it is highly desirable to be able to remove the RAFT-endgroup once the reaction has finished, and several techniques have been reported in the literature:[45]

- Reaction with nucleophiles (hydrolysis, aminolysis)[43,44,51]
- Radical induced termination[52]
- Radical induced reduction (tribuylstannane, *N*-ethylpiperidine hypophosphite)[53]
- Thermal elimination[54]
- UV radiation[20]

Although a number of procedures are available to remove the RAFT-endgroup, each of the techniques has a drawback. Aminolysis of RAFT-endcapped polystyrene leads to the formation of a disulfide linkage, whereas the removal of the RAFT-endgroup from a

poly(methyl methacrylate) chain results in intramolecular thiolactone formation.[51] The formation of a disulfide linkage can be suppressed by the addition of a reducing agent. Excess tributylstannane and derived byproducts are difficult to remove and remain as impurities in the final product. *N*-ethylpiperidine hypophosphite (EPHP) has proved to be a good alternative because the excess EPHP and its byproducts are water-soluble, although this proton-donor is not as effective as tributylstannane.[53] Thermolysis does not require any chemical treatment, but the polymer (and its functional groups) needs to be stable under the thermolysis conditions.

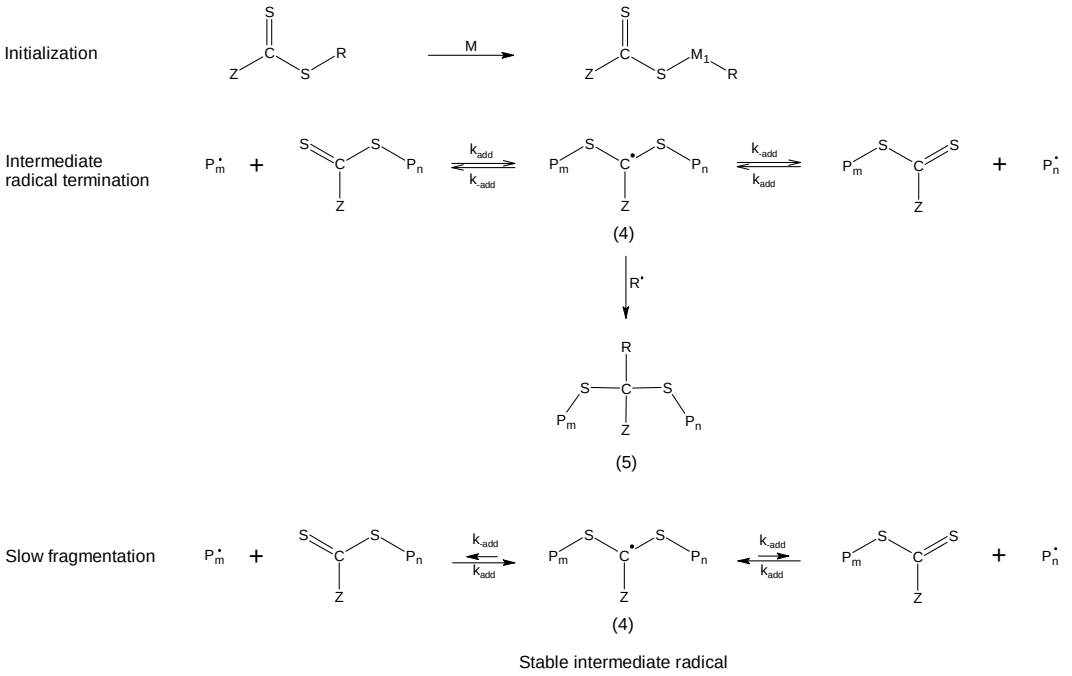

Scheme 3.2: Proposed mechanisms for induction and rate retardation in RAFT-mediated polymerization.

3.1.1 Kinetics in RAFT-mediated polymerization[55-57]

Along with the unraveling of the mechanism of RAFT-mediated polymerization a debate has arisen on induction period and rate retardation phenomena observed during the polymerization.[14,58] The induction period refers to the phenomenon that the start of the polymerization is delayed, that is, no conversion is observed at all. Rate retardation on the other hand is the reduction in the rate of polymerization compared to a conventional

free-radical polymerization where no RAFT-agent is employed. The occurrence of these observations is particularly strong in RAFT-polymerizations mediated by dithiobenzoate-moieties.[59] Although no theory exists currently that satisfies all, several plausible mechanisms have been proposed:

- Initialization period
- Intermediate radical termination, either reversible or irreversible
- Slow fragmentation

The term *initialization* was introduced by McLeary *et al.* in 2004 and refers to the very early stages of RAFT-mediated polymerization, where the initial RAFT-agent is highly selectively converted into a 'macroRAFT'-agent with one monomer unit inserted.[60-62] Via *in-situ* ^{1}H-NMR experiments they followed the consumption of the RAFT-agent and monomer, and the formation of the first and second monomer adducts. They noted that the RAFT-agent is first completely consumed before further growth of the polymer chains takes place. They explained their results by distinguishing between the addition rate constant of a leaving group radical to monomer and the propagation rate constant of the monomer. When a monomer with a high propagation rate constant is used, so that $k_p > k_{p,I}$ (where k_p is the propagation rate constant of the monomer and $k_{p,I}$ the addition rate constant of a leaving group radical to a monomer unit), and high molecular weight polymers are targeted, the monomer conversion during initialization remains very low (<1%), and this might mistakenly be interpreted as an inhibition period. The kinetics that were observed were rather attributed to this initialization period than to an inhibition period, because the RAFT-agent was converted into a macroRAFT-agent with a single monomer unit inserted, which for a fast propagating monomer might have the appearance of an inhibition period. The complete consumption of the RAFT-agent while only one monomer unit is being inserted before further growth of polymer chains takes place, is also observed in polymerizations aiming for higher target molecular weights and for RAFT-mediated copolymerizations as will be discussed in more detail in Section 3.3.[63-66] Drache and Schmidt-Naake analyzed the initialization period via size exclusion chromatography (SEC) and also derived transfer coefficients via the time-dependent

concentrations of the RAFT-agent and monomer.[67] It must be emphasized however, that this selective conversion of the RAFT-agent into a first monomer adduct is system dependent and that in some systems, such as methacrylates, different behavior is observed, where the RAFT-agent is consumed throughout the polymerization, dependent on the molecular weight targeted.[68] Also the choice of the RAFT-agent employed may result in different behavior, as observed by Li *et al.*[69] Although they did not focus on the fate of the RAFT-agent during the early stage of the polymerization they observed, via *in-situ* ^{1}H-NMR spectroscopy, that RAFT-agents bearing the same leaving group, but different stabilizing groups, have an equal period where hardly any conversion takes place, for all RAFT-agents employed, and this was attributed to the slow re-initiation of the leaving group radical. Guo observed via *in-situ* ^{1}H-NMR spectroscopy a selective conversion of a trithiocarbonate RAFT-agent, inserting one monomer unit, before a second monomer unit is added to the growing chain.[70]

Reversible or irreversible termination of the intermediate radical has been suggested as a cause of the induction and rate retardation phenomena observed during RAFT-mediated polymerization. By the involvement of the intermediate radical in termination reactions, radicals are removed from the system and this decreases the radical flux, automatically leading to a decrease in the rate of polymerization. Intermediate radical termination of the RAFT-agent has been observed in experiments aiming to detect intermediate radical termination products, but so far only limited evidence is available that intermediate radical termination does occur in a typical RAFT-mediated polymerization system.[38,71-73] Kwak *et al.* performed a structural investigation on the formation of three- and four-armed stars by using low molecular weight compounds as a model system for styrene.[74] They confirmed via ^{1}H-NMR, ^{13}C-NMR, MALDI-ToF-MS and elemental analysis the formation and structure of mainly three-armed star compounds formed from the reaction of the intermediate radical with an ATRP-derived initiator radical. They also investigated the kinetics of a polystyryl dithiobenzoate-mediated styrene polymerization by means of Electron Spin Resonance (ESR) spectroscopy and derived addition and fragmentation rate coefficients.[75,76] They calculated $k_{-add} = 7 \times 10^{4} s^{-1}$ and concluded that slow fragmentation could not be the cause of rate retardation. After heating polystyryl

dithiobenzoate in the presence of bromine-functionalized polystyrene they observed two distributions via SEC. Apart from the initial polystyrene distribution, they could ascribe the second distribution to the formation of three-arm stars via cross-termination of the intermediate radical with a polystyryl-radical. Venkatesh and coworkers adopted a similar approach as Kwak *et al.*: they used poly(butyl acrylate) instead of polystyrene, and were able to detect three- and four-arm star intermediate radical termination products via a combination of SEC and MALDI-ToF-MS analysis.[77] The above experiments clearly show that the intermediate radical is prone to attack from either a propagating radical (cross-termination) or from another intermediate radical (self-termination), forming a three- or four-arm star polymer respectively. It must be stated however that the experiments described by Kwak *et al.* and Venkatesh *et al.* were designed for the detection of intermediate radical termination products and that none of the intermediate radical termination products could be identified in a common RAFT-mediated polymerization. Detection of intermediate radical termination products would be a difficult task altogether since termination of the intermediate radical can take place throughout the polymerization, leading to a broad distribution in molecular weight and very low concentrations of the specific termination products, often below the detection limit of common analytical methods.

Bathfield *et al.* observed an additional rate retardation in their experiments, apart from the common rate retardation observed in some RAFT-mediated polymerizations. This could be attributed to intermediate radical termination, as detected by MALDI-ToF-MS.[78] This additional rate retardation was only observed for experiments aiming for low molecular weight polymers, and it was suggested that the intermediate radical termination is assumingly insufficient to explain the rate retardation phenomena occurring in RAFT-mediated polymerization. Favier *et al.* investigated *t*-butyl dithiobenzoate-mediated acrylamide polymerizations via MALDI-ToF-MS and suggested the occurrence of intermediate radical termination, although there was insufficient evidence to assign the peaks to an intermediate radical termination product.[79,80] Buback and Vana suggested that the intermediate radical that is involved in termination reactions undergoes a subsequent reaction with a propagating radical to form a dead polymer and the intermediate radical

itself.[81] Coote and coworkers adopted a different approach to derive addition- and fragmentation rate constants in RAFT-mediated polymerizations.[82-84] They used high level *ab initio* molecular orbital calculations, which is an independent method that is not influenced by model-dependent assumptions, and that makes use of direct calculations of the rates and equilibrium constants from first principles. However, accurate calculations on polymeric radicals are not possible, and in order to reduce computer time, small radicals are analyzed rather than polymeric radicals. They included chain-length dependence when determining the rate constants in their calculations and arrived at equilibrium constants ($K = \frac{k_{add}}{k_{-add}}$, where k_{add} is the rate constant of addition to the RAFT-agent and k_{-add} is the rate constant of fragmentation) of $>10^5 L \cdot mol^{-1}$ for the radicals investigated. From this they suggested that the rate of fragmentation is low, because the rate constant of addition to the RAFT-agent is generally accepted to be in the order of $10^5 - 10^6 L \cdot mol^{-1} \cdot s^{-1}$. The intermediate radical concentration according to ESR experiments is $<10^{-5} mol \cdot L^{-1}$,[58,75,85-87] depending on the system under investigation, which they interpreted as evidence for reversible termination of the intermediate radical.

The theory of slow fragmentation was proposed by Barner-Kowollik *et al.* Via Predici simulations, they estimated addition and fragmentation rate constants for cumyl phenyldithioacetate (CPDA)-mediated styrene and methyl methacrylate (MMA) polymerizations, and compared those to rate constants predicted for a cumyl dithiobenzoate (CDB)-mediated styrene polymerization.[88] For the CPDA-mediated styrene polymerization they did not observe any rate retardation when varying the RAFT-agent concentration as opposed to a CDB-mediated RAFT polymerization. They attributed this to the difference in the fragmentation rate coefficients between the two systems and the radical lifetime of the intermediate radical. For the CPDA-mediated MMA polymerization they observed a bimodal molecular weight distribution for reactions carried out at 60 °C and at low conversions. They believed that this was due to hybrid behavior of the polymerization, *i.e.* conventional chain transfer in combination with controlled radical polymerization via RAFT. Additional evidence for the theory of slow fragmentation during the pre-equilibrium was claimed via the investigation of

RAFT-mediated methyl acrylate polymerizations using dithiobenzoate RAFT-agents with varying leaving groups.[89] By comparing the relative stabilities of the RAFT-agents and the leaving group radicals with their kinetic data, they concluded that the stability of the intermediate radical is the likely cause of the induction period observed, although there was no direct experimental evidence to support this conclusion. Additional circumstantial evidence was obtained from modeling of kinetic data from a CDB-mediated styrene polymerization initiated via γ-radiation at 30 °C.[32] The experimental observation of a delayed onset of steady-state behavior could only be accurately fitted with the slow fragmentation model and not with the irreversible termination model. They concluded that the intermediate radical is a long-lived species (close to 2.5 seconds), which in turn could increase the likelihood of intermediate radical termination. After exposing samples to a γ-radiation source and implementing a waiting time before polymerizing the samples (at 60 °C for styrene or 80 °C for methyl acrylate (MA)) they observed that controlled polymerization took place.[33,37,90] This was explained by suggesting that stable intermediates are present, which are either radical or non-radical in nature. Calitz *et al.* also reported on the observation of intermediate radicals via ESR spectroscopy at 90 °C after 19 hours, a time when almost no initiator would be expected to remain.[85] They suggested that the presence of radicals in the virtual absence of initiator and their disappearance upon cooling implies very long-lived, non-radical species, which may act as a thermally activated radical source. In this way the (active) radicals would be protected from termination events, possibly via reversible reaction pathways. Barner-Kowollik *et al.* also carried out RAFT-mediated MA polymerizations using a retarding (CDB) and non-retarding (CPDA) RAFT-agent and analyzed the product stream using coupled SEC-ESI-MS.[91,92] Although they were able to assign peaks to (conventional) bimolecular termination products formed via combination and disproportionation, they were not able to detect any 3- or 4-arm star intermediate radical termination products. They realized however, that although these products were not detected via mass spectrometry (a highly sensitive technique) this does not prove their absence. They thought it to be more likely that reversible or irreversible intermediate radical termination events do not occur to a significant extent, and hence has a minor influence on the rate retardation phenomena observed in some RAFT-agent/monomer systems. Vana *et al.*

further investigated the kinetics of RAFT-mediated polymerizations during the pre- and main equilibrium via simulations with Predici to probe for conditions leading to induction, rate retardation and optimal living conditions.[93]

Much effort has been made to put the experimental data obtained into models. It must be emphasized however that the models used focus on specific conditions and/or reactions. This provides the possibility of fitting the kinetic experimental data into models. However, as there are still many unknown variables that can only be reasonably estimated, a number of models can be tuned to fit experimental data by the appropriate choice of such kinetic variables. Care has therefore to be taken in modeling RAFT-mediated polymerizations, because the two equilibria in which the RAFT-agent is involved are governed by the addition and fragmentation rate constants that are not experimentally determined yet, although reasonable estimates can be derived. Furthermore, it is important to distinguish between the pre- and main equilibrium of the RAFT-process, because it is likely that both equilibria are governed by largely different rate constants.[86,87,94] Buback *et al.* recently initiated a RAFT-mediated polymerization via a laser pulse and examined the formation and decay of the intermediate radical concentration via ESR spectroscopy.[87] Via modeling of the intermediate radical concentration versus time they derived values for the addition and fragmentation rate constants simultaneously.

Another study carried out by Plummer and coworkers focused on the purity of the RAFT-agent.[95] They polymerized 2-hydroxyethyl methacrylate (HEMA), styrene and MA using cumyl dithiobenzoate either purified via column chromatography or via preparative HPLC. The overall conclusion of their work was that impurities present in the RAFT-agent, such as dithiobenzoic acid, act to inhibit or retard the polymerization. Therefore caution has to be taken when trying to distinguish between models or simulating polymerizations, especially at the early stages of the polymerization. Hosseini Nejad and coworkers investigated the stability of the RAFT-agent for a dithiobenzoate-mediated polymerization of oligomeric methacrylate derivatives and detected dithiobenzoic acid as a degradation product.[96] Dithiobenzoic acid was also detected as a degradation product

when targeting for higher molecular weights, but the degradation occurred to a lesser extent.

There is no doubt that RAFT-mediated polymerization is a highly efficient way to prepare polymers of controlled structure, with the additional advantage of functionalization, either by incorporating a suitable functional group in the leaving group or via post-polymerization endgroup modification. The polymers synthesized via RAFT-mediated polymerization find widespread application. One of the applications is the formation of nanocapsules, either via miniemulsion polymerization or via the spontaneous self-assembly of block copolymers into micelles, as will be highlighted in Chapter 4.

This chapter focuses on the kinetics during the early stages of RAFT-mediated (co)polymerizations in an effort to elucidate the origin of induction phenomena reported for some dithiobenzoate-mediated polymerizations. Section 3.3 provides supporting evidence for the occurrence of an initialization period in RAFT-mediated polymerizations targeting various molecular weights (MWs) and in RAFT-mediated copolymerizations. Initially relatively high molecular weights are targeted using various dithioester RAFT-agents for the polymerization of MA. These experiments are complementary to the low target molecular weight initialization studies carried out by McLeary *et al.*,[60-62] where high RAFT-agent and initiator concentrations were employed. The study is extended with an investigation into the initialization behavior of RAFT-mediated styrene-maleic anhydride (Sty-MAh) copolymers using common dithioester RAFT-agents.

3.2 Experimental details

3.2.1 Chemicals

Methyl acrylate (Aldrich 99% (GC), [96-33-3]) was purified by passing it through a column of inhibitor remover (Aldrich, [9003-70-7]). Styrene (Plascon Research Centre, University of Stellenbosch, estimated purity ~99% by ^{1}H-NMR) was washed three times with an aqueous 0.3 M KOH solution to remove the inhibitor and subsequently distilled under reduced pressure. 2,2'-Azobis(isobutyronitrile) (AIBN, Riedel de Haën) was

recrystallized from ethanol and dried under vacuum. Benzene (R&S Enterprises), maleic anhydride (Acros organics 99%, [108-31-6]), 1,4-dioxane (Saarchem uniLAB 99%) and benzene-*d*6 (Acros organics, [1076-43-3]) were used as received.

The RAFT-agents that were used in this study are 2-cyanoprop-2-yl dithiobenzoate (CIPDB), cumyl dithiobenzoate (CDB) and cumyl phenyldithioacetate (CPDA), the structures of which are shown in Scheme 3.3. All three RAFT-agents were synthesized according to procedures available in the literature.[88,97,98] The purities of the RAFT-agents were determined via ^{1}H-NMR spectroscopy and were 96% for CIPDB, 99% for CDB and 99% for CPDA.

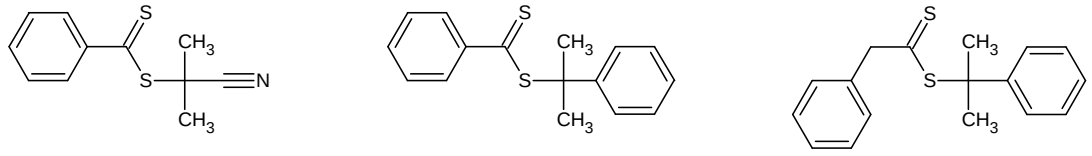

Scheme 3.3: Structures of the RAFT-agents used in this kinetic study.

3.2.2 RAFT-mediated methyl acrylate polymerizations

Solution polymerizations were carried out using MA, benzene and AIBN as monomer, solvent and initiator respectively, and three different RAFT-agents, namely CDB, CIPDB and CPDA. In a typical experiment a 250 mL three-neck round-bottom flask was charged with 47 g of MA (0.55 mol), 1.14 g of CDB (4.18×10^{-3} mol), 0.16 g of AIBN (0.97×10^{-3} mol) and 44 g of benzene. The concentrations of the various compounds used for all the experiments are tabulated in Table 3.1. A magnetic stirrer bar was placed in the three-neck round-bottom flask and the homogeneous solution was purged with nitrogen at room temperature for half an hour in order to remove the oxygen from the system. The polymerization was carried out at 70 °C and was run for about 6 hours. During the early stage of the experiment samples were taken for investigation of the initialization period via ^{1}H-NMR spectroscopy, and conversion was determined gravimetrically. Samples taken at later stages were subjected to SEC for molecular weight analysis.

Table 3.1: Formulation used for the RAFT-mediated MA polymerizations[a]

Exp	[MA] (mol/L)	[RAFT] (mol/L)	[AIBN] (mmol/L)	$M_{n,th}$ (g/mol)	Ratio RAFT/AIBN
1[b]	5.488	0.042	9.75	1.16×10^4	4.29
2[c]	5.488	0.042	9.77	1.15×10^4	4.28
3[d]	5.492	0.043	9.72	1.14×10^4	4.39
4[c]	5.494	0.016	3.72	3.00×10^4	4.27
5[c]	5.488	0.007	1.57	6.98×10^4	4.32

[a] The polymerizations were carried out at 70 °C in benzene

[b] RAFT-agent used is cumyl dithiobenzoate (CDB)

[c] RAFT-agent used is 2-cyanoprop-2-yl dithiobenzoate (CIPDB)

[d] RAFT-agent used is cumyl phenyldithioacetate (CPDA)

3.2.3 RAFT-mediated copolymerization of styrene and maleic anhydride

For a typical *in-situ* ^{1}H-NMR experiment 0.101 g of styrene (0.97×10^{-3} mol), 0.090 g of maleic anhydride (0.92×10^{-3} mol), 0.123 g of 1,4-dioxane (1.39×10^{-3} mol), 0.053 g of RAFT-agent (0.24×10^{-3} mol), 0.008 g of AIBN (0.05×10^{-3} mol) and 0.302 g of benzene-*d*6 (3.59×10^{-3} mol) were accurately weighed into a glass vial and homogenized. The solution was degassed in the NMR tube by purging with nitrogen. The experiment was conducted in a closed NMR tube and the cavity of the magnet was kept under a nitrogen flux to maintain an inert atmosphere. Table 3.2 shows the concentrations of the various compounds used for the copolymerizations carried out. The copolymerizations were carried out at either 60 or 70 °C and followed online via *in-situ* ^{1}H-NMR spectroscopy: a spectrum was recorded every minute over a period of about three hours.

Table 3.2: Formulation used for the RAFT-mediated Sty-MAh copolymerizations[a]

Exp	[Sty] (mol/L)	[MAh] (mol/L)	[RAFT] (mol/L)	[AIBN] (mol/L)	[Solv.] (mol/L)	$M_{n,th}$ (g/mol)	Ratio RAFT/AIBN
1[b]	1.773	1.672	0.436	0.088	2.542	1.02×10^3	4.93
2[c]	1.976	1.907	0.534	0.106	2.764	1.01×10^3	5.03

[a] The solutions (without benzene-*d*6) were first separately prepared and transferred to an NMR tube. Then benzene-*d*6 was added to the mixture. The concentrations given in the table are the final concentrations

[b] RAFT-agent used is CIPDB and the polymerization was carried out at 70 °C

[c] RAFT-agent used is CDB and the polymerization was carried out at 60 °C

3.2.4 Characterization

^{1}H-NMR spectra were recorded on a 600 MHz Varian Unity Inova spectrometer at room temperature in $CDCl_3$. A 5 mm inverse detection PFG probe was used for the experiments and ^{1}H-NMR spectra were acquired with a 3 μs (40°) pulse width and a 4 s acquisition time. Integration of spectra was carried out using ACD Labs 7.0 1D ^{1}H-NMR processor®. Equation 3-2 shows how the percentages of initial RAFT-agent $(n=0)$, first monomer adduct $(n=1)$ and second monomer adduct $(n=2)$ can be calculated:

$$AM_nD = \frac{I_{methyl,n}}{3I_{ortho}} \times 100\% \qquad \textit{equation 3-2}$$

AM_nD is the percentage of initial RAFT-agent $(n=0)$, first monomer adduct $(n=1)$ or second monomer adduct $(n=2)$. $I_{methyl,n}$ is the integral of the methyl protons of the leaving group for the three different species of interest and I_{ortho} is the integral of the ortho protons of the dithioester moiety, which serves as a reference for the total amount of dithioester species present.

The same instrument was used for the *in-situ* ^{1}H-NMR experiments. The probe temperature was calibrated using an ethylene glycol sample, in the manner suggested by the manufacturer, using the method of Van Geet.[99] ^{1}H-NMR spectra were acquired with a

3 μs (40°) pulse width and a 4 s acquisition time. For the *in-situ* ^{1}H-NMR kinetic experiments, samples were inserted into the magnet at 25 °C and the magnet fully shimmed on the sample. A reference spectrum was collected at 25 °C. The sample was then removed from the magnet and the cavity of the magnet was raised to the required temperature (60 °C or 70 °C). Once the magnet cavity had stabilized at the required temperature, the sample was re-inserted (time zero) and allowed to equilibrate. Additional shimming was carried out to fully optimize the system and the first spectra were recorded approximately 5 min after the sample was inserted into the magnet. For integration purposes, a sealed glass insert containing formic acid in benzene-*d*6 was inserted into the NMR tube and integration of the spectra was carried out using ACD Labs 7.0 1D ^{1}H-NMR processor®.

Molecular weight distributions were determined via size exclusion chromatography (SEC). The SEC instrument consisted of a Waters 717plus autosampler, Waters 600E system controller (run by Millennium^{32} V3.05 software) and a Waters 610 fluid unit. A Waters 410 differential refractometer was used at 35 °C in series with a Waters 2487 dual wavelength absorbance UV-Vis detector operating at 320 nm, the wavelength at which the thiocarbonyl thio moiety of the RAFT-agent shows intense absorption. Tetrahydrofuran (THF, HPLC-grade) sparged with IR-grade helium was used as eluent at a flow rate of 1 mL/min. The column oven was kept at 30 °C and the injection volume was 100 μL. Two PLgel 5 μm Mixed-C columns and a pre-column (PLgel 5 μm Guard) were used. Calibration was done using narrow polystyrene standards ranging from 800 to $2x10^{6}$ g/mol. All molecular weights are reported as polystyrene equivalents.

3.3 Results and discussion

3.3.1 Initialization behavior in RAFT-mediated methyl acrylate polymerization

This section focuses on high target molecular weight RAFT-mediated MA polymerizations using low RAFT-agent concentrations. In earlier work it was demonstrated that during the early stages of RAFT-mediated polymerization the RAFT-agent inserts one monomer unit before further growth of the chains takes place.[60,62] This was done under conditions aiming for low target molecular weight polymer and thus high

RAFT-agent concentrations were employed. Here high target molecular weight polymers are aimed to show the importance of the first step that takes place during RAFT-mediated polymerizations, *i.e.* an initialization period during which the initial RAFT-agent is converted into a macroRAFT species containing one monomer unit. Analysis of the early stages of polymerization was done via ^{1}H-NMR spectroscopy and the data were analyzed in a way similar to that used in earlier published work.[60,62]

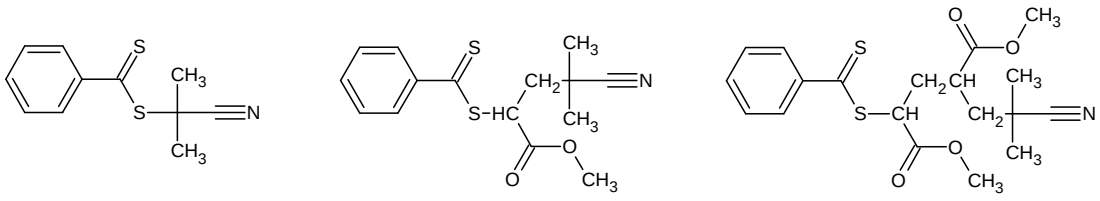

Scheme 3.4: The species of interest investigated via ^{1}H-NMR spectroscopy, formed during and shortly after initialization, in a CIPDB (AD)-mediated MA polymerization using AIBN as the initiator at 70 °C.

Scheme 3.4 shows the species of interest in a CIPDB (AD)-mediated MA polymerization. Note that for the first monomer adduct (AMD) a pair of enantiomers is formed and for the second monomer adduct (AM_2D) a pair of diastereomers, resulting in two peaks for the first monomer adduct (R and S) and four peaks for the second monomer adduct (RR, RS, SR and SS) in the ^{1}H-NMR spectra. The assignment for the CDB (CD)- and CPDA (CDtA)-mediated MA polymerizations proceeds in a similar way. The main focus was on the peaks belonging to the methyl protons of the leaving group, as these signals are well defined and intense. Figure 3.1 shows a trace of a ^{1}H-NMR spectrum in the region of the methyl protons of the leaving group for a CIPDB-mediated MA polymerization at 70 °C during the first 60 minutes of the polymerization. All signals are clearly identified, which was also done in previous work.[60,62]

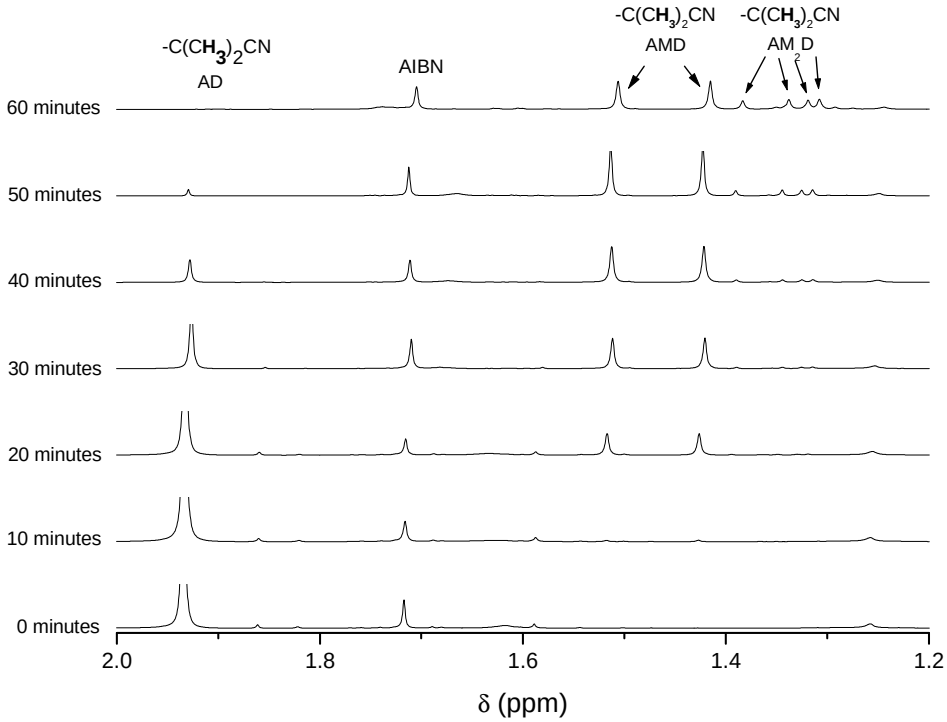

Figure 3.1: Typical ^{1}H-NMR spectra for a CIPDB-mediated MA polymerization at 70 °C with target molecular weight of 11,000 g/mol during the first 60 minutes of the polymerization. The region shown is that of the methyl protons of the leaving group. AD refers to the initial RAFT-agent (A represents the leaving group and D the dithiobenzoate moiety). AMD refers to the first monomer adduct and AM_2D to the second monomer adduct (M for one MA unit and M_2 for two MA units).

Figure 3.2 shows the conversion of the RAFT-agent versus time for three RAFT-mediated MA polymerizations at 70 °C with a target molecular weight of 11,000 g/mol. Each polymerization undergoes initialization, only after which the chains continue to grow. This means that the majority of chains only have one monomer unit inserted in the RAFT-agent during this period. Longer chains begin to form only after initialization is completed. It must be noted however, that beyond initialization the total amount of dithiobenzoates integrated is decreasing. Higher adducts are being formed that can not be resolved from the ^{1}H-NMR spectra. Furthermore, as can be deduced from Figure 3.2, at

the end of the initialization period, by which time almost all of the RAFT-agent has been consumed (and the maximum in the concentration of first monomer adduct is reached), it seems that already a considerable amount of the second monomer adduct has formed. However, at this stage higher adducts are being formed simultaneously, which gives a lot of overlap of signals in the NMR spectra, leading to an overestimation of the amount of second monomer adduct formed (this is particularly obvious for the CPDA-mediated MA polymerization).

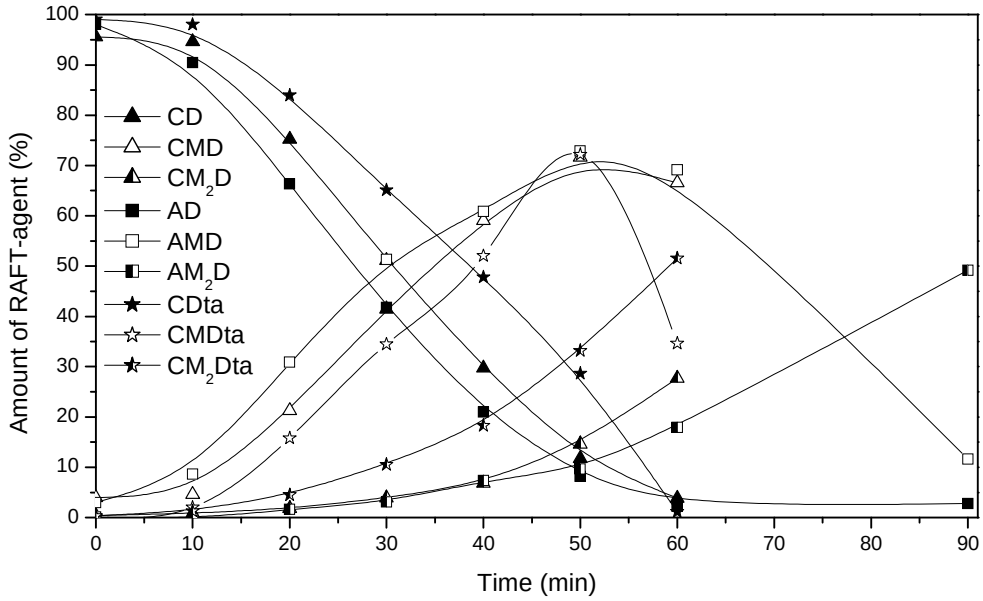

Figure 3.2: Percentage of the RAFT-agent present as specific species vs. time for three RAFT-mediated MA polymerizations with a target molecular weight of 11,000 g/mol at 70 °C using CDB (CD), CIPDB (AD) and CPDA (CDta) as the RAFT-agents (see Table 3.1, reactions 1–3). The figure shows the conversion of the initial RAFT-agent into its first (AMD) and second (AM_2D) monomer adducts (AD for the RAFT-endgroup and M for one and M_2 for two MA unit(s)).

As concluded from a previous study in which RAFT-agents with different stabilizing groups were used,[61] the pseudo zero-order kinetics during this initialization period implies that the rate-determining step is the addition of the leaving group radical to a

monomer unit. During initialization the amount of RAFT-agent that is present as first monomer adduct (AMD) reaches a maximum of approximately 70% (of the initial RAFT-agent concentration) for all three RAFT-mediated MA polymerizations with a target molecular weight of 11,000 g/mol, and only a small amount is present as a second monomer adduct at this stage. This means that for higher target molecular weight RAFT-mediated polymerizations (thus using low(er) RAFT-agent concentration) the conversion of the initial RAFT-agent into a macroRAFT-agent is still a critical step that governs the kinetics during the very early stage of the polymerization.

The initialization behavior of RAFT-agents with 2-cyanoprop-2-yl and cumyl radical leaving groups has been thoroughly investigated and described in literature.[60,62] It was deduced that, although both leaving group radicals are tertiary radicals whose addition rate coefficients are claimed to be similar,[100] the cumyl radical appears to have a higher termination rate coefficient than the 2-cyanoprop-2-yl radical. Thus, the steady-state radical concentration of a RAFT-mediated reaction in which a cumyl leaving group is used will be lower during initialization, which potentially leads to a longer initialization period, although the differences observed between the CIPDB- and CDB-mediated MA polymerizations described here were small. This apparent discrepancy is possibly related to the high concentrations used in previous studies. In CPDA-mediated MA polymerizations the leaving group radical is a cumyl group in the same fashion as cumyl dithiobenzoate, but the stabilizing group is different, that is, a benzyl compared to a phenyl group. The intermediate radical formed with CPDA does not have the enhanced stability due to conjugation in the manner of dithiobenzoate intermediate radicals. This explains the higher propagating radical concentration for the CPDA-mediated MA polymerization after initialization. The less stable intermediate radical is much more prone to fragmentation and will rapidly release an oligomeric radical that can continue to grow. It must be noted that for the experiments reported here a much lower RAFT-agent and initiator concentration (about 15x lower) are used than in the experiments reported previously.[61] These concentrations are also such that there is slightly more initiator present per RAFT-agent and the degree of polymerization targeted is more than an order of magnitude higher than discussed previously, both of which should decrease the

initialization time.[61] As the ratio of initiator to RAFT-agent and the degree of polymerization are not identical, direct comparisons are however difficult to draw. Once the RAFT-agent has been fully consumed, *i.e.* at the end of the initialization period when the RAFT-agent has been fully converted into predominantly the single monomer adduct of the original RAFT-agent, the polymer chain growth really starts to occur. This is shown in Figure 3.3, where the conversion versus time data is presented.

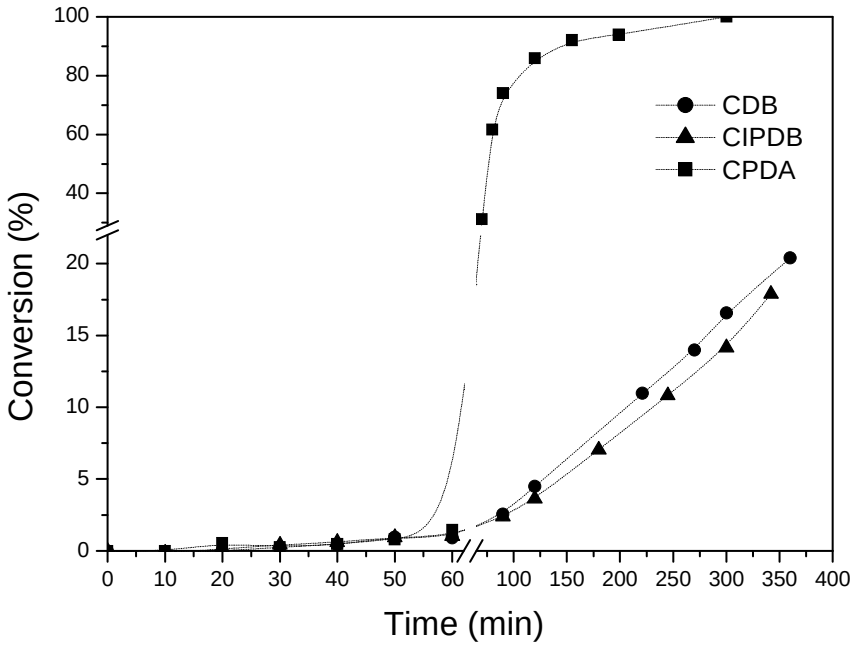

Figure 3.3: Conversion vs. time plot for CDB-, CIPDB- and CPDA-mediated MA polymerizations at 70 °C with target molecular weight of 11,000 g/mol (see Table 3.1, reactions 1–3).

Note that during the initialization period the conversion for all three polymerizations remains very low, as can be calculated from the conversion for one monomer unit insertion (conversion <1%). In the case of the CPDA RAFT-agent the rate of polymerization increases drastically. Similar behavior was also observed during an *in-situ* ^{1}H-NMR experiment for a CPDA-mediated MA polymerization.[61] On the other hand, the CIPDB- and CDB-mediated MA polymerizations proceed at a similar rate throughout the

reaction. It is expected that both polymerizations proceed at a similar rate after initialization, because the fragmenting radicals and stabilizing groups are the same in both experiments. As mentioned previously, the difference in behavior between CPDA-mediated MA polymerizations on the one hand and CDB- and CIPDB-mediated MA polymerizations on the other hand might be ascribed to differences in the intermediate radical stability.

Table 3.3: Molecular weight and polydispersity index data for the final samples of the RAFT-mediated MA polymerizations

Experiment	Conversion[a] (%)	$M_{n,th}$ [b] (g/mol)	M_n [c] (g/mol)	PDI[c] (-)
1[d]	22	2.8×10^3	2.4×10^3	1.12
2[e]	20	2.5×10^3	2.1×10^3	1.18
3[f]	~100[g]	1.1×10^4	9.7×10^3	1.26
4[e]	17	5.2×10^3	4.5×10^3	1.12
5[e]	23	1.6×10^4	1.4×10^4	1.21

[a] Conversion determined gravimetrically

[b] Theoretical molecular weight at the given conversion

[c] Molecular weight and molecular weight distribution as determined via SEC

[d] RAFT-agent used is CDB

[e] RAFT-agent used is CIPDB

[f] RAFT-agent used is CPDA

[g] Judged from SEC results that show a plateau in the M_n versus time

The addition rate constant of a leaving group radical to MA ($k_{p,I,MA}$) during initialization is much lower (for both cumyl and 2-cyanoprop-2-yl radicals) than the propagation rate constant of MA ($k_{p,MA}$). The observed induction period for some RAFT-mediated polymerization systems can rather be ascribed to this lower addition rate constant during initialization than to slow fragmentation of the intermediate radical. Hua *et al.*[38] recently came to the same conclusions for their RAFT-mediated polymerization system initiated via gamma radiation. After initialization the propagating radicals are identical in dithiobenzoate-mediated polymerizations and there should not be significant differences

between the rates of polymerization in CIPDB- and CDB-mediated MA polymerization once the polymerization has passed initialization.

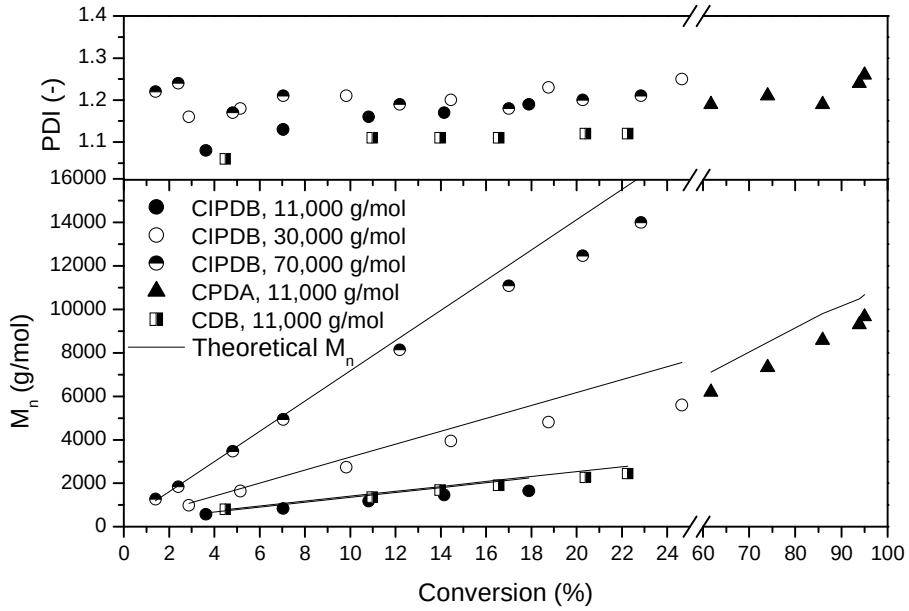

Figure 3.4: Development of the molecular weight and PDI vs. conversion for the RAFT-mediated MA polymerizations. The RAFT-agents used are CDB, CIPDB and CPDA and the molecular weights targeted were 11,000, 30,000 and 70,000 g/mol (see Table 3.1, reactions 1–5). The reaction temperature was 70 °C.

Figure 3.4 shows the molecular weight and polydispersity index development versus conversion for the RAFT-mediated MA polymerizations carried out and discussed in this section. As stated, the conversion of monomer for the CPDA-mediated MA polymerization increases rapidly after initialization has finished (not shown in Figure 3.4, but obvious from Figure 3.3). The final molecular weight is in good agreement with the theoretical value at 100% conversion. The final conversions, molecular weights and polydispersity index values of all RAFT-mediated MA polymerizations are shown in Table 3.3. As expected, all polymerizations show a linear increase in molecular weight vs. conversion and all molecular weight distributions remain very narrow.

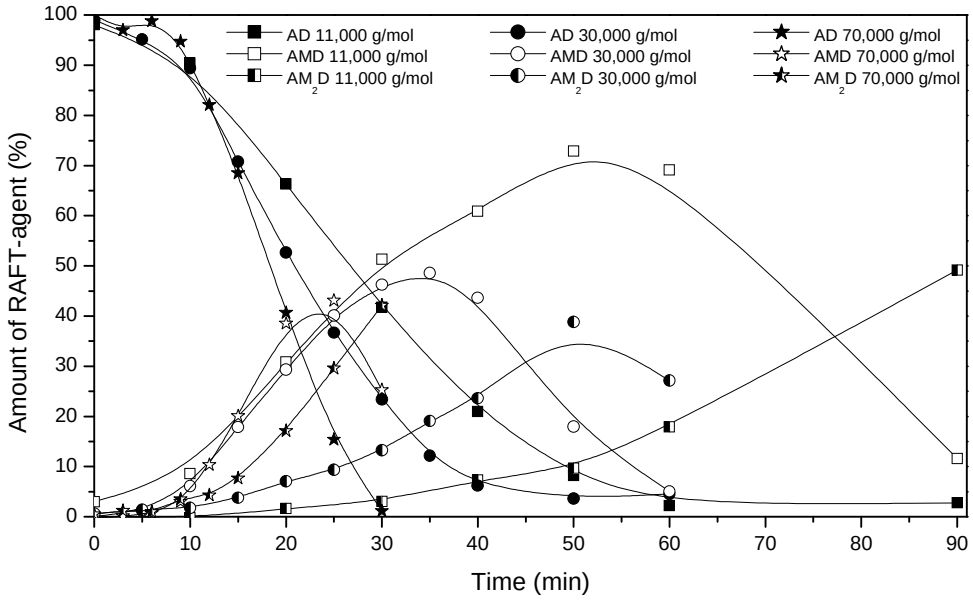

Figure 3.5: Percentage of the RAFT-agent present as specific species vs. time for three RAFT-mediated MA polymerizations with target molecular weights of 11,000, 30,000 and 70,000 g/mol at 70 °C using CIPDB (AD) as the RAFT-agent (see Table 3.1, reactions 2, 4 and 5). The figure shows the conversion of the initial RAFT-agent into its first (AMD) and second (AM_2D) monomer adducts (AD represents the RAFT-endgroup and M one MA unit and M_2 two MA units).

Figure 3.5 shows the consumption of the initial RAFT-agent along with the formation of the first and second monomer adducts for three CIPDB-mediated MA polymerizations targeting molecular weights of 11,000, 30,000 and 70,000 g/mol. As expected, from Figure 3.5 it can be observed that the higher the target molecular weight (lower RAFT-agent concentration), the shorter the initialization period. For the lower target molecular weight polymerizations (experiments 1–3) it was already shown that the selectivity (the amount of RAFT-agent converted to first monomer adduct before higher adducts are being formed) during the initialization period is high for all three experiments. One should expect, however, that for higher target molecular weight polymerizations the selectivity will decrease. The RAFT-agent and initiator concentrations (using the same RAFT-agent to initiator ratio) are lower and the system is diluted considerably. As the

concentration of RAFT-agent relative to monomer is decreased, the probability of adding multiple monomer units during initialization is increased, thus lowering the selectivity of the initialization process. Although the selectivity for the experiments with higher target molecular weight has been reduced, the CIPDB-mediated MA polymerization with target molecular weight of 70,000 g/mol still shows a maximum fraction of about 50% monoadduct.

Thus it becomes evident from the current experiments, for which RAFT-agents with different stabilizing and leaving groups have been used, that the conversion of RAFT-agent to a macroRAFT-agent containing one monomer unit is still a very important effect in determining the rate of polymerization during the early stages of the reaction. Since the chain length of the oligomers remains short and unimers predominate, the observed fractional conversion remains very low, especially for high target molecular weight polymerizations.

3.3.2 Initialization behavior in RAFT-mediated styrene-maleic anhydride copolymerization

The ^{1}H-NMR spectra obtained from the Sty-MAh copolymerizations were analyzed in a similar way to that of earlier published work and as described above.[60-62] The first monomer adduct of the reaction of CIPDB and styrene was identified via a detailed NMR study (Table 3.4).

During the analysis of the NMR spectra of the copolymerizations some interesting observations were made regarding the stereochemistry of the products formed, which are discussed briefly here. During a radical addition reaction, the carbon bearing the unpaired electron in the radical intermediate is sp^2 hybridized and the three substituent groups on the carbon lie in a plane. The added monomer has equal access to both sides of the plane, resulting in the equal formation of both R and S enantiomers. To understand the copolymerization of styrene and maleic anhydride it should be noted that styrene may homopolymerize while maleic anhydride does not. For this reason it is relevant to examine the behavior of styrene homopolymerization.

Table 3.4: Peak assignment and numbering of the atoms for the first monomer adduct of a CIPDB-mediated styrene homopolymerization

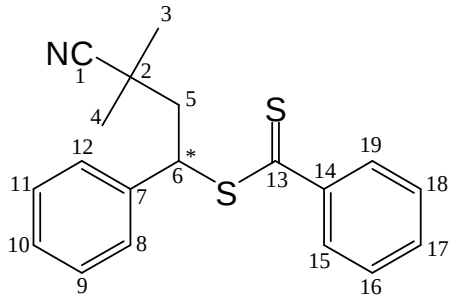

Position	δ_C [ppm]	δ_H [ppm] (^3J [Hz])
1	123.55	
2	31.49	
3/4	26.62 27.44	1.18 s 1.36 s
5	44.46	2.32 dd (9.9, 14.2) 2.39 dd (4.9, 14.2)
6	51.99	5.34 dd (4.9, 9.9)
7	138.29	
8/12	128.06	7.30 m
9/11	128.38	
10	128.23	
13	225.10	
14	144.28	
15/19	126.65	7.91 dd (1.2, 8.5)
16/18	128.69	7.43 m
17	132.29	

For the second monomer addition of styrene to a styrene unimer, a chiral centre already exists in the propagating radical and the addition of a second monomer results in the formation of a second chiral centre (after addition to the RAFT-agent) resulting in diastereomers. Unequal formation of R and S configurations occurs in the second centre, due to greater access on one side of the radical intermediate as a result of steric

constraints when adding to the RAFT-agent. Four stereo-combinations are now possible, being RR, SS, RS or SR. The RR and SS configurations are one enantiomer pair (R^*R^*), while the RS and SR configurations constitute another (R^*S^*). It should be noted at this point that NMR spectroscopy only allows one to distinguish between diastereomers but not between enantiomers (unless an auxillary reagent is used which was not feasible in this work due to the complexity of the systems). Thus the R^*R^* stereoisomers appear as one signal and the R^*S^* pair appear also as a single resonance though at a different chemical shift from the R^*R^* pair. In the ^{1}H-NMR spectrum of the second Sty-Sty monomer adduct the peaks exhibit a ratio of 45:55, indicating that stereoselectivity occurred during the addition reaction to the RAFT-agent. Bulk polystyrene is approximately P(m) = 0.46, *i.e.* an excess of syndiotacticity exists over isotacticity. Syndiotacticity implies that the relative configuration of the chiral centres alternate and that racemic dyads dominate. From 1D nuclear Overhauser effect (NOE) spectra it was possible to determine that R*R* configurations were preferred over R*S* implying that the stereochemistry was similar to bulk polystyrene as R*R* corresponds to a racemic dyad in the second monomer addition.

For the determination of the position of the methyl protons of the RAFT-agent for the first monomer adduct containing a MAh unit, either A-MAh-D or C-MAh-D (A and C represent the leaving groups 2-cyanoprop-2-yl and cumyl respectively and D represents the dithiobenzoate moiety), two *in-situ* ^{1}H-NMR experiments were conducted with MAh, CDB or CIPDB, AIBN and 1,4-dioxane in benzene-*d*6. From these experiments the structure, peaks and couplings of the first monomer adducts were determined. It was observed in these experiments that the first monomer adduct containing a MAh unit (A-MAh-D and C-MAh-D) contained only two peaks for the methyl groups instead of four as expected due to the two chiral carbon centres (since the methyl groups behave diastereotopically). With the addition of styrene to form the second monomer adduct four methyl peaks were observed. The stereochemistry of the second monomer adduct was more closely investigated for C-MAh-Sty-D. From 1D NOE spectra it was found that the CH protons of the maleic anhydride unit are anti for both the diastereomers that can be observed in the ^{1}H-NMR spectrum, thus also explaining the observations from the ^{1}H-

NMR spectra of the first monomer adducts A-MAh-D and C-MAh-D. The chiral centre formed with the addition of styrene can be either R or S and it was found that the $R^*R^*S^*$ diastereomer is marginally preferred with a ratio to the $S^*R^*S^*$ diastereomer being approximately 58:42. The assignment of the peaks in the ^{1}H-NMR spectrum due to the two diastereomers present was again achieved using selective 1D NOE experiments. Figure 3.6 shows selected NOE correlations observed for the diastereomer $R^*R^*S^*$ which made the assignment possible.

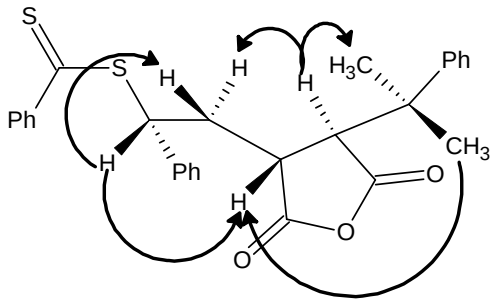

Figure 3.6: $R^*R^*S^*$ stereoisomer of the second monomer adduct C-MAh-Sty-D showing selected NOE interactions that were detected via 1D NOE spectra.

The peaks used for quantification of species in this study were predominantly the methyl peaks of the leaving group of the RAFT-agent (2-cyanoprop-2-yl or cumyl) for the initial RAFT-agent (AD/CD, A and C represent 2-cyanoprop-2-yl and cumyl respectively and D represents the dithiobenzoate-moiety), the first monomer adduct (AMD/CMD, M represents one monomer unit) and the second monomer adduct (AM_2D/CM_2D, M_2 represents two monomer units). The main focus of the study was to investigate the presence of an initialization period[60-62] for these copolymerizations together with the preference of the leaving group of the RAFT-agent to add to one of the monomers (styrene or maleic anhydride) during the initialization period. The peaks belonging to the monomers were also analyzed in order to calculate the conversion and examine the alternating behavior of the copolymerizations.

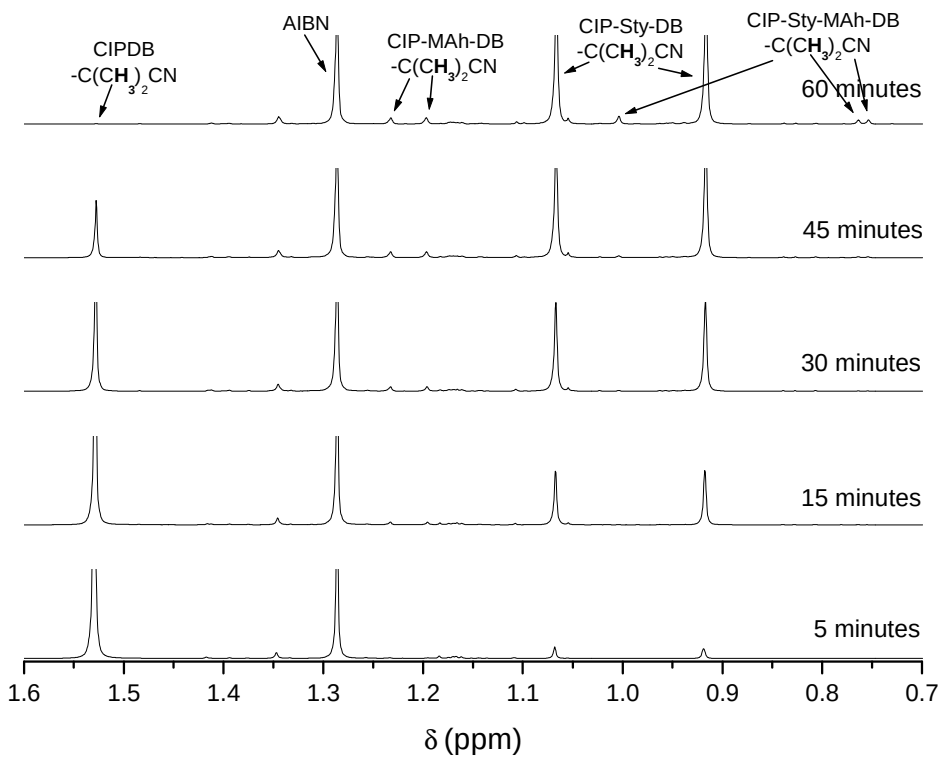

Figure 3.7: ^{1}H-NMR spectra of a CIPDB-mediated styrene-maleic anhydride copolymerization at 70 °C, enlarged at the methyl region of the leaving group of the RAFT-agent (δ = 0.7–1.6 ppm). The spectra have been taken after 5, 15, 30, 45 and 60 minutes and shown are the leaving group CIP, –C(CH$_3$)$_2$CN, the MAh-derived first monoadduct, CIP-MAh-DB, the styrene-derived first monoadduct, CIP-Sty-DB and the second monomer adduct derived from one styrene unit and one maleic anhydride unit, CIP-Sty-MAh-DB.

In Figures 3.7 and 3.8 spectra are shown obtained from *in-situ* ^{1}H-NMR experiments of CIPDB- and CDB-mediated Sty-MAh copolymerizations at 70 °C and 60 °C respectively. The expansion of the spectra in the methyl region of the leaving group shows that all relevant species can clearly be observed, *i.e.* the peaks of the leaving group of the RAFT-agent belonging to the initial RAFT-agent (AD or CD), the first (A-Sty-D, A-MAh-D or C-MAh-D) and the second (A-Sty-MAh-D or C-MAh-Sty-D) monomer adducts.

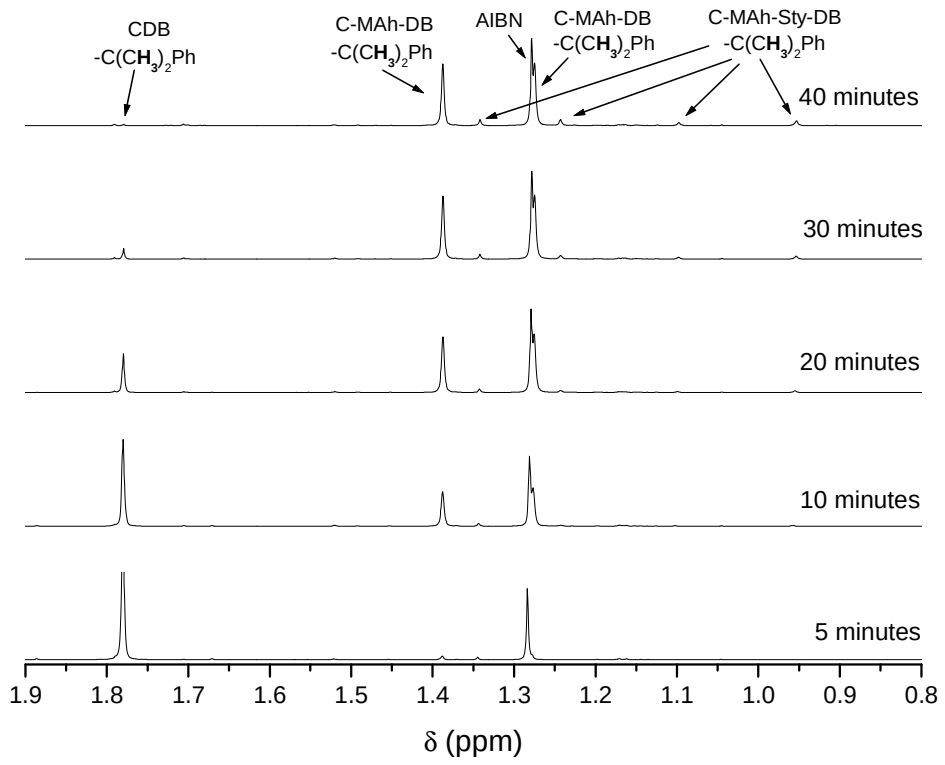

Figure 3.8: ^{1}H-NMR spectra of a CDB-mediated styrene-maleic anhydride copolymerization at 60 °C, enlarged at the methyl region of the leaving group of the RAFT-agent (δ = 0.8–1.9 ppm). The spectra have been taken after 5, 10, 20, 30 and 40 minutes and shown are the leaving group C, –C(CH$_3$)$_2$Ph, the MAh-derived first monoadduct, C-MAh-DB and the second monomer adduct derived from one maleic anhydride unit and one styrene unit, C-MAh-Sty-DB.

Figure 3.9 shows the consumption of the initial RAFT-agent and the formation of the first, second and third monomer adducts for a CIPDB-mediated Sty-MAh copolymerization at 70 °C, monitored via *in-situ* ^{1}H-NMR spectroscopy (Table 3.2, experiment 1). The initialization period can clearly be observed for the copolymerization of Sty and MAh, meaning that the RAFT-agent is highly selectively converted into a macroRAFT-agent, and that only one monomer unit is attached to this RAFT-agent during the initialization period.

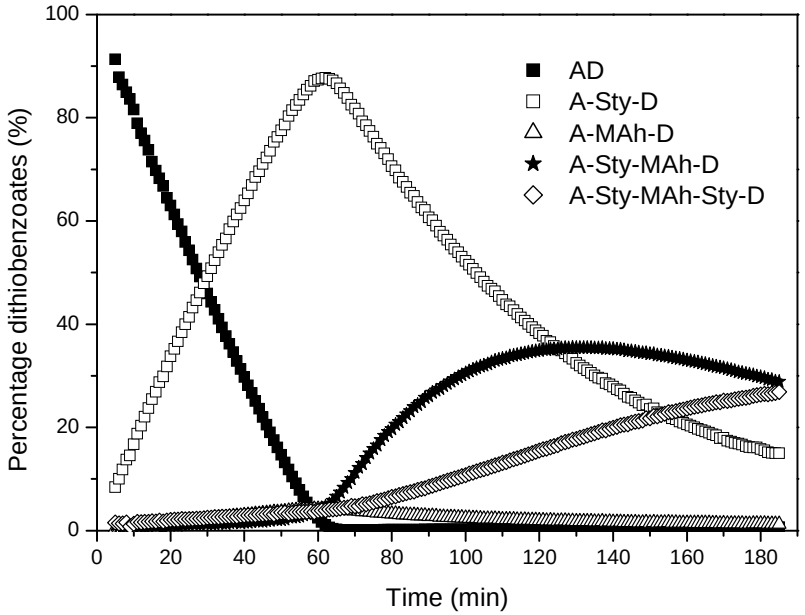

Figure 3.9: Conversion of the initial RAFT-agent and the formation of the first, second and third monomer adducts for a CIPDB-mediated Sty-MAh copolymerization at 70 °C. AD represents the initial RAFT-agent CIPDB, and A-Sty-D and A-MAh-D are the first monomer adducts in case of a styrene monomer unit and a maleic anhydride monomer unit addition respectively to the initial RAFT-agent. A-Sty-MAh-D and A-Sty-MAh-Sty-D are the second and third monomer unit adducts formed from a styrene-derived first monomer adduct.

As Figure 3.9 indicates, the majority of the RAFT-agent is converted into the styrene-derived monoadduct, and only a very small amount of the RAFT-agent is converted into the maleic anhydride-derived monoadduct. Therefore it can be deduced that for this copolymerization the addition rate of the leaving group to styrene is higher than the addition rate of the leaving group to maleic anhydride. The second monomer adduct, which is being formed in very low concentrations from early in the polymerization, consists entirely of one styrene and one MAh unit, as evidenced from ^{1}H-NMR analysis and conversion determination of both monomers. Only after the RAFT-agent has been initialized, does the concentration of the second monomer adduct start to increase

significantly. Furthermore, the third monomer adduct could be resolved from the spectra, consisting of an A-Sty-MAh-Sty-D sequence, as confirmed by 1D Total Correlation Spectroscopy (TOCSY) experiments. From this single experiment several conclusions can be drawn. First of all, Du *et al.* previously investigated the nature of the intermediate radical via ESR studies and concluded that the intermediate radical is derived from active MAh-terminal propagating radicals.[101] From this they suggested that the mechanism of propagation is via the charge-transfer-complex (CTC) model, although they were not able to detect the propagating radical itself. Although in their experiments they used benzyl dithiobenzoate (BDB) and for our experiment we used CIPDB, the effect of the leaving group should not change the nature of the propagation reaction from the CTC model to the penultimate unit model (PU). In the case of the CTC model operating, two monomer units add during one addition-fragmentation cycle, as the electron donor (Sty) and the electron acceptor (MAh) form a charge-transfer-complex. From the data obtained from the *in-situ* ^{1}H-NMR copolymerization, it is obvious that only one monomer unit is added to the growing chain during each addition-fragmentation cycle, which favors the penultimate unit model.[102,103] Du *et al.* based their findings on the appearance of the intermediate radical via ESR experiments, which indicated that the MAh unit was attached to the intermediate radical, suggesting that the propagating radical has a MAh terminal unit. Although only this type of intermediate radical could be observed, it is evident from the current experiment that chains with a styrene terminal unit can also be attached to the RAFT-agent moiety and thus will form a portion of the intermediate radical population in the reaction. The reason that no intermediate radicals formed by the addition of propagating chains with a Sty terminal unit could be observed via ESR studies can be attributed to the difference in the rate of fragmentation between a MAh leaving group and a Sty leaving group. The ESR spectroscopy experiment only allows easy observation of the intermediate radical species of highest concentration. Therefore, during the course of the polymerization, if the rate of fragmentation is substantially higher for a chain with a styrene terminal unit, only intermediate radicals formed by two chains with a MAh terminal unit will be observed via ESR. The intermediate radicals formed from a combination of chains that include a styrene terminal unit would have a much lower lifetime, and therefore a lower steady-state concentration.

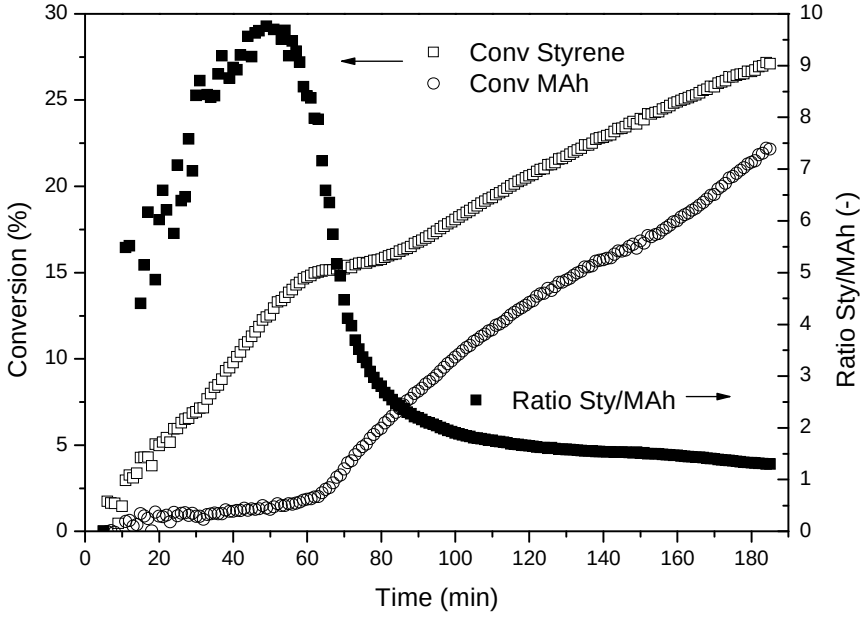

Figure 3.10: Conversion vs. time plot for a CIPDB-mediated Sty-MAh copolymerization at 70 °C. The ratio of Sty to MAh consumption is also plotted vs. time.

Figure 3.10 shows the monomer conversion for the CIPDB-mediated copolymerization of styrene and maleic anhydride (Table 3.2, experiment 1). During the initialization period, styrene monomer is preferentially consumed and only a very small amount of maleic anhydride is consumed. This is in agreement with Figure 3.9, which shows that the majority of the first monomer adduct consists of a styrene-derived monoadduct. Once the copolymerization has passed the initialization period, maleic anhydride is being consumed much more rapidly, confirming that a maleic anhydride unit is being added to the styrene-derived monoadduct. This is also in agreement with copolymer reactivity ratios given in the literature.[104] When Figures 3.9 and 3.10 are examined in more detail, it can be observed that styrene is being consumed much slower and maleic anhydride much faster up to the point that the formation of the second monomer adduct (consisting of one styrene and one maleic anhydride unit) reaches its maximum. After this point the third monomer adduct is being formed. After the second monomer adduct has been formed, the slopes of both the styrene and the maleic anhydride conversion vs. time become fairly

similar, which means that both monomers are being consumed at approximately the same rate. This, together with the copolymer reactivity ratios given in the literature,[104] implies that the Sty-MAh copolymerization proceeds in an alternating fashion leading to a well-defined structure. The ratio of the styrene and maleic anhydride consumption is also shown in Figure 3.10, which decreases from a maximum during the initialization period to a value close to unity after the initialization period, indicating that an alternating copolymer is being formed.

A second Sty-MAh copolymerization was carried out at 70 °C and followed by *in-situ* ^{1}H-NMR spectroscopy, using CDB instead of CIPDB as the RAFT-agent. Again the focus was on the initialization period of this copolymerization and the alternating behavior of the monomers in the copolymerization. It appeared that the rate of addition of the leaving group radical (cumyl radical) to maleic anhydride was so fast that by the time the first ^{1}H-NMR spectrum was obtained, the copolymerization had already proceeded past the initialization period. The two peaks belonging to the first monomer adduct C-MAh-D could be observed to decrease, indicating that the second monomer adduct C-MAh-Sty-D was already being formed. The increase in the mean rate of polymerization with an increase of the MAh content for a Sty-MAh copolymerization has been observed previously and, as the electronic structure of the cumyl radical is similar to that of styrene and it acts as an electron donor to MAh, the addition rate is expected to be at least similar to that of cross propagation in a Sty-MAh polymerization.[102,105,106] To achieve more resolution of the formation of oligomers the same experiment was repeated at 60 °C.

Figure 3.11 shows the consumption of CDB and the formation of the first (C-MAh-D) and second (C-MAh-Sty-D) monomer adducts for the CDB-mediated Sty-MAh copolymerization at 60 °C, as followed by *in-situ* ^{1}H-NMR spectroscopy (Table 3.2, experiment 2). An initialization period was observed for the CDB-mediated Sty-MAh copolymerization, which took about 40 minutes to complete. The first monomer adduct consists almost entirely of single MAh adducts, forming C-MAh-D, and no peaks were observed for a styrene addition to the initial RAFT-agent. From Figure 3.11 it can be seen that the addition rate of the cumyl leaving group to a MAh unit is much faster than to a

Sty unit. Close to the end of the initialization period, the formation of the second monomer adduct starts to increase in frequency, which consists entirely of a styrene unit that forms C-MAh-Sty-D. This can also be observed from Figure 3.12, which shows the conversion-time plot for a CDB-mediated Sty-MAh copolymerization.

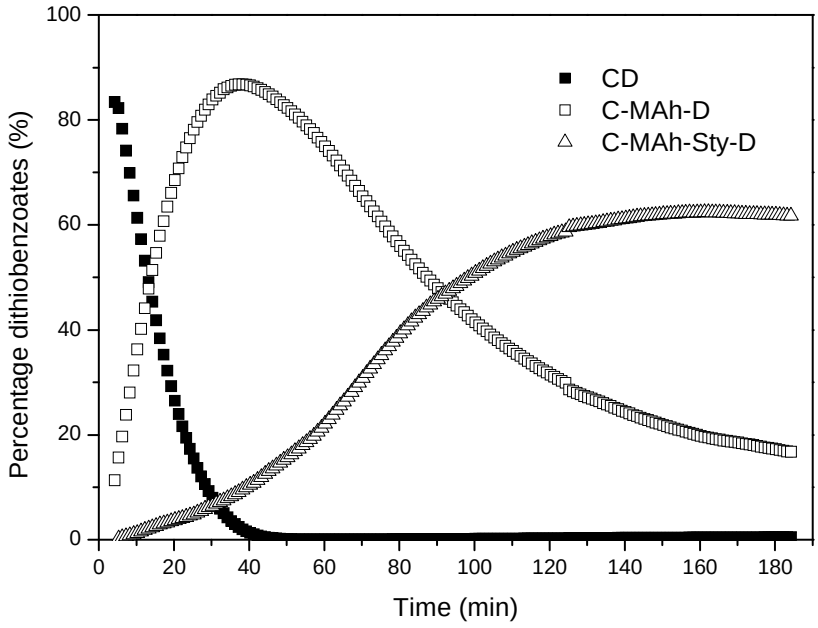

Figure 3.11: Conversion of the initial RAFT-agent and the formation of the first and second monomer adducts for a CDB-mediated Sty-MAh copolymerization at 60 °C. CD represents the initial RAFT-agent CDB, and C-MAh-D and C-MAh-Sty-D are the first and second monomer adducts respectively.

The preference of CDB to add a MAh unit can be attributed to the leaving group. As the leaving group radical is nucleophilic, it acts as an electron donor to maleic anhydride. The 2-cyanoprop-2-yl radical fragmented from CIPDB on the other hand is electrophilic, which therefore adds to styrene that acts as an electron donor. Initially the conversion of styrene remains very low and only once the majority of the RAFT-agent has been converted into the first monomer adduct C-MAh-D, does the conversion of styrene start

to increase to form the second monomer adduct C-MAh-Sty-D. The ratio of the Sty to MAh consumption shows a minimum just before the end of the initialization period, indicating that the first monomer adduct consists mainly of C-MAh-D and only after initialization is styrene being consumed more rapidly. During the addition of the second monomer unit the ratio of the styrene to maleic anhydride consumption increases to form the second monomer adduct C-MAh-Sty-D and tends towards unity. This is in agreement with alternating behavior for the Sty-MAh copolymerization.

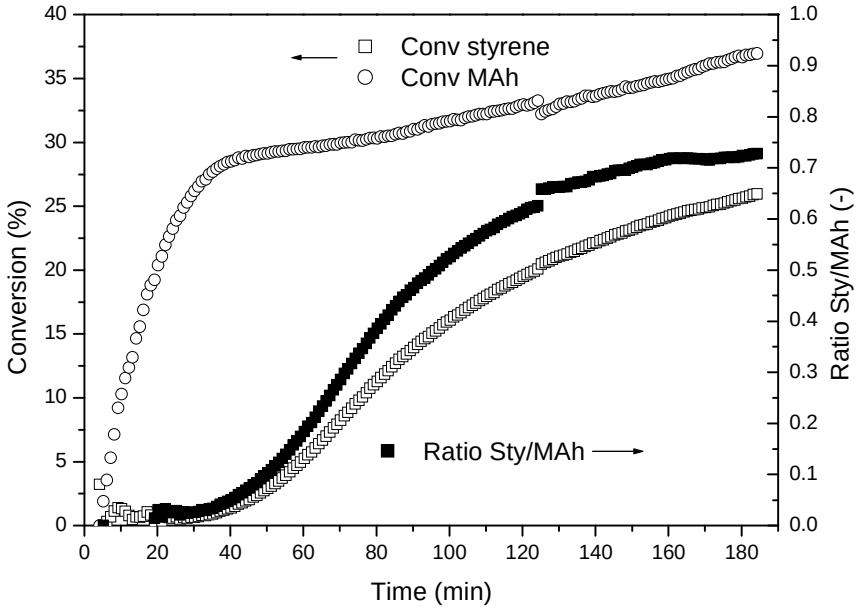

Figure 3.12: Conversion vs. time plot for a CDB-mediated Sty-MAh copolymerization at 60 °C. The ratio of Sty to MAh consumption is also plotted vs. time.

3.4 Conclusions

Along with the unraveling of the RAFT-mechanism, a debate arose on the origin of induction period and rate retardation phenomena observed in some RAFT-mediated polymerizations. These kinetic irregularities were especially strong in dithiobenzoate-mediated acrylate polymerizations. This is often attributed to the stability of the intermediate radical of the RAFT-agent in the pre-equilibrium as well as in the main

equilibrium. Some researchers argue that the intermediate radical is so stable and that the rate of fragmentation is very slow and therefore its lifetime is long (a few seconds), which results in induction and rate retardation of the polymerization. Other researchers claim that the intermediate radical is involved in termination reactions, either via cross-termination with a propagating chain or via self-termination with another intermediate radical, leading to 3- or 4-arm stars respectively. There is only circumstantial evidence available for the slow fragmentation theory. Limited evidence is available that the intermediate radical does undergo termination reactions with other radicals. As a consequence, there is no unanimous agreement among all researchers about the exact cause of the induction and rate retardation phenomena.

This chapter described the investigation into the very early stages of RAFT-mediated polymerizations of MA using CIPDB, CDB and CPDA as the RAFT-agents and aiming for common target molecular weights (up to 70,000 g/mol). Furthermore, the study was extended with an investigation into the early stages of RAFT-mediated Sty-MAh copolymerizations using CIPDB and CDB as the RAFT-agents. In both cases, during the early stages of the polymerization the RAFT-agent is selectively converted into a 'macroRAFT'-agent containing only one monomer unit. That is, an *initialization period* is observed during which the initial RAFT-agent is converted into its first monomer adduct and only after the complete conversion of the initial RAFT-agent, further growth of the polymer chains takes place. This means that for the RAFT-agent/monomer systems investigated here, a highly selective conversion of the RAFT-agent takes place during which unimers predominate and higher adducts are only able to form in considerable amounts after the complete consumption of the initial RAFT-agent. This behavior is in agreement with earlier studies, and proves that this initial step in RAFT-mediated polymerizations is an important step, also for common target molecular weight polymerizations (up to 70,000 g/mol) and copolymerizations. An important outcome of this study is that the induction period often observed in dithiobenzoate-mediated (acrylate) polymerizations can rather be described by this selective initialization period. During this initialization period, where unimers predominate, the monomer conversion remains so low, that this often mistakenly is interpreted as an inhibition period, rather

than as an initialization period. The observed behavior is particularly strong for fast propagating monomers, where the propagation rate constant of the monomer is much higher than the addition rate constant of the leaving group radical to a monomer unit. In this case the monomer conversion remains very low (<1%).

An additional conclusion from this study is that the RAFT-mediated alternating copolymerization of styrene and maleic anhydride is very selective in the choice of the RAFT-agent leaving group to preferentially add to one monomer. For CIPDB the leaving group preferably adds to a styrene unit, whereas for CDB the cumyl radical preferably adds to a maleic anhydride unit. This preference for selective addition can be explained by the electronic structure of the leaving group of the RAFT-agents and the monomers. CIPDB, which has an electron-withdrawing group, preferably adds to styrene, which has an electron-rich double bond. CDB on the other hand, acts as an electron-donor for maleic anhydride and preferably adds to this monomer. Besides this preferential addition to one of the monomers, the fact that the monomers are added individually to the growing chain favors the penultimate unit (PU) model and is in contradiction with the charge-transfer-complex (CTC) model, which requires that the monomers add in pairs to the growing chain. After initialization, the copolymerization proceeds in both cases in an alternating fashion, resulting in the formation of an alternating styrene-maleic anhydride copolymer.

References

1. D.A. Shipp, *J. Macromol. Sci., part C: Polym. Rev.* **2005**, *45*, 171-194
2. G. Moad, E. Rizzardo and S.H. Thang, *Aust. J. Chem.* **2005**, *58*, 379-410
3. S. Perrier and P. Takolpuckdee, *J. Polym. Sci., Part A: Polym. Chem.* **2005**, *43*, 5347-5393
4. G. Delaittre and B. Charleux, *Macromolecules* **2008**, *41*, 2361-2367
5. K. Matyjaszewski, K. Davis, T.E. Patten and M. Wei, *Tetrahedron* **1997**, *53*, (45), 15321-15329
6. K. Matyjaszewski, T.E. Patten and J. Xia, *J. Am. Chem. Soc.* **1997**, *119*, 674-680
7. N.V. Tsarevsky, S.A. Bencherif and K. Matyjaszewski, *Macromolecules* **2007**, *40*, 4439-4445
8. H. Gao, G. Louche, B.S. Sumerlin, N. Jahed, P. Golas and K. Matyjaszewski, *Macromolecules* **2005**, *38*, 8979-8982
9. M. Spiniello, A. Blencowe and G.G. Qiao, *J. Polym. Sci., Part A: Polym. Chem.* **2008**, *46*, 2422-2432
10. J. Chiefari, B.Y.K. Chong, F. Ercole, J. Krstina, J. Jeffery, T.P.T. Le, R.T.A. Mayadunne, G.F. Meijs, C.L. Moad, E. Rizzardo and S.H. Thang, *Macromolecules* **1998**, *31*, 5559-5562
11. E. Rizzardo, J. Chiefari, B.Y.K. Chong, F. Ercole, J. Krstina, J. Jeffery, T.P.T. Le, R.T.A. Mayadunne, G.F. Meijs, C.L. Moad, G. Moad and S.H. Thang, *Macromol. Symp.* **1999**, *143*, 291-307
12. E. Rizzardo, J. Chiefari, R.T.A. Mayadunne, G. Moad and S.H. Thang, *ACS Symp. Ser.* **2000**, *768*, 278-296
13. B.Y.K. Chong, T.P.T. Le, G. Moad, E. Rizzardo and S.H. Thang, *Macromolecules* **1999**, *32*, 2071-2074
14. L. Albertin and N.R. Cameron, *Macromolecules* **2007**, *40*, 6082-6093
15. S. Venkataraman and K.L. Wooley, *J. Polym. Sci., Part A: Polym. Chem.* **2007**, *45*, 5420-5430
16. H. Gemici, T.M. Legge, M. Whittaker, M.J. Monteiro and S. Perrier, *J. Polym. Sci., Part A: Polym. Chem.* **2007**, *45*, 2334-2340

17. R.T.A. Mayadunne, E. Rizzardo, J. Chiefari, J. Krstina, G. Moad, A. Postma and S.H. Thang, *Macromolecules* **2000**, *33*, 243-245
18. S. Perrier, P. Takolpuckdee, J. Westwood and D.M. Lewis, *Macromolecules* **2004**, *37*, 2709-2717
19. J.J. Vosloo, M.P. Tonge, C.M. Fellows, F. D'Agosto, R.D. Sanderson and R.G. Gilbert, *Macromolecules* **2004**, *37*, 2371-2382
20. H. de Brouwer, M.A.J. Schellekens, B. Klumperman, M.J. Monteiro and A.L. German, *J. Polym. Sci., Part A: Polym. Chem.* **2000**, *38*, 3596-3603
21. Z. Deng, H. Bouchékif, K. Babooram, A. Housni, N. Choytun and R. Narain, *J. Polym. Sci., Part A: Polym. Chem.* **2008**, *46*, 4984-4996
22. C.L. McCormick and A.B. Lowe, *Acc. Chem. Res.* **2004**, *37*, 312-325
23. J.B. McLeary and B. Klumperman, *Soft Matter* **2006**, *2*, 45-53
24. D.E. Ganeva, E. Sprong, H. de Bruyn, G.G. Warr, C.H. Such and B.S. Hawkett, *Macromolecules* **2007**, *40*, 6181-6189
25. S.W. Prescott, M.J. Ballard, E. Rizzardo and R.G. Gilbert, *Macromolecules* **2002**, *35*, 5417-5425
26. M. Lansalot, T.P. Davis and J.P.A. Heuts, *Macromolecules* **2002**, *35*, 7582-7591
27. J. Bozovic-Vukic, H.T. Mañon, J. Meuldijk, C. Koning and B. Klumperman, *Macromolecules* **2007**, *40*, 7132-7139
28. F. Stoffelbach, L. Tibiletti, J. Rieger and B. Charleux, *Macromolecules* **2008**, *41*, 7850-7856
29. J.K. Oh, *J. Polym. Sci., Part A: Polym. Chem.* **2008**, *46*, 6983-7001
30. J.F. Quinn, L. Barner, C. Barner-Kowollik, E. Rizzardo and T.P. Davis, *Macromolecules* **2002**, *35*, 7620-7627
31. W. Jiang, L. Lu and Y. Cai, *Macromol. Rapid Commun.* **2007**, *28*, 725-728
32. A. Feldermann, M.L. Coote, M.H. Stenzel, T.P. Davis and C. Barner-Kowollik, *J. Am. Chem. Soc.* **2004**, *126*, 15915-15923
33. C. Barner-Kowollik, P. Vana, J.F. Quinn and T.P. Davis, *J. Polym. Sci., Part A: Polym. Chem.* **2002**, *40*, 1058-1063
34. D. Hua, K. Cheng, R. Bai, W. Lu and C. Pan, *Polym. Int.* **2004**, *53*, 821-823

35. J.F. Quinn, L. Barner, E. Rizzardo and T.P. Davis, *J. Polym. Sci., Part A: Polym. Chem.* **2002**, *40*, 19-25
36. J.F. Quinn, L. Barner, T.P. Davis, S.H. Thang and E. Rizzardo, *Macromol. Rapid Commun.* **2002**, *23*, 717-721
37. L. Barner, J.F. Quinn, C. Barner-Kowollik, P. Vana and T.P. Davis, *Eur. Polym. J.* **2003**, *39*, 449-459
38. D. Hua, X. Ge, R. Bai, W. Lu and C. Pan, *Polymer* **2005**, *46*, 12696-12702
39. B.Y.K. Chong, J. Krstina, T.P.T. Le, G. Moad, A. Postma, E. Rizzardo and S.H. Thang, *Macromolecules* **2003**, *36*, 2256-2272
40. J. Chiefari, R.T.A. Mayadunne, C.L. Moad, G. Moad, E. Rizzardo, A. Postma, M.A. Skidmore and S.H. Thang, *Macromolecules* **2003**, *36*, 2273-2283
41. G. Moad, Y.K. Chong, A. Postma, E. Rizzardo and S.H. Thang, *Polymer* **2005**, *46*, 8458-8468
42. D.B. Thomas, A.J. Convertine, R.D. Hester, A.B. Lowe and C.L. McCormick, *Macromolecules* **2004**, *37*, 1735-1741
43. V. Lima, X. Jiang, J. Brokken-Zijp, P.J. Schoenmakers, B. Klumperman and R.v.d. Linde, *J. Polym. Sci., Part A: Polym. Chem.* **2005**, *43*, 959-973
44. X.-P. Qiu and F.M. Winnik, *Macromol. Rapid Commun.* **2006**, *27*, 1648-1653
45. A. Postma, T.P. Davis, R.A. Evans, G. Li, G. Moad and M.S. O'Shea, *Macromolecules* **2006**, *39*, 5293-5306
46. Y. Li, J. Yang and B.C. Benicewicz, *J. Polym. Sci., Part A: Polym. Chem.* **2007**, *45*, 4300-4308
47. F. Segui, X.-P. Qiu and F.M. Winnik, *J. Polym. Sci., Part A: Polym. Chem.* **2008**, *46*, 314-326
48. J.T. Lai, D. Filla and R. Shea, *Macromolecules* **2002**, *35*, 6754-6756
49. J. Liu, C.-Y. Hong and C.-Y. Pan, *Polymer* **2004**, *45*, 4413-4421
50. M. Li, P. De, S.R. Gondi and B.S. Sumerlin, *Macromol. Rapid Commun.* **2008**, *29*, 1172-1176
51. J. Xu, J. He, D. Fan, X. Wang and Y. Yang, *Macromolecules* **2006**, *39*, 8616-8624
52. S. Perrier, P. Takolpuckdee and C.A. Mars, *Macromolecules* **2005**, *38*, 2033-2036

53. Y.K. Chong, G. Moad, E. Rizzardo and S. Thang, *Macromolecules* **2007**, *40*, 4446-4455

54. A. Postma, T.P. Davis, G. Moad and M.S. O'Shea, *Macromolecules* **2005**, *38*, 5371-5374

55. C. Barner-Kowollik, M. Buback, B. Charleux, M.L. Coote, M. Drache, T. Fukuda, A. Goto, B. Klumperman, A.B. Lowe, J.B. McLeary, G. Moad, M.J. Monteiro, R.D. Sanderson, M.P. Tonge and P. Vana, *J. Polym. Sci., Part A: Polym. Chem.* **2006**, *44*, 5809-5831

56. A.R. Wang, S. Zhu, Y. Kwak, A. Goto, T. Fukuda and M.J. Monteiro, *J. Polym. Sci., Part A: Polym. Chem.* **2003**, *41*, 2833-2839

57. C. Barner-Kowollik, M.L. Coote, T.P. Davis, L. Radom and P. Vana, *J. Polym. Sci., Part A: Polym. Chem.* **2003**, *41*, 2828-2832

58. E. Chernikova, A. Morozov, E. Leonova, E. Garina, V. Golubev, C. Bui and B. Charleux, *Macromolecules* **2004**, *37*, 6329-6339

59. J.F. Quinn, E. Rizzardo and T.P. Davis, *Chem. Commun.* **2001**, 1044-1045

60. J.B. McLeary, F.M. Calitz, J.M. McKenzie, M.P. Tonge, R.D. Sanderson and B. Klumperman, *Macromolecules* **2004**, *37*, 2383-2394

61. J.B. McLeary, J.M. McKenzie, M.P. Tonge, R.D. Sanderson and B. Klumperman, *Chem. Commun.* **2004**, 1950-1951

62. J.B. McLeary, F.M. Calitz, J.M. McKenzie, M.P. Tonge, R.D. Sanderson and B. Klumperman, *Macromolecules* **2005**, *38*, 3151-3161

63. E.T.A. van den Dungen, H. Matahwa, J.B. McLeary, R.D. Sanderson and B. Klumperman, *J. Polym. Sci., Part A: Polym. Chem.* **2008**, *46*, 2500-2509

64. B. Klumperman, J.B. McLeary, E.T.A. van den Dungen, W.-J. Soer and J.S. Bozovic, *ACS Symp. Ser.* **2006**, *944*, 501-513

65. E.T.A. van den Dungen, J. Rinquest, N.O. Pretorius, J.M. McKenzie, J.B. McLeary, R.D. Sanderson and B. Klumperman, *Aust. J. Chem.* **2006**, *59*, 742-748

66. B. Klumperman, J.B. McLeary, E.T.A. van den Dungen and G. Pound, *Macromol. Symp.* **2007**, *248*, 141-149

67. M. Drache and G. Schmidt-Naake, *Macromol. Symp.* **2007**, *259*, 397-405

68. X. Han, J. Fan, J. He, J. Xu, D. Fan and Y. Yang, *Macromolecules* **2007**, *40*, 5618-5624
69. C. Li and B.C. Benicewicz, *J. Polym. Sci., Part A: Polym. Chem.* **2005**, *43*, 1535-1543
70. M.M. Guo, *Polym. Preprints* **2005**, *46*, (2), 261-262
71. F.M. Calitz, J.B. McLeary, J.M. McKenzie, M.P. Tonge, B. Klumperman and R.D. Sanderson, *Macromolecules* **2003**, *36*, 9687-9690
72. P. Geelen and B. Klumperman, *Macromolecules* **2007**, *40*, 3914-3920
73. M.J. Monteiro and H. de Brouwer, *Macromolecules* **2001**, *34*, 349-352
74. Y. Kwak, A. Goto, K. Komatsu, Y. Sugiura and T. Fukuda, *Macromolecules* **2004**, *37*, 4434-4440
75. Y. Kwak, A. Goto, Y. Tsujii, Y. Murata, K. Komatsu and T. Fukuda, *Macromolecules* **2002**, *35*, 3026-3029
76. Y. Kwak, A. Goto and T. Fukuda, *Macromolecules* **2004**, *37*, 1219-1225
77. R. Venkatesh, B.B.P. Staal, B. Klumperman and M.J. Monteiro, *Macromolecules* **2004**, *37*, 7906-7917
78. M. Bathfield, F. D'Agosto, R. Spitz, C. Ladavière, M.-T. Charreyre and T. Delair, *Macromol. Rapid Commun.* **2007**, *28*, 856-862
79. A. Favier, C. Ladavière, M.-T. Charreyre and C. Pichot, *Macromolecules* **2004**, *37*, 2026-2034
80. A. Favier, M.-T. Charreyre, P. Chaumont and C. Pichot, *Macromolecules* **2002**, *35*, 8271-8280
81. M. Buback and P. Vana, *Macromol. Rapid Commun.* **2006**, *27*, 1299-1305
82. M.L. Coote, E.H. Krenske and E.I. Izgorodina, *Macromol. Rapid Commun.* **2006**, *27*, 473-497
83. E.I. Izgorodina and M.L. Coote, *Macromol. Theory Simul.* **2006**, *15*, 394-403
84. M.L. Coote, E.I. Izgorodina, E.H. Krenske, M. Busch and C. Barner-Kowollik, *Macromol. Rapid Commun.* **2006**, *27*, 1015-1022
85. F.M. Calitz, M.P. Tonge and R.D. Sanderson, *Macromolecules* **2003**, *36*, 5-8
86. M. Drache, G. Schmidt-Naake, M. Buback and P. Vana, *Polymer* **2005**, *46*, 8483-8493

87. M. Buback, P. Hesse, T. Junkers and P. Vana, *Macromol. Rapid Commun.* **2006**, *27*, 182-187

88. C. Barner-Kowollik, J.F. Quinn, T.L. Uyen Nguyen, J.P.A. Heuts and T.P. Davis, *Macromolecules* **2001**, *34*, 7849-7857

89. S. Perrier, C. Barner-Kowollik, J.F. Quinn, P. Vana and T.P. Davis, *Macromolecules* **2002**, *35*, 8300-8306

90. P. Vana, J.F. Quinn, T.P. Davis and C. Barner-Kowollik, *Aust. J. Chem.* **2002**, *55*, 425-431

91. A. Ah Toy, P. Vana, T.P. Davis and C. Barner-Kowollik, *Macromolecules* **2004**, *37*, 744-751

92. A. Feldermann, A. Ah Toy, T.P. Davis, M.H. Stenzel and C. Barner-Kowollik, *Polymer* **2005**, *46*, 8448-8457

93. P. Vana, T.P. Davis and C. Barner-Kowollik, *Macromol. Theory Simul.* **2002**, *11*, (8), 823-835

94. J.B. McLeary, M.P. Tonge and B. Klumperman, *Macromol. Rapid Commun.* **2006**, *27*, 1233-1240

95. R. Plummer, Y.-K. Goh, A.K. Whittaker and M.J. Monteiro, *Macromolecules* **2005**, *38*, 5352-5355

96. E.H. Nejad, P. Castignolles, R.G. Gilbert and Y. Guillaneuf, *Journal of Polymer Science, Part A: Polymer Chemistry* **2008**, *46*, 2277-2289

97. S.H. Thang, B.Y.K. Chong, R.T.A. Mayadunne, G. Moad and E. Rizzardo, *Tetrahedron Lett.* **1999**, *40*, 2435-2438

98. T.P. Le, G. Moad, E. Rizzardo and S.H. Thang, *PCT Int. Appl.*, **1998**, *WO 98/01478*

99. A.L.v. Geet, *Anal. Chem.* **1968**, *40*, (14), 2227-2229

100. H. Fischer and L. Radom, *Angew. Chem. Int. Ed.* **2001**, *40*, 1340-1371

101. F.-S. Du, M.-Q. Zhu, H.-Q. Guo, Z.-C. Li, F.-M. Li, M. Kamachi and A. Kajiwara, *Macromolecules* **2002**, *35*, 6739-6741

102. H.K. Hall Jr. and A.B. Padias, *J. Polym. Sci., Part A: Polym. Chem.* **2001**, *39*, 2069-2077

103. R.A. Sanayei, K.F. O'Driscoll and B. Klumperman, *Macromolecules* **1994**, *27*, 5577-5582

104. B. Klumperman and G. Vonk, *Eur. Polym. J.* **1994**, *30*, (8), 955-960

105. E. Chernikova, P. Terpugova, C. Bui and B. Charleux, *Polymer* **2003**, *44*, 4101-4107

106. E.-S. Park, M.-N. Kim, I.-M. Lee, H.S. Lee and J.-S. Yoon, *J. Polym. Sci., Part A: Polym. Chem.* **2000**, *38*, 2239-2244

Chapter 4: Synthesis of core-shell particles via miniemulsification

Abstract

This chapter describes the synthesis of well-defined core-shell particles via miniemulsification. Pentaerythritol tetrakis(3-mercaptopropionate) (TetraThiol), a tetrafunctional thiol that is employed as monomer in step-growth free-radical thiol-ene polymerization as described in subsequent chapters, is employed as the oil phase. The use of this monomer eliminates the possibility of miniemulsion polymerization, as TetraThiol would simultaneously act as a chain-transfer agent. Various styrene-maleic anhydride (SMA) copolymers were employed as surfactant, based on the well-known properties of SMA copolymers as surfactant. Commercial SMA1000 (Sartomer) as well as SMA copolymers of various molecular weight synthesized via Reversible Addition-Fragmentation chain Transer (RAFT)-mediated polymerization were used. In addition, P[(Sty-*alt*-MAh)-*b*-Sty] block copolymers of various molecular weight were synthesized via chain-extension of the SMA copolymers obtained from RAFT-mediated polymerization. Well-defined SMA copolymers and P[(Sty-*alt*-MAh)-*b*-Sty] block copolymers with controlled molecular weight and narrow molecular weight distribution were obtained. The molecular weight ratio of the SMA copolymer block to the polystyrene block varied from about two to approximately one. Well-defined core-shell particles were synthesized with TetraThiol as the core and SMA1000 and various SMA copolymers as the shell material. The core-shell particles had a diameter of 150–350 nm and the particle size distribution was fairly narrow. The stability of these core-shell particles was not very good however, and therefore extra stabilization was provided with the addition of formaldehyde. Formaldehyde reacts with the amic acid functionality of ring-opened (with ammonia) maleic anhydride and introduces a hydroxymethyl functionality that provides additional steric stabilization. A slight excess of formaldehyde introduces oxymethylene oligomer chains. The use of P[(Sty-*alt*-MAh)-*b*-Sty] block copolymers as surfactant in combination with steric stabilization provided by reaction with formaldehyde, significantly improved the stability of the core-shell particles. Although a fair amount of very small (25–35 nm) particles was present, core-shell particles with improved stability were obtained with a size around 100 nm.

4.1 Introduction

Free-radical polymerization in heterogeneous media has established itself as a versatile technique via which stable latexes can be prepared that may consist of particles of various advanced morphologies. High rates of polymerization are obtained and high molecular weight polymers can easily be prepared.[1] Control over the molecular weight is obtained via the addition of chain-transfer agents.[2] Emulsion polymerization is widely applied in industry and many polymers are prepared via this technique. It must be noted though, that while emulsion polymerization is easily applicable to the free-radical homopolymerization of certain (hydrophobic) monomers, it also suffers from certain drawbacks. Generally it is a challenge to obtain advanced structures, such as core-shell particles that show a high degree of homogeneity in composition throughout the molecular weight and particle size distribution. This is also related to the nucleation mechanism of emulsion polymerization. The primary nucleation mechanisms in emulsion polymerization are homogeneous and micellar nucleation and during the early stages of the polymerization (referred to as Interval I) continuously new particles are formed. For (co)polymerizations that require a long nucleation time, final latex particles are obtained that lack homogeneity in particle size and chemical composition.

By realizing that the monomer droplets could compete with micelles for incoming radicals, as long as the monomer droplets are small (<1 μm) so that their surface area is large, the monomer droplets themselves could be nucleated and transformed into latex particles.[3] The process where nucleation occurs in the monomer droplets is nowadays known as miniemulsion polymerization, and the formation of a miniemulsion is achieved by subjecting the premixed oil- and aqueous phases to high shear, so that the droplet size is brought in a kinetic equilibrium via fission and fusion events.[4-6] The major advantage of miniemulsion polymerization is that it opens the way for the preparation of more complex architectures, as the whole polymerization process takes place in the monomer droplets that are transformed into polymer particles. Ideally the latex particles are a one-to-one copy of the monomer droplets, retaining their original size and identity. However, to obtain a one-to-one copy of the monomer droplets into latex particles, several criteria must be met simultaneously.[6] The nucleation of the monomer droplets must be very fast

and the rate of polymerization must be much higher than the mass transport of monomer among particles. Furthermore, coalescence between droplets and particles must be negligible. Stability against monomer diffusion from the small to the large droplets (Ostwald ripening) in miniemulsion polymerization is obtained via the addition of an ultrahydrophobe, a highly water insoluble compound such as hexadecane, and colloidal stability is obtained via the use of a surfactant. In contrast to emulsion polymerization where the monomer has to diffuse through the aqueous phase and supply the polymerization loci with monomer, in miniemulsion polymerization the monomer is already present at the reaction loci so that no transport through the aqueous phase is required. As a consequence, the synthesis of copolymers will result in the formation of particles that are more homogeneous in their chemical composition throughout the latex particle distribution.

Although the concept of miniemulsion polymerization was introduced over three decades ago,[3] recently an increased interest in the synthesis of complex structures, such as core-shell particles has emerged. In a similar manner as introduced by Torza and Mason,[7] Chen *et al.* predicted the particle morphology of a three-phase polymer system via experimentally determined interfacial tensions. Their system consisted of polystyrene and poly(methyl methacrylate) in the aqueous phase and the predicted morphology showed good agreement with the observed particle morphologies.[8] Also the effect of conversion on particle morphology was investigated and indicated that especially at high conversions the experimentally obtained morphologies are in good agreement with predicted morphologies.[9] A different approach for the synthesis of core-shell particles was described by Jhaveri *et al.*[10] They simultaneously polymerized and cross-linked methyl methacrylate in emulsion, while embedding a dormant Atom Transfer Radical Polymerization (ATRP)-initiator with its functional group present at the surface. The core-shell particles were then synthesized via ATRP of various monomers. The encapsulation of a wide variety of inorganic compounds via miniemulsion polymerization has been reported over the last decade, such as TiO_2,[11] Fe_3O_4,[12,13], Y_2O_2S[14] and polyoxometalates (POMs),[15] and also the formation of hollow nanocapsules was described.[16-21] Crespy *et al.* synthesized hollow nanocapsules via interfacial

polycondensation reactions in inverse miniemulsion and demonstrated that the hollow nanocapsules can be used as nanoreactor for model reactions.[22]

The introduction and rapid development of new controlled/living radical polymerization techniques over the past decades, such as Nitroxide-Mediated Polymerization (NMP), ATRP and Reversible Addition-Fragmentation chain Transfer (RAFT)-mediated polymerization[23] allowed for precision polymerization, in terms of controlled growth and formation of narrow molecular weight distribution polymers, to synthesize advanced architectures. Among these techniques, RAFT-mediated polymerization has established itself as the most robust and versatile technique because the polymerization can be conducted under the same conditions (solvent, temperature and initiator) as employed in conventional free-radical polymerization and it can be applied to the same wide range of monomers and functional groups. Because the controlled radical polymerization techniques are conducted in the presence of a transfer agent that is endcapped at the polymer chain-ends and preserved after polymerization, easy access to the formation of diblock copolymers and more advanced architectures is readily available.

Chen *et al*. reported on the synthesis of well-defined di- and triblock copolymers and the subsequent use of these polymers as surfactant in miniemulsion polymerization.[24,25] In addition, a lot of research has focused on the synthesis of amphiphilic or double hydrophilic block copolymers that self-assemble into micelles in a selective solvent.[26-28] Cheng and coworkers synthesized Polymeric Micelles with Aqueous Core (PMAC) and demonstrated that the micelles could be employed as nanoreactor for the preparation of inorganic nanoparticles.[29] Also block copolymers that reversibly self-assemble into micelles via the application of an external stimulus such as temperature or pH has been reported extensively.[30-32] Stabilization of these block copolymer micelles is readily achieved via cross-linking of either the core- or shell block using well-established chemistries.[33-37] Retention of the micellar structure after cross-linking in various solvents and at various temperatures or pH for the thermo- and pH-responsive polymers respectively has been reported. The swelling-deswelling behavior of these cross-linked micelles makes them potential candidates as nano-sized drug-delivery vehicles.[38-41] The

degree of cross-linking has also been shown to influence and control this release behavior.[42] In addition, attention has been paid to reversible cross-linking of the polymers for application in controlled release experiments.[43,44] Because the majority of monomers that are employed contain functional groups in either the core or shell, these sites are not only suitable for cross-linking, but give an additional advantage for further functionalization of the micelles with specific target compounds such as fluorescent labels and specific receptors for recognition that are available at the micellar surface or in the core.[45-49] Recently Ievins and coworkers demonstrated the availability of terpyridine functional groups within the core for complexation with metals and the subsequent catalytic activity of these complexes for the click reaction of azido and alkynyl-functionalized small molecules.[50]

Here we present the synthesis of well-defined core-shell latex particles consisting of a tetrafunctional thiol compound as the core material (pentaerythritol tetrakis(3-mercaptopropionate), TetraThiol) and a styrene-maleic anhydride copolymer shell via miniemulsification of an oil-in-water emulsion. First the synthesis of styrene-maleic anhydride (SMA) alternating copolymers via RAFT-mediated polymerization and the chain-extension of this alternating copolymer with styrene to form a P[(Sty-*alt*-MAh)-*b*-Sty] block copolymer is described. A detailed analysis of these copolymers via size exclusion chromatography (SEC) and ^{1}H-NMR spectroscopy is given to determine the control over the polymerization in terms of molecular weight and molecular weight distribution, and the retention of the RAFT-endgroup at the polymer chain-end. The SMA copolymers obtained via RAFT-mediated polymerization and also a commercially available SMA copolymer (SMA1000) are employed as surfactant for the encapsulation of TetraThiol. The maleic anhydride units of the copolymer are ring-opened with ammonia to introduce and control the hydrophilicity and, after encapsulation of TetraThiol, used in post-encapsulation reactions for stability purposes. The resulting core-shell particles are analyzed via dynamic light scattering (DLS) and transmission electron microscopy (TEM).

4.2 Experimental details

4.2.1 Chemicals

Styrene (Plascon Research Centre, University of Stellenbosch, estimated purity ~99% by ^{1}H-NMR) was washed three times with an aqueous 0.3 M KOH solution to remove the inhibitor, and the styrene was subsequently distilled under reduced pressure. 2,2'-Azobis(isobutyronitrile) (AIBN, Riedel de Haën) was recrystallized from ethanol and dried under vacuum before use. Dichloromethane (Kimix, CP grade) was distilled at 40 °C and stored over molecular sieves (pore size 4Å). Maleic anhydride (Acros Organics 99%), 1,4-dioxane (Saarchem uniLAB 99%), 2-butanone (methyl ethyl ketone (MEK), Sasol solvents), SMA1000 (Elf Atochem (Sartomer) >98%, styrene to maleic anhydride ratio 1:1, molecular weight $M_n = 2.6\times10^3 g/mol$, PDI=1.68), SMA3000 (Elf Atochem (Sartomer) >98%, styrene to maleic anhydride ratio 3:1, molecular weight $M_n = 4.9\times10^3 g/mol$, PDI=5.41), pentaerythritol tetrakis(3-mercaptopropionate) (TetraThiol, Fluka ≥96%, [7575-23-7]), formaldehyde (37 wt% solution in water, Sigma-Aldrich ACS reagent, [50-00-0]), ammonia (25% solution, Saarchem uniLAB) and adipic acid dihydrazide (Sigma 98%, [1071-93-8]) were all used without further purification. Distilled deionized (DDI) water, obtained from a Millipore Milli-Q purification system, was used throughout the experiments described in this chapter.

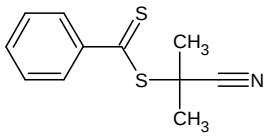

2-cyanoprop-2-yl dithiobenzoate (CIPDB)

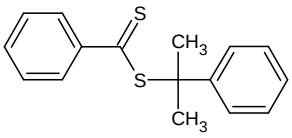

cumyl dithiobenzoate (CDB)

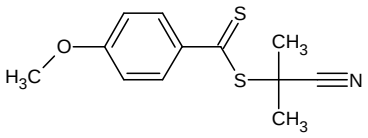

p-(2-cyanoprop-2-yl dithiocarboxy) anisole (p-CIPDCA)

Scheme 4.1: Structures of the RAFT-agents used for the synthesis of styrene-maleic anhydride copolymers.

4.2.2 RAFT-mediated copolymerization of styrene and maleic anhydride

The RAFT-agents that were employed for this study (Scheme 4.1) were 2-cyanoprop-2-yl dithiobenzoate (CIPDB), cumyl dithiobenzoate (CDB) and p-(2-cyanoprop-2-yl dithiocarboxy) anisole (p-CIPDCA) and these transfer agents were synthesized according

to the procedures described in Chapter 3. Table 4.1 shows the recipes for the different copolymers synthesized in this study.

Table 4.1: Formulation used for the RAFT-mediated styrene-maleic anhydride copolymerizations and the chain-extension with styrene[a]

Exp	Time (hrs)	T (°C)	$M_{n,target}$[b] (g/mol)	[Sty] (mol/L)	[MAh] (mol/L)	[RAFT] (mol/L)	[AIBN] (mol/L)
1[c]	6	60	$5.0x10^3$	2.830	2.829	0.121	0.024
2[d]	6	60	$8.0x10^3$	2.913	2.915	0.076	0.015
3[d]	6	60	$2.0x10^4$	2.964	2.968	0.030	0.006
4[e]	4.5	60	$2.0x10^4$	2.909	2.910	0.030	0.006
5[f]	22	70	$8.0x10^3$	2.184	x	0.045	0.009
6[g]	21	70	$4.8x10^4$	2.186	x	0.006	0.001
7[h]	24	70	$8.6x10^4$	2.409	x	0.004	0.001

[a] Experiments 1–6 were carried out in 1,4-dioxane and experiment 7 was carried out in MEK

[b] The target molecular weight was calculated with the following equation: $M_{n,target} = \frac{[M_1]_0}{[RAFT]_0} \cdot MW_{M_1} + \frac{[M_2]_0}{[RAFT]_0} \cdot MW_{M_2} + MW_{RAFT}$, where $[M_1]_0$, $[M_2]_0$ and $[RAFT]_0$ are the initial concentrations of both monomers and the RAFT-agent respectively and MW_{M_1}, MW_{M_2} and MW_{RAFT} the molecular weights of both monomers and the RAFT-agent respectively

[c] The RAFT-agent used is cumyl dithiobenzoate (CDB)

[d] The RAT-agent used is 2-cyanoprop-2-yl dithiobenzoate (CIPDB)

[e] The RAFT-agent used is p-(2-cyanoprop-2-yl dithiocarboxy) anisole (p-CIPDCA)

[f] The RAFT-agent used is the macroRAFT-agent obtained from experiment 1

[g] The RAFT-agent used is the macroRAFT-agent obtained from experiment 3

[h] The RAFT-agent used is the macroRAFT-agent obtained from experiment 4

A typical copolymerization was carried out as follows. To a 100 mL three-neck round-bottom flask were added 1.27 g of CDB (RAFT-agent, 4.7 mmol), 0.15 g of AIBN (0.9 mmol), 26 g of 1,4-dioxane, 11.4 g of styrene (0.11 mol) and 10.7 g of maleic anhydride (0.11 mol), together with a magnetic stirrer bar. The flask was connected to a condenser

and one neck was fitted with a nitrogen inlet and the other neck was fitted with a rubber septum so that samples could be taken for conversion and molecular weight analysis. The homogeneous solution was purged with nitrogen to remove the dissolved oxygen from the system while an oil bath was simultaneously heated to the reaction temperature of 60 °C. Once the temperature was stabilized, the flask was immersed in the oil bath and the reaction was allowed to proceed for six hours. During this period, samples were taken at regular time intervals. After the polymerization was stopped and cooled down to room temperature, the alternating styrene-maleic anhydride (SMA) copolymer was collected via precipitation in diethyl ether and analyzed via size exclusion chromatography and NMR spectroscopy.

For the formation of a (styrene-*alt*-maleic anhydride)-*b*-styrene block copolymer (P[(Sty-*alt*-MAh)-*b*-Sty]), the alternating copolymer obtained as described above was used as a macroRAFT-agent and chain-extended with styrene. For a typical reaction, 4.4 g of macroRAFT-agent (1.5 mmol, macroRAFT-agent obtained from experiment 1, Table 4.1), 0.05 g of AIBN (0.3 mmol), 7.4 g of styrene (0.07 mol) and 25 g of 1,4-dioxane were added to a 100 mL 3-neck round-bottom flask and deoxygenated by purging with nitrogen. The polymerization was carried out at 70 °C and allowed to react overnight. Precipitation of the block copolymer was accomplished in diethyl ether.

The SMA copolymers were intended for use as surfactant in the formation of core-shell particles in the aqueous phase and as such, they needed to be transformed into water soluble polymers. This was accomplished via reaction with a three times molar excess of a 25% ammonia solution with respect to the maleic anhydride units.[51] The water soluble polymer was then subsequently precipitated in THF prior to use in order to remove the excess ammonia, as TetraThiol contains ester groups that can be cleaved via nucleophilic attack. Care must be taken that no ring-closure (and formation of the more hydrophobic imide) occurs upon drying (for example in a vacuum oven or at elevated temperatures). The removal of excess ammonia in case of the block copolymers was achieved by exposing the solution to air and allowing the ammonia to evaporate. The complete removal of ammonia was confirmed via a neutral pH of the aqueous solution.

4.2.3 Formation of latex via miniemulsification

The synthesis of core-shell particles was carried out via the following steps. First the aqueous phase containing DDI water and surfactant (SMA copolymer, ring-opened with ammonia) and the oil phase containing TetraThiol (Scheme 4.2) and dichloromethane were prepared separately. Dichloromethane was added to the system to facilitate the dispersion of the highly viscous TetraThiol in the aqueous phase. Tables 4.2–4.5 show details of the various experiments for the synthesis of core-shell particles. The aqueous phase and oil phase were then combined and an oil-in-water pre-emulsion was formed with a Silverson L4R homogenizer operating at 9500 rpm for three minutes or via stirring with a magnetic stirrer bar at 1250 rpm for one hour. The obtained pre-emulsion was then subjected to ultrasonication using a Sonics Vibra cell VCX 750 Watt ultrasonic processor with a replaceable ½'' tip. Ultrasonication was conducted for 20–30 minutes with an amplitude of 50% during which a total amount of 50–75 kJ was delivered to the miniemulsion system.

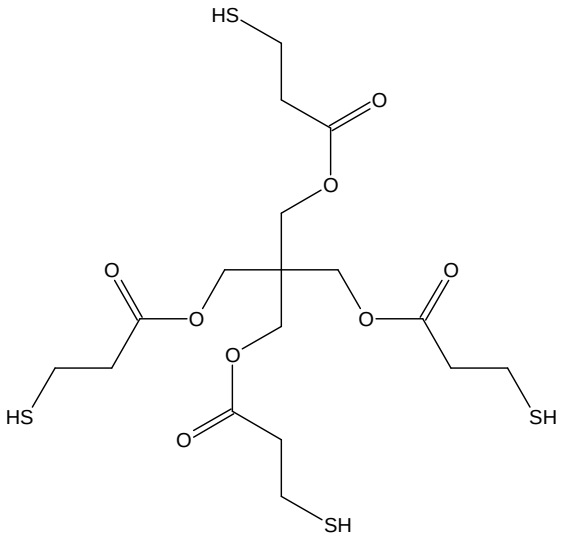

pentaerythritol tetrakis(3-mercaptopropionate)
(TetraThiol)

Scheme 4.2: Structure of the tetrafunctional thiol compound that serves as the core material.

Table 4.2: Formulation used for the synthesis of core-shell particles without extra stabilization[a]

Experiment	$m_{SMA1000}$ **(g)**	$m_{TetraThiol}$ **(g)**	m_{DCM} **(g)**	**TetraThiol content[b] (wt%)**
1	0.25	0.50	1.0	1.77
2	0.50	0.50	1.0	1.75
3	1.0	0.50	1.0	1.72
4	2.0	0.50	1.0	1.67
5	1.0	0.50	0.30	1.72

[a] The miniemulsions were prepared using 28 g of DDI water

[b] TetraThiol content with respect to the aqueous phase (DDI water and surfactant)

Cross-linking of the shell was investigated to improve the stability of the core-shell particles, as the non-stabilized core-shell particles degraded via phase separation over a period of a few weeks. For this purpose, the ring-opening of the maleic anhydride units in the copolymer was performed via the addition of a mixture of ammonia and urea (30–35 mol% of urea). After encapsulation of the core compound, formaldehyde (ratio formaldehyde to urea of 1.8) was added to the system to achieve cross-linking of the shell via urea-formaldehyde cross-linking reactions.

Table 4.3: Formulation used for the synthesis of core-shell particles with extra stabilization induced via cross-linking of urea and formaldehyde[a]

Experiment	$m_{SMA1000}$ **(g)**	$m_{TetraThiol}$ **(g)**	m_{DCM} **(g)**	**TetraThiol content[b] (wt%)**
6	1.0	0.50	1.0	1.72
7	1.0	0.50	1.0	1.72
8	1.0	1.0	2.0	3.45
9	0.50	1.0	2.0	3.51
10	1.0	0.50	1.0	1.72
11	1.0	1.0	2.0	3.45

[a] The miniemulsions were prepared using 28 g of DDI water

[b] TetraThiol content with respect to the aqueous phase (DDI water and surfactant)

Table 4.4: Formulation used for the synthesis of core-shell particles with various SMA copolymers as surfactant and with extra stabilization induced via cross-linking of urea and formaldehyde[a]

Experiment	m_{SMA} **(g)**	$m_{TetraThiol}$ **(g)**	m_{DCM} **(g)**	**TetraThiol content[b] (wt%)**
12[c]	0.25	1.0	1.0	3.54
13[c]	0.50	1.0	1.0	3.51
14[c]	1.0	1.0	1.0	3.45
15[d]	0.25	1.0	1.0	3.54
16[d]	0.50	1.0	1.0	3.51
17[d]	1.0	1.0	1.0	3.45

[a] The miniemulsions were prepared using 28 g of DDI water

[b] TetraThiol content with respect to the aqueous phase (DDI water and surfactant)

[c] SMA copolymer used as surfactant obtained from experiment 1, Table 4.1

[d] SMA copolymer used as surfactant obtained from experiment 2, Table 4.1

Table 4.5: Formulation used for the synthesis of core-shell particles with various P[(Sty-*alt*-MAh)-*b*-Sty] block copolymers as surfactant and with extra stabilization induced via addition of formaldehyde[a]

Experiment	$m_{P[(Sty-alt-MAh)-b-Sty]}$ **(g)**	$m_{TetraThiol}$ **(g)**	m_{DCM} **(g)**	**TetraThiol content[b] (wt%)**
18[c]	0.50	0.50	0.75	1.75
19[c]	0.50	1.0	1.50	3.51
20[d]	0.50	1.0	1.50	3.51
21[e]	0.50	1.0	1.50	3.51

[a] The miniemulsions were prepared using 28 g of DDI water

[b] TetraThiol content with respect to the aqueous phase (DDI water and surfactant)

[c] P[(Sty-*alt*-MAh)-*b*-Sty] block copolymer used as surfactant obtained from experiment 5, Table 4.1

[d] P[(Sty-*alt*-MAh)-*b*-Sty] block copolymer used as surfactant obtained from experiment 6, Table 4.1

[e] P[(Sty-*alt*-MAh)-*b*-Sty] block copolymer used as surfactant obtained from experiment 7, Table 4.1

As mentioned above, the ring-opening of the maleic anhydride units of the block copolymer P[(Sty-*alt*-MAh)-*b*-Sty] was achieved via reaction with ammonia. Excess ammonia was removed via evaporation until the pH reached a neutral value. Stabilization of the core-shell particles was investigated via the addition of formaldehyde.

4.2.4 Characterization

The molecular weight distribution of the styrene-maleic anhydride (SMA) copolymers was obtained via size exclusion chromatography (SEC). The instrument consisted of a Waters 1515 isocratic HPLC pump, a Waters 717 plus autosampler, a Waters 2487 dual λ absorbance detector and a Waters 2414 refractive index detector at 30 °C. Separation was achieved by using two PLgel 5 μm Mixed-C (300 x 7.5 mm) columns (Polymer Laboratories) connected in series along with a PLgel 5 μm guard column (50 x 7.5 mm). The columns were kept at a constant temperature of 30 °C and THF (Chromasolve, HPLC-grade) stabilized with 0.0125% BHT was used as the eluent at a flow rate of 1.0 mL/min. The system was calibrated with narrow molecular weight polystyrene standards (Polymer Laboratories) ranging from 580–3x10^6 g/mol. Data processing was performed using Breeze Version 3.30 SPA (Waters) software.

^{1}H-NMR spectra were collected from a 400 MHz Varian Unity Inova spectrometer at room temperature in acetone-*d*6 or D_2O and integration of the spectra was carried out with ACD Labs 10.08 1D ^{1}H-NMR processor.

Dynamic light scattering (DLS) was carried out on a Malvern Instruments ZetaSizer 1000HS_a equipped with a He-Ne laser operating at a wavelength of 633.0 nm and the scattered light was detected at an angle of 90°. The latex was diluted with a 1.0 mM aqueous solution of NaCl. The sample was diluted until the rate meter indicated a rate of about 300 kilocounts per second (kCps). The final particle size and particle size distribution were obtained from five measurements, each consisting of ten sub-runs. The particle size and particle size distribution were calculated via a CONTIN analysis[52] and presented as the Z-average particle size (Z_{avg}).

The core-shell morphology of the particles was investigated via transmission electron microscopy (TEM) analysis. The latex was diluted with DDI water until the latex became translucent and 3 μL was transferred onto a hydrophilic carbon-coated copper grid by pipette. Excess sample was removed by blotting with filter paper and the remainder was allowed to dry at ambient temperature before analysis was carried out. No staining agent was required to facilitate contrast, as the core material contains the sufficiently electron-dense sulfur element. The analyses were done on a LEO912 TEM instrument operating with an accelerating voltage of 120 kV. Each sample was analyzed at different areas of the copper grid to obtain representative data and the particle size was determined manually. The particle sizes determined from TEM analysis as presented in this chapter are average values of the different sections.

Fourier transform infrared (FTIR) spectra were recorded on a Nexus FTIR spectrophotometer equipped with a Smart Golden Gate attenuated total reflectance (ATR) diamond from Thermo Nicolet with ZnSe lenses. Each spectrum was scanned 32 times with 4.0 cm^{-1} resolution and data analysis was performed with Omnic Software version 7.2.

4.3 Results and discussion

4.3.1 RAFT-mediated copolymerization of styrene and maleic anhydride

It is well-known that the free-radical copolymerization of styrene and maleic anhydride results in the formation of a close to alternating copolymer, which is governed by the copolymer reactivity ratios r_1 and r_2 ($r_1 << 1, r_2 << 1$ and $r_1 \cdot r_2 \to 0$). Also it is well-documented that the polymerization of styrene and maleic anhydride via living radical polymerization, such as RAFT-mediated polymerization, does not alter the reactivity ratios and consequently also leads to an alternating copolymer (see Chapter 3).[23,35] The tendency of the monomer pair to form an alternating copolymer allows for the one-pot synthesis of a P[(Sty-*alt*-MAh)-*b*-Sty] block copolymer by simply adding an excess of styrene monomer to the reaction formulation.[28,34] Here we employ the RAFT-mediated copolymerization of styrene and maleic anhydride to form alternating styrene-maleic anhydride (SMA) copolymers of different molecular weight. Also chain-extension of this

macroRAFT-agent with styrene after purification of the SMA block is carried out. Although styrene and maleic anhydride have a strong natural tendency to form an alternating copolymer, the most well-defined alternating copolymer will be obtained when both monomers are fed in a one-to-one ratio. The results of the RAFT-mediated styrene-maleic anhydride copolymerizations that are described in this chapter are summarized in Table 4.6.

Table 4.6: SEC results of the RAFT-mediated styrene-maleic anhydride copolymerizations and the chain-extension with styrene

Exp	T (°C)	Time (hrs)	Conversion (%)	$M_{n,th}$ [a] (g/mol)	M_n [b] (g/mol)	PDI[b] (-)
1[c]	60	6	57[i]	3.0×10^3	3.0×10^3	1.14
2[d]	60	6	64[i]	5.2×10^3	4.6×10^3	1.13
3[d]	60	6	60[i]	1.2×10^4	1.0×10^4	1.17
4[e]	60	4.5	75[i]	1.5×10^4	1.6×10^4	1.07
5[f]	70	22	37[j]	x	4.9×10^3	1.17
6[g]	70	21	19[j]	x	1.7×10^4	1.19
7[h]	70	24	20[j]	x	3.0×10^4	1.38

[a] The theoretical molecular weight is calculated via the equation shown at the footnote of Table 4.1 at the final conversion

[b] The molecular weight and the polydispersity are determined via SEC calibrated with narrow PS standards

[c] The RAFT-agent used is cumyl dithiobenzoate (CDB)

[d] The RAFT agent used is 2-cyanoprop-2-yl dithiobenzoate (CIPDB)

[e] The RAFT agent used is p-(2-cyanoprop-2-yl dithiocarboxy) anisole (p-CIPDCA)

[f] The RAFT agent used is the macroRAFT-agent obtained from experiment 1

[g] The RAFT-agent used is the macroRAFT-agent obtained from experiment 3

[h] The RAFT-agent used is the macroRAFT-agent obtained from experiment 4

[i] Conversion determined via ^{1}H-NMR spectroscopy

[j] Conversion estimated from M_n according to SEC analysis and the equation at the footnote of Table 4.1

It can be concluded that the control over the polymerizations was good, as the final molecular weights are in good agreement with the theoretical molecular weight and the

polydispersity indices are low, although no evolution of molecular weight and polydispersity index with conversion was obtained for the polymerizations. For experiments 5–7 no conversion (and consequently theoretical molecular weight) data could be calculated, as during the polymerization some evaporation of solvent, and possibly monomer, took place. It can be seen however, that the loss of solvent did not have a significant influence on the control over the polymerization, as the molecular weights are in the range targeted and the molecular weight distributions are narrow. Additional proof of the control over the polymerizations was obtained from size exclusion chromatography (SEC). For the analysis of the copolymers, the SEC instrument was equipped with an RI-detector in series with a dual wavelength UV-detector. At 320 nm, the thiocarbonyl thio moiety of the RAFT-agents show intense absorption and the absorption at 254 nm is related to the amount of styrene present in the copolymer. Figure 4.1 shows the RI and UV overlap of the molecular weight distributions obtained from experiment 1.

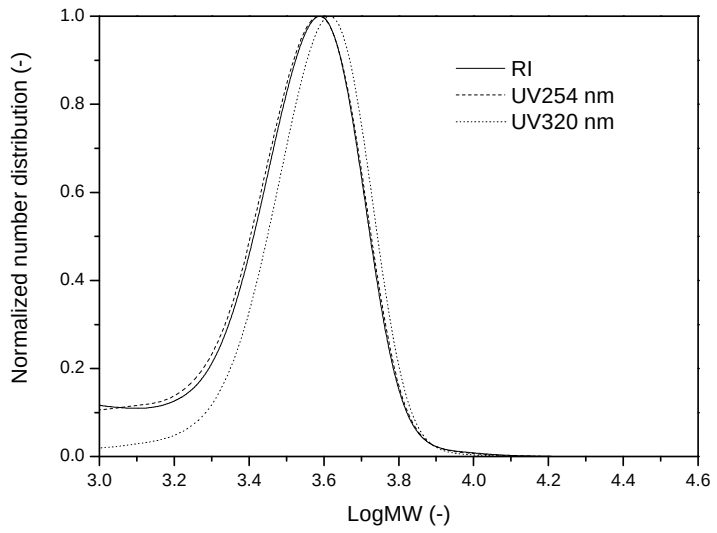

Figure 4.1: Molecular weight distributions obtained from the RI and UV (at 254 and 320 nm) detectors for PSMA (experiment 1, Table 4.6).

The RI and UV254 nm signals show good overlap as expected, although a significant tail towards the low molecular weight side is present. The tailing can be explained by interaction of (partially) hydrolyzed maleic anhydride units with the SEC column, as THF was the eluent.[53] The delay between the RI and UV detector has been compensated for so that both signals overlap at their peak maximum. Furthermore, for a valid approximate comparison between all three signals, the RI and UV254 nm data have been transformed into the number distribution by dividing each point through the molecular weight before normalization to their peak maxima.[54] The UV320 nm data already represent a number distribution, as they are related to the thiocarbonyl thio moiety of the RAFT-agent. It is assumed that all chains do contain the RAFT-moiety as an endgroup. A small fraction of the RI and UV254 nm signals at higher molecular weight do not completely overlap with the UV320 nm signal. This can either be explained by the interaction of the copolymer with the SEC column or that there is a small amount of chains at the high molecular weight side that does not contain the RAFT-endgroup. This imperfection might indicate the occurrence of bimolecular termination of chains.

Another indication of the good control over the polymerizations is provided by the chain-extension of the SMA copolymers with styrene (experiments 5–7, Table 4.6). Figures 4.2 and 4.3 show the molecular weight distributions of the PSMA copolymer and the chain-extended P[(Sty-*alt*-MAh)-*b*-Sty] block copolymer (experiment 5, Table 4.6). Figure 4.2 shows the RI and UV signals of the block copolymer and indicates that good control over the polymerization was obtained. Again, as was seen for the SMA copolymer shown in Figure 4.1, the RI and UV254 nm data show a tail towards low molecular weight, indicating interaction of the block copolymer with the SEC column. The RI and UV254 nm signals also show a small deviation among each other at the low molecular weight side of the distribution. The UV254 nm data have higher intensity, which reveals the (uncontrolled) free-radical homopolymerization of styrene. Also a pronounced shoulder at the high molecular weight side of the distribution of about twice the molecular weight of the peak maximum is observed, indicating that bimolecular termination reactions took place to a small extent.

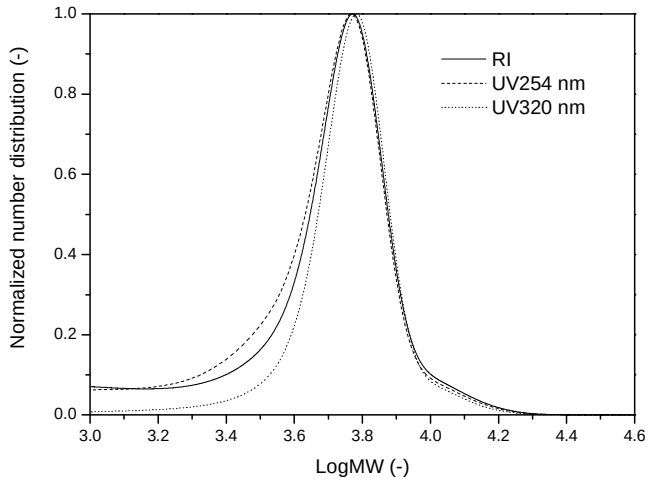

Figure 4.2: Molecular weight distributions obtained from the RI and UV (at 254 and 320 nm) detectors for P[(Sty-*alt*-MAh)-*b*-Sty] (experiment 5, Table 4.6).

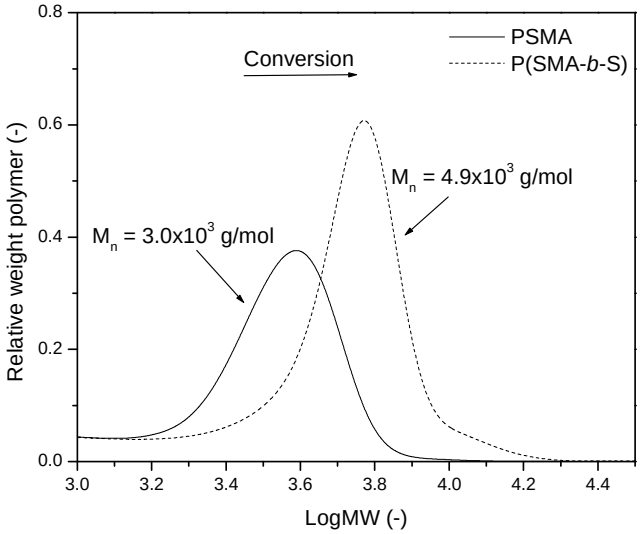

Figure 4.3: Molecular weight distributions (RI-signal) showing the chain-extension of PSMA to P[(Sty-*alt*-MAh)-*b*-Sty] block copolymer (experiment 5, Table 4.6).

Figure 4.3 clearly shows that the chains shift to higher molecular weight indicating that the majority of the polymer chains contain the RAFT-moiety as an endgroup which allows for further growth of the SMA copolymer with styrene, while the distribution remains narrow.

4.3.2 RAFT-endgroup removal and simultaneous ring-opening of maleic anhydride units via ammonolysis

The polymers obtained from the RAFT-mediated copolymerization of styrene and maleic anhydride (Table 4.6) and also commercial SMA1000 ($M_n = 2.6\times10^3 g/mol$, PDI=1.68) were intended to be used as polymeric surfactant for the synthesis of core-shell particles.

It is well-known that SMA copolymers exhibit unique properties for protection of surfaces as wetting agents and that they improve both water resistance and thermal resistance of composite materials.[51,55] In order to become water soluble, the copolymer needs to be hydrophilized by (partial) ring-opening of the maleic anhydride units and this can be accomplished by reaction with a variety of nucleophiles such as sodium hydroxide and primary and secondary amines. Special properties of the SMA copolymer can be obtained by partial reaction of the maleic anhydride units with an alcohol to form an ester. In this way the hydrophilic properties of the SMA copolymer can be tuned. In the work described here, SMA copolymers were synthesized via RAFT-mediated copolymerization and also a commercial SMA1000 was employed for the synthesis of core-shell particles. Because the polymers synthesized via RAFT-mediated polymerization are intensely colored, which is not always practical from an industrial point of view, a lot of research has focused on methods for the removal of the RAFT-endgroup. The methods commonly referred to in the literature include nucleophilic attack by primary or secondary amines,[56-58] thermal elimination,[59] radical induced reduction[60] and radical induced termination.[61] Here we adopted the nucleophilic attack of ammonia to remove the RAFT-endgroup and convert the endgroup of the polymer chain into a thiol. An advantage of this method is that while the RAFT-endgroup is being removed from the polymer chains and thus the color is removed, the maleic anhydride units of the SMA copolymer are simultaneously ring-opened which renders them water soluble. For

the experiments carried out here, a three times molar excess of ammonia over the maleic anhydride units was used to ensure that all the maleic anhydride units would react with ammonia[51] and a twenty times molar excess of ammonia to polymer was used to fully remove the thiocarbonyl thio moiety from the polymer chains.

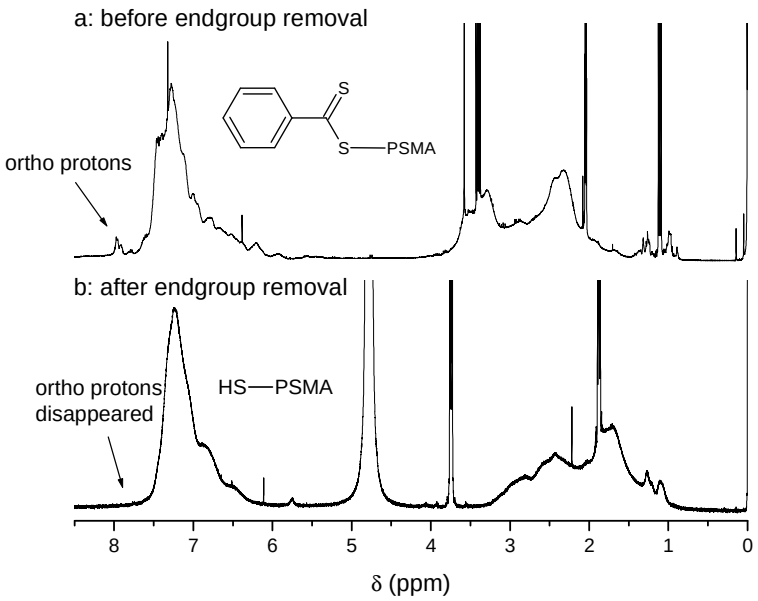

Figure 4.4: RAFT-endgroup removal from PSMA experiment 2, Table 4.6 before (a) and after (b) reaction with ammonia.

The successful removal of the thiocarbonyl thio moiety was confirmed via both ^{1}H-NMR spectroscopy and UV-Vis spectroscopy. Figure 4.4 shows the ^{1}H-NMR spectrum in acetone-*d*6 of the SMA copolymer before endgroup-removal and ring-opening of maleic anhydride units (spectrum a) and also the ^{1}H-NMR spectrum in D_2O after reaction with NH_3 and precipitation of the copolymer in THF (spectrum b). The successful endgroup removal is confirmed by the disappearance of the ortho-protons of the dithiobenzoate-moiety at 7.9 ppm. Before the nucleophilic attack an intense doublet is present, whereas after the reaction this doublet has disappeared. Figure 4.5 shows the corresponding UV-Vis spectroscopy results before and after endgroup removal. It can clearly be observed that the intense absorption of the C=S bond (at 305 nm) has vanished after treatment with ammonia.

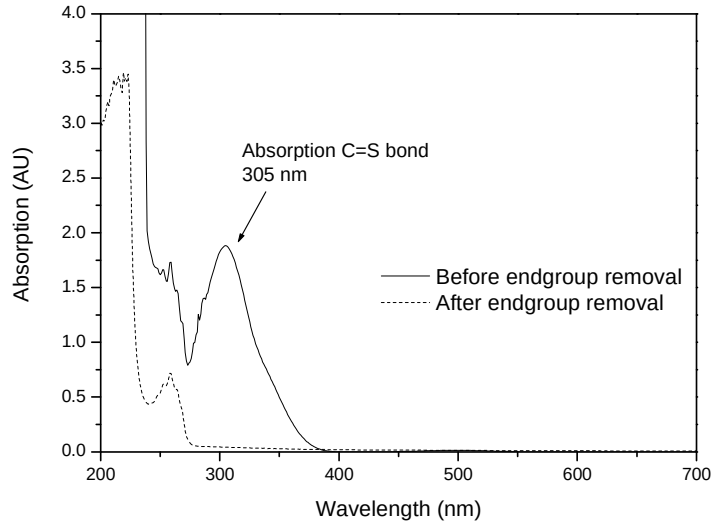

Figure 4.5: Confirmation of RAFT-endgroup removal by UV-Vis spectroscopy.

It must be pointed out that the RAFT-endgroup removal from the block copolymers (P[(Sty-*alt*-MAh)-*b*-Sty]), experiments 5–7, Table 4.6) was not as straightforward as for the SMA copolymers. Several methods have been attempted, such as nucleophilic attack with ammonia and radical attack with a 50 times molar excess of hydrogen peroxide at different temperatures, but although in some cases a color-change was observed, no complete removal of the endgroup was obtained. In addition, the precipitation of the ring-opened version of the block copolymer was unsuccessful, as the P[(Sty-*alt*-MAh)-*b*-Sty] automatically self-assembles into polymeric micelles in a wide variety of solvents. Both aspects might be related, as the thiocarbonyl thio moiety is attached to the hydrophobic side of the block copolymer and therefore will be present in the core of the polymeric micelles and as such be less available at the surface to react with ammonia. Therefore, the P[(Sty-*alt*-MAh)-*b*-Sty] was treated slightly differently from the other SMA copolymers in that the RAFT-endgroup was maintained at the polymer chains and the maleic anhydride units were ring-opened with a three times molar excess of ammonia. Because no suitable solvent could be selected for the precipitation of the block copolymer, excess ammonia was removed by exposing the solution to air, allowing the ammonia to evaporate. This was confirmed by a neutral pH of the solution.

4.3.3 Potential side-reactions of TetraThiol during encapsulation

An investigation into the reactivity of the functional groups of the core material was carried out to assess potential side-reactions that may occur with compounds present in the miniemulsion formulation. Care has to be taken that none of the compounds that are used in excess during the polymerization of the SMA copolymers and during the post-polymerization reactions are present during the emulsification. First of all, TetraThiol contains four ester-groups that are susceptible to nucleophilic attack from ammonia. Therefore, after ring-opening of the maleic anhydride units with excess ammonia, the SMA copolymer needs to be purified by precipitation to assure that all excess ammonia has been removed.

For extra stabilization of the core-shell particles, the SMA copolymer can be cross-linked via various straightforward cross-linking chemistries.[40] Wooley and coworkers reported the cross-linking of acrylic acid with an alkyl diamine in the presence of carbodiimide[47], while Armes and coworkers described the cross-linking of (dimethylamino)ethyl methacrylate (DMAEMA) via quaternization of the tertiary-amine group in the presence of 1,2-bis(2-iodoethoxyethane) and the cross-linking of 2-aminoethyl methacrylate hydrochloride (AMA) via Michael-addition with a diacrylate.[36,37,39,62] An easily accessible route for the cross-linking of the maleic anhydride units in the SMA copolymer is via the reaction with an alkyl dihydrazide.[63] Maleic anhydride is well-known to react with primary and secondary amines and hydrazides and inter- as well as intramolecular cross-linking via the maleic anhydride units takes place. There are two important factors that have to be considered, however. First of all, during cross-linking of the core-shell particles the amount of inter-micellar cross-linking needs to be suppressed. This can be achieved by using low concentrations of core material in the miniemulsion formulation so as to obtain a diluted system. Second, the application of an alkyl dihydrazide for cross-linking purposes must be carefully approached, since the excess of hydrazide might destructively react with TetraThiol via ester hydrolysis, resulting in a monofunctional thiol. Therefore the best approach would be to use a limited amount of alkyl dihydrazide with respect to the available maleic anhydride units during cross-linking.

Another approach for stabilization of the core-shell particles is via the introduction of non-ionic hydrophilic chains that extend into the aqueous phase and as such provide steric stability to the core-shell particles. A model compound for this approach is formaldehyde, which is known to react readily with primary and secondary amines, introducing a hydroxymethyl functionality or an oxymethylene oligomer chain (dependent on the excess of formaldehyde employed). As Figure 4.6 shows, attention needs to be paid that not too much excess of formaldehyde is used during this step, as the formaldehyde is also capable of reacting with the thiol functionalities of the core material, leading to the formation of a thio-ether and the concomitant loss of thiol functionality.

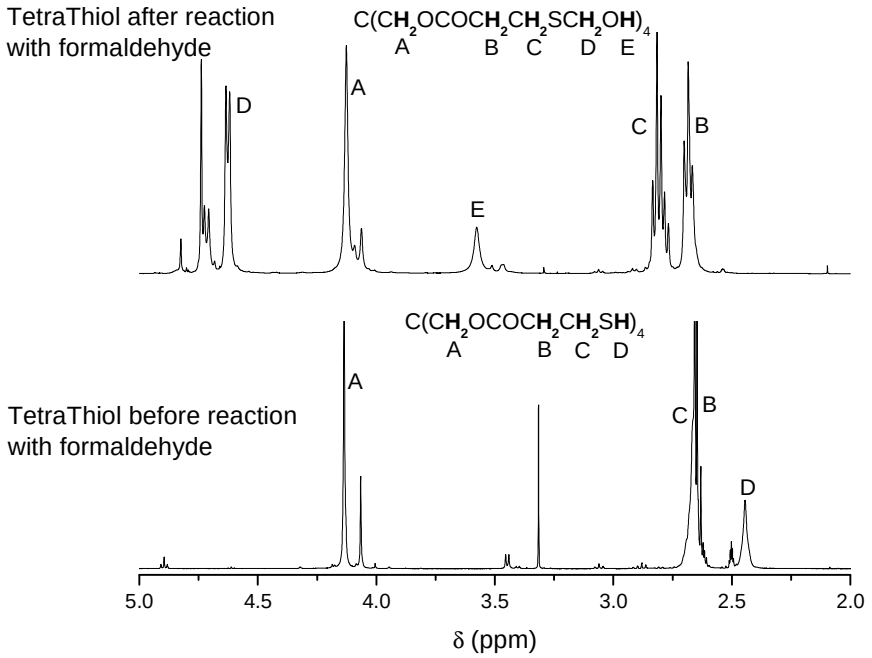

Figure 4.6: ^{1}H-NMR spectra indicating that the reaction of TetraThiol with formaldehyde results in the loss of thiol functionality.

4.3.4 Encapsulation of TetraThiol with SMA1000

After ring-opening of the maleic anhydride units via reaction with ammonia, the SMA copolymers synthesized via RAFT-mediated polymerization and SMA1000 were used as surfactant for the encapsulation of TetraThiol. This section discusses the synthesis of core-shell particles without additional stabilization via either cross-linking or steric stabilization. Only the commercial SMA1000 was employed for this purpose (experiments 1–5, Table 4.2). The oil phase comprised TetraThiol and dichloromethane and the aqueous phase consisted of DDI water and SMA1000 and both phases were premixed via simple stirring with a stirrer bar at 1250 rpm before subjecting the pre-emulsion to ultrasonication. The sole reason for the addition of dichloromethane is to facilitate the dispersion of TetraThiol in the aqueous phase, as TetraThiol is a highly viscous compound. The fact that a tetrafunctional thiol is adopted as the core material eliminated the possibility of (miniemulsion) polymerization, as TetraThiol would simultaneously act as a chain-transfer agent. Stability against coalescence is provided by the addition of a sufficient amount of surfactant whereas TetraThiol itself, having a low vapor pressure and a high viscosity, acts as the osmotic pressure agent. The size of the final particles is dependent on a combination of factors, such as amount of core material, amount of surfactant, the miniemulsification process (stirring speed, time of sonication), the miniemulsion formulation and the viscosity of the core material.[14,64] For the experiments described here it was decided to use a low amount of core material (~2 wt% relative to the aqueous phase) to minimize coalescence and to facilitate encapsulation. The effect of the amount of SMA1000 on the particle size was investigated. The ultrasonication conditions were determined to be optimal when the pre-emulsion was subjected to ultrasonication for 20–30 minutes, during which about 50–75 kJ of energy was supplied to the miniemulsion. The viscosity of the core was controlled by the addition of dichloromethane, which facilitated the dispersion of TetraThiol in the aqueous phase and the break-up of the droplets to provide stable droplets in the nanometer size-range. Table 4.7 shows the particle size and particle size distribution of the core-shell particles synthesized via miniemulsification without the introduction of extra stability via either steric stabilization or cross-linking. Figure 4.7 shows images of the resulting core-shell particles obtained from TEM analysis for experiments 1 and 5 in Table 4.7.

Table 4.7: Particle size and particle size distribution of the core-shell particles synthesized without additional stabilization

Experiment	DLS analysis		TEM analysis
	Particle size (nm)	**Polydispersity (-)**	**Particle size (nm)**
1	309.6±8.6	0.112	300–350
2	274.7±8.1	0.085	250–350
3	275.1±3.8	0.072	175–325
4	242.9±3.0	0.028	250–350
5	298.8±4.7	0.100	250–325

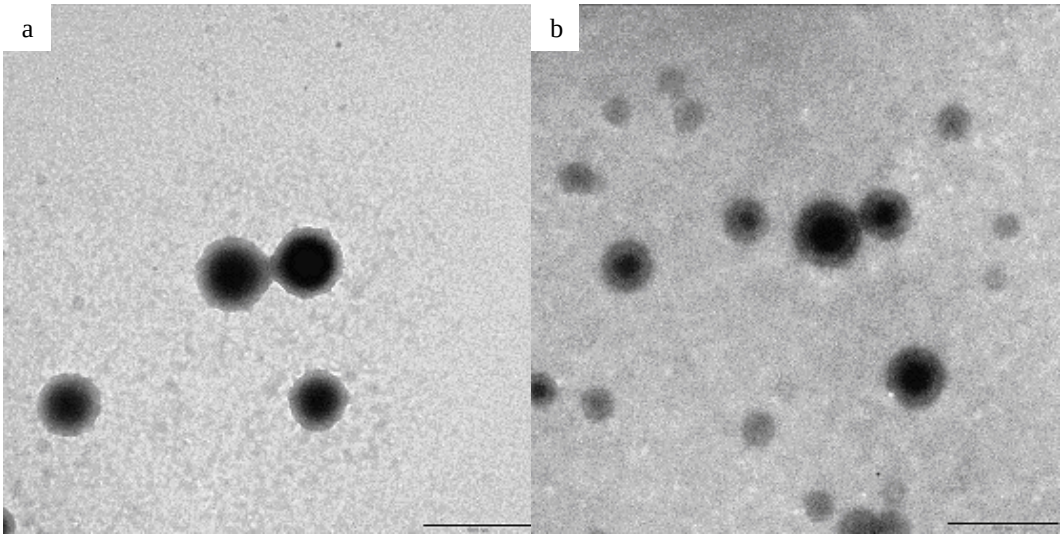

Figure 4.7: TEM images of core-shell particles synthesized with SMA1000 as surfactant, without additional stability (experiments 1 (a) and 5 (b) in Table 4.7). The scale bar in the images represents 500 nm.

From Table 4.7 and Figure 4.7 it can be concluded that well-defined core-shell particles are obtained from the miniemulsification of TetraThiol with SMA1000 as surfactant. The particle sizes obtained from DLS and TEM analysis show good agreement and the particle size distribution is narrow. It must be mentioned though, that certain areas on the copper grid for TEM analysis showed deviation in the particle size from the mean particle size. Therefore Table 4.7 shows the range of particle sizes obtained from TEM analysis at

different sections on the copper grid. Figure 4.7b also shows a distribution of small particles that appear to be empty. This might indicate that the particles consist of a shell of SMA1000 copolymer with only a very small amount or even no core material at all. There are two possible reasons for this. The first one is that the core material could have diffused out of the particles over time, meaning that the surfactant does not provide sufficient stability for the core-shell particles to survive. The second reason is that the initial amount of surfactant present was too high and exceeded the required amount of surfactant to stabilize the core-shell particles. This would lead to the formation of micelles if the surfactant concentration is higher than the critical micelle concentration (cmc), which for copolymers is generally very low.[24] The size of the apparent empty particles appear to be rather big however (~100 nm), which suggests that the empty particles arise from the diffusion of the core-component out of the core-shell particles. This conclusion is further supported by the fact that the long-term stability of the latexes was not optimal, as over a period of a couple of weeks the latexes degraded via precipitation and phase separation. Therefore alternative pathways were approached to synthesize core-shell particles which would provide sufficient stability to the particles so that they would not rapidly degrade to a large extent over time.

4.3.5 Shell cross-linking with urea and formaldehyde

Again SMA1000 was employed as the surfactant for the encapsulation of TetraThiol. It was attempted to stabilize the core-shell particles via cross-linking of the shell with urea and formaldehyde. For this purpose, the maleic anhydride units of the copolymer were ring-opened via reaction with a mixture of urea and ammonia (30–35 mol% of urea). After formation of the pre-emulsion and subjecting the pre-emulsion to ultrasonication, formaldehyde (ratio formaldehyde to urea of 1.8) was added to the system. The temperature of the reaction mixture was raised to 55 °C and allowed to react for four hours. It was anticipated that formaldehyde would react with urea in a similar fashion as during the *in-situ* polymerization of urea and formaldehyde for the synthesis of microcapsules.[65,66] This would result in a densely cross-linked shell and the core-shell particles would be stabilized accordingly. Table 4.8 shows the particle size and particle size distribution of the core-shell particles synthesized with the addition of urea and

formaldehyde for cross-linking purposes. Figures 4.8 and 4.9a–c show images of core-shell particles obtained from TEM analysis.

Table 4.8: Particle size and particle size distribution of core-shell particles synthesized with SMA1000 as surfactant and stabilized via shell cross-linking of urea and formaldehyde

Experiment	DLS analysis		TEM analysis
	Particle size (nm)	Polydispersity (-)	Particle size (nm)
6	355.8±5.4	0.136	300–350
7	395.4±8.4	0.144	200–300
8	204.2±2.3	0.177	150–250
9	261.9±3.8	0.138	300–500
10	253.3±3.9	0.186	200–300
11	253.1±8.3	0.164	200–300

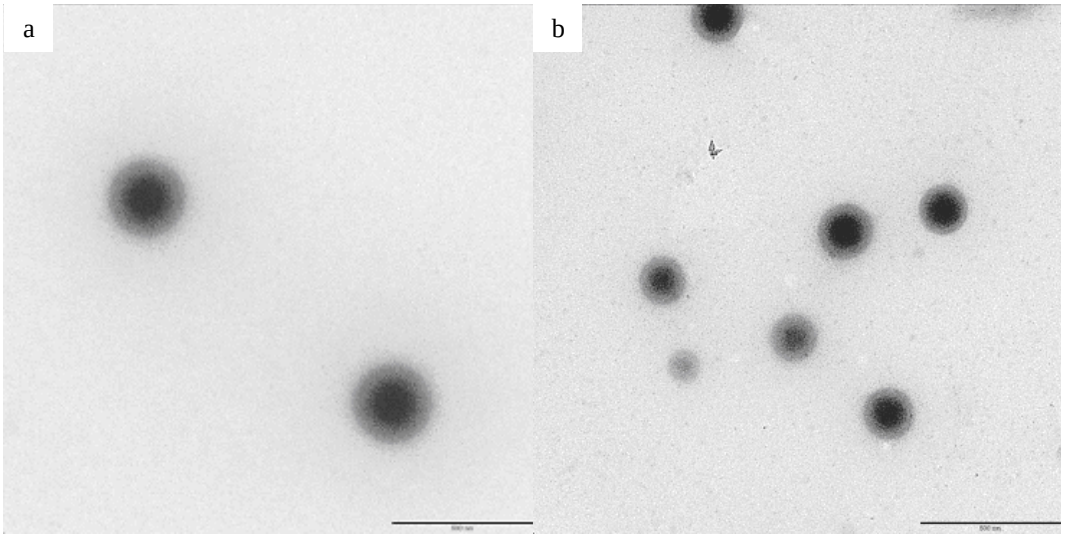

Figure 4.8: TEM images of core-shell particles synthesized with SMA1000 as surfactant and shell cross-linking with urea and formaldehyde (experiments 6 (a) and 7 (b) in Table 4.8). The scale bar in the images represents 500 nm.

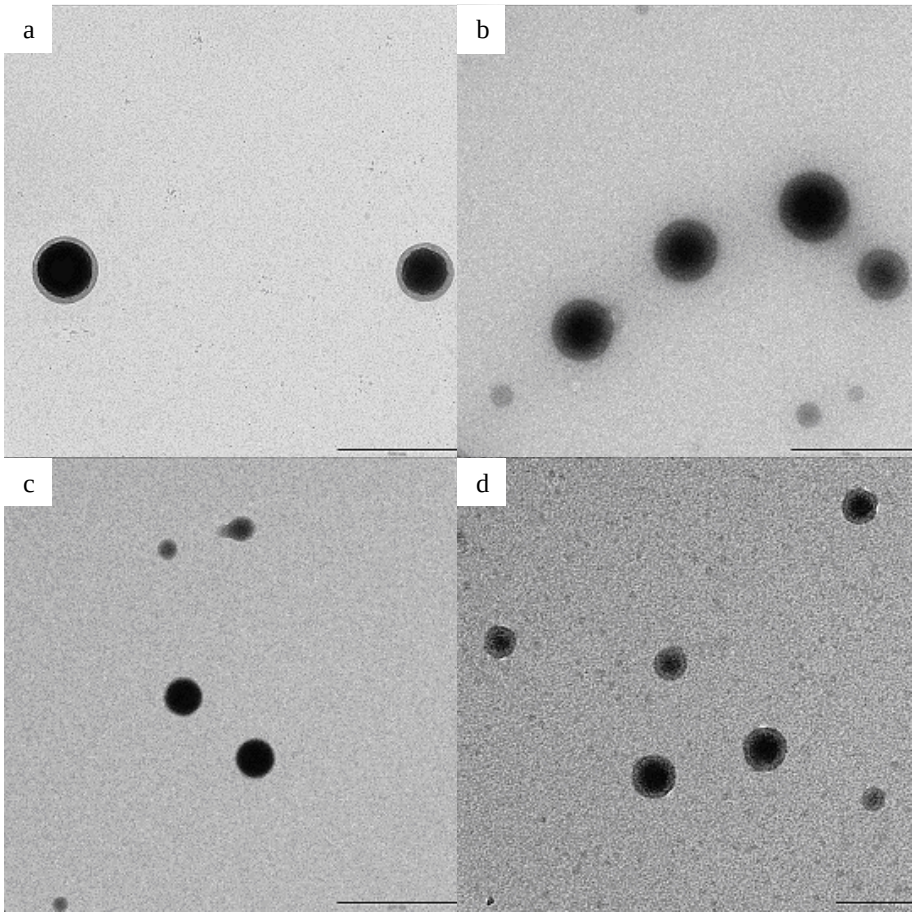

Figure 4.9: TEM images of core-shell particles synthesized with SMA1000 (a–c) or SMA copolymer (d, experiment 1, Table 4.6) as surfactant and shell cross-linking with urea and formaldehyde (experiments 8 (a), 10 (b), 11 (c) and 14 (d) in Tables 4.8 and 4.9). The scale bars in figures a-c represent 500 nm and the scale bar in figure d represents 200 nm.

From Figures 4.8 and 4.9a–c it can be concluded that well-defined core-shell particles are obtained via miniemulsification of TetraThiol and subsequent cross-linking of the shell with urea and formaldehyde. It must be pointed out again that the core-shell particles observed via TEM analysis showed a distribution in size within one sample. The average particle sizes obtained from DLS were in fairly good agreement with those of TEM

analysis, but the particle size distributions (PSD) were rather broad. This may have been caused by bimodality in the particle size distribution.

The amount of SMA1000 was varied for experiments 8 and 9 to get an indication of the influence of the amount of surfactant on particle size and stability. For experiment 8, a higher concentration of surfactant was used and as a result, a smaller particle size was obtained. Figure 4.9a shows that well-defined core-shell particles are obtained. The TetraThiol content in experiment 11 was twice as high as in experiment 10 and from Table 4.8 and Figures 4.9b and 4.9c it can be seen that, although the sizes are comparable, the shell formed in experiment 11 is much thinner.

Table 4.9: Particle size and particle size distribution of core-shell particles synthesized with SMA copolymer as surfactant and stabilized via shell cross-linking of urea and formaldehyde

Experiment	DLS analysis		TEM analysis
	Particle size (nm)	Polydispersity (-)	Particle size (nm)
12[a]	271.2±3.7	0.127	350–450
13[a]	228.5±4.0	0.102	150–250
14[a]	178.6±3.3	0.161	100–200
15[b]	249.1±6.8	0.083	75–100[c]
16[b]	224.4±3.9	0.094	200–250[c]
17[b]	190.2±4.9	0.138	120–150[c]

[a] SMA copolymer used as surfactant obtained from experiment 1, Table 4.6

[b] SMA copolymer used as surfactant obtained from experiment 2, Table 4.6

[c] The majority of particles appear to be empty according to TEM analysis

Another series of experiments was carried out with the SMA copolymers synthesized via RAFT-mediated polymerization and subsequent endgroup removal. Ring-opening of the maleic anhydride units was achieved with a mixture of ammonia and urea (30–35 mol% of urea, Table 4.9). Two different SMA copolymers were used for the encapsulation of TetraThiol, one having a molecular weight of 3.0×10^3 g/mol and the other one with a

molecular weight of $4.6x10^3$ g/mol (Table 4.6). Figure 4.9d shows that small, well-defined core-shell particles are formed, when SMA copolymer is used as surfactant. Table 4.9 shows that the particle sizes obtained from DLS are in fairly good agreement with those obtained from TEM analysis, while the particle size distributions remained reasonably narrow. In experiments 12–14 and 15–17 the concentration of surfactant was varied to investigate the influence of the amount of surfactant on particle size. A common behavior was observed in that the particle size decreased with increasing amount of surfactant, although the particle size distribution slightly broadened. This effect may be accounted for by the introduction of bimodality in the particle size distribution. It is important to note however, that the majority of particles obtained from experiments 15–17 appear to be empty as observed from TEM analysis. As mentioned previously, this may be caused by the diffusion of TetraThiol out of the particles due to instability, leaving small amounts of core material or even empty particles.

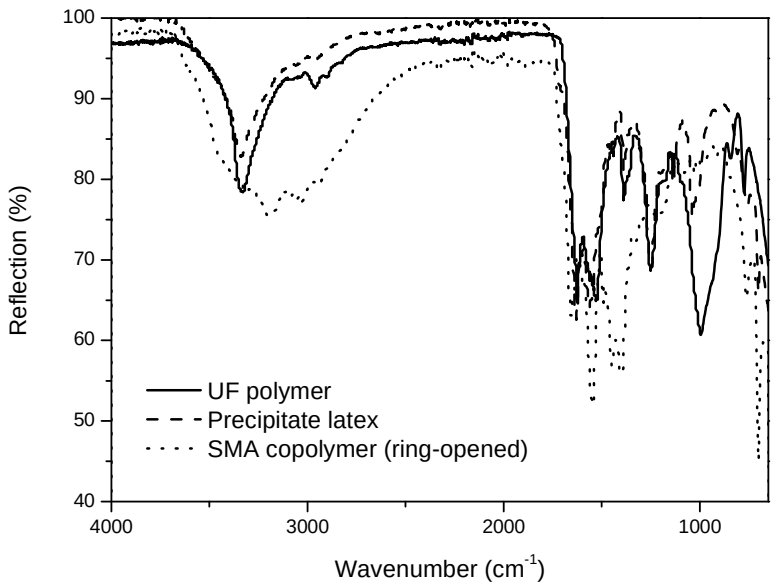

Figure 4.10: IR-spectra suggesting that the precipitate of the latex consists of urea-formaldehyde polymer that is formed in the aqueous phase.

Urea and formaldehyde were introduced into the miniemulsion formulation to increase the stability of the core-shell particles via cross-linking of the shell. In comparison to the experiments where no extra stabilization was applied to the core-shell particles, the stability had indeed improved. However, it is difficult to assess whether urea reacts as efficiently with maleic anhydride as ammonia does and therefore it is hard to determine the exact amount of urea on the polymer backbone. Furthermore, although the *in-situ* polymerization of urea and formaldehyde is well-documented,[65,66] it is unknown whether the experimental conditions employed here allow for the cross-linking reaction as suggested. The incomplete reaction of urea with maleic anhydride is further supported by analysis via IR spectroscopy of the precipitate that formed after a few weeks (Figure 4.10). The precipitate formed consisted mainly of urea-formaldehyde polymer formed in the aqueous phase. This also leads to the conclusion that at least part of the urea employed for reaction with maleic anhydride remained in the aqueous phase, and as such was available for reaction with formaldehyde. Therefore the fraction of urea functionality on the polymer backbone is lower than anticipated, which reduces the extent of cross-linking. In addition, the conditions employed here might not prove suitable for the reaction of formaldehyde with urea.

4.3.6 Alternatives to cross-linking with urea and formaldehyde

Although the previous sections described the synthesis of well-defined core-shell particles, the stability generally was an issue that had to be considered and improved. Because urea did not quantitatively react with maleic anhydride and unknown amounts of urea were left in the aqueous phase, ammonia was adopted for the ring-opening of maleic anhydride. The SMA copolymer was subsequently precipitated and dried in air to assure that no excess ammonia was left in the aqueous phase. It must be realized that drying the SMA copolymer in a vacuum oven would result in ring-closure of the maleic anhydride units, rendering it more hydrophobic and less suitable for use as surfactant. The oil-in-water pre-emulsion was then formed by mixing the oil phase and aqueous phase via homogenization at 9500 rpm. This was done to achieve an optimal dispersion of the oil phase in the aqueous phase and to create small droplets in the nanometer size-range.

Next, the pre-emulsion was subjected to ultrasonication, during which small stable droplets were formed via droplet fission and fusion processes.

For steric stabilization, formaldehyde was chosen to react with the amide of amic acid (maleic anhydride after ring-opening with ammonia/amine) to introduce a hydroxymethyl ($-CH_2OH$) functionality that extends into the aqueous phase. Although formaldehyde is a highly reactive compound towards a large number of functional groups during which it introduces a hydroxymethyl group, the reactivity of formaldehyde with amic acid needs to be assessed. The most well-known reaction of formaldehyde is probably with urea and/or melamine to form a cross-linked urea/melamine-formaldehyde network.[65] Amic acid contains an amide functionality and formaldehyde is likely to react with amic acid in a similar fashion, introducing a hydroxymethyl group. The reaction of maleimide with formaldehyde under basic conditions has been reported.[67] In addition, it has been reported that formaldehyde readily reacts with acetone under basic conditions and introduces a hydroxymethyl group.[68] Only protons on one of the methyl groups of acetone were replaced by a hydroxymethyl group and the number of hydroxymethyl groups introduced was dependent on the ratio of acetone to formaldehyde and the temperature at which the reaction was carried out. Furthermore, it was found that under certain conditions the formation of hemiacetal groups ($-O-CH_2-O-$) was favored over the introduction of additional hydroxymethyl groups. By using higher ratios of formaldehyde to acetone and carrying out the reaction at higher temperatures lead to an increase in the formation of oxymethylene ($-O-[CH_2-O]_n-H$) units (oligomer). In this study a similar approach was adopted and via ^{1}H-NMR and IR spectroscopy it was assessed that the protons of the amide functionality of succinic anhydride (model compound for maleic anhydride, Scheme 4.3) disappear upon reaction with formaldehyde. Paraformaldehyde (oxymethylene oligomer) may be present as a side product. The resulting hydroxymethyl functionality extends into the aqueous phase and provides additional stability to the latex particles.

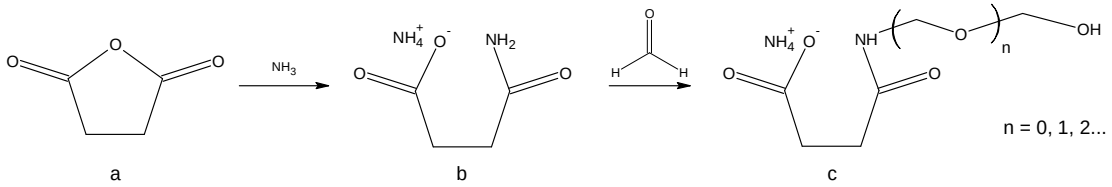

Scheme 4.3: Proposed mechanism for the reaction of succinic anhydride (a) with ammonia to give compound b and subsequent reaction with formaldehyde to give compound c. Succinic anhydride is used as a model compound for maleic anhydride.

By carefully controlling the amount of formaldehyde employed, side-reactions with TetraThiol would be suppressed. Furthermore, as the reaction of formaldehyde with the amide functionality occurs at the interface of the shell and the aqueous phase, side-reactions with the thiol functionality of TetraThiol are probably minimized. Although the addition of formaldehyde did increase the stability of the core-shell particles, the addition of formaldehyde to the latex resulted in a decrease in the pH (~5). By realizing that the acid functionality of the SMA copolymers are protonated at lower pH-values (pH <4) and that the SMA copolymers are only dissolved in the aqueous solution and act as surfactant at pH >4, the core-shell particles will be destabilized at low pH. Therefore, the pH of the latex needs to be controlled so that the SMA copolymer can act as a stabilizer for the core-shell particles.

A different approach to improve the stability of core-shell particles is via the use of a more hydrophobic copolymer as the shell material. It has been reported that the encapsulation of hydrophobic compounds with SMA copolymers is achieved via the reduction of the maleic anhydride content (less hydrophilic), which simultaneously increases the hydrophobicity of the copolymer.[69] Therefore, in this study the commercially available copolymer SMA3000 (Elf Atochem (Sartomer) >98%, styrene to maleic anhydride ratio 3:1, molecular weight $M_n = 4.9\times10^3 g/mol$, PDI=5.41) was chosen to decrease the maleic anhydride content of the copolymer. However, no improvement in the stability of the core-shell particles was obtained.

An alternative to cross-linking of the shell with urea and formaldehyde is via cross-linking with adipic acid dihydrazide.[63,70,71] Soer *et al.* recently reported on the cross-linking of maleic anhydride containing copolymers via 1,6-diaminohexane and adipic acid dihydrazide.[63] It was observed that although 1,6-diaminohexane reacts faster with maleic anhydride (more nucleophilic) than adipic acid dihydrazide, the former interacted with the latex particles leading to destabilization of the latex particles, whereas the latter did not show any interaction with the latex particles. An additional advantage was that the ring-closure of the amic acid functionality into an imide functionality using adipic acid dihydrazide could be carried out at much lower temperatures (<100 °C) and showed no degradation or reversibility towards ring-opening. Therefore, in this study cross-linking of the shell with adipic acid dihydrazide was attempted. A combination of ammonia (to control the hydrophilicity of the polymer) and adipic acid dihydrazide was investigated, but the stability of the core-shell particles proved not to be optimal.

4.3.7 Employment of a block copolymer as surfactant

The use of a P[(Sty-*alt*-MAh)-*b*-Sty] block copolymer as surfactant in the synthesis of core-shell particles was investigated. Precipitation of the ring-opened version of the block copolymer in a non-solvent was unsuccessful due to self-assembly of the block copolymer into polymeric micelles. Therefore excess ammonia used for the ring-opening of maleic anhydride units (while retaining the RAFT-endgroup) was removed by exposing the solution to air and allowing the ammonia to evaporate. The complete removal of ammonia was ascertained by measuring the pH which indicated pH ~7–8. Table 4.10 summarizes details of the core-shell particles synthesized with P[(Sty-*alt*-MAh)-*b*-Sty] as surfactant and reaction with formaldehyde at 55 °C overnight (ratio formaldehyde to amide functionality of approximately eight). Formaldehyde was added for stabilization purposes, as discussed in the previous section. Table 4.6 showed that block copolymers of varying molecular weight were synthesized. Also the molecular weight ratio of the polystyrene block to the SMA copolymer block varied. The ratio of molecular weight of SMA copolymer block to polystyrene block varied from about two to one. This means that the length of the SMA copolymer block varied from roughly twice as large as the polystyrene block to similar size of the blocks.

Table 4.10: Particle size and particle size distribution of core-shell particles synthesized with P[(Sty-*alt*-MAh)-*b*-Sty] block copolymer as surfactant and stabilized via reaction with formaldehyde

Experiment	DLS analysis		TEM analysis
	Particle size (nm)	Polydispersity (-)	Particle size (nm)
18[a]	123.0±2.0	0.376	25–30/150
19[a]	124.2±1.6	0.369	15–20/70
20[b]	86.9±2.3	0.255	25–30
21[c]	105.8±1.7	0.316	25–30/90

[a] P[(Sty-*alt*-MAh)-*b*-Sty] block copolymer used as surfactant obtained from experiment 5, Table 4.6

[b] P[(Sty-*alt*-MAh)-*b*-Sty] block copolymer used as surfactant obtained from experiment 6, Table 4.6

[c] P[(Sty-*alt*-MAh)-*b*-Sty] block copolymer used as surfactant obtained from experiment 7, Table 4.6

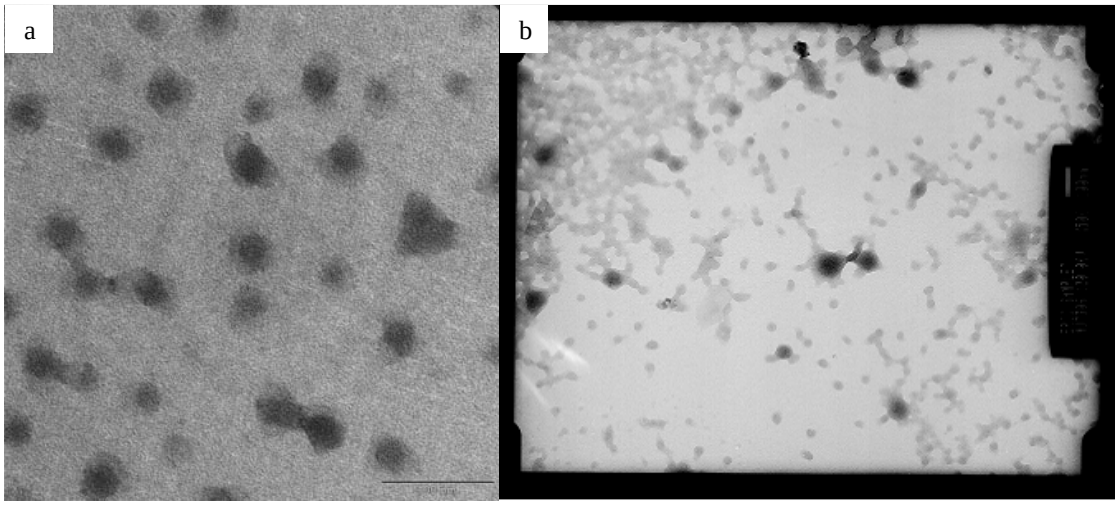

Figure 4.11: TEM images of core-shell particles synthesized with P[(Sty-*alt*-MAh)-*b*-Sty] block copolymer as surfactant and stabilized with formaldehyde (experiment 21 in Table 4.10). The scale bar in image a represents 100 nm. The core-shell particles in image b have a size of about 90 nm and the small particles have a size of about 25–30 nm.

Table 4.10 indicates that although the molecular weight of the block copolymer surfactant increases, the particle size remains roughly the same with a size of around 100

nm. Also the particle size distribution remains broad and DLS analysis showed that the particle size distribution was bimodal. The particle sizes are considerably smaller though, than those obtained for core-shell particles that were stabilized by SMA copolymer. In addition, the stability of the core-shell particles induced by the P[(Sty-*alt*-MAh)-*b*-Sty] block copolymer, after stabilization with formaldehyde, had improved significantly. The bimodal distribution obtained from DLS analysis are in good agreement with those obtained from TEM analysis. DLS analysis only provides a Z_{avg} particle size, but the intensity and volume distributions of the analysis clearly show the presence of a bimodal distribution. The core-shell particles obtained from experiment 21 in Table 4.10 are shown in Figure 4.11. Image a shows that very small particles are present with a size of about 25–35 nm. Image b reveals that in between the numerous small particles also big(ger) core-shell particles are present with a size of about 90 nm, which is in rather good agreement with the sizes of both distributions obtained from DLS analysis. The bimodal distribution can be closely related to the intensity and volume distributions obtained from DLS analysis. The intensity and volume distribution particle sizes are about 120 and 50 nm respectively, which is in reasonably good agreement with the sizes obtained from TEM analysis. The slightly smaller particle sizes obtained from TEM analysis may be related to the fact that TEM analysis considers dry particles whereas DLS analyzes particles in diluted solution.

Although the particles show a considerable improvement in stability, there are a large number of very small particles present. TEM analysis of block copolymer micelles formed in the aqueous phase after reaction with ammonia indicates that the block copolymer micelles have a size of approximately 10–20 nm. Even though the size of the small distribution is only 25–35 nm, they may still contain small amounts of TetraThiol as the core material. This increase in particle size may also be due to reaction of the block copolymer with formaldehyde, which potentially extends into the aqueous phase and provides stability. The large number of small particles seen in the TEM images could indicate that the amount of surfactant was too high to provide sufficient stability to TetraThiol as the core material. However, the amount of surfactant was just below 2 wt% of the aqueous phase, which is not particularly high for standard (mini)emulsion

formulations. The bigger particles in Figure 4.11b clearly show that TetraThiol is present as the core material. Although it was anticipated that TetraThiol would be sufficiently hydrophobic to act as an ultrahydrophobe, the miniemulsification could have benefited from an additional costabilizer that would have provided the formation of a monomodal particle size distribution.

It should be mentioned that the higher molecular weight block copolymer surfactants (experiments 6 and 7 in Table 4.6) provided improved stability to the core-shell particles. This could be explained by the molecular weight of the hydrophobic styrene block, which is very short for the low molecular weight block copolymers. If the attachment of a hydrophobic (polystyrene) block would provide additional stability to the core-shell particles, this block should be of sufficient length and at least be of similar size to the hydrophilic (SMA copolymer) block that forms the shell and separates the aqueous phase from the (TetraThiol) oil phase. Finally, although TetraThiol can not participate in miniemulsion polymerization, because it would act as a chain-transfer agent, miniemulsion polymerization could further improve the stability and homogeneity of the core-shell particles. The stability of monomer droplets obtained from a pre-emulsion are generally not as good as the stability of the polymer particles obtained after polymerization of the pre-emulsion.

4.4 Conclusions

Miniemulsion polymerization allows for the synthesis of (co)polymer latex particles with homogeneity in chemical composition and molecular weight throughout the entire particle size distribution. Via miniemulsion polymerization well-defined, ordered structures can be obtained, such as core-shell particles.

This chapter described the synthesis of core-shell particles via miniemulsification, *i.e.* the formation of a miniemulsion without subsequent polymerization. As core component was chosen TetraThiol, a tetrafunctional thiol that is used in step-growth free-radical thiol-ene polymerization as described in Chapters 5 and 6. The use of this monomer eliminated the possibility of (controlled) free-radical polymerization as it would simultaneously act as a

chain-transfer agent. Initially a commercial SMA1000 copolymer was employed as surfactant, because of its well-documented surfactant-like properties. Also SMA copolymers and P[(Sty-*alt*-MAh)-*b*-Sty] block copolymers were employed as surfactant that were synthesized via RAFT-mediated polymerization. The SMA copolymers were chain-extended with styrene to form well-defined P[(Sty-*alt*-MAh)-*b*-Sty] block copolymers of varying molecular weight. The molecular weight ratio of both blocks was varied and ratios of SMA copolymer to polystyrene of two to approximately one were obtained.

The initial core-shell particles synthesized, using SMA1000 and SMA copolymers (obtained via RAFT-mediated polymerization) as surfactant, were well-defined. The size of the core-shell particles ranged between 150 and 350 nm and the particle size distribution was fairly narrow. The stability of these core-shell particles was not optimal, however. Therefore, formaldehyde was employed as reactant to improve the stability of the core-shell particles by introducing hydroxymethyl groups to the amic acid. Small excess of formaldehyde leads to the introduction of oxymethylene units. Care must be taken that formaldehyde does not react with TetraThiol, as this could lead to the formation of thioether compounds. It was anticipated that TetraThiol would not react as fast with formaldehyde as the amic acid functionality, as the stabilization reaction takes place at the interface of the shell and the aqueous phase. The employment of P[(Sty-*alt*-MAh)-*b*-Sty] block copolymers as surfactant and stabilization via reaction with formaldehyde improved the stability of the core-shell particles considerably. Especially the higher molecular weight block copolymers that contained a polystyrene block of sufficient length provided enhanced stabilization. However, DLS analysis showed a bimodal distribution and TEM images showed a fair amount of very small particles that may not contain a large amount of TetraThiol. The big(ger) particles from the bimodal distribution showed well-defined core-shell particles with a size around 100 nm.

References

1. J.K. Oh, *J. Polym. Sci., Part A: Polym. Chem.* **2008**, *46*, 6983-7001
2. J. Stubbs, R. Carrier and D.C. Sundberg, *Macromol. Theory Simul.* **2008**, *17*, 147-162
3. J. Ugelstad, M.S. El-Aasser and J.W. Vanderhoff, *Polym. Lett. Ed.* **1973**, *11*, 503-513
4. M. Antonietti and K. Landfester, *Prog. Polym. Sci.* **2002**, *27*, 689-757
5. K. Landfester, N. Bechthold, F. Tiarks and M. Antonietti, *Macromolecules* **1999**, *32*, 5222-5228
6. J.M. Asua, *Prog. Polym. Sci.* **2002**, *27*, 1283-1346
7. S. Torza and S.G. Mason, *J. Colloid Interface Sci.* **1970**, *33*, 67-83
8. Y.-C. Chen, V. Dimonie and M.S. El-Aasser, *J. Appl. Polym. Sci.* **1991**, *42*, 1049-1063
9. Y.-C. Chen, V. Dimonie and M.S. El-Aasser, *J. Appl. Polym. Sci.* **1992**, *45*, 487-499
10. S.B. Jhaveri, D. Koylu, D. Maschke and K.R. Carter, *J. Polym. Sci., Part A: Polym. Chem.* **2007**, *45*, 1575-1584
11. B. Erdem, E.D. Sudol, V.L. Dimonie and M.S. El-Aasser, *J. Polym. Sci., Part A: Polym. Chem.* **2000**, *38*, 4431-4440
12. Y.-D. Luo, C.-A. Dai and W.-Y. Chiu, *J. Polym. Sci., Part A: Polym. Chem.* **2008**, *46*, 1014-1024
13. R. Faridi-Majidi, N. Sharifi-Sanjani and F. Agend, *Thin Solid Films* **2006**, *515*, 368-374
14. H. Kim, E.S. Daniels, S. Li, V.K. Mokkapati and K. Kardos, *J. Polym. Sci., Part A: Polym. Chem.* **2007**, *45*, 1038-1054
15. H. Li, P. Li, Y. Yang, W. Qi, H. Sun and L. Wu, *Macromol. Rapid Commun.* **2008**, *29*, 431-436
16. Y. Chen, H. Liu, Z. Zhang and S. Wang, *Eur. Polym. J.* **2007**, *43*, 2848-2855
17. F. Tiarks, K. Landfester and M. Antonietti, *Langmuir* **2001**, *17*, 908-918
18. Y. Luo and H. Gu, *Macromol. Rapid Commun.* **2006**, *27*, 21-25
19. B. Klumperman, *Macromol. Chem. Phys.* **2006**, *207*, 861-863

20. A.J.P. van Zyl, D. de Wet-Roos, R.D. Sanderson and B. Klumperman, *Eur. Polym. J.* **2004**, *40*, 2717-2725
21. C. Scott, D. Wu, C.-C. Ho and C.C. Co, *J. Am. Chem. Soc.* **2005**, *127*, 4160-4161
22. D. Crespy, M. Stark, C. Hoffmann-Richter, U. Ziener and K. Landfester, *Macromolecules* **2007**, *40*, 3122-3135
23. G. Moad, E. Rizzardo and S.H. Thang, *Aust. J. Chem.* **2005**, *58*, 379-410
24. M.-S. Lim and H. Chen, *J. Polym. Sci., Part A: Polym. Chem.* **2000**, *38*, 1818-1827
25. J.-L. Ou, M.-S. Lim and H. Chen, *J. Appl. Polym. Sci.* **2003**, *87*, 2230-2237
26. L. Houillot, C. Bui, M. Save, B. Charleux, C. Farcet, C. Moire, J.-A. Raust and I. Rodriguez, *Macromolecules* **2007**, *40*, 6500-6509
27. K. Stubenrauch, C. Moitzi, G. Fritz, O. Glatter, G. Trimmel and F. Stelzer, *Macromolecules* **2006**, *39*, 5865-5874
28. M.-Q. Zhu, L.-H. Wei, M. Li, L. Jiang, F.-S. Du, Z.-C. Li and F.-M. Li, *Chem. Commun.* **2001**, 365-366
29. F. Cheng, X. Yang, H. Peng, D. Chen and M. Jiang, *Macromolecules* **2007**, *40*, 8007-8014
30. R. Narain and S.P. Armes, *Biomacromolecules* **2003**, *4*, 1746-1758
31. C. He, C. Zhao, X. Chen, Z. Guo, X. Zhuang and X. Jing, *Macromol. Rapid Commun.* **2008**, *29*, 490-497
32. Z. Ge, D. Xie, D. Chen, X. Jiang, Y. Zhang, H. Liu and S. Liu, *Macromolecules* **2007**, *40*, 3538-3546
33. C. Tang, K. Qi, K.L. Wooley, K. Matyjaszewski and T. Kowalewski, *Angew. Chem. Int. Ed.* **2004**, *43*, 2783-2787
34. S. Harrisson and K.L. Wooley, *Chem. Commun.* **2005**, 3259-3261
35. D.S. Germack, S. Harrisson, G.O. Brown and K.L. Wooley, *J. Polym. Sci., Part A: Polym. Chem.* **2006**, *44*, 5218-5228
36. V. Bütün, X.-S. Wang, M.V. de Paz Báñez, K.L. Robinson, N.C. Bilingham, S.P. Armes and Z. Tuzar, *Macromolecules* **2000**, *33*, 1-3
37. V. Bütün, N.C. Bilingham and S.P. Armes, *J. Am. Chem. Soc.* **1998**, *120*, 12135-12136

38. X. Jiang, J. Zhang, Y. Zhou, J. Xu and S. Liu, *J. Polym. Sci., Part A: Polym. Chem.* **2008**, *46*, 860-871
39. S. Liu and S.P. Armes, *J. Am. Chem. Soc.* **2001**, *123*, 9910-9911
40. Y. Li, B.S. Lokitz and C.L. McCormick, *Macromolecules* **2006**, *39*, 81-89
41. Y. Zhang, Z. Wang, Y. Wang, J. Zhao and C. Wu, *Polymer* **2007**, *48*, 5639-5645
42. K.S. Murthy, Q. Ma, C.G. Clark Jr., E.E. Remsen and K.L. Wooley, *Chem. Commun.* **2001**, 773-774
43. J. Zhang, X. Jiang, Y. Zhang, Y. Li and S. Liu, *Macromolecules* **2007**, *40*, 9125-9132
44. J. Babin, M. Lepage and Y. Zhao, *Macromolecules* **2008**, *41*, 1246-1253
45. R.K. O'Reilly, C.J. Hawker and K.L. Wooley, *Chem. Soc. Rev.* **2006**, *35*, 1068-1083
46. K. Qi, Q. Ma, E.E. Remsen, C.G. Clark Jr. and K.L. Wooley, *J. Am. Chem. Soc.* **2004**, *126*, 6599-6607
47. R.K. O'Reilly, M.J. Joralemon, C.J. Hawker and K.L. Wooley, *J. Polym. Sci., Part A: Polym. Chem.* **2006**, *44*, 5203-5217
48. H. Liu, X. Jiang, J. Fan, G. Wang and S. Liu, *Macromolecules* **2007**, *40*, 9074-9083
49. R.K. O'Reilly, M.J. Joralemon, C.J. Hawker and K.L. Wooley, *Chem. Eur. J.* **2006**, *12*, 6776-6786
50. A.D. Ievins, X. Wang, A.O. Moughton, J. Skey and R.K. O'Reilly, *Macromolecules* **2008**, *41*, 2998-3006
51. S.-S. Lee and T.O. Ahn, *J. Appl. Polym. Sci.* **1999**, *71*, 1187-1196
52. R.T.C. Ju, C.W. Frank and A.P. Gast, *Langmuir* **1992**, *8*, 2165-2171
53. J.C.J.F. Tacx, N.L.J. Meijerink and K. Suen, *Polymer* **1996**, *37*, 4307-4310
54. F.M. Saoud, M.P. Tonge, W.G. Weber and R.D. Sanderson, *Macromolecules* **2008**, *41*, 1598-1600
55. J.A. Marsella, C.J. Mammarella and I.K. Meier, *Collloids Surf., A: Physiochem. Eng. Aspects* **2004**, *234*, 63-69
56. V. Lima, X. Jiang, J. Brokken-Zijp, P.J. Schoenmakers, B. Klumperman and R.v.d. Linde, *J. Polym. Sci., Part A: Polym. Chem.* **2005**, *43*, 959-973

57. X.-P. Qiu and F.M. Winnik, *Macromol. Rapid Commun.* **2006**, *27*, 1648-1653
58. J. Xu, J. He, D. Fan, X. Wang and Y. Yang, *Macromolecules* **2006**, *39*, 8616-8624
59. A. Postma, T.P. Davis, G. Moad and M.S. O'Shea, *Macromolecules* **2005**, *38*, 5371-5374
60. Y.K. Chong, G. Moad, E. Rizzardo and S. Thang, *Macromolecules* **2007**, *40*, 4446-4455
61. S. Perrier, P. Takolpuckdee and C.A. Mars, *Macromolecules* **2005**, *38*, 2033-2036
62. L. He, E.S. Read, S.P. Armes and D.J. Adams, *Macromolecules* **2007**, *40*, 4429-4438
63. W.-J. Soer, W. Ming, C.E. Koning and R.A.T.M. van Benthem, *Polymer* **2008**, *49*, 3399-3412
64. B. Sæthre, P.C. Mørk and J. Ugelstad, *J. Polym. Sci., Part A: Polym. Chem.* **1995**, *33*, 2951-2959
65. K. Dietrich, H. Herma, R. Nastke, E. Bonatz and W. Teige, *Acta Polym.* **1989**, *40*, (4), 243-251
66. B.R. Nair and D.J. Francis, *Polymer* **1983**, *24*, 626-630
67. S. Jothibasu, A. Ashok Kumar and M. Alagar, *J. Sol-Gel Sci. Technol.* **2007**, *43*, 337-345
68. Z. Wirpsza, M. Kucharski and J. Lubczak, *J. Appl. Polym. Sci.* **1998**, *67*, 1039-1049
69. A. Shulkin and H.D.H. Stöver, *J. Membrane Sci.* **2002**, *209*, 421-432
70. A. Satoh, K. Kojima, T. Koyama, H. Ogawa and I. Matsumoto, *Anal. Biochem.* **1998**, *260*, 96-102
71. A. Satoh, E. Fukui, S. Yoshino, M. Shinoda, K. Kojima and I. Matsumoto, *Anal. Biochem.* **1999**, *275*, 231-235

Chapter 5: Development of self-healing coatings based on microcapsules[a]

Abstract

This chapter describes the development of a self-healing coating based on urea-formaldehyde microcapsules containing pentaerythritol tetrakis(3-mercaptopropionate) (TetraThiol) and 1,6-hexanediol diacrylate (DiAcrylate) as the healing agents. Thiol-ene step-growth free-radical polymerization serves as the healing mechanism and TetraThiol, DiAcrylate and 1,6-hexanediol di-(*endo, exo*-norborn-2-ene-5-carboxylate) (DiNorbornene) are the monomers used in thiol-ene (photo)polymerization. Kinetic experiments indicate that TetraThiol-DiNorbornene and TetraThiol-DiAcrylate monomer combinations show high rates of polymerization and rapid network formation upon exposure to UV radiation with the addition of a photoinitiator. In addition, the TetraThiol-DiNorbornene system shows fast network formation without the addition of a photoinitiator and/or without exposure to UV radiation. TetraThiol and DiAcrylate are encapsulated separately via *in-situ* polymerization of urea and formaldehyde and microcapsules with a very smooth surface and a particle size of one to ten micrometers are obtained. The rupture of the TetraThiol microcapsules upon crack formation in a coating (poly(methyl acrylate) (PMA) film) is examined with the aid of a rhodamine-based fluorescent probe. Only reaction of the probe with TetraThiol could lead to fluorescence emission. It appears that intense fluorescence emission is observed under a fluorescence microscope after the formation of a cut in the composite PMA film with a razor blade. This means that upon crack formation in the coating, the microcapsules are ruptured and that the healing agent is attracted to the (propagating) crack. The potential self-healing ability of a composite coating containing TetraThiol and DiAcrylate microcapsules (5 wt% relative to the solid content of the matrix) and 0.5 wt% of photoinitiator in a PMA film are investigated. From visual inspection by SEM it seems that the composite coating shows partial recovery at the place of the crack. It can be concluded that the microcapsules do rupture upon crack formation and that the thiol and ene compounds are present at the place where the coating fails. The primary cause for only partial recovery is due to the formation of large aggregates of mainly DiAcrylate microcapsules that do not rupture, which reduces the efficiency of self-healing.

[a] The results described in this chapter are filed in a patent application with number EP09150796.2

5.1 Introduction

During the last decade a considerable amount of research has focused on the exploration of the concept of self-healing coatings.[1] Generally, a coating applied onto a metal surface serves to protect the surface from corrosion caused by exposure to air, water and chloride ions. This type of coating can be classified as a passive anti-corrosive coating. Recently, research has focused on the development of an active anti-corrosive coating that (autonomously) repairs the coating upon the formation of an invisible microcrack within the coating, and restores its (mechanical) properties and prevents the coating from failing.

In order to protect a metal substrate against corrosion, hexavalent chromium ions are usually incorporated in the coating formulation. Although chromium(VI) compounds are the most effective solution for the design of anti-corrosive coatings so far, they suffer from serious drawbacks as they are highly toxic and are suspected carcinogens.[2-5] Research has focused therefore on potential alternatives. In this regard Aramaki reported on the anti-corrosive properties of a zinc-electrode that was coated with a film containing sodium silicate and cerium(III)nitrate.[2] By scratching the surface of the coated electrode and immersing it into a sodium chloride solution, no corrosion at the surface of the electrode could be detected. It was hypothesized that the silicate and cerium ions diffuse out of the scratched film and suppress zinc corrosion. The current approach and a potential substitute for the chromium(VI) compounds focuses on sol-gel derived films.[3-6] However, although inorganic sol-gel coatings show good adhesion to the metal surface and provide a dense barrier for corrosive agents, the coating alone is not sufficient to protect the metal surface from corrosion. Because the coating contains micropores, cracks and areas of low cross-link density, these defects provide a path for diffusion of corrosive agents to the coating/metal interface. Addition of an organic component to the inorganic sol-gel (hybrid sol-gel) leads to the formation of thicker and more flexible films with better compatibility with organic top coats. These hybrid sol-gel coatings can be reinforced by doping with nanoparticles that improve corrosion protection properties. This improvement results from the reduced porosity and cracking potential of such films. Corrosion protection of the metal surface can be further improved by the incorporation of inorganic or organic inhibitors into the sol-gel film.[7] Common examples of inorganic

inhibitors are phosphates, vanadates and cerium salts and examples of organic inhibitors are phenylphosphonic acid, mercaptobenzothiazole and triazole.[5,8] The limitation of this approach is that only a low critical concentration of free inhibitor can be incorporated in the matrix, because at higher concentrations the sol-gel matrix suffers from defects such as crack-formation due to the incorporation of these inhibitors.[5,7] To overcome the negative effects of incorporating free inhibitor in the matrix, the inhibitor can be incorporated in nanometer-scale reservoirs.[8,9] These nanoreservoirs can be homogeneously distributed in the coating and store the inhibitor and only release the substance on demand over a prolonged time.[5]

Apart from protecting a substrate against environmental influences, considerable advancements have been made over the past decade in the development of a self-healing polymer coating.[1] Upon the formation of an invisible microcrack, this type of coatings aims to autonomously self-repair the crack and restore its mechanical properties and prevent the coating from failing.[10] This brings about huge advantages, as non-destructive techniques aiming to detect internal cracks have a limited resolution. The general approach is to embed microcapsules that contain a healing agent in the coating. Dependent on the healing mechanism that is approached, a catalyst is embedded in the matrix. For the coating to function as a self-healing coating, certain criteria have to be met.[11,12] The capsules with their reactive content should be homogeneously distributed in the matrix and only break and release their charge upon the formation of a crack in the coating. The content should be released into the propagating crack via capillary action and the healing reaction should be autonomously triggered, for example by making contact with a catalyst that is embedded in the coating. Furthermore, the reaction should be fast, be able to take place at room temperature and proceed in an environment exposed to oxygen or moisture. This means that the resin that is chosen as the wall material for the synthesis of the microcapsules forms a strong, impermeable, durable shell that is resistant to mechanical and thermal stress. A well-documented procedure for the preparation of such microcapsules is via the condensation reaction of urea and/or melamine with formaldehyde to form the wall material.[13-21] A different approach for the synthesis of

microcapsules was reported by Xiao *et al.* who adopted epoxy resin as the wall material for the UV radiation induced interfacial polymerization.[22]

One interesting approach for the development of a self-healing coating recently put forward by Caruso *et al.* describes a solvent-promoted healing mechanism.[23] This approach is based on the encapsulation of a solvent via *in-situ* polymerization of urea and formaldehyde (UF). Upon the occurrence of a crack, the UF capsules break and release their content. It was suggested that the solvent plasticizes the matrix and allows the mobility of the solvent molecules which promotes further curing reactions. A number of reports have appeared on the encapsulation of self-healing agents via *in-situ* polymerization of UF.[11,12,24-26] These UF microcapsules were embedded in various polymer matrices and tested for their self-healing ability. It appeared that the UF microcapsules provided good stability and only released the healing agent when they were ruptured. Also the healing efficiency of the self-healing coatings, defined as the ratio of the fracture toughness of the healed specimen to the fracture toughness of the virgin specimen, was high and in some cases even higher than 100%.[12,24] The concentration of microcapsules and the size and concentration of the catalyst had a significant influence on the fracture toughness of the composite material, and under optimized conditions the fracture toughness was improved compared to that of the virgin material. White and coworkers extensively investigated one particular self-healing coating based on UF microcapsules containing dicyclopentadiene that were embedded in an epoxy matrix together with Grubbs' catalyst. They investigated separately the cure kinetics of dicyclopentadiene with different amounts of Grubbs' catalyst via differential scanning calorimetry (DSC) and concluded that the amount of catalyst has a large effect on the cure kinetics.[27] By observing that the catalyst is not homogeneously distributed in the epoxy matrix and that only large aggregates are present along the crack surface, they tried to improve the efficiency of the healing mechanism by encapsulating the catalyst in wax.[28] They found that the protected catalyst is homogeneously distributed in the epoxy matrix and that the catalyst is released upon crack formation. Much lower concentration of catalyst is needed to perform equally well to the system where the catalyst is not homogeneously dispersed and present as large aggregates. They further investigated the

influence of UF microcapsules toughened epoxy on crack-tip shielding mechanisms during fatigue.[29] They initially embedded UF microcapsules containing dicyclopentadiene in the epoxy matrix without the addition of catalyst. Upon crack formation they injected pre-catalyzed monomer into the crack plane and observed that under certain conditions crack arrest and extension of the fatigue life was obtained. They extended these experiments with the embedding of the catalyst into the epoxy matrix.[30] Under the applied range of cyclic stress intensity (ΔK_I) investigated, significant crack arrest and life extension from the *in-situ* healing mechanism was obtained. Recently Keller *et al.* and Yuan *et al.* reported on self-healing polymeric materials based on a two-component healing agent.[31,32] Both components of the healing agent were encapsulated separately in microcapsules via *in-situ* urea-formaldehyde polymerization. The rupture of the capsules upon crack formation and the subsequent healing of the matrix was reported.

A promising cross-linking chemistry that can be approached as healing mechanism in self-healing coatings and that meets the requirements for autonomic reparation of coatings, is cross-linking via thiol-ene chemistry. A recent review on thiol-ene chemistry by Hoyle *et al.* describes the development of thiol-ene photopolymerization during recent years and highlights the flexibility and advantages of thiol-ene chemistry regarding polymerization mechanism and conditions employable in comparison with traditional free-radical polymerization.[33] In thiol-ene chemistry, linear polymer chains can be formed by using dithiols and dienes, whereas a densely cross-linked network can be build by the adoption of tri- or tetrafunctional thiols and enes. Because thiol-ene chemistry proceeds via a step-growth polymerization mechanism, gelation of the network occurs at high conversions resulting in a homogeneous network with improved mechanical properties. Bowman *et al.* and Hoyle *et al.* extensively investigated the kinetics of thiol-ene chemistry for a variety of functional enes.[34-37] It appeared that the electron density of the double bond of the ene is related to the reactivity of the ene in thiol-ene chemistry. The higher the electron density of the double bond, the higher is the reactivity of the ene towards chain-transfer reactions with thiol. Furthermore, by using an ene with an acrylate functionality introduces the possibility of acrylate homopolymerization parallel with thiol-ene polymerization. This approach was further exploited by the investigation of

ternary thiol-ene systems by the same authors.[38-41] Because thiol-ene chemistry shows great flexibility in the type of ene that is employed and because the densely cross-linked network is only formed at high conversions, mechanical properties of the resulting network and the glass transition temperature (T_g) can be tuned.[42-44]

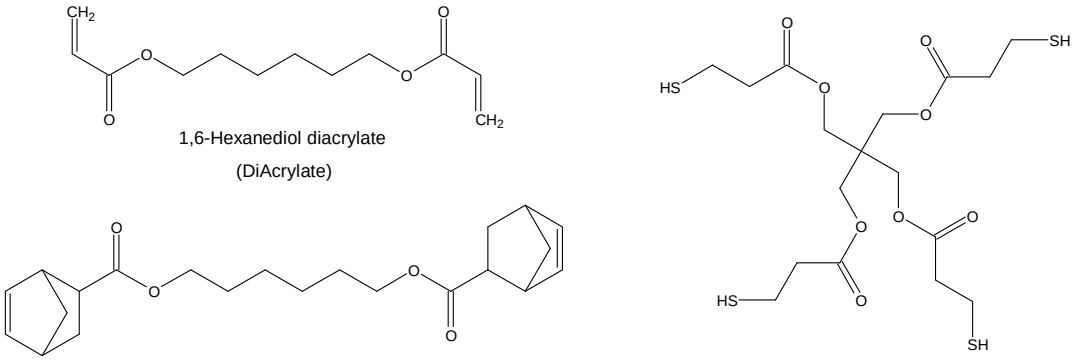

Scheme 5.1: Compounds that serve as core material for the synthesis of microcapsules via *in-situ* polymerization of urea and formaldehyde.

This chapter focuses on the development of a self-healing coating via the incorporation of urea-formaldehyde microcapsules that contain a reactive healing agent, either pentaerythritol tetrakis(3-mercaptopropionate) (TetraThiol), 1,6-hexanediol diacrylate (DiAcrylate) or 1,6-hexanediol di-(*endo*, *exo*-norborn-2-ene-5-carboxylate) (DiNorbornene) (Scheme 5.1). These compounds are encapsulated separately and are designed to react according to thiol-ene cross-linking chemistry. Some of the main advantages of thiol-ene chemistry for the current investigation are that no initiator is required to initiate the polymerization and that the reaction takes place at room temperature under the influence of UV radiation. The subsequent embedding of these microcapsules into an acrylic coating formulation is described together with the self-healing ability of the resultant coating upon the introduction of a crack with a razor blade. The morphology and size of the urea-formaldehyde microcapsules are investigated via scanning electron microscopy (SEM) as well as the morphology of the cross-section of

the cracked coating before healing and the surface of the cracked coating after exposure to UV radiation.

5.2 Experimental details

5.2.1 Chemicals

Methyl acrylate (MA, Aldrich 99% (GC), [96-33-3]) was purified by passing it through a column of inhibitor remover (Aldrich, [9003-70-7]) and 2,2'-azobis(isobutyronitrile) (AIBN, Riedel de Haën) was recrystallized from ethanol and dried under vacuum. Urea (Merck 99.5%), formaldehyde (37 wt% solution in water, Sigma-Aldrich ACS reagent, [50-00-0]), resorcinol (Saarchem uniLAB 99%), NaCl (Scienceworld 99.5%), pentaerythritol tetrakis(3-mercaptopropionate) (TetraThiol, Fluka ≥96%, [7575-23-7]), SMA1000 (Elf Atochem (Sartomer) >98%, styrene to maleic anhydride ratio 1:1, molecular weight $M_n = 2.6\times10^3\, g/mol$, PDI=1.68), sodium hydroxide (NaOH, Saarchem uniLAB ≥97%), 3-dimethylamino-1-propylamine (Fluka ≥98% (GC), [109-55-7]), 1,6-hexanediol diacrylate (DiAcrylate, Aldrich technical grade 80%, [13048-33-4]), dicyclopentadiene (Aldrich, [77-73-6]), phenothiazine (Fluka ≥98% (GC), [92-84-2]), potassium persulfate (KPS, Riedel de Haën 99%, [7727-21-1]), sodium hydrogencarbonate ($NaHCO_3$, R&S Enterprises 99.5%), sodium dodecylsulfate (SDS, BDH Laboratory Supplies 90%), rhodamine 110 chloride (Fluka Analytical ≥99% (UV), [13558-31-1]), 2,4-dinitrobenzenesulfonyl chloride (Aldrich, [1656-44-6]), potassium *tert*-butoxide (KO-*t*-Bu, Fluka ≥97.0%, [865-47-4]), *N*,*N*-dimethylformamide (DMF, Saarchem univAR ≥99.0%), tetrahydrofuran (THF, Kimix CP), ethyl acetate (Sasol Class 3) and 2,2-dimethoxy-2-phenylacetophenone (Aldrich 99%, [24650-42-8]) were all used without further purification. Distilled water was used throughout the experiments described in this chapter, unless stated otherwise.

*5.2.2 Synthesis of 1,6-hexanediol di-(*endo, exo-*norborn-2-ene-5-carboxylate)*

The synthesis of 1,6-hexanediol di(*endo, exo*-norborn-2-ene-5-carboxylate) (DiNorbornene) was achieved in two steps. In the first step dicyclopentadiene was cracked to form its monomer cyclopentadiene. Cyclopentadiene was then reacted via a Diels-Alder reaction with 1,6-hexanediol diacrylate to form DiNorbornene.

A distillation setup was used for the cracking of dicyclopentadiene. A 250 mL round-bottom flask containing boiling stones was charged with 73.85 g of dicyclopentadiene (0.56 mol) and heated in a heating mantle until the dicyclopentadiene started boiling (at approximately 160 °C). The fraction of cyclopentadiene monomer distilled smoothly at a temperature around 40 °C. Care has to be taken that cyclopentadiene is immediately used in the next step, as the monomer rapidly dimerizes at room temperature.[45]

A 250 mL three-neck round-bottom flask equipped with a dropping funnel, a condenser and a nitrogen inlet was charged with 50 g of 1,6-hexanediol diacrylate (0.22 mol) and the flask was purged with nitrogen gas. To prevent the monomer from polymerizing at elevated temperatures, 0.082 g of phenothiazine (~2000 ppm) was added as a thermal stabilizer. The three-neck round-bottom flask was preheated to 80 °C and 37 g of cyclopentadiene monomer (0.56 mol) was slowly added to 1,6-hexanediol diacrylate via the dropping funnel. After complete addition of cyclopentadiene, the mixture was allowed to react for a further four hours. The resulting solution was subjected to vacuum distillation to remove impurities cyclopentadiene and dicyclopentadiene. The yield of DiNorbornene was ~75 g (95%) and the purity checked with ^{1}H-NMR spectroscopy was >98%. ^{1}H-NMR ($CDCl_3$), δ (ppm) downfield from TMS: 1.19–2.26 (-C**H$_2$**-, 17H), 2.80–3.27 (-C**H**(CH_2)-, 5H), 3.94–4.14 (-C**H$_2$**-O-, 4H) and 5.85–6.25 (-C**H**=C**H**-, 4H).

5.2.3 Synthesis of rhodamine-based fluorescent probe

A glass vial was charged with 0.1018 g of rhodamine 110 chloride (0.28 mmol) and dissolved in 1.90 g of DMF. Separately, 0.0919 g of KO-*t*-Bu (0.82 mmol, three times molar excess to rhodamine 110 chloride) was dissolved in 1.77 g of THF. The KO-*t*-Bu solution was added dropwise to the rhodamine solution while being cooled in an ice bath and left to stir for half an hour. After half an hour, 0.2214 g of 2,4-dinitrobenzenesulfonyl chloride (0.83 mmol, three times molar excess to rhodamine 110 chloride) was added to the rhodamine solution while the temperature was kept at 0 °C. After stirring for two hours, 0.2226 g of 2,4-dinitrobenzenesulfonyl chloride (0.83 mmol, three times molar excess to rhodamine 110 chloride) was added to the solution and the reaction was allowed to proceed for 16 hours at room temperature. The solution was diluted with ethyl

acetate and washed three times with a saturated $NaHCO_3$ solution. The solvent was removed under reduced pressure and the raw product was purified by column chromatography using silica (Silica Gel 60, 0.063–0.12 mm/70–230 mesh) as the stationary phase. The initial eluent was hexane:ethyl acetate 2:1 and this was gradually changed to hexane:ethyl acetate 1:1 and eventually to hexane:ethyl acetate 1:2. The disubstituted rhodamine-based fluorescent probe eluted with hexane:ethyl acetate 1:1 and the monosubstituted rhodamine-based fluorescent probe eluted with hexane:ethyl acetate 1:2. The disubstituted rhodamine-based fluorescent probe is the compound of interest and the yield of the reaction was 26.1 mg (12%). The purity was checked with ^{1}H-NMR spectroscopy and was 98%. ^{1}H-NMR (acetone-*d*6), δ (ppm) downfield from TMS: 6.83 (2H, d, ^{3}J=8.6), 7.12 (2H, dd, ^{3}J=8.6, ^{4}J=2.2), 7.24–7.28 (1H, m), 7.35 (2H, d, ^{4}J=2.2), 7.74 (1H, td, ^{3}J=7.5, ^{4}J=1.0), 7.79 (1H, td, ^{3}J=7.5, ^{4}J=1.1), 7.97–8.01 (1H, m), 8.43 (2H, d, ^{3}J=8.6), 8.62 (2H, dd, ^{3}J=8.7, ^{4}J=2.3) and 8.80 (2H, d, ^{4}J=2.4).

5.2.4 Emulsion polymerization of methyl acrylate

To a 250 mL three-neck round-bottom flask was added 70 g of distilled deionized water, 0.70 g of SDS (1 wt% of the aqueous phase) and 0.036 g of $NaHCO_3$ (0.05 wt% of the aqueous phase). To this solution was added 30 g of MA and an emulsion was formed by stirring at 500 rpm for 30 minutes. A solution containing 0.024 g of KPS (0.075 wt% of MA) was added to the emulsion and the solution was purged with a nitrogen flow to remove the oxygen from the system. An oil bath was heated to 85 °C while the solution was being degassed and once the oil bath reached 85 °C, the flask was immersed in the oil bath and the reaction was allowed to proceed for 4 hours. After polymerization a latex was obtained with 30% solid content and with a particle size of 125 nm and a particle size distribution of 0.025. The molecular weight and molecular weight distribution of the final polymer were $5.1x10^5$ g/mol and 2.24 respectively.

5.2.5 Synthesis of urea-formaldehyde microcapsules

For the synthesis of the urea-formaldehyde (UF) microcapsules a styrene-maleic anhydride copolymer (SMA1000 or SMI1000) was used to provide stabilization of the oil droplets during emulsification and to facilitate encapsulation of the oil phase via *in-situ*

polymerization of urea and formaldehyde. In case SMA1000 was used as the surfactant, the maleic anhydride units were ring-opened by reaction with NaOH. For this purpose 5.02 g of SMA1000 (0.025 mol of maleic anhydride) and 2.09 g of NaOH (0.052 mol) were mixed in distilled water and after the polymer had dissolved in the aqueous phase, the pH of the solution was decreased to approximately 7 by the addition of an appropriate amount of a 5 wt% solution of hydrochloric acid. The SMI1000 copolymer was synthesized via ring-opening of the maleic anhydride units of SMA1000 by reaction with 3-dimethylamino-1-propylamine. The subsequent ring-closure to form the imide took place under vacuum at 100 °C. A 50 mL three-neck round-bottom flask was charged with 5.01 g of SMA1000 (0.025 mol of maleic anhydride) and 5.67 g of 3-dimethylamino-1-propylamine (0.055 mol) in distilled water. After the copolymer had dissolved in the aqueous phase, the copolymer was precipitated in THF and dried under vacuum at 100 °C to afford ring-closure and formation of maleimide. The resulting SMA1000 and SMI1000 copolymers were water soluble at acidic pH (~3–4).

A typical procedure for the synthesis of the UF microcapsules was as follows. To a 50 mL three-neck round-bottom flask was charged 2.0 g of urea (0.033 mol) and 5.2 g of a 37% solution of formaldehyde (0.064 mol of formaldehyde) so that the ratio of formaldehyde to urea was kept above 1.8. After homogenization, the pH of the mixture was raised to ~9 via the addition of a few drops of a 5 wt% solution of NaOH. The flask was immersed in an oil bath preheated to 70 °C and left to react for one hour. This resulted in the formation of UF prepolymer. Separately, 6.59 g of a SMA1000 solution in distilled water (0.80 g of SMA1000), 0.20 g of resorcinol and 0.20 g of NaCl were dissolved in distilled water (the total mass of distilled water was 100 g) and the pH was decreased to ~3. Then 20.0 g of TetraThiol (Scheme 5.1) was added to the aqueous phase and the oil-in-water emulsion was formed by stirring for about half an hour at a stirring speed of 500 rpm. The UF prepolymer was added to the oil-in-water emulsion and the pH of the mixture was corrected to pH ~3.0 via the addition of a few drops of a 5 wt% solution of hydrochloric acid. The *in-situ* polymerization of urea and formaldehyde was allowed to continue for two hours at 55 °C while the pH was carefully monitored and kept at ~2.5–3.0. After two hours the dispersion was cooled down and the pH was raised

to 7. The capsules were washed three times with distilled water and rinsed twice with chloroform or acetone to remove excess TetraThiol that was not encapsulated. The microcapsules were collected and dried in a vacuum oven overnight at 50 °C. The yield of UF microcapsules was ~10–12 g (70–90%).

The synthesis of UF microcapsules with hexadecane or diene (1,6-hexanediol diacrylate or 1,6-hexanediol di(*endo, exo*-norborn-2-ene-5-carboxylate)) as core compound (Scheme 5.1) proceeded in a similar way as the synthesis of the UF microcapsules with TetraThiol core. The reaction generally resulted in a poor yield of about 10% (2.5–3.0 g of UF microcapsules).

5.2.6 Thiol-ene (photo)polymerizations

Thiol-ene polymerizations were carried out either *in-situ* in a DSC instrument to determine the cure kinetics or by exposing the sample to UV radiation. In either case the experiment was carried out with and without the addition of a photo- (UV) or thermal (DSC) initiator. For a typical experiment 0.50 g of TetraThiol (1.02 mmol), 0.74 g of DiNorbornene (2.06 mmol) and 0.0045 g of 2,2-dimethoxy-2-phenylacetophenone (0.9 wt% to TetraThiol) were mixed in a vial. Once homogeneous, the solution was placed in an aluminum sample pan and the solution was exposed to UV radiation for a predetermined time. Generally the exposure to UV radiation resulted in the formation of a polymer network within a couple of minutes.

5.2.7 Incorporation of microcapsules in a paint formulation

Initially only microcapsules containing TetraThiol or DiAcrylate were embedded in the coating. 5–10 wt% of microcapsules, relative to the solid content of the paint, were mixed with the paint and homogeneously distributed via stirring. As matrix was used the poly(methyl acrylate) (PMA) latex prepared as described in Section 5.2.4. The composite coating was then air-dried in an aluminum pan and the cross-section was investigated via scanning electron microscopy (SEM) upon crack formation induced with a razor blade.

The preparation of a self-healing coating was approached in a similar way, but in this case 5–10 wt% of both DiAcrylate or DiNorbornene and TetraThiol microcapsules, relative to the solid content of the paint, were incorporated in the coating. In addition, ~0.5 wt% of photoinitiator (2,2-dimethoxy-2-phenylacetophenone) relative to TetraThiol was dispersed in the composite coating.

5.2.8 Characterization

SEM analysis was carried out on a Leica S440 instrument. The samples were placed on a SEM grid and coated with a layer of gold-palladium to induce contrast and reduce charging of the sample. Powder samples were dispersed in water and a few drops were placed on the SEM grid and left to dry. The size of the microcapsules was determined manually. The dried (composite) coatings were cut with a razor blade and placed on the SEM grid to analyze the cross-section of the cut.

Fluorescence spectroscopy was carried out on a Perkin Elmer Model LS50B Luminescence spectrometer using FL Winlab version 4.0 for data processing. Analyses were done in fluorescence mode and emission spectra were recorded at a constant excitation wavelength of 490 nm.

Samples for fluorescence microscopy were observed on an Olympus Cell$^{\mathbb{R}}$ system attached to an IX-81 inverted fluorescence microscope. The microscope was equipped with a F-view-II cooled CCD camera (Soft Imaging Systems), using 572 nm excitation and UBG triple band pass emission filter. For the z-stack image frames, an Olympus Plan Apo N 60x/1.4 oil objective and the Cell$^{\mathbb{R}}$ imaging software have been used for the image acquisition and analysis.

Fourier transform infrared (FTIR) spectra were recorded on a Nexus FTIR spectrophotometer equipped with a Smart Golden Gate attenuated total reflectance (ATR) diamond from Thermo Nicolet with ZnSe lenses. Each spectrum was scanned 32 times with 4.0 cm^{-1} resolution and data analysis was performed with Omnic Software version 7.2.

Dynamic scanning calorimetry (DSC) was carried out on a TA Instruments Q100 system calibrated with indium metal. Heating and cooling rates were 10 °C/min under a nitrogen atmosphere and the glass transition temperature (T_g) was determined from the second heating cycle. Cure kinetics of the thiol-ene polymerizations were analyzed from room temperature to 200 °C at heating rates of 1, 5, 10 and 20 °C/min. An equimolar ratio of the thiol and ene functional groups was used and 2 mol% of AIBN with respect to thiol was added to initiate the polymerization.

Thermogravimetric analysis (TGA) was carried out on a TA Instruments Q500 thermogravimetric analyzer. The runs were performed under a nitrogen atmosphere and run from room temperature up to 600 °C at a heating rate of 10 °C/min.

5.3 Results and discussion

*5.3.1 Synthesis of 1,6-hexanediol di-(*endo, exo-*norborn-2-ene-5-carboxylate)*

The synthesis of 1,6-hexanediol di(*endo*, *exo*-norborn-2-ene-5-carboxylate) (DiNorbornene) was carried out as described by Jacobine and coworkers and Carioscia and coworkers (Scheme 5.2).[43,44]

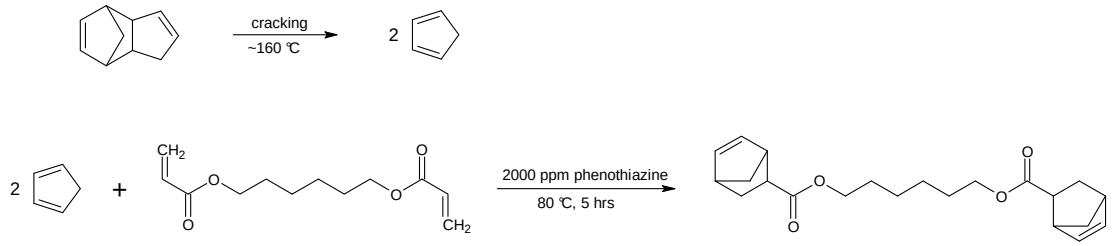

Scheme 5.2: Reaction mechanism for the synthesis of DiNorbornene.

Firstly, dicyclopentadiene is cracked in a distillation setup to provide the monomer cyclopentadiene. This monomer is so reactive that it undergoes a Diels-Alder reaction with itself at room temperature and therefore has to be used immediately.[45] Secondly, the cyclopentadiene is reacted with 1,6-hexanediol diacrylate (DiAcrylate). To achieve high conversion of the acrylate, the reaction is commonly carried out at elevated temperatures

in the presence of a thermal stabilizer which prevents the monomer from polymerizing. The resultant DiNorbornene is purified by vacuum distillation, which removes the unreacted cyclopentadiene and dicyclopentadiene monomers. The final product is obtained in a mixture of the *endo* and *exo* isomers in high yield. The excess thermal stabilizer (phenothiazine) is not removed from the synthesized monomer, although this might inhibit the polymerization to some extent. Figure 5.1 and Figure 5.2 show the ^{1}H-NMR and IR spectra respectively of DiNorbornene monomer. All the peaks were clearly identified, both in the ^{1}H-NMR and IR spectra. No residual peaks related to DiAcrylate could be observed, indicating that the synthesis proceeded to high conversion.

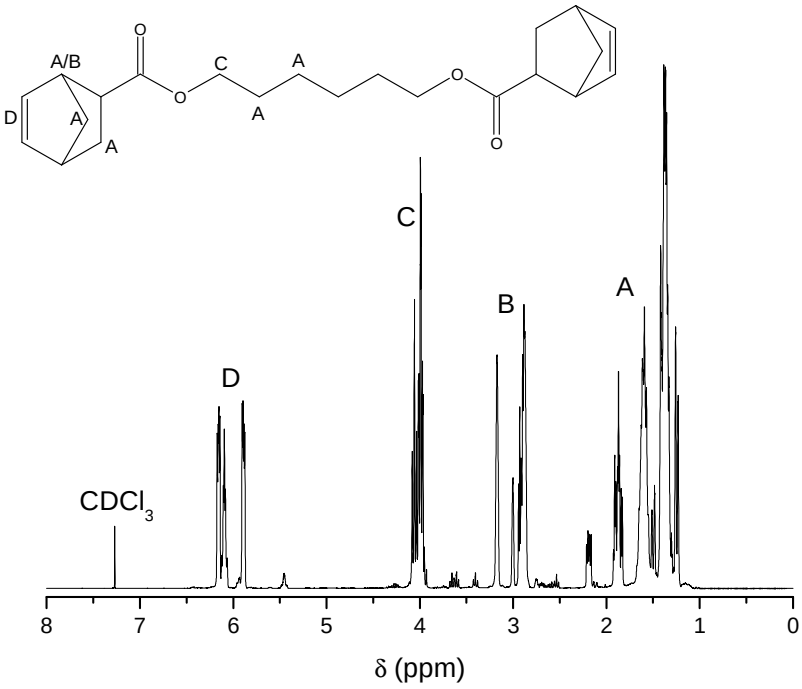

Figure 5.1: ^{1}H-NMR spectrum of DiNorbornene.

5.3.2 Synthesis of urea-formaldehyde microcapsules

As was outlined in the introduction, the synthesis of microcapsules via *in-situ* polymerization of urea and/or melamine with formaldehyde is well documented. Microcapsules with high strength and durability and low permeability are formed which can be used as containers that are suitable for storage of (reactive) compounds for application in self-healing coatings.

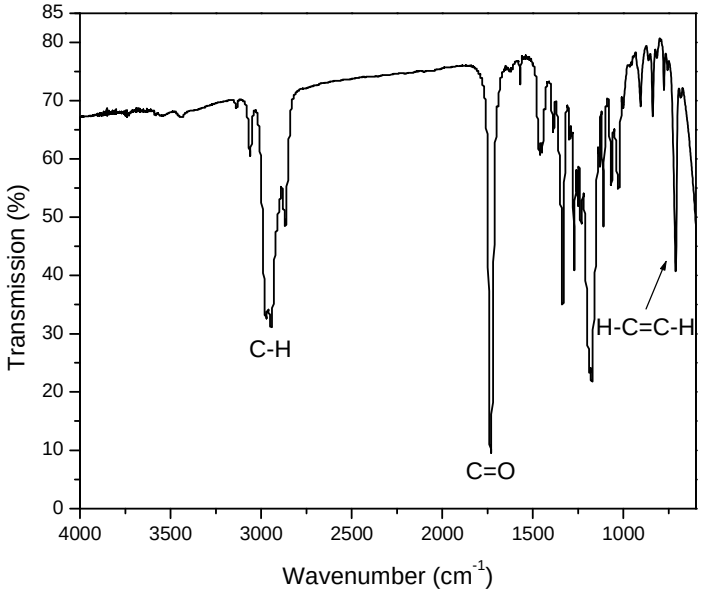

Figure 5.2: IR spectrum of DiNorbornene.

In this study microcapsules were synthesized via *in-situ* polymerization of urea and formaldehyde and reactive thiol and ene compounds were encapsulated. The *in-situ* polymerization of urea and formaldehyde proceeds via two steps, that is, an addition reaction and a condensation polymerization.[46]

Firstly, urea-formaldehyde (UF) prepolymer is formed, a reaction which can take place at acidic as well as alkaline pH.[47] During this reaction monomethylol-, dimethylol- and trimethylolurea condensates are formed, whereas tetramethylolurea has never been isolated.[17] Methylolation refers to the number of formaldehyde molecules that has reacted with one molecule of urea. In this study the UF prepolymer was prepared at alkaline pH ~9. Excessive basicity would lead to the precipitation of white solids as the prepolymer began to polymerize.[12] These white solids could not be used as the wall material in the final product. Furthermore, in order to obtain a homogeneously cross-linked UF polymer network, the molar ratio of formaldehyde to urea must be kept above 1.8.[17]

Separately an aqueous solution containing NaCl, resorcinol and water soluble polymer was prepared to which the oil phase was added to form an emulsion. It has been reported that the addition of salts such as NaCl in amounts of 1 to 10 wt% relative to urea is of great importance for control over the viscosity and the capsule wall permeability.[13] The addition of NH_4Cl in amounts of 1 to 10 wt% relative to urea is claimed to accelerate the polycondensation. Resorcinol, which acts as a brancher and is added in amounts of 1 to 10 wt% relative to urea, is said to enhance the membrane strength and the membrane formation to proceed more regularly. For the synthesis of UF microcapsules, a water soluble polymer is added to the formulation, which has the following functions:

- Accelerates the emulsification of the hydrophobe to be encapsulated
- Stabilizes the emulsion
- Acts as an accelerator for the formation of the capsule wall
- Acts as a dispersing agent for the capsules

The UF prepolymer is then added to the emulsion and the pH is decreased to approximately 3. The polycondensation between the low molecular weight urea and formaldehyde species proceeds mainly at acidic pH. When the initial pH is too low, the rate of reaction is too high and therefore the pH was only gradually decreased to ~2.

The procedure outlined above was employed for the synthesis of microcapsules with TetraThiol, DiAcrylate, DiNorbornene and hexadecane (HD) as the core material. Figure 5.3 shows SEM images obtained from microcapsules with TetraThiol core. Although the microcapsules have a broad particle size distribution, the particles are composed of a very smooth surface. The particle size ranges between about one and eight micrometers. Microencapsulation via *in-situ* polymerization of urea and formaldehyde generally results in particle sizes between 3 and 800 micrometers, dependent on the conditions employed.[15,20] A factor that influences the final particle size of the microcapsules is the stirring speed. It has been reported that smaller microcapsules are obtained with narrower particle size distribution if the stirring speed is increased.[12,16,19,48] Furthermore, as has been discussed above, the pH of the system during the synthesis of the prepolymer and

during the polycondensation between urea and formaldehyde has a huge impact on the rate of polymerization and will also influence the size and the morphology of the microcapsules. In addition, temperature will play a role in the kinetics of the UF polymerization.

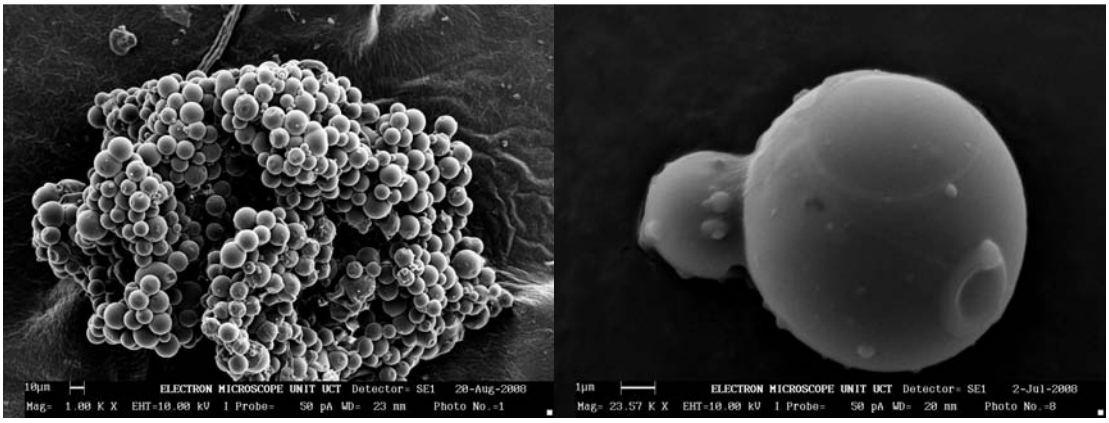

Figure 5.3: SEM images of UF microcapsules with TetraThiol as the core material.

For the experiments carried out and described in this chapter, the emulsion was formed via stirring with a magnetic stirrer bar at 500 rpm. Similar to emulsion polymerization where large monomer droplets are formed during emulsification, the oil droplets will have a distribution in particle size. Moreover, the UF polymer that serves as the wall material is formed in the aqueous phase and deposits onto the surface of the oil droplets. Therefore it is likely that the microcapsules synthesized have a rather broad particle size distribution. Because the wall material is formed in the aqueous phase and deposits homogeneously throughout the suspension onto the surface of the oil droplets, the shell thickness of the microcapsules should be equal, regardless the size of the microcapsules.[14]

Figures 5.4 and 5.5 show SEM images of UF microcapsules that contain hexadecane and DiAcrylate as the core material, respectively. As was the case for TetraThiol containing microcapsules, microcapsules with a very smooth surface are obtained. Again the size distribution is broad in both cases, giving a particle size range for the hexadecane

containing microcapsules of one to three micrometers and for the DiAcrylate containing microcapsules of one to four micrometers.

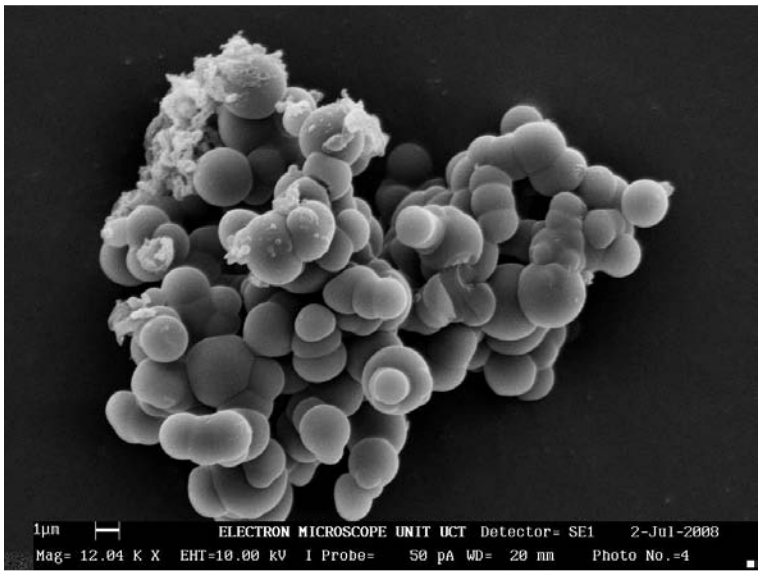

Figure 5.4: SEM images of UF microcapsules with hexadecane as the core material.

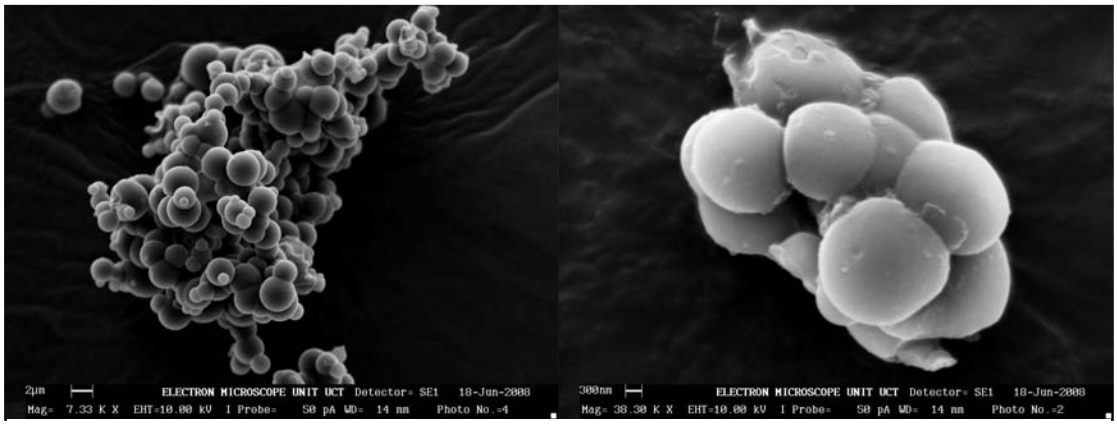

Figure 5.5: SEM images of UF microcapsules with DiAcrylate as the core material.

It must be noted that the size of the microcapsules synthesized via *in-situ* polymerization of urea and formaldehyde is very small. Only microcapsules with a maximum size of around ten micrometers were obtained. The microencapsulation of a variety of compounds such as dicyclopentadiene,[16] bisphenol-F-type epoxy resin (PY306),[17] bisphenol-A-type epoxy resin,[12] TetraThiol[32] and phase change materials (PCMs, such as *n*-octadecane)[15,48] synthesized in a similar way as described here, are reported to consist of a wide range of sizes. Microcapsules as small as 0.2–5.6 micrometers and microcapsules as large as 200 micrometers have been reported. It has been pointed out above, that the most important parameter in controlling the encapsulation process is the pH. According to literature, the *in-situ* polymerization of urea and formaldehyde can be carried out both in one step and in two steps. For the one-step synthetic procedure, the polymerization is carried out at acidic pH, because the polycondensation of urea and formaldehyde prepolymer takes mainly place at acidic pH. Initial values of pH reported are around 3.5 at a temperature between 55 and 60 °C. The pH and the temperature of the system must both be carefully matched, as the rate of UF polymerization will get too high for a successful encapsulation when the pH is too low. For the two-step synthetic procedure, an initial pH value between 9 and 10 is adopted to synthesize UF prepolymer. Too high a pH value will again result in too high a rate of prepolymer formation. The synthesis of the prepolymer is usually carried out at 70 °C. The prepolymer synthesized is then added to the emulsion formulation and the pH is decreased to a value around 3. If the initial pH is too low, as mentioned above, the rate of UF polymerization is too fast and the deposition of the prepolymer onto the surface of the oil droplets will not be efficient. Moreover, when the rate of polymerization is too high, UF nanoparticles will be formed that remain in suspension in the aqueous phase and this will lower the encapsulation efficiency. Generally poor quality microcapsules are obtained and the yield is low.

Considering the importance of both the pH and the temperature, additional experiments were carried out where the pH and temperature were varied. Step one, the synthesis of prepolymer was not changed and carried out at pH ~9 at 70 °C. Only the second step of the UF polymerization, the polycondensation of the various methylolurea species, was

changed. The temperature was varied between 55 and 70 °C and the initial pH was varied between 2 and 4 to gain insight in and obtain control over the rate of polymerization. The change of initial pH and temperature had a marginal effect on the size and smoothness of the TetraThiol containing microcapsules. Too low an initial pH however, resulted in coagulation of the microcapsules. The various initial pH and temperature values employed had a much larger impact on the microcapsules containing the ene compound. Bigger capsules were formed with sizes ranging between 50 and 100 micrometers. The smoothness of the capsule surface was replaced with a shell consisting of a smooth inner membrane with a rough outer surface. The rough outer surface is a result of the deposition of agglomerated UF nanoparticles that are formed in the aqueous phase. As Figure 5.6 shows, many capsules appeared to have broken shells and the yield (the amount of core compound encapsulated) was generally very low.

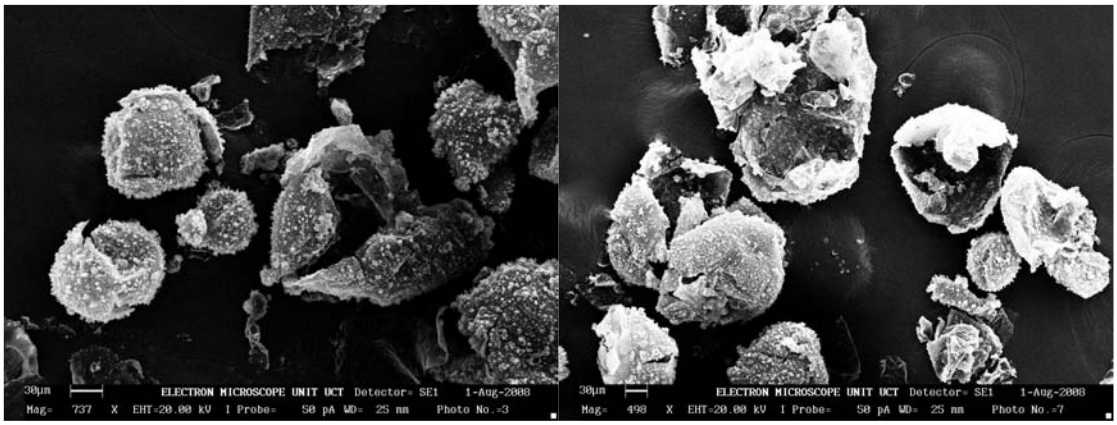

Figure 5.6: SEM images of broken UF microcapsules after encapsulation of DiAcrylate as the core material.

5.3.3 Synthesis of rhodamine-based fluorescent probe

In this study the development of a self-healing coating is based on thiol-ene chemistry. The reactive thiol and ene compounds that are encapsulated in the UF microcapsules should be released upon the occurrence of a crack in the coating and provide a mechanism for self-healing. In the introduction it was pointed out that thiol-ene chemistry is highly robust regarding conditions under which curing of the network can take place. For the healing mechanism to be efficient, the concentration of both thiol and

ene compounds must be high at the location of crack formation. An efficient method to prove that the compound of interest is present at the desired location is via the use of a fluorescent probe. Fluorescent compounds such as rhodamine are widely used for labeling biomolecules. By protecting the amino group of the highly fluorescent rhodamine with an electron-withdrawing 2,4-dinitrobenzenesulfonamide group, the rhodamine-based molecule becomes practically non-fluorescent.[49,50] The sulfonamide group resists hydrolysis and yields no undesired background fluorescence. However, the nucleophilic attack of a thiol group on the 2,4-dinitrobenzenesulfonamide group results in the cleavage of the sulfonamide linkage and the recovery of rhodamine, which results in highly intense fluorescence emission.

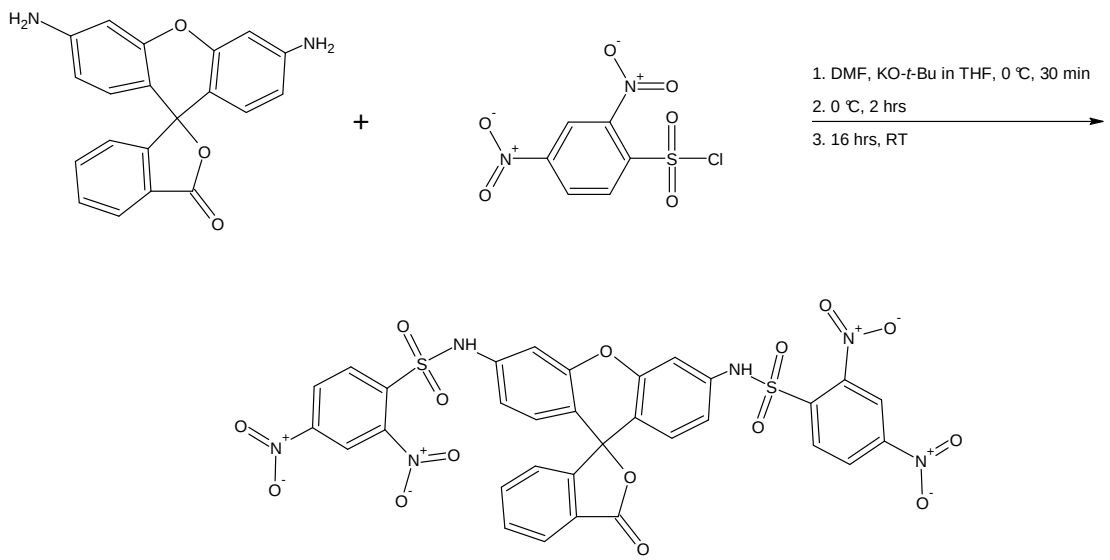

Scheme 5.3: Reaction mechanism for the synthesis of the rhodamine-based fluorescent probe.

The synthesis of the rhodamine-based fluorescent probe was carried out via a substitution reaction (Scheme 5.3).[49] The presence of an excess of a strong base, KO-*t*-Bu, provided the proton abstraction at both amine functionalities of rhodamine 110 chloride. The subsequent addition of 2,4-dinitrobenzenesulfonyl chloride resulted in the formation of a sulfonamide bond and the release of potassium chloride as a salt. Although the synthesis of the fluorescent probe was straightforward, the yield of the reaction was low (26.1 mg,

12%). As side product was present the mono-substituted 2,4-dinitrobenzenesulfonamide, which has only weak fluorescence emission. The disubstituted 2,4-dinitrobenzenesulfonamide that was employed as the fluorescent probe is practically non-fluorescent. The purity of the fluorescent probe was high and the assignment of the peaks was confirmed via a combination of ^{1}H and ^{13}C-NMR spectroscopy (Figures 5.7 and 5.8 respectively) and ^{1}H-^{1}H Correlation Spectroscopy (^{1}H-^{1}H COSY, Figure 5.9), ^{1}H-^{13}C gradient-selective Heteronuclear Single Quantum Coherence (gHSQC) spectroscopy and ^{1}H-^{13}C gradient-selective Heteronuclear Multiple Bond Correlation (gHMBC) spectroscopy (Figure 5.10).

5.3.4 Cure kinetics of thiol-ene chemistry

In this study thiol-ene chemistry was adopted as the mechanism for the concept of autonomous self-healing of coatings. Thiol-ene chemistry is a highly robust step-growth free-radical polymerization technique via which polymer networks can be formed. The flexibility of thiol-ene chemistry stems from the conditions at which the polymer networks can be formed and the vast number of monomers that can be chosen from. Thiol-ene networks can be formed at ambient temperature by exposing the sample to UV radiation without the necessity of the addition of a photoinitiator. Although the rate of polymerization in air is slightly reduced to that under inert atmosphere, the rate of polymerization in air proceeds sufficiently rapidly and does not suffer from inhibition as compared to (meth)acrylate free-radical polymerizations. A homogeneous network with reduced stress and shrinkage built into the network is formed. This is a result of the delayed onset of gel formation which is a consequence of its step-growth polymerization mechanism. The reactivity of a thiol-ene monomer combination is mainly associated with the reactivity of the ene and it appears that the higher the electron density of the carbon-carbon double bond, the higher is its reactivity in thiol-ene chemistry. An exception is norbornene. Upon the addition of a thiyl-radical to the carbon-carbon double bond of norbornene, the monomer is relieved from ring-strain which favors this radical addition. Furthermore, this results in the formation of a highly reactive radical that readily abstracts a proton from the thiol in a subsequent chain-transfer reaction.[33,43]

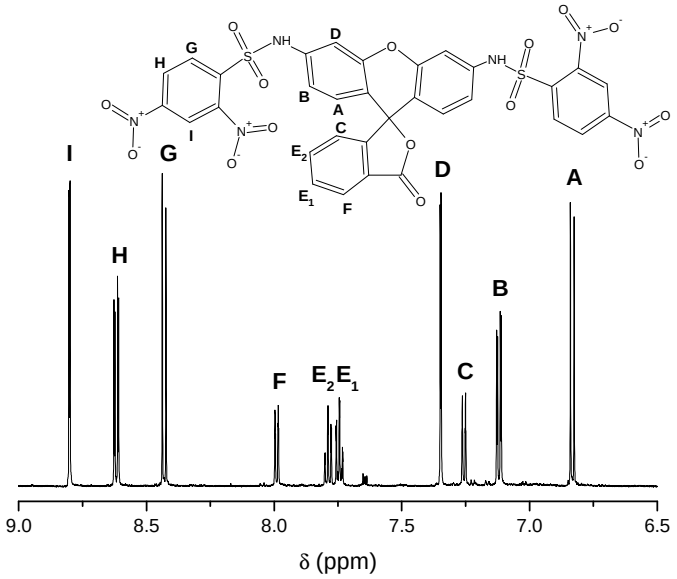

Figure 5.7: ^{1}H-NMR spectrum of the disubstituted rhodamine-based fluorescent probe.

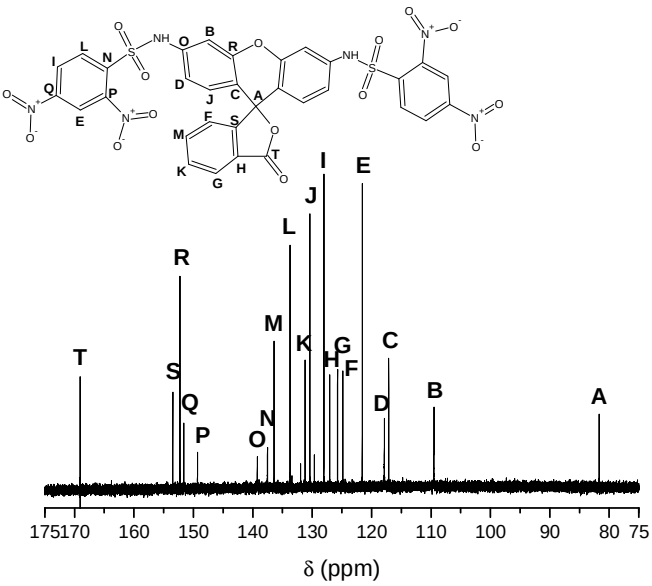

Figure 5.8: ^{13}C-NMR spectrum of the disubstituted rhodamine-based fluorescent probe.

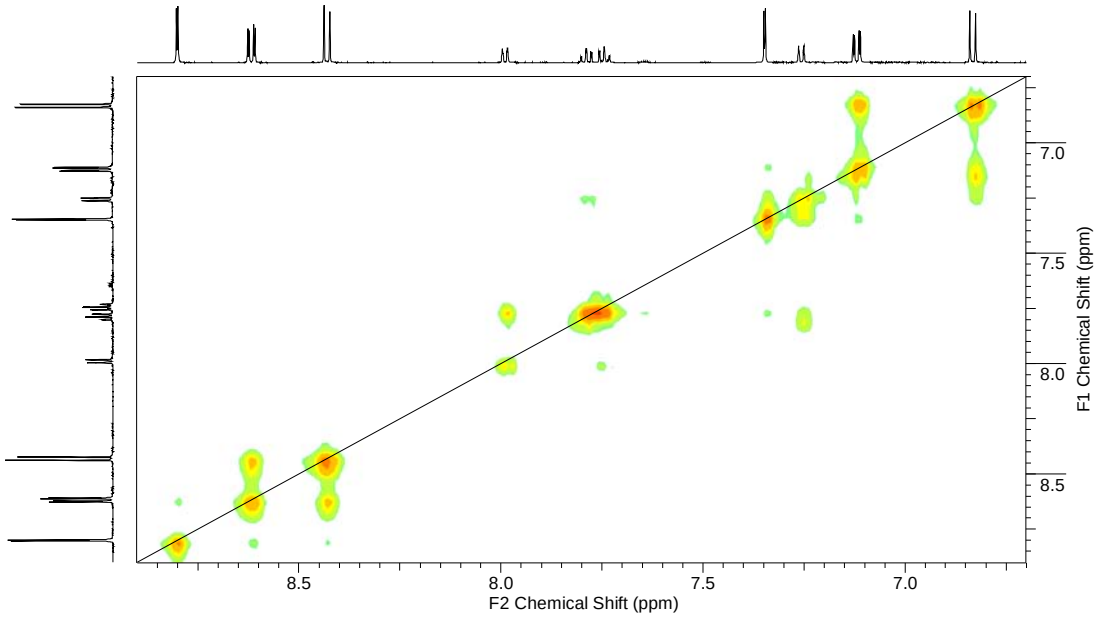

Figure 5.9: ^{1}H-^{1}H COSY spectrum of the disubstituted rhodamine-based fluorescent probe.

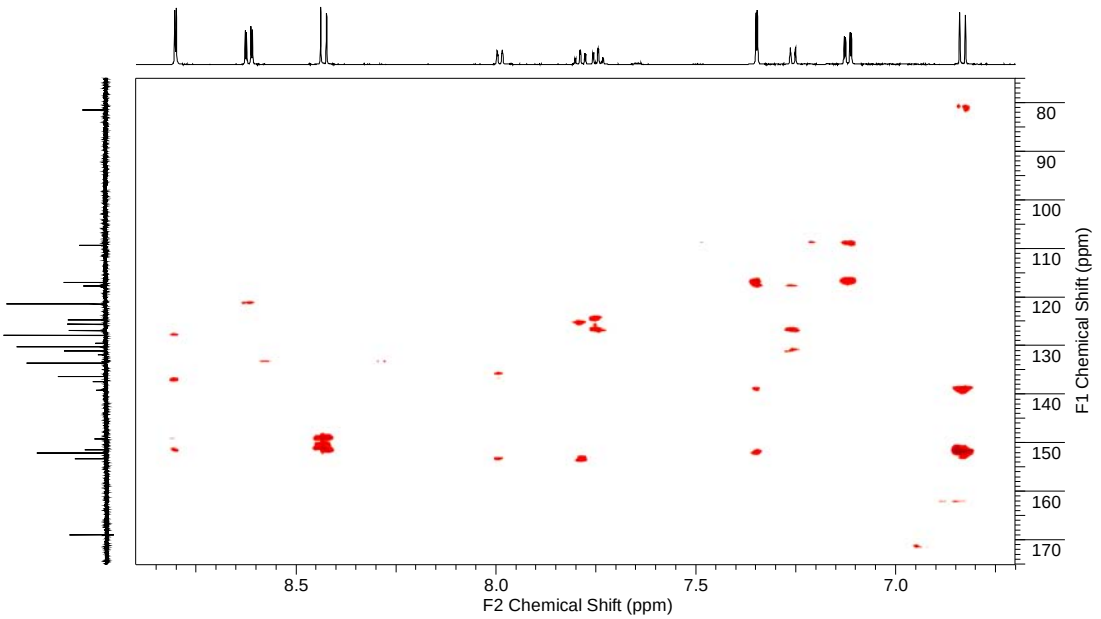

Figure 5.10: ^{1}H-^{13}C gHMBC spectrum of the disubstituted rhodamine-based fluorescent probe.

The above discussion presents the main advantages of thiol-ene chemistry over conventional ((meth)acrylate) free-radical polymerizations. In this study the adoption of thiol-ene chemistry as a healing mechanism in self-healing coatings was investigated. In literature several approaches have been reported. White and coworkers used Ring-Opening Metathesis Polymerization (ROMP) as a mechanism for their self-healing coatings and embedded a catalyst in the polymer matrix.[11] Although the approach was successful, the deactivation of the catalyst over long(er) time spans was mentioned. By adopting thiol-ene chemistry as the healing mechanism, there is no need for the addition of a catalyst/initiator in the matrix, although the rate is significantly enhanced by the addition of a photoinitiator. The thiol and ene compounds can be encapsulated separately and upon the occurrence of crack formation, the thiol and ene will react under the influence of UV radiation. In this study norbornene is employed as the monomer of choice, because it is reported as one of the most reactive monomers in thiol-ene chemistry. Together with TetraThiol, one of the most widely used thiols in thiol-ene chemistry, it forms a densely cross-linked network.

A well-established and popular method to investigate the cure kinetics of polymer network formation is via thermal analysis methods such as thermogravimetric analysis (TGA) and dynamic scanning calorimetry (DSC).[51,52] The determination of kinetic parameters via DSC can be accomplished via either isothermal or dynamic analysis. Isothermal experiments are carried out at a constant temperature, whereas dynamic experiments are carried out at a constant heating or cooling rate. Isothermal experiments have the disadvantage that a significant advancement of the reaction can take place before the DSC can reach and stabilize at the desired temperature. In addition, the reaction may not proceed to completion at low temperature. Figure 5.11 shows dynamic DSC-exotherms for the reaction of TetraThiol and DiNorbornene initiated with AIBN at different heating rates. An equimolar ratio of the thiol and ene functional groups and 2 mol% of AIBN with respect to TetraThiol was employed in all experiments. As the heating rate increases, the peak temperature shifts to higher temperatures. Tables 5.1 and 5.2 summarize the total enthalpy of reaction and the peak temperature for a given heating rate for all TetraThiol-DiNorbornene and TetraThiol-DiAcrylate curing experiments

carried out, respectively. The average reaction enthalpy for the TetraThiol-DiNorbornene curing experiments is 321 ± 2.2 J/g for the first three experiments, whereas the reaction enthalpy for the last experiment is slightly higher. The average reaction enthalpy for the TetraThiol-DiAcrylate curing experiments is 336 ± 7.4 J/g.

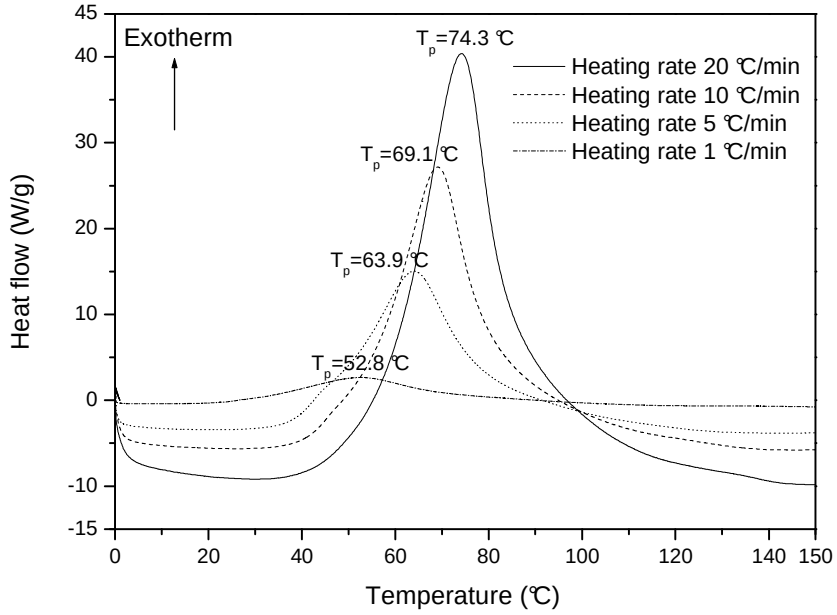

Figure 5.11: DSC-exotherms for TetraThiol-DiNorbornene network formation at different heating rates.

Table 5.1: Characteristics of the DSC-exotherms for the TetraThiol-DiNorbornene network formation

Experiment	**Heating rate (°C/min)**	T_p **(°C)**	$\Delta H_{reaction}$ **(J/g)**
1	20	74.33	319.6
2	10	69.11	319.3
3	5	64.21	323.3
4	1	53.01	357.6

Table 5.2: Characteristics of the DSC-exotherms for the TetraThiol-DiAcrylate network formation

Experiment	Heating rate (°C/min)	T_p (°C)	$\Delta H_{reaction}$ (J/g)
1	20	77.55	345.0
2	10	71.99	329.8
3	5	64.31	337.7
4	1	46.66	329.6

The main equations that allow for calculation of various kinetic parameters from data obtained from thermal analysis, such as activation energy (E_{act}) and pre-exponential factor (A), were developed in the late fifties and early sixties.[51,52] The most widely used methods are known as the Kissinger equation, the Friedman method and the Ozawa equation.[53-57] The Kissinger equation is a so-called single-step kinetic equation and it produces a single value for E_{act} and A. As a result, the obtained values are only sound if there is no variation of E_{act} and A with the degree of cure throughout the process. However, more often than not, E_{act} and A are found to vary with the extent of conversion. The Friedman method and the Ozawa equation on the other hand, both take into account the variation of E_{act} and A with degree of cure. By carrying out multiple experiments at varying heating rates, a value of E_{act} and A is obtained for every degree of cure. The latter two equations make use of the so-called isoconversional principle which states that at a constant extent of conversion, the rate of reaction is only a function of the temperature. The isoconversional method enables the separation and analysis of complex reaction mechanisms.

The degree of cure as measured via DSC is defined as:

$$\alpha(t) = \frac{H(t)}{H_R} \qquad \textit{equation 5-1}$$

where $\alpha(t)$ is the degree of cure, $H(t)$ the enthalpy of reaction up to time t and H_R the total enthalpy of reaction. The rate of reaction can then be described by equation 5-2:

$$\frac{d\alpha}{dt} = K(T) \cdot f(\alpha) \qquad \textit{equation 5-2}$$

where $\frac{d\alpha}{dt}$ is the rate of reaction, $f(\alpha)$ corresponds to the reaction model (first order, second order, *n*th order, *n*th order with autocatalysis, etc.) and $K(T)$ is a temperature dependent rate constant, which is described by the Arrhenius equation:

$$K(T) = A \cdot \exp\left(-\frac{E_{act}}{RT}\right) \qquad \textit{equation 5-3}$$

where A is the pre-exponential factor, E_{act} the activation energy, R the universal gas constant ($8.3145\ {}^{J}\!/_{mol \cdot K}$) and T the absolute temperature. By carrying out dynamic DSC experiments with a constant heating rate, the rate of reaction can be described as a function of temperature:

$$\frac{d\alpha}{dT} \propto \frac{K(T)}{\beta} \qquad \textit{equation 5-4}$$

where $\beta = \frac{dT}{dt}$ is the (constant) heating rate.

The Kissinger equation is expressed as:

$$\frac{E_{act}\beta}{RT_p^2} = A \cdot \exp\left(-\frac{E_{act}}{RT_p}\right) \qquad \textit{equation 5-5}$$

where T_p is the peak temperature. By taking the natural logarithm of the Kissinger equation the following equation is obtained:

$$-\ln\left(\frac{\beta}{T_p^2}\right) = -\ln\left(\frac{AR}{E_{act}}\right) + \frac{E_{act}}{R}\cdot\frac{1}{T_p} \qquad \textit{equation 5-6}$$

E_{act} and A can be obtained from the slope and intercept respectively, when $-\ln\left(\frac{\beta}{T_p^2}\right)$ is plotted against $\frac{1}{T_p}$. As mentioned above, the Kissinger equation produces a single value for E_{act} and A and does not take into account a variation of E_{act} and A with degree of cure. An estimate of the reaction order can be obtained from the Crane equation:[53,55]

$$\frac{d(\ln\beta)}{d\left(1/T_p\right)} = -\left[\frac{E_{act,k}}{nR} + 2T_p\right] \qquad \textit{equation 5-7}$$

where $E_{act,k}$ is the E_{act} obtained from the Kissinger equation and n is the reaction order. From a plot of $\ln(\beta)$ against $1/T_p$ a value for the reaction order n can be obtained if $\frac{E_{act,k}}{nR} >> 2T_p$.

The Friedman method is directly derived from the Arrhenius equation and reads as:

$$\ln\left[\beta\cdot\left(\frac{d\alpha}{dT}\right)_\alpha\right] = \ln(A_\alpha) - \frac{E_{act,\alpha}}{R}\cdot\frac{1}{T_\alpha} \qquad \textit{equation 5-8}$$

where the subscript α indicates that both E_{act} and A are a function of the degree of cure. By plotting $\ln\left[\beta\cdot\left(\frac{d\alpha}{dT}\right)_{\alpha}\right]$ against $\frac{1}{T_{\alpha}}$ a value for E_{act} and A can be obtained for each degree of cure.

The Ozawa equation is defined as:

$$\ln(\beta)=\left[\ln\left(\frac{AE_{act,\alpha}}{R}\right)-2.315\cdot\ln(10)\right]-\frac{1.052\cdot E_{act,\alpha}}{R}\cdot\frac{1}{T_{\alpha}} \qquad \textit{equation 5-9}$$

From a plot of $\ln(\beta)$ against $\frac{1}{T_{\alpha}}$ both E_{act} and A can be calculated for each degree of cure.

Table 5.3 shows the results obtained from the Kissinger equation for both TetraThiol-DiNorbornene and TetraThiol-DiAcrylate curing reactions. The reaction order was obtained via the Crane equation.

Table 5.3: Estimation of E_{act} and A obtained from the Kissinger equation and the curing reaction order obtained from the Crane method

	E_{act} **(kJ/mol)**	A **(s^{-1})**	n
Thiol-Norbornene	126.9	$5.09\text{x}10^{17}$	0.958
Thiol-Acrylate	96.2	$6.42\text{x}10^{12}$	0.944

Figure 5.12 shows an example of a linear fit to the data obtained from applying the Friedman method at a degree of cure of 0.3 to the TetraThiol-DiNorbornene experimental data. Each data point is obtained from one experiment at varying heating rates. From the experimental data E_{act} and A can be calculated via the Friedman method and the Ozawa equation at every degree of cure. Figures 5.13 to 5.16 show the results obtained for E_{act} and A via both methods for both experiments.

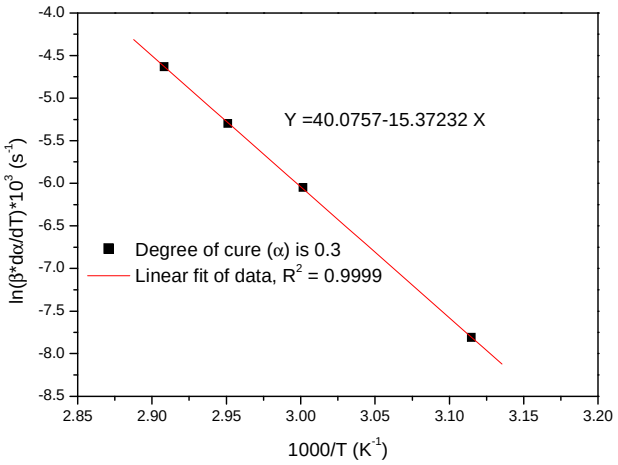

Figure 5.12: Linear fit obtained from the Friedman plot at a degree of cure (α) of 0.3.

For both experiments, E_{act} and A increase with degree of cure up to about a degree of cure of 0.9, after which both slightly decrease. Both Friedman method and Ozawa equation show a similar development of E_{act} and A with degree of cure, where the Friedman method results in slightly higher values as compared to the Ozawa equation. As both methods show an increase of E_{act} and A with degree of cure, the single values obtained via the Kissinger equation should be considered as an approximation. The development of E_{act} and A with degree of cure obtained for the thiol-ene curing reactions has also been reported for other cross-linking reactions, such as epoxy systems.[52] The TetraThiol-DiNorbornene system shows an increase in E_{act} and A from the beginning of the reaction, whereas E_{act} and A for the TetraThiol-DiAcrylate system remain fairly constant up to about 60% conversion, after which it increases significantly.

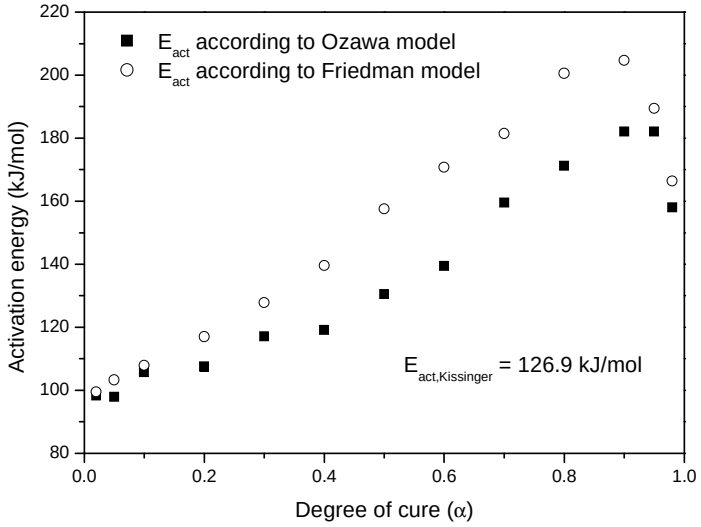

Figure 5.13: Variation of E_{act} with degree of cure for TetraThiol-DiNorbornene curing reaction obtained from the Friedman method and the Ozawa equation.

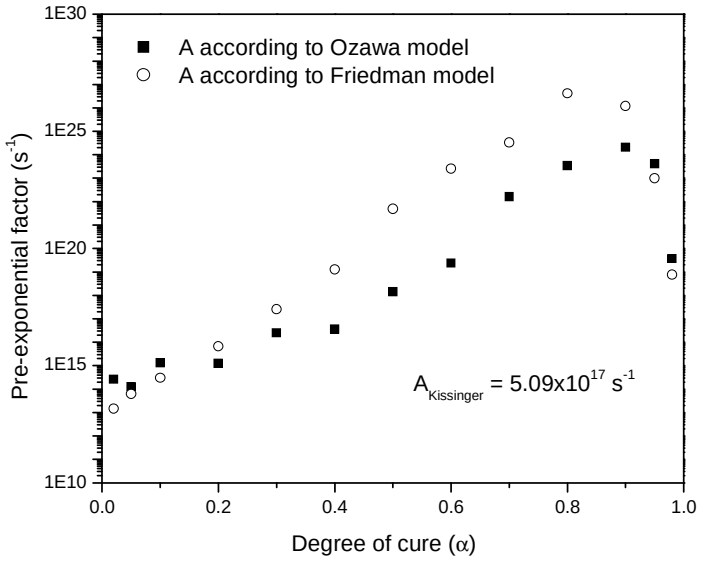

Figure 5.14: Variation of A with degree of cure for TetraThiol-DiNorbornene curing reaction obtained from the Friedman method and the Ozawa equation.

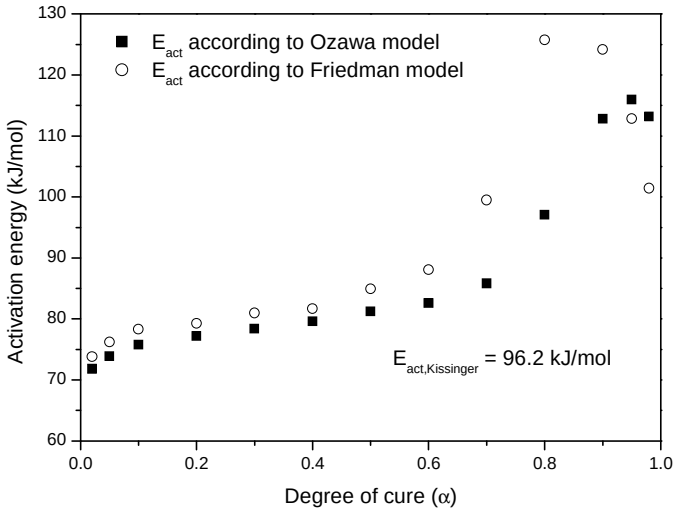

Figure 5.15: Variation of E_{act} with degree of cure for TetraThiol-DiAcrylate curing reaction obtained from the Friedman method and the Ozawa equation.

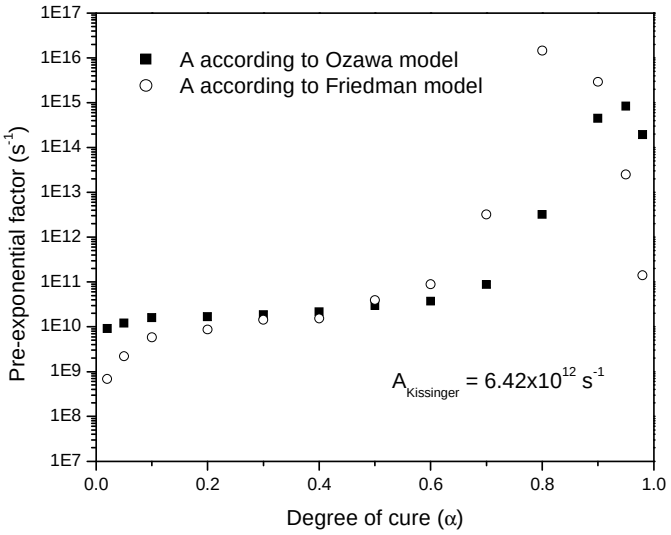

Figure 5.16: Variation of A with degree of cure for TetraThiol-DiAcrylate curing reaction obtained from the Friedman method and the Ozawa equation.

The gel point of a network that is formed via a step-growth polymerization mechanism is given by equation 5-10:[33]

$$gelpoint = \left[\frac{1}{r \cdot (f_{thiol} - 1) \cdot (f_{ene} - 1)} \right]^{1/2} \qquad \textit{equation 5-10}$$

where r is the molar ratio of the thiol and ene functional groups, f_{thiol} is the thiol functionality and f_{ene} is the ene functionality. For the thiol-ene curing reactions carried out, the gel point is reached at a conversion of 58%. Although E_{act} and A for the TetraThiol-DiNorbornene reaction increase throughout the curing process, E_{act} and A only significantly increase after a degree of cure of 60% for the TetraThiol-DiAcrylate system. This increase in E_{act} and A can be attributed to the gel point, which results in a decrease in molecular mobility. The lower values of both E_{act} and A after about 90% conversion for both curing reactions are consistent with diffusion of small molecules in a so-called liquid-solid medium, and the effect can be explained by diffusion control that is associated with vitrification.[52]

Cramer *et al.* investigated the kinetics of thiol-ene chemistry and Table 5.4 shows the kinetc parameters they obtained for the TetraThiol-DiNorbornene and TetraThiol-DiAcrylate step-growth polymerizations.[33,35]

Table 5.4: Kinetic rate constants for TetraThiol-DiEne step-growth polymerization[33,35]

Monomer	k_p / k_{ct}	n	m
DiNorbornene	1	0.5	0.5
DiAcrylate	13	0.4	0.6

The kinetic parameters are related to the rate of polymerization as defined in equation 5-11:

$$R_{polymerization} \propto [RSH]^n [C=C]^m \qquad \textit{equation 5-11}$$

where $R_{polymerization}$ is the rate of polymerization, $[RSH]$ and $[C=C]$ are the thiol and ene concentrations respectively and the exponents n and m relate the rate of polymerization to the thiol and ene concentrations respectively. It must be noted that the values reported in Table 5.4 for the TetraThiol-DiAcrylate step-growth polymerization are related to the initial polymerization rate if DiAcrylate homopolymerization is taken into account. If the DiAcrylate homopolymerization is not taken into account, thus assuming only step-growth polymerization, the rate of polymerization would scale with the first order of the thiol concentration ($R_p \propto [RSH]$).[35] The reaction order obtained from the Crane method, which gives a value of 0.958 and 0.944 for the TetraThiol-DiNorbornene and TetraThiol-DiAcrylate system respectively, are in good agreement with the values obtained by Cramer *et al.* However, for the experiments carried out here, no distinction can be made between the reaction order of the thiol and ene.

A couple of isothermal curing experiments have been carried out for both TetraThiol-DiNorbornene and TetraThiol-DiAcrylate formulations. Values for E_{act} and A obtained from the Kissinger equation (Table 5.3) have been put into the Arrhenius equation at various temperatures ranging from 40–65 °C, to get an estimation of the rate constant $K(T)$ at each temperature. The time necessary to reach a degree of cure of 0.99 has been calculated via the integration of equation 5-2, where $f(\alpha)=(1-\alpha)$ (first order reaction). Table 5.5 shows the predicted time to reach a degree of cure of 0.99 for both curing systems and the actual time that was necessary to reach a degree of cure of 0.99.

Table 5.5: Prediction of the time it will take to reach 99% conversion for the isothermal curing reaction of DiNorbornene and DiAcrylate with TetraThiol. The reactions were initiated with AIBN and E_{act} and A were calculated via the Kissinger equation

Temperature (°C)	**Norbornene**		**Acrylate**	
	$t_{experimental}$ **(min)**	$t_{prediction}$ **(min)**	$t_{experimental}$ **(min)**	$t_{prediction}$ **(min)**
40	28.6	225	x	x
45	20.8	105	x	x
50	20.9	49.8	25.6	42.8
55	x	x	24.0	24.8
60	x	x	14.1	14.6
65	3.4	6.2	11.9	8.7

Table 5.5 shows that for the TetraThiol-DiAcrylate system the predicted time is in very good agreement with the actual time that the curing reaction took to reach a degree of cure of 0.99. For the TetraThiol-DiNorbornene the opposite is true. Although for the isothermal experiments carried out at 50 and 65 °C the prediction is relatively close to the experimental value, the values obtained for the experiments carried out at 40 and 45 °C are far off. There are several explanations for these deviations. First of all, the TetraThiol-DiNorbornene system is very reactive and upon storing, the system starts polymerizing, even without the application of heat. Therefore, as this system is very sensitive, the experimental values should be regarded as a lower limit. Another explanation is inherent to isothermal experiments carried out at elevated temperatures. Before the DSC instrument reaches the isothermal temperature and has stabilized at that temperature, a considerable progression in the reaction could have taken place already. This phenomenon was particularly strong for the experiments carried out with the TetraThiol-DiNorbornene system. A third explanation for the deviation arises from reading errors. Generally the experiment is stopped after a long period of (visibly) constant heat flow. This may have introduced an error in that the curing reaction had not reached 100% conversion yet and the subsequent time necessary to reach a degree of cure of 0.99 could have been underestimated. Finally, as was concluded from the dynamic

DSC experiments, the E_{act} and A obtained from the Kissinger equation give only one value for both E_{act} and A over the whole range of cure. These values for E_{act} and A should therefore be taken as approximations, as both the Friedman method and the Ozawa equation show that the E_{act} and A are a function of the degree of cure.

Figure 5.17 shows the T_g and the thermal stability of both TetraThiol-DiNorbornene and TetraThiol-DiAcrylate networks formed after exposing the monomer mixtures, containing ~0.1 wt% photoinitiator with respect to TetraThiol, to UV radiation. It can be seen that both networks are very stable up to temperatures of around 300 °C.

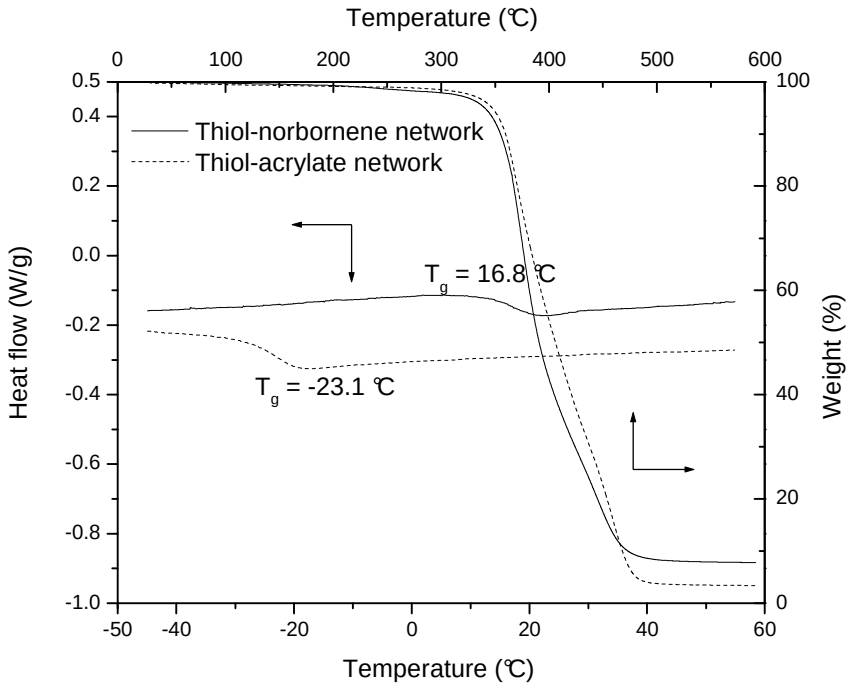

Figure 5.17: T_g and the thermal stability of TetraThiol-DiNorbornene and TetraThiol-DiAcrylate networks.

5.3.5 Incorporation of either TetraThiol or DiAcrylate microcapsules in a coating

The microcapsules synthesized as described in Section 5.3.2 were embedded in a film (Section 5.2.4). Initial focus was put on a PMA film because of its inherently low T_g which renders the matrix soft. This would facilitate the easy introduction of a cut in the film with a razor blade and the consequent rupture of the microcapsules. The rupture of the microcapsules is a prerequisite for the successful development of a self-healing coating and therefore the detection of a thiol compound by means of fluorescence spectroscopy was investigated. The rhodamine-based fluorescent probe described in Section 5.3.3 was employed for this purpose. The probe shows hardly any fluorescence emission at a wavelength of 520 nm, whereas rhodamine shows highly intense fluorescence emission at this wavelength (Scheme 5.4). The reaction of a thiol compound with the probe results in the cleavage of the sulfonamide bond and the formation of rhodamine. Thus, upon reaction of the probe with TetraThiol present in the UF microcapsules, rhodamine is recovered and this would result in fluorescence emission.

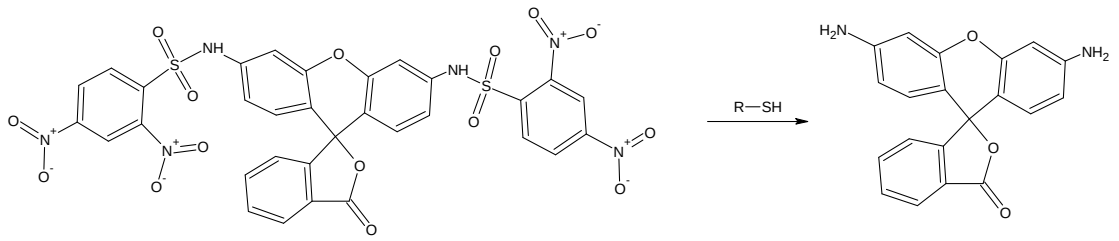

Rhodamine-based fluorescent probe
Very low fluorescence emission

Rhodamine
Very high fluorescence emission

Scheme 5.4: Application of rhodamine-based fluorescent probe, showing that after reaction with a thiol intense fluorescence emission is detected.

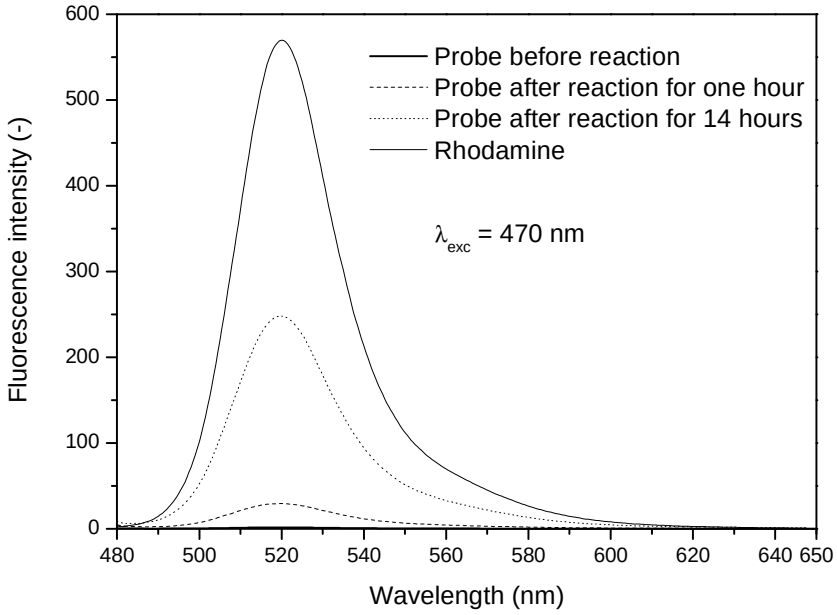

Figure 5.18: Emission spectra showing the fluorescence intensity of the various rhodamine-based compounds.

Figure 5.18 shows the emission spectra of rhodamine and the probe before and after reaction with TetraThiol at different times. The excitation wavelength was set at 470 nm and the emission spectra were recorded from 480–650 nm. The concentration of the various rhodamine-based compounds was about 15 µM. It is easily observed that the probe itself shows hardly any fluorescence at the maximum wavelength of emission ($\lambda_{em,\max}$ =520 nm). Rhodamine on the other hand shows significant fluorescence emission at this wavelength. Rhodamine shows even at very low concentrations (~50 nM) intense fluorescence emission. Therefore, after reaction of the probe with TetraThiol, which basically leads to the recovery of rhodamine itself, intense fluorescence emission is observed. It has been reported that mercapto-based compounds show only a limited increase in fluorescence emission as compared to the probe itself, which is related to the pK_a of the thiol compound.[49,50] However, the mercapto-based compound was only allowed to react with the probe for half an hour at 37 °C,[49] whereas the reaction solution was examined for fluorescence emission at different times in this study. Even though the

reaction proceeds very slowly, after 14 hours intense fluorescence emission is observed. This means that the fluorescent probe is able to detect whether TetraThiol is present or not. Therefore, the rhodamine-based fluorescent probe can be successfully applied for the detection of TetraThiol in the self-healing coating formulations.

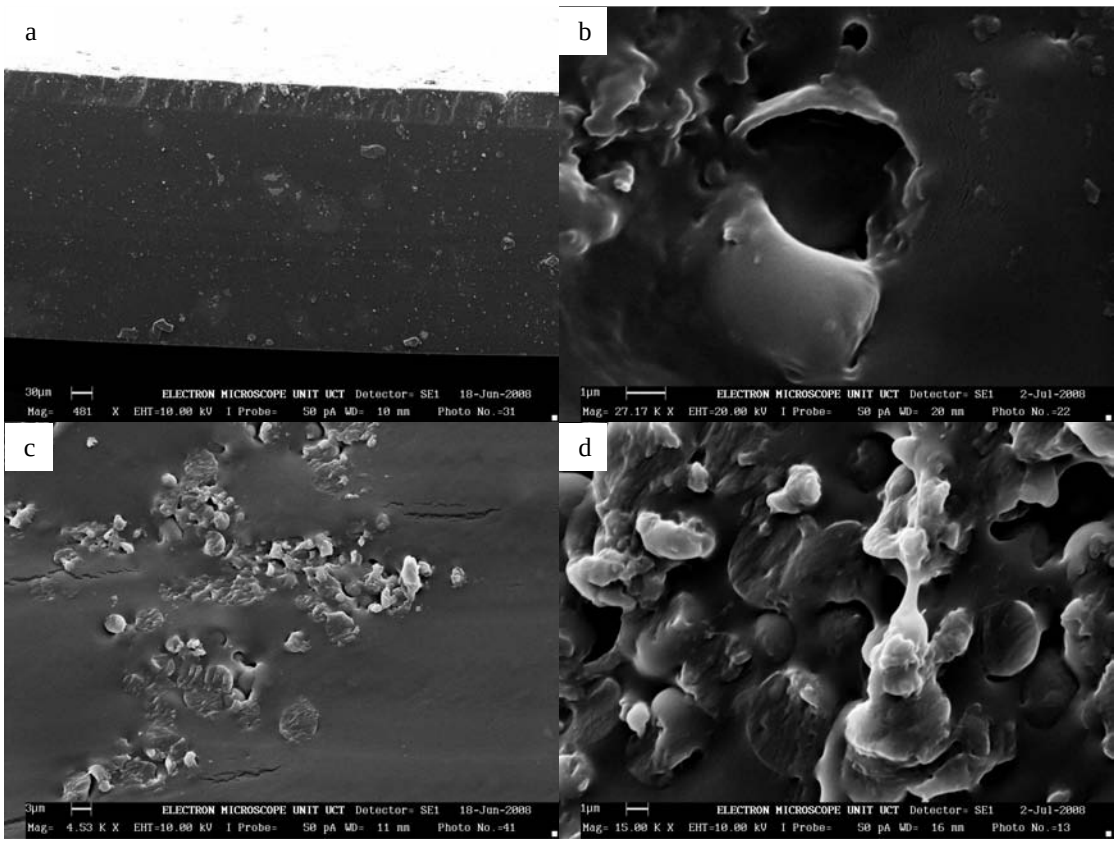

Figure 5.19: SEM images showing the cross-section of PMA films without microcapsules (a) and with DiAcrylate (b) and TetraThiol (c and d) microcapsules.

For the development of a self-healing coating, initially either TetraThiol *or* DiAcrylate capsules were dispersed in the coating. The dispersion of the microcapsules throughout the PMA film and the response of the microcapsules to a cut made with a razor blade were investigated with SEM. For this purpose the microcapsules with either TetraThiol *or* DiAcrylate as the core material were dispersed in a PMA latex and the composite coating was left to dry in an aluminum pan. 5–10 wt% of microcapsules relative to the solid content of the PMA latex was employed. The resulting film was cut with a razor

blade and the cross-section of the film was analyzed with SEM. Figure 5.19 shows the cross-section of PMA films without microcapsules (a) and with DiAcrylate (b) and TetraThiol (c and d) microcapsules. It can clearly be observed that the microcapsules were ruptured after the PMA film was cut with a razor blade. The PMA film that does not contain microcapsules shows a rather smooth cross-section, whereas the cross-sections of the PMA films with microcapsules show ruptured capsules. In Figure 5.19b the ruptured capsule and also the thickness of the shell can be observed.

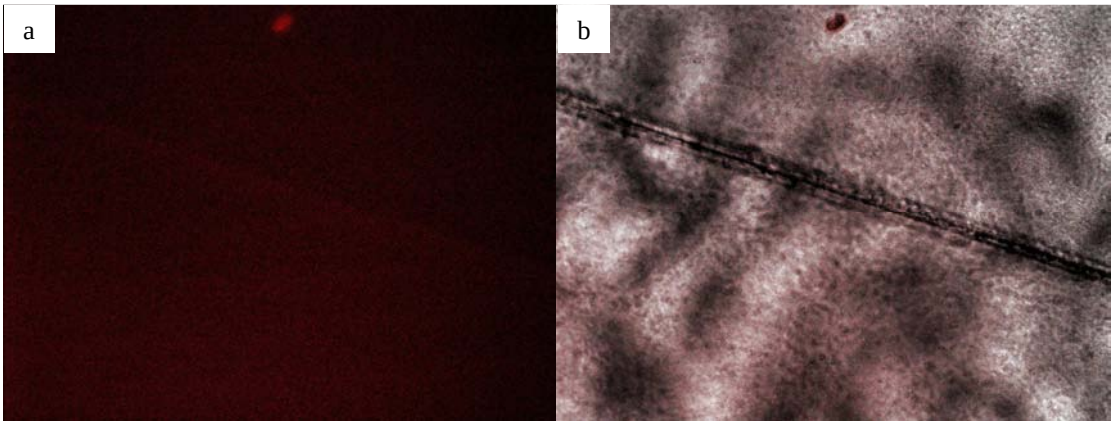

Figure 5.20: Images showing hardly any fluorescence emission at a cut made with a razor blade in a PMA film containing only fluorescent probe. The images are obtained at 20x magnification. Image a shows the fluorescence image and image b shows the overlay of the fluorescence image with the non-fluorescence image.

To further investigate the rupture of the capsules and the presence of the core compound along the cut, TetraThiol microcapsules were dispersed in the PMA latex together with the rhodamine-based fluorescent probe described earlier this section. The composite coating was air-dried in an aluminum pan and after that a small, shallow cut was inserted with a razor blade. In a similar fashion as investigated for the reaction of the rhodamine-based fluorescent probe with TetraThiol (Figure 5.18), intense fluorescence emission would appear if TetraThiol is present along the cut. This would mean that the microcapsules that are embedded in the coating contain TetraThiol as the core material and above all, the microcapsules do rupture upon the occurrence of a cut in the coating.

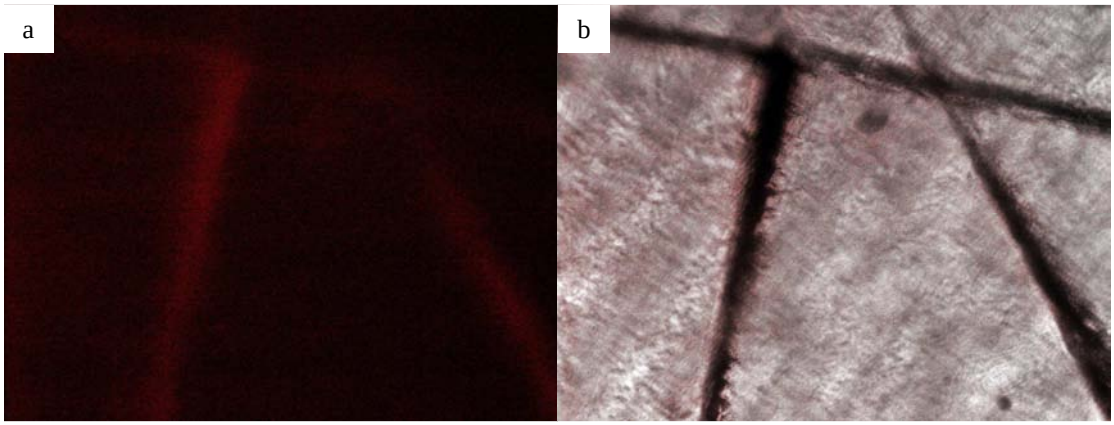

Figure 5.21: Images showing hardly any fluorescence emission at a cut made with a razor blade in a PMA film containing only microcapsules with TetraThiol core. The images are obtained at 20x magnification. Image a shows the fluorescence image and image b shows the overlay of the fluorescence image with the non-fluorescence image.

Figures 5.20 to 5.22 show images obtained from the fluorescence microscope. Figures 5.20 and 5.21 serve as a reference and are composed of a PMA film with either rhodamine-based fluorescent probe *or* TetraThiol microcapsules dispersed in the coating. Both reference films show hardly any fluorescence emission. The coating containing TetraThiol microcapsules *and* rhodamine-based fluorescent probe on the other hand, shows highly intense fluorescence emission (Figure 5.22). This means that upon inserting a cut with a razor blade in a PMA film, the microcapsules do rupture and the core material is released in the cut. The images obtained from the fluorescence microscope are an addition to the SEM images (Figures 5.19a–d) that already indicated that the microcapsules do rupture upon insertion of a cut with a razor blade. This means that embedding TetraThiol *and* DiAcrylate microcapsules together in a coating formulation (with or without the addition of a photoinitiator), could potentially serve as a self-healing mechanism for the autonomous repair of the coating.

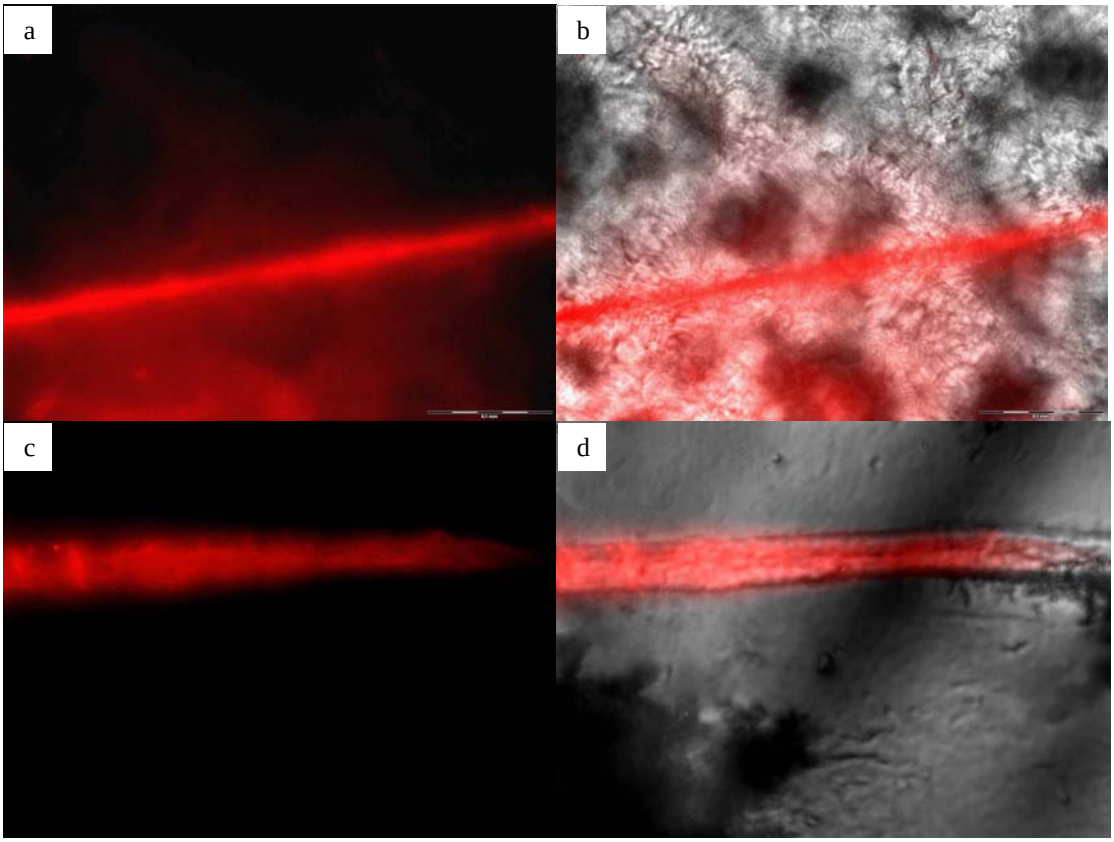

Figure 5.22: Images showing fluorescence emission at a cut made with a razor blade in a PMA film containing microcapsules with TetraThiol core and fluorescent probe. Images a and b are obtained at 20x magnification and images c and d are obtained at 60x magnification. Images a and c show the fluorescence image and images b and d show the overlay of the fluorescence image with the non-fluorescence image.

5.3.6 Incorporation of both TetraThiol and DiAcrylate microcapsules in a coating

To investigate the self-healing ability of the current system, both TetraThiol and DiAcrylate microcapsules are embedded in a PMA film, together with a small amount of photoinitiator (~0.5 wt% relative to TetraThiol). In a similar way as described above, a shallow cut with a width of about 10–20 µm is introduced in the composite coating with a razor blade. The composite coating is subsequently exposed to UV radiation for one hour and the resulting coating is analyzed with SEM.

Scheme 5.5 shows an illustration with the concept of self-healing based on the incorporation of microcapsules with TetraThiol and DiAcrylate as the core material in the composite coating. Upon the formation of a (micro)crack (with)in the coating, the microcapsules should rupture and release their content at the place of the defect. The thiol-ene polymerization that subsequently takes place, should heal the crack and prevent the substrate from exposure to environmental influences. Although the place of the crack might still be visible after healing, the substrate is protected and the coating prevents the substrate from failing.

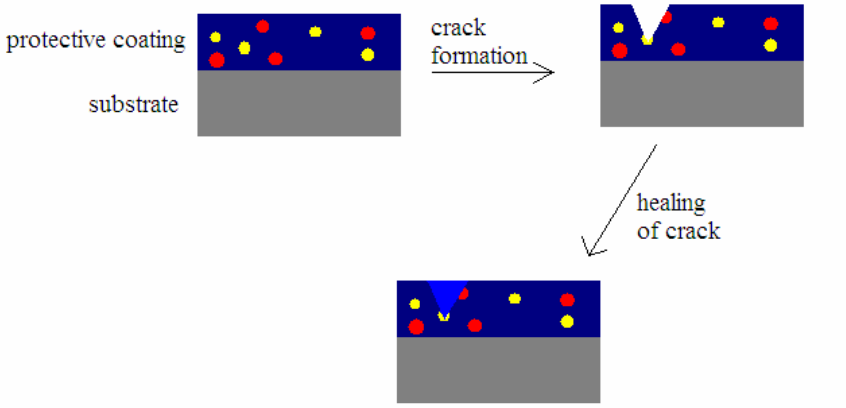

Scheme 5.5: Illustration showing the concept of a self-healing coating that results in protection of the substrate.

Figures 5.23a–d show representative SEM images of a partially repaired cut in a composite PMA film containing TetraThiol and DiAcrylate microcapsules. The microcapsule content in the PMA film was about 5 wt% of both TetraThiol and DiAcrylate microcapsules relative to the solid content of the PMA latex. It was already observed from the SEM images of the cross-section that the microcapsules do rupture upon insertion of a cut with a razor blade. The fluorescence microscope images show in addition that TetraThiol is released in the cut. Although the cut was not completely healed, the images in Figures 5.23a–d clearly indicate that a healing process took place. One important cause for the partial recovery of the composite coating is related to the inhomogeneous dispersion of the microcapsules in the coating. Although the TetraThiol

microcapsules were dispersed fairly homogeneously throughout the composite coating, the DiAcrylate microcapsules aggregated considerably. This resulted in an inhomogeneous distribution of the microcapsules in the composite coating. As a consequence, regions of large aggregates are present that are not efficient in the self-healing process and areas of low concentration of capsules were present. Although the recovery efficiency of the coating has to be improved, the potential use of microcapsules as reservoirs for healing agents in combination with thiol-ene chemistry as a self-healing mechanism has been demonstrated.

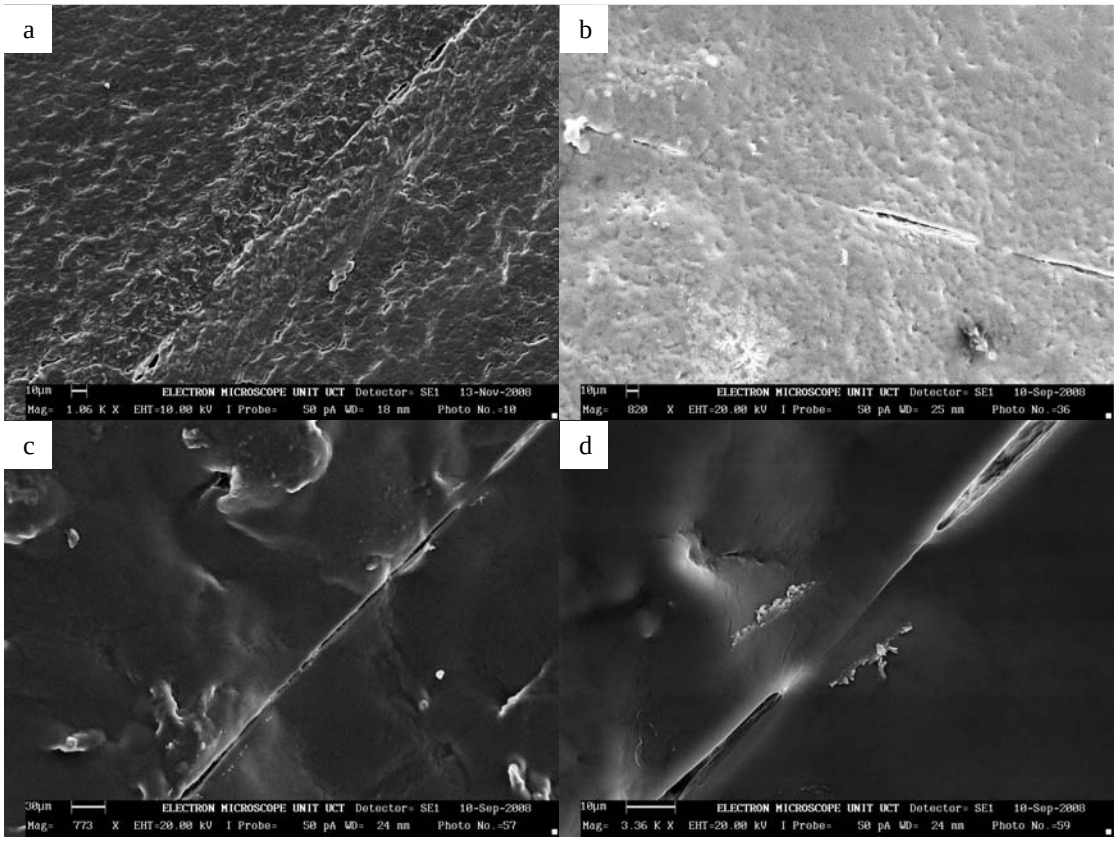

Figure 5.23: SEM images of a partially repaired PMA film via thiol-ene chemistry.

5.4 Conclusions

Considerable advancements in the development of (autonomous) self-healing coatings have been made over the past decade. This chapter described the development of a self-healing coating based on urea-formaldehyde microcapsules as reservoir for reactive

healing agents in combination with thiol-ene chemistry as the healing mechanism. The system contains two different types of microcapsules, *i.e.* a two-component healing system with TetraThiol and DiAcrylate microcapsules. The kinetics of TetraThiol-DiNorbornene and TetraThiol-DiAcrylate polymerizations have been investigated via thermal analysis using DSC. The results indicated that both systems undergo rapid network formation with a concomitant increase in E_{act} and A, which was especially pronounced after reaching the gel point. Kinetic experiments carried out via initiation with UV radiation indicated that the addition of a photoinitiator to the reaction formulation resulted in a significant increase in the rate of polymerization. TetraThiol-DiNorbornene polymerization resulted in fast formation of a polymer network, even without the addition of a photoinitiator and/or without exposure to UV radiation. This might prove to be highly advantageous for (industrial) application purposes.

The synthesis of urea-formaldehyde microcapsules with TetraThiol, DiAcrylate, DiNorbornene or hexadecane as the core component, resulted in small microcapsules with very smooth surface. The particle size ranged from one to ten micrometers. Attempts to increase the particle size resulted in bigger microcapsules ranging from 50–100 micrometers. The smooth surface was replaced however, with a smooth inner membrane on top of which agglomerated urea-formaldehyde nanoparticles had deposited from the aqueous phase. A large fraction of microcapsules appeared to have broken shells and the encapsulation yield was low. Therefore, the smaller microcapsules with smooth surface were embedded in a PMA film and employed for investigation into the self-healing ability of the composite coating.

The rupture of microcapsules upon the formation of a cut in a PMA film with a razor blade has primarily been investigated with the aid of a rhodamine-based fluorescent probe. Reaction between the probe and TetraThiol leads to the formation of rhodamine, which shows intense fluorescence emission, whereas the probe itself shows no significant fluorescence emission. It appeared that reference coating formulations consisting of PMA film and TetraThiol microcapsules (no probe) and PMA film and rhodamine-based fluorescent probe (no TetraThiol microcapsules), showed only marginal fluorescence

emission. The PMA film that contained both TetraThiol microcapsules *and* rhodamine based fluorescent probe on the other hand, showed a significant increase in fluorescence emission after introduction of a cut with a razor blade. This strongly indicated that the microcapsules rupture and release their content, which then becomes available at the place of defect. In addition, SEM images taken from the cross-section of PMA films with microcapsules embedded indicated that the microcapsules do rupture upon crack formation with a razor blade.

The composite coating consisting of PMA film, 5 wt% DiAcrylate and 5 wt% TetraThiol microcapsules (both amounts are relative to the solid content of the PMA latex) and 0.5 wt% photoinitiator (relative to TetraThiol) was investigated for its self-healing ability. After introduction of a cut with a razor blade and exposing the composite coating to UV radiation, the coatings were examined with SEM. It appeared that the coatings were only partially repaired. This means that the microcapsules do rupture upon crack formation with a razor blade and that the healing agent is attracted to the place where the coating fails. The thiol-ene polymerization is initiated and partially restores the original coating, providing protection of the substrate against *e.g.* oxidation. The main reason for only partial recovery of the coating was the formation of large aggregates of DiAcrylate microcapsules. These aggregates of microcapsules appeared not to rupture, which reduced the efficiency of the healing process.

References

1. J.-L. Wietor and R.P. Sijbesma, *Angew. Chem. Int. Ed.* **2008**, *47*, 8161-8163
2. K. Aramaki, *Corros. Sci.* **2002**, *44*, 1375-1389
3. J.H. Osborne, K.Y. Blohowiak, S.R Taylor, C. Hunter, G. Bierwagon, B. Carlson, D. Bernard and M.S. Donley, *Progr. Org. Coatings* **2001**, *41*, 217-225
4. J.H. Osborne, *Progr. Org. Coatings* **2001**, *41*, 280-286
5. D.G. Shchukin, M. Zheludkevich, K. Yasakau, S. Lamaka, M.G.S. Ferreira and H. Möhwald, *Adv. Mater.* **2006**, *18*, 1672-1678
6. M.L. Zheludkevich, I.M. Salvado and M.G.S. Ferreira, *J. Mater. Chem.* **2005**, *15*, 5099-5111
7. M. Garcia-Heras, A. Jimenez-Morales, B. Casal, J.C. Galvan, S. Radzki and M.A. Villegas, *J. Alloys Comp.* **2004**, *380*, 219-224
8. M.L. Zheludkevich, R. Serra, M.F. Montemor, K.A. Yasakau, I.M.M. Salvado and M.G.S. Ferreira, *Electrochim. Acta* **2005**, *51*, 208-217
9. M.L. Zheludkevich, R. Serra, M.F. Montemor and M.G.S. Ferreira, *Electrochem. Commun.* **2005**, *7*, 836-840
10. C. Dry, *Composite Structures* **1996**, *35*, 263-269
11. S.R. White, N.R. Sottos, P.H. Geubelle, J.S. Moore, M.R. Kessler, S.R. Sriram, E.N. Brown and S. Viswanathan, *Nature* **2001**, *409*, 794-797
12. T. Yin, M.Z. Rong, M.Q. Zhang and G.C. Yang, *Compos. Sci. Tech.* **2007**, *67*, 201-212
13. K. Dietrich, H. Herma, R. Nastke, E. Bonatz and W. Teige, *Acta Polym.* **1989**, *40*, (4), 243-251
14. B. Boh, E. Knez and M. Staresinic, *J. Microencapsulation* **2005**, *22*, (7), 715-735
15. X.-X. Zhang, X.-M. Tao, K.-L. Yick and X.-C. Wang, *Colloid. Polym. Sci.* **2004**, *282*, 330-336
16. E.N. Brown, M.R. Kessler, N.R. Sottos and S.R. White, *J. Microencapsulation* **2003**, *20*, (6), 719-730
17. S. Cosco, V. Ambrogi, P. Musto and C. Carfagna, *J. Appl. Polym. Sci.* **2007**, *105*, 1400-1411

18. S. Cosco, V. Ambrogi, P. Musto and C. Carfagna, *Macromol. Symp.* **2006**, *234*, 184-192
19. L. Yuan, G. Liang, J. Xie, L. Li and J. Guo, *Polymer* **2006**, *47*, 5338-5349
20. I.B. Jang, J.H. Sung and H.J. Choi, *J. Mater. Sci.* **2005**, *40*, 1031-1033
21. K.S. Kim, J.Y. Lee, B.J. Park, J.H. Sung, I. Chin, H.J. Choi and J.H. Lee, *Colloid. Polym. Sci.* **2006**, *284*, 813-816
22. D.S. Xiao, M.Z. Rong and M.Q. Zhang, *Polymer* **2007**, *48*, 4765-4776
23. M.M. Caruso, D.A. Delafuente, V. Ho, N.R. Sottos, J.S. Moore and S.R. White, *Macromolecules* **2007**, *40*, 8830-8832
24. E.N. Brown, N.R. Sottos and S.R. White, *Exp. Mech.* **2002**, *42*, (4), 372-379
25. M.W. Keller, S.R. White and N.R. Sottos, *Polymer* **2008**, *49*, 3136-3145
26. A. Kumar, L.D. Stephenson and J.N. Murray, *Progr. Org. Coatings* **2006**, *55*, 244-253
27. M.R. Kessler and S.R. White, *J. Polym. Sci., Part A: Polym. Chem.* **2002**, *40*, 2373-2383
28. J.D. Rule, E.N. Brown, N.R. Sottos, s.R. White and J.S. Moore, *Adv. Mater.* **2005**, *17*, 205-208
29. E.N. Brown, S.R. White and N.R. Sottos, *Comp. Sci. Tech.* **2005**, *65*, 2466-2473
30. E.N. Brown, S.R. White and N.R. Sottos, *Comp. Sci. Tech.* **2005**, *65*, 2474-2480
31. M.W. Keller, S.R. White and N.R. Sottos, *Adv. Funct. Mater.* **2007**, *17*, 2399-2404
32. Y.C. Yuan, M.Z. Rong, M.Q. Zhang, J. Chen, G.C. Yang and X.M. Li, *Macromolecules* **2008**, *41*, 5197-5202
33. C.E. Hoyle, T.Y. Lee and T. Roper, *J. Polym. Sci., Part A: Polym. Chem.* **2004**, *42*, 5301-5338
34. N.B. Cramer and C.N. Bowman, *J. Polym. Sci., Part A: Polym. Chem.* **2001**, *39*, 3311-3319
35. N.B. Cramer, S.K. Reddy, A.K. O'Brien and C.N. Bowman, *Macromolecules* **2003**, *36*, 7964-7969
36. T.Y. Lee, T.M. Roper, E.S. Jönsson, C.A. Guymon and C.E. Hoyle, *Macromolecules* **2004**, *37*, 3606-3613

37. S.K. Reddy, N.B. Cramer and C.N. Bowman, *Macromolecules* **2006**, *39*, 3673-3680
38. S.K. Reddy, N.B. Cramer and C.N. Bowman, *Macromolecules* **2006**, *39*, 3681-3687
39. T.Y. Lee, Z. Smith, S.K. Reddy, N.B. Cramer and C.N. Bowman, *Macromolecules* **2007**, *40*, 1466-1472
40. T.Y. Lee, J. Carioscia, Z. Smith and C.N. Bowman, *Macromolecules* **2007**, *40*, 1473-1479
41. H. Wei, A.F. Senyurt, S. Jönsson and C.E. Hoyle, *J. Polym. Sci., Part A: Polym. Chem.* **2007**, *45*, 822-829
42. Q. Li, H. Zhou, D.A. Wicks and C.E. Hoyle, *J. Polym. Sci., Part A: Polym. Chem.* **2007**, *45*, 5103-5111
43. J.A. Carioscia, L. Schneidewind, C. O'Brien, R. Ely, C. Feeser, N. Cramer and C.N. Bowman, *J. Polym. Sci., Part A: Polym. Chem.* **2007**, *45*, 5686-5696
44. A.F. Jacobine, D.M. Glaser, P.J. Grabek, D. Mancini, M. Masterson, S.T. Nakos, M.A. Rakas and J.G. Woods, *J. Appl. Polym. Sci.* **1992**, *45*, 471-485
45. B.S. Furniss, A.J. Hannaford, P.W.G. Smith and A.R. Tatchell, *Vogel's textbook of practical organic chemistry*, fifth edition, **1989**, ISBN 0-582-46236-3
46. Y.T. Wang, X.P. Zhao and D.W. Wang, *J. Microencapsulation* **2006**, *23*, (7), 762-768
47. B.R. Nair and D.J. Francis, *Polymer* **1983**, *24*, 626-630
48. X.-X. Zhang, Y.-F. Fan, X.-M. Tao and K.-L. Yick, *J. Colloid Interface Sci.* **2005**, *281*, 299-306
49. A. Shibata, K. Furukawa, H. Abe, S. Tsuneda and Y. Ito, *Bioorg. Med. Chem. Lett.* **2008**, *18*, 2246-2249
50. W. Jiang, Q. Fu, H. Fan, J. Ho and W. Wang, *Angew. Chem. Int. Ed.* **2007**, *46*, 8445-8448
51. T. Ozawa, *Thermochim. Acta* **2000**, *355*, 35-42
52. S. Vyazovkin and N. Sbirrazzuoli, *Macromol. Rapid Commun.* **2006**, *27*, 1515-1532
53. W. Liu, Q. Qiu, J. Wang, Z. Huo and H. Sun, *Polymer* **2008**, *49*, 4399-4405

54. Y. Cheng, Y. Huang, K. Alexander and D. Dollimore, *Thermochim. Acta* **2001**, *367-368*, 23-28

55. C.F. Deng, X.X. Zhang, D.Z. Wang and Y.X. Ma, *Mater. Lett.* **2007**, *61*, 3221-3223

56. M. Ghaemy, S.M. Amini Nasab and M. Barghamadi, *Polym. Compos.* **2008**, *29*, 165-172

57. P. Sajkiewicz, L. Carpaneto and A. Wasiak, *Polymer* **2001**, *42*, 5365-5370

Chapter 6: Development of self-healing coatings based on nanocapsules[a]

Abstract

This chapter describes the development of a self-healing coating based on nanocapsules containing pentaerythritol tetrakis(3-mercaptopropionate) (TetraThiol) and 1,6-hexanediol di-(*endo, exo*-norborn-2-ene-5-carboxylate) (DiNorbornene) as the healing agents. The nanocapsules are embedded in a poly(methyl acrylate) (PMA) film and thiol-ene step-growth free-radical polymerization serves as the healing mechanism. In addition, TetraThiol and 1,6-hexanediol diacrylate (DiAcrylate) microcapsules and TetraThiol and DiNorbornene nanocapsules are embedded in commercial styrene-acrylate and pure acrylic coating formulations for assessment of self-healing ability. The rupture of TetraThiol nanocapsules embedded in a PMA film after introduction of a cut with a razor blade is examined by means of fluorescence microscopy. The addition of a rhodamine-based fluorescent probe to the coating formulation requires the probe to react with TetraThiol, before any fluorescence emission can be observed. It appears that the PMA film containing both TetraThiol nanocapsules *and* rhodamine-based fluorescent probe shows significant fluorescence emission. This means that the TetraThiol nanocapsules do rupture upon crack formation, allowing for potential self-healing of the coating. The microcapsules embedded in the commercial coatings (5 wt% relative to the solid content of the coating) allow for only partial recovery of the film after crack formation with a razor blade. Due to the aggregation of DiAcrylate microcapsules that do not rupture upon crack formation, the efficiency of self-healing is reduced. The embedding of 10 wt% TetraThiol and ~15 wt% DiNorbornene nanocapsules in the PMA coating also allows for only partial recovery of the coating upon crack formation with a razor blade. The nanocapsules embedded in the commercial coatings show reduced ability of self-healing compared to nanocapsules embedded in the PMA coating. All composite coatings with nanocapsules are very brittle, which is mainly due to the DiNorbornene nanocapsules, which were synthesized via miniemulsion homopolymerization of styrene. Moreover, the commercial coatings are of more brittle nature than the PMA coating and the resulting severe cuts require large amounts of healing agent at the place of the defect.

[a] The results described in this chapter are filed in a patent application with number EP09150796.2

6.1 Introduction

Chapter 5 described the development of a self-healing coating based on the incorporation of microcapsules with TetraThiol and DiAcrylate core in a poly(methyl acrylate) (PMA) film. Also a small amount of photoinitiator was embedded in the coating to enhance the rate of thiol-ene photopolymerization upon exposure to UV radiation. In an identical way as described for the development of a self-healing coating based on microcapsules, this chapter describes the development of a self-healing coating based on nanocapsules. The nanocapsules containing TetraThiol or DiNorbornene as the core material are synthesized via the miniemulsion polymerization method. Chapter 4 described the synthesis of TetraThiol containing core-shell nanoparticles via miniemulsification of an oil-in-water emulsion with various styrene-maleic anhydride (block) copolymers as surfactant. This chapter first describes the synthesis of nanocapsules with DiNorbornene as the core material via miniemulsion polymerization, where DiNorbornene simultaneously acts as the costabilizer. Then the development of a self-healing coating based on nanocapsules is examined. An investigation into the rupture of TetraThiol nanocapsules is carried out with fluorescence microscopy in a similar fashion as described for the TetraThiol microcapsules in Chapter 5. Then both types of nanocapsules are embedded in a PMA film together with a small amount of photoinitiator. After the introduction of a cut in the coating with a razor blade, the composite coating is exposed to UV radiation. If the nanocapsules are ruptured upon failure of the composite coating, TetraThiol and DiNorbornene are released and flow into the cut, where the thiol-ene free-radical step-growth polymerization will be initiated upon exposure to UV radiation. This would result in arrest of the crack-growth and healing of the coating, consequently protecting the substrate against environmental influences such as corrosion.

6.2 Experimental details

6.2.1 Chemicals

Methyl acrylate (MA, Aldrich 99% (GC), [96-33-3]) was purified by passing it through a column of inhibitor remover (Aldrich, [9003-70-7]). Styrene (Plascon Research Centre, University of Stellenbosch, estimated purity ~99% by ^{1}H-NMR) was washed three times with an aqueous 0.3 M KOH solution to remove the inhibitor and subsequently distilled

under reduced pressure. 2,2'-Azobis(isobutyronitrile) (AIBN, Riedel de Haën) was recrystallized from ethanol and dried under vacuum. Pentaerythritol tetrakis(3-mercaptopropionate) (TetraThiol, Fluka ≥96%, [7575-23-7]) and 2,2-dimethoxy-2-phenylacetophenone (DMPA, Aldrich 99%, [24650-42-8]) were used without further purification. A poly(methyl acrylate) (PMA) latex, synthesized as described in Chapter 5, was adopted as matrix for the composite coating. Also commercial pure acrylic and styrene-acrylate latexes, obtained from Plascon Research Centre, University of Stellenbosch, were used as matrix for the incorporation of micro- and nanocapsules. Texanol (film forming agent (coalescent), Plascon Research Centre, University of Stellenbosch) was used as received. Distilled water was used throughout the experiments described in this chapter, unless stated otherwise.

6.2.2 Encapsulation of DiNorbornene via miniemulsion polymerization

To a 250 mL beaker was added 40 g of distilled deionized (DDI) water and 0.40 g of SDS (1 wt% of the aqueous phase). Separately 10 g of styrene, 0.16 g of AIBN (1.0 mol% with respect to styrene) and 2.0 g of DiNorbornene (synthesized as described in Chapter 5, simultaneously acts as costabilizer) were mixed together in a 100 mL beaker. Both homogeneous solutions were put together and a pre-emulsion was formed via stirring with a stirrer bar at 400 rpm for half an hour. The pre-emulsion was then subjected to ultrasonication for 20 minutes during which 95 kJ of energy was delivered. The miniemulsion that was formed was transferred to a 100 mL 3-neck round-bottom flask and the miniemulsion was purged with nitrogen gas to remove the oxygen from the system. Simultaneously the oil bath was preheated to the desired reaction temperature of 70 °C. After 30 minutes of purging with nitrogen, the flask was immersed in the oil bath. The polymerization was allowed to continue overnight, after which the miniemulsion was cooled down to room temperature. After polymerization, a latex was obtained with 20 wt% solid content and with a particle size of 132 nm and a particle size distribution of 0.233 (bimodal distribution). The number average molecular weight and polydispersity index of the final polymer were 1.2×10^5 g/mol and 4.52 respectively.

6.2.3 Incorporation of micro- or nanocapsules in various coating formulations

First it was investigated whether the nanocapsules embedded in the coating do rupture upon the introduction of a crack with a razor blade. This was done via fluorescence microscopy in a similar fashion as described in Chapter 5. For this purpose TetraThiol nanocapsules (synthesized as described in Chapter 4) and rhodamine-based fluorescent probe (synthesized as described in Chapter 5) were homogeneously dispersed in a PMA latex (synthesized as described in Chapter 5) that served as the matrix. The composite coating was air-dried and a crack was introduced with a razor blade. After allowing the fluorescent probe and TetraThiol to react for sufficient time (longer than 24 hours), the fluorescence emission of the composite coating was examined with fluorescence microscopy. The fluorescence emission was compared with reference coatings that were composed of PMA matrix with only rhodamine-based fluorescent probe or PMA matrix with only TetraThiol nanocapsules.

The self-healing ability of the coatings was tested on a composite coating containing both 10 wt% TetraThiol nanocapsules and about 15 wt% DiNorbornene nanocapsules (molar ratio of thiol to ene functionality of 1) with respect to the solid content of the matrix. As matrix were used a PMA film, a styrene-acrylate film or a pure acrylic film. Also TetraThiol and DiAcrylate microcapsules were embed in the commercial coating formulations. A small amount of photoinitiator (DMPA, ~0.5 wt% with respect to TetraThiol) was dispersed in the composite coating. The composite coating was air-dried and a cut was introduced with a razor blade. The coating was then exposed to UV radiation and subsequently examined with SEM.

6.2.4 Characterization

Ultrasonication was done on a Sonics Vibra cell VCX 750 Watt ultrasonic processor with a replaceable ½'' tip. Ultrasonication was conducted for 20 minutes with an amplitude of 70% during which a total amount of 95 kJ was delivered to the miniemulsion system.

The molecular weight distribution of the polymers was obtained via size exclusion chromatography (SEC). The instrument consisted of a Waters 1515 isocratic HPLC

pump, a Waters 717 plus autosampler, a Waters 2487 dual λ absorbance detector and a Waters 2414 refractive index detector at 30 °C. Separation was achieved by using two PLgel 5 μm Mixed-C (300 x 7.5 mm) columns (Polymer Laboratories) connected in series along with a PLgel 5 μm guard column (50 x 7.5 mm). The columns were kept at a constant temperature of 30 °C and THF (Chromasolve, HPLC-grade) stabilized with 0.0125% BHT was used as the eluent at a flow rate of 1.0 mL/min. The system was calibrated with narrow molecular weight polystyrene standards (Polymer Laboratories) ranging from 580–3x10^6 g/mol. Data processing was performed using Breeze Version 3.30 SPA (Waters) software.

^{1}H-NMR spectra were collected from a 400 MHz Varian Unity Inova spectrometer at room temperature in $CDCl_3$ and integration of the spectra was carried out with ACD Labs 10.08 1D ^{1}H-NMR processor.

Dynamic light scattering (DLS) was carried out on a Malvern Instruments ZetaSizer 1000HS_a equipped with a He-Ne laser operating at a wavelength of 633.0 nm and the scattered light was detected at an angle of 90°. The latex was diluted with a 1.0 mM aqueous solution of NaCl. The sample was diluted until the rate meter indicated a rate of about 300 kilocounts per second (kCps). The final particle size and particle size distribution were obtained from five measurements, each consisting of ten sub-runs. The particle size and particle size distribution were calculated via a CONTIN analysis[1] and presented as the Z-average particle size (Z_{avg}).

The morphology of the miniemulsion particles was investigated via transmission electron microscopy (TEM) analysis. The latex was diluted with DDI water until the latex became translucent and 3 μL was transferred onto a hydrophilic carbon-coated copper grid by pipette. Excess sample was removed by blotting with filter paper and the remainder was allowed to dry at ambient temperature before analysis was carried out. The analyses were done on a LEO912 TEM instrument operating with an accelerating voltage of 120 kV. Each sample was analyzed at different areas of the copper grid to obtain representative data and the particle size was determined manually.

Fourier transform infrared (FTIR) spectra were recorded on a Nexus FTIR spectrophotometer equipped with a Smart Golden Gate attenuated total reflectance (ATR) diamond from Thermo Nicolet with ZnSe lenses. Each spectrum was scanned 32 times with 4.0 cm^{-1} resolution and data analysis was performed with Omnic Software version 7.2.

SEM analysis was carried out on a Leica S440 instrument. The samples were placed on a SEM grid and coated with a layer of gold-palladium to induce contrast and reduce charging of the sample.

Samples for fluorescence microscopy were observed on an Olympus Cell$^{\mathbb{R}}$ system attached to an IX-81 inverted fluorescence microscope. The microscope was equipped with a F-view-II cooled CCD camera (Soft Imaging Systems), using 572 nm excitation and UBG triple band pass emission filter. For the z-stack image frames, an Olympus Plan Apo N 60x/1.4 oil objective and the Cell$^{\mathbb{R}}$ imaging software have been used for the image acquisition and analysis.

6.3 Results and discussion

6.3.1 Encapsulation of DiNorbornene via miniemulsion polymerization

The synthesis of nanocapsules that contain DiNorbornene as the core component was initially attempted via miniemulsification in a similar fashion as described for TetraThiol in Chapter 4. Because of the poor stability of the nanocapsules, as evidenced by phase separation and DLS analysis, which showed large particles with a very broad particle size distribution, the encapsulation of DiNorbornene was attempted via miniemulsion polymerization. Although DiNorbornene contains a carbon-carbon double bond that may participate in free-radical (co)polymerization, norbornene is generally polymerized in the presence of a (Ruthenium) catalyst via Ring-Opening Methathesis Polymerization (ROMP).[2] Therefore, norbornene may be sufficiently inert toward radical polymerization and the compound can be encapsulated via free-radical miniemulsion polymerization.

For the development of a self-healing coating, nanocapsules are synthesized that should consist of a hard shell that does not allow diffusion of the core component through the shell into the matrix. Furthermore, the shell needs to be brittle so that upon the formation of a crack the capsule shell does rupture. A soft shell may deform instead of rupture upon the occurrence of a crack in the coating, causing the crack to continue propagating instead of being healed. For this reason styrene was chosen as the monomer of choice for the encapsulation of DiNorbornene. DiNorbornene would simultaneously act as a costabilizer in the miniemulsion homopolymerization of styrene, as it is a very hydrophobic compound with a very high boiling point.

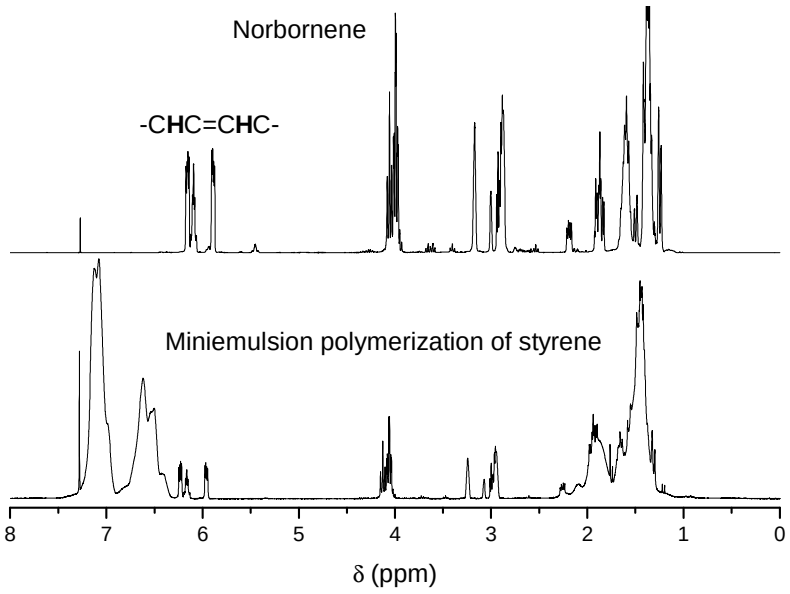

Figure 6.1: ^{1}H-NMR spectra of pure norbornene (top) and the retention of the norbornene peaks after miniemulsion polymerization of styrene (bottom).

Figure 6.1 shows both the ^{1}H-NMR spectra of pure DiNorbornene and of the polymer obtained via miniemulsion polymerization after drying. Special attention is paid to the protons of the carbon-carbon double bond of DiNorbornene. It can clearly be observed that after polymerization of styrene at 70 °C overnight, the protons attached to the carbon-carbon double bond of DiNorbornene are retained. Moreover, the integral ratio of

the double bond protons with the other protons of DiNorbornene is still in good agreement. This means that DiNorbornene did not participate in free-radical copolymerization with styrene and that DiNorbornene was successfully encapsulated. The DLS analysis showed that very small nanocapsules were obtained with a Z_{avg} diameter of 132 nm and a particle size distribution of 0.233. The broad particle size distribution may be the result of a combination of miniemulsion polymerization and emulsion polymerization. The former allows for nucleation of the monomer droplets that ensures that DiNorbornene is encapsulated, as no transport of the highly hydrophobic compound through the aqueous phase is required. The second distribution of particles that is formed via micellar (or homogeneous) nucleation, explains the very small size of these particles.[3] The simultaneous operation of both emulsion and miniemulsion polymerization may be caused by unstable monomer droplets and/or a too large amount of surfactant. However, the surfactant concentration is low, being 1 wt% of the aqueous phase, which makes this argument rather unrealistic. Another possibility could be that DiNorbornene is not as effective as costabilizer as initially anticipated, which would result in degradation of the monomer droplets via diffusion (Ostwald ripening). This would lead to a distribution in the particle size, although each particle would still contain DiNorbornene as the core material.

A significant shoulder in the SEC data confirms that two particle size distributions are present, as both particle size distributions should have significantly different molecular weights. The small particle size distribution would give a higher molecular weight, whereas the large(r) particle size distribution would lead to a lower molecular weight. Figure 6.2 shows TEM images of nanocapsules obtained via miniemulsion homopolymerization of styrene. The TEM images clearly show that two particle size distributions are present. The small nanoparticles constitute the majority of the nanoparticles and have a size of about 65 nm. The size of the larger particles (Figure 6.2b) is about 200 nm and there are a few nanoparticles present with a size of about 100 nm or slightly larger. Although DiNorbornene does not contain an electron dense element to facilitate contrast in the TEM images, it can be assessed that the particles do have a core-shell morphology. In addition, the encapsulation of DiNorbornene with retention of

the carbon-carbon double bond was already assessed via ^{1}H-NMR and ATR-FTIR spectroscopy. Although the Z_{avg} diameter of the particles according to DLS is 132 nm, the DLS analysis shows a bimodal distribution in the particle size. The small particles have a size of 60–70 nm and the large particles have a size of about 150 nm. These data are in good agreement with the particle sizes obtained from TEM analysis.

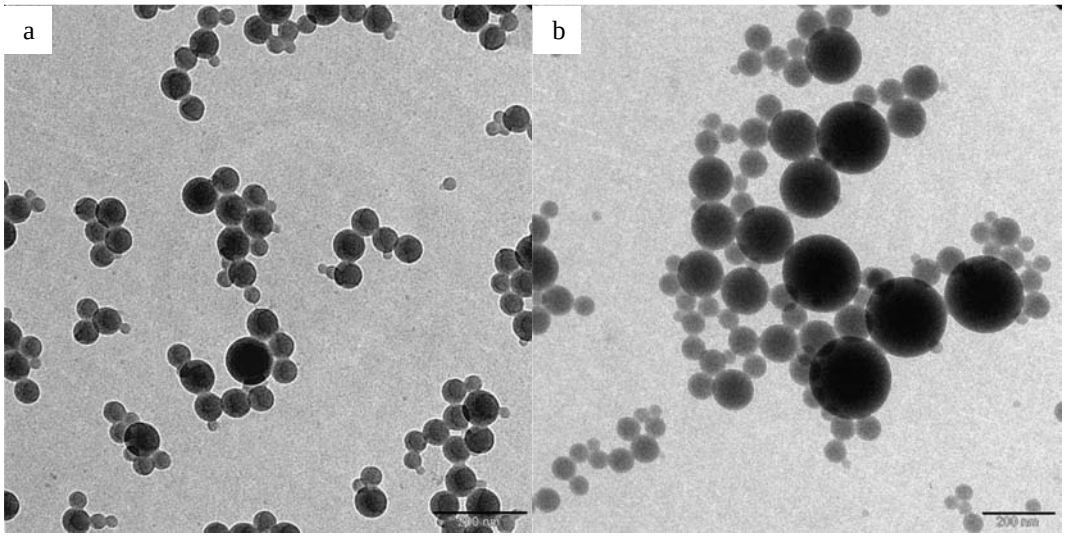

Figure 6.2: TEM images of nanocapsules synthesized via miniemulsion homopolymerization of styrene. The scale bar in the images represents 200 nm.

6.3.2 Investigation into the rupture of nanocapsules via fluorescence microscopy

In a similar fashion as described in Chapter 5, a self-healing coating is developed via the embedding of thiol- and ene-containing capsules in a coating formulation. In this chapter the focus is on nanocapsules, whereas the focus in Chapter 5 was on microcapsules. A very important aspect in the development of a self-healing coating via the introduction of capsules in a polymer matrix, is whether the capsules do rupture upon the formation of a (micro)crack (with)in the coating. Therefore, it needs to be assessed whether the nanocapsules synthesized via miniemulsification (Chapter 4) and miniemulsion polymerization do rupture and subsequently release their reactive load at the place where the crack in the coating occurs. As described in Chapter 5 in detail, a rhodamine-based fluorescent probe was synthesized that shows hardly any fluorescence emission.

However, upon the nucleophilic attack of a thiol, the sulfonamide bond of the rhodamine-based fluorescent probe is broken and rhodamine is formed, which shows intense fluorescence emission. Therefore, incorporating the rhodamine-based fluorescent probe in the polymer matrix together with TetraThiol nanocapsules, would allow determining if the nanocapsules do rupture upon the formation of a crack in the coating.

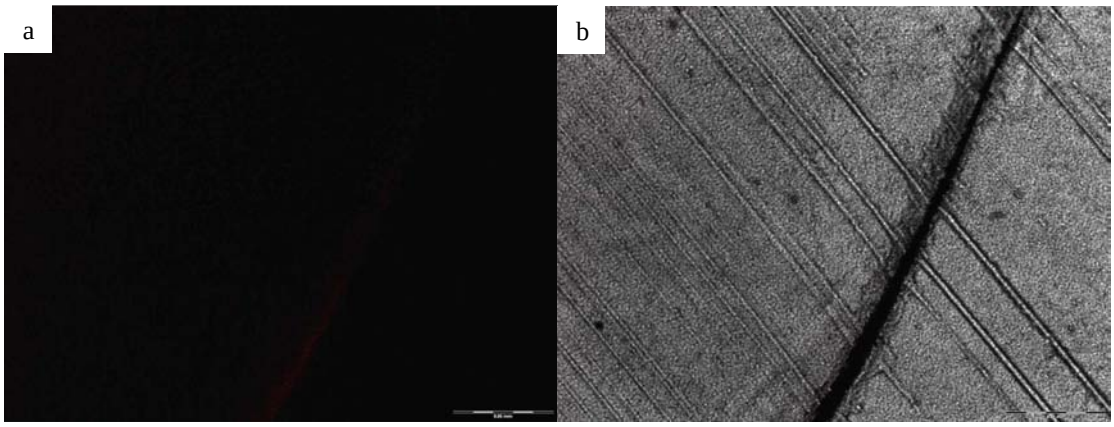

Figure 6.3: Images showing hardly any fluorescence emission at a cut made with a razor blade in a PMA film containing only nanocapsules with TetraThiol core. The images are obtained at 20x magnification. Image a shows the fluorescence image and image b shows the overlay of the fluorescence image with the non-fluorescence image.

As was shown earlier, the PMA film with only rhodamine-based fluorescent probe dispersed in the matrix shows hardly any fluorescence emission. It was also observed that embedding only TetraThiol microcapsules in the PMA film does not result in significant fluorescence emission. Figure 6.3 shows that the same holds for TetraThiol nanocapsules embedded in the PMA film. Practically no fluorescence emission is observed along the cut. Figure 6.4 on the other hand, shows that the incorporation of both TetraThiol nanocapsules *and* rhodamine-based fluorescent probe in the matrix results in intense fluorescence emission. Although the background shows low fluorescence emission, a significant increase in fluorescence emission is observed along the cut introduced in the PMA film. From these results it can be concluded that TetraThiol nanocapsules embedded in the PMA film do rupture upon the introduction of a crack with a razor

blade. The TetraThiol nanocapsules do rupture and release their content along the cut, which allows the reaction with the rhodamine-based fluorescent probe to take place. The rupture of the nanocapsules and the subsequent release of their content in the cut allows for the potential self-healing of the coating.

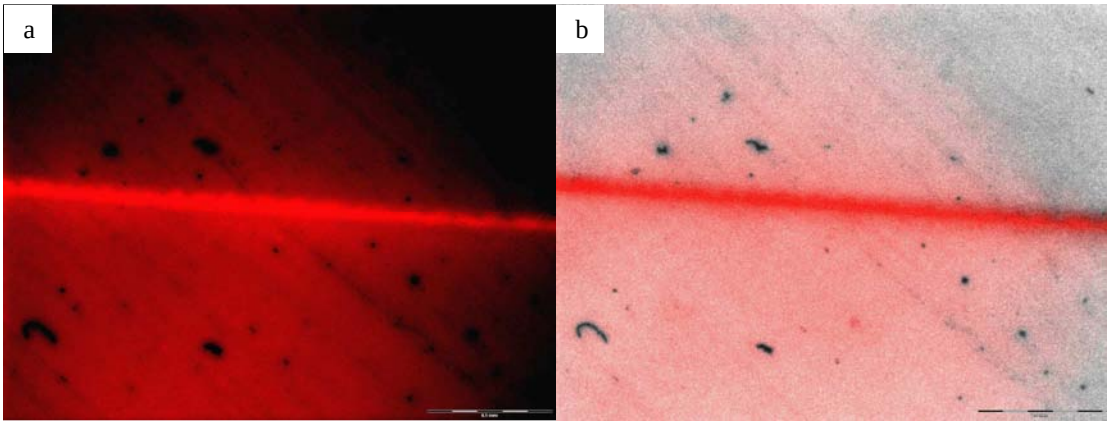

Figure 6.4: Images showing fluorescence emission at a cut made with a razor blade in a PMA film containing nanocapsules with TetraThiol core and rhodamine-based fluorescent probe. The images are obtained at 20x magnification. Image a shows the fluorescence image and image b shows the overlay of the fluorescence image with the non-fluorescence image. The scale bar in the images represents 0.1 mm.

6.3.3 Assessing the self-healing ability of nanocapsules embedded in a PMA film

The results obtained in the previous section indicate that the TetraThiol nanocapsules do rupture upon the introduction of a crack in the PMA film. This means that the coating may have the potential to serve as a self-healing coating. For this purpose both TetraThiol and DiNorbornene nanocapsules are embedded in a PMA film and a small amount of photoinitiator is dispersed in the film to enhance the rate of thiol-ene polymerization. If the nanocapsules would rupture upon the formation of a defect within the coating, the step-growth free-radical thiol-ene photopolymerization would be initiated. The crack-growth would come to an arrest and the coating would subsequently be healed, resulting in the protection of the substrate against environmental influences such as oxygen and chloride ions. It must be pointed out that DiNorbornene was encapsulated via

miniemulsion polymerization of styrene. Polystyrene has inherently a high glass transition temperature (T_g) and the polystyrene film is therefore brittle. The introduction of DiNorbornene nanocapsules in the soft PMA matrix renders the matrix brittle too. This considerably affects the introduction of a crack in the composite film. Caution has to be taken that the film does not break because of its brittle nature, as this would complicate analysis. An advantage of the nanocapsules over the microcapsules is that the nanocapsules are well distributed in the PMA film and do not show any aggregation, unlike the microcapsules that showed (significant) aggregation, especially for the DiAcrylate microcapsules.

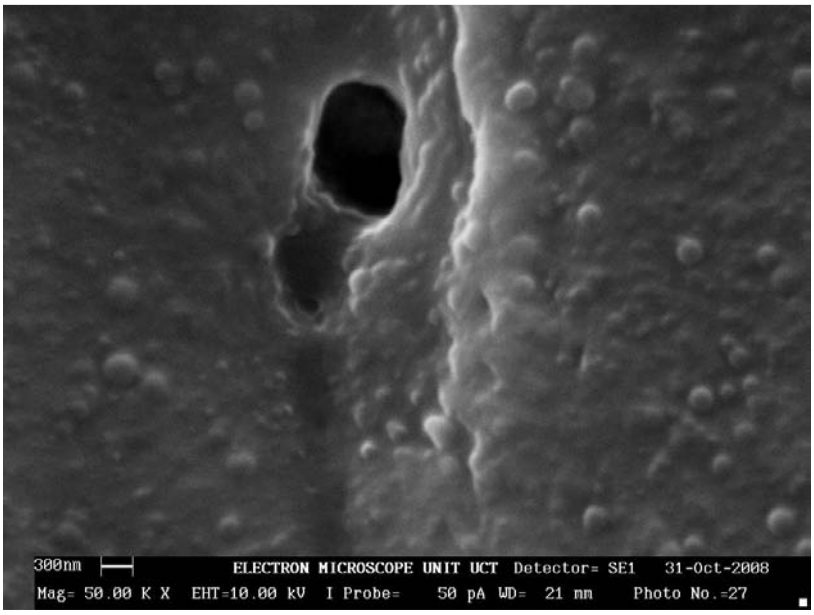

Figure 6.5: SEM image of TetraThiol and DiNorbornene nanocapsules homogeneously distributed in the PMA film. The size of the nanocapsules ranges from about 50–250 nm.

Figure 6.5 shows a SEM image obtained from TetraThiol and DiNorbornene nanocapsules homogeneously distributed in a PMA film. The size of the nanocapsules can be estimated to be approximately 50–250 nm, which is in rather good agreement with DLS and TEM analyses. The Z_{avg} diameter for the TetraThiol and DiNorbornene nanocapsules is 148 and 132 nm respectively, whereby the DLS analysis also indicates

bimodality in the particle size distribution. Moreover, the nanocapsules retain their spherical morphology and do not deform or crack upon film formation. This indicates that the wall material of the nanocapsules shows sufficient strength and allows for embedding of both TetraThiol and DiNorbornene nanocapsules in the PMA film without deterioration of the quality of the nanocapsules.

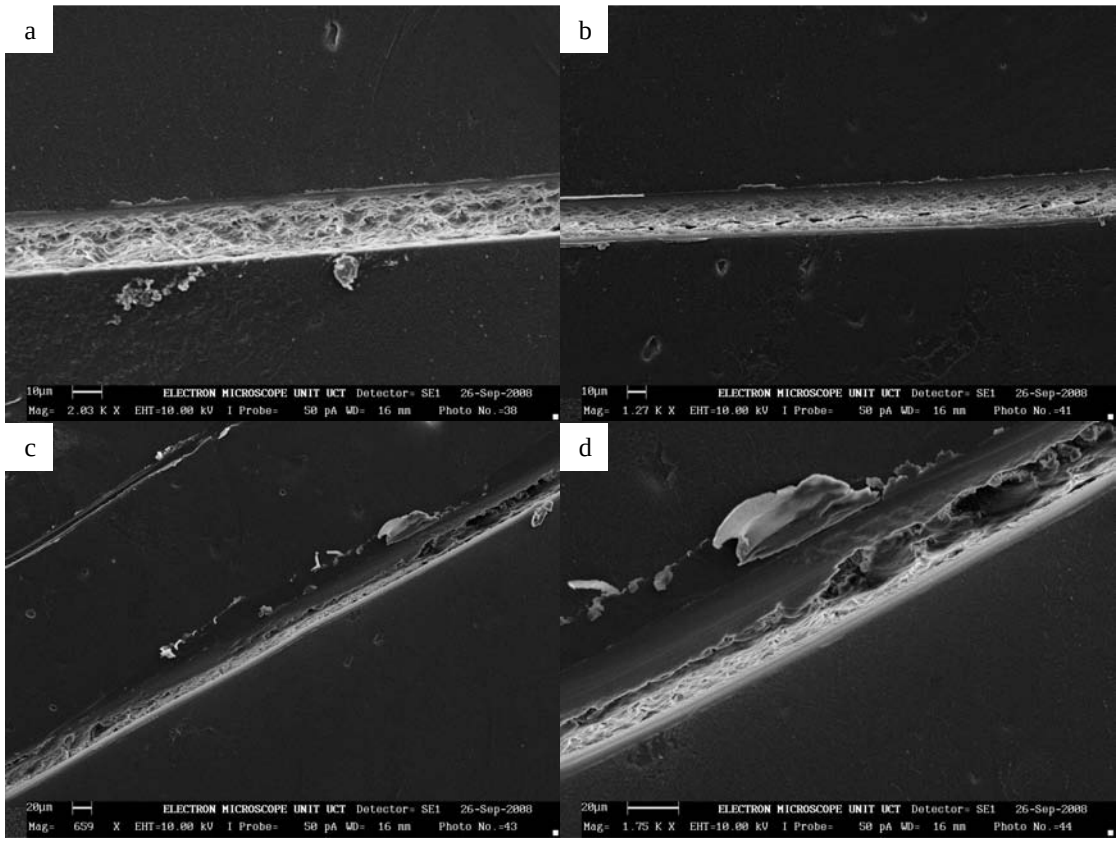

Figure 6.6: SEM images of a partially repaired PMA film via thiol-ene chemistry.

Figure 6.6 shows representative SEM images of a PMA film with both TetraThiol and DiNorbornene nanocapsules (10 wt% of TetraThiol and about 15 wt% of DiNorbornene with respect to the solid content of the matrix, so that a molar ratio of thiol to ene functionality of one is obtained) and a small amount of photoinitiator (~0.5 wt% with respect to TetraThiol) embedded in the matrix. It can be observed that a severe cut is introduced in the composite coating (about 20 µm in diameter) and that the cut has a shallow appearance over the whole length. Figures 6.6c and 6.6d show a region with both

a deep and a shallow cut. This may indicate that the nanocapsules embedded in the matrix were ruptured upon the introduction of a cut and that the thiol-ene polymerization was initiated in the presence of photoinitiator upon exposure to UV radiation. The thiol-ene polymer network recovered the crack partially, probably as a result of a severe cut in combination with a small amount of healing agent present at the cut.

6.3.4 Assessing the self-healing ability of capsules embedded in a commercial film

Both TetraThiol and DiAcrylate microcapsules and TetraThiol and DiNorbornene nanocapsules were embedded in commercial styrene-acrylate and pure acrylic films to examine the potential self-healing ability of the composite coatings. Both films have a T_g slightly above room temperature and therefore film formation cannot takes place via simply drying the composite coating on air. The minimum film-forming temperature (MFFT) is closely related to the T_g of the polymer film and the MFFT can be adjusted by the addition of a film-forming agent (coalescent).[4,5] Texanol was used as coalescent, which acts as a plasticizer and evaporates slowly from the composite coating after film-formation. In case no precautions would have been taken, the emulsion would form a non-coherent, fissured, mechanically unstable film. Another possibility is to dry the coating at elevated temperatures, at least above the MFFT.

Figure 6.7 shows representative SEM images of both styrene-acrylate (images a and b) and pure acrylic (image c) composite coatings with embedded 5 wt% TetraThiol as well as 5 wt% DiAcrylate microcapsules, relative to the solid content of the latex. A small amount of photoinitiator was added to the formulation (~0.5 wt% with respect to TetraThiol). These films were formed with the aid of Texanol (coalescent) and 11 wt% relative to the solid content of the latex was added. A smooth film was obtained with microcapsules embedded in the composite coating. Similar to the composite PMA films with TetraThiol and DiAcrylate microcapsules, the SEM images indicate that partial recovery of the coating was obtained. The DiAcrylate microcapsules in particular, were not homogeneously distributed throughout the film and formed aggregates that were not efficient in the self-healing process. It must also be pointed out that the films were not as

flexible (soft) as the PMA films, which is caused by the difference in T_g between the commercial films and the PMA film. This caused some brittleness in the film, but not as pronounced as for the PMA films that contained nanocapsules. The addition of Texanol, which merely acts as a plasticizer, allowed for proper film-formation and provided that the film did not become brittle during film-formation. After film-formation however, Texanol slowly evaporates and the film restores its brittle nature. Although the self-healing ability might appear not to be as pronounced as for the PMA composite coatings containing microcapsules, the results strongly indicate that thiol-ene chemistry has potential as a healing mechanism for the development of self-healing coatings. The less efficient healing ability may be related to the nature of the commercial styrene-acrylate and pure acrylic films, which is less flexible than the PMA films previously described.

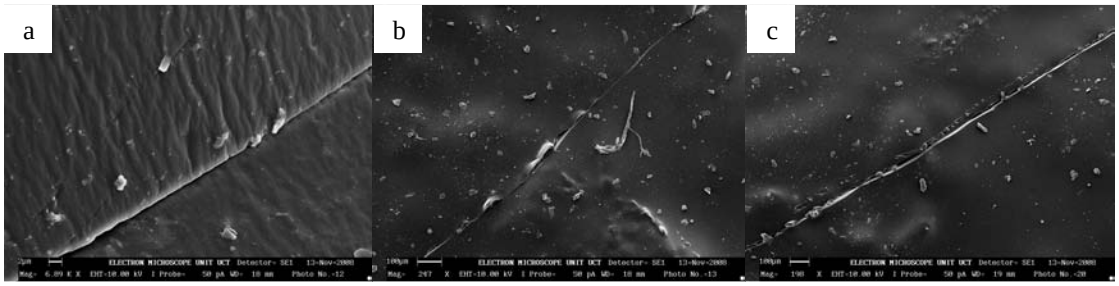

Figure 6.7: SEM images of a partially repaired styrene-acrylate film (a and b) and pure acrylic film (c) resulting from the rupture of microcapsules embedded in the films and subsequent reparation via thiol-ene chemistry.

Figure 6.8 shows representative SEM images of both styrene-acrylate (images a and b) and pure acrylic (image c) composite coatings with embedded 10 wt% TetraThiol and about 15 wt% DiNorbornene nanocapsules with respect to the solid content of the latex, so that the thiol-ene molar ratio is one. About 0.5 wt% of photoinitiator (relative to TetraThiol) is added to the coating formulation to allow for an optimized rate of thiol-ene photopolymerization. The composite coatings were dried both with the aid of Texanol as coalescent (11 wt% with respect to the solid content of the latex, image a) and at an elevated temperature of about 50 °C in a drying oven (images b and c). Again very smooth films were obtained with both TetraThiol and DiNorbornene nanocapsules

homogeneously distributed throughout the coating. These coatings turned out to be of brittle nature due to the DiNorbornene latex that was obtained via miniemulsion homopolymerization of styrene and due to the inherently higher T_g of the commercial styrene-acrylate and pure acrylic films compared to the PMA film.

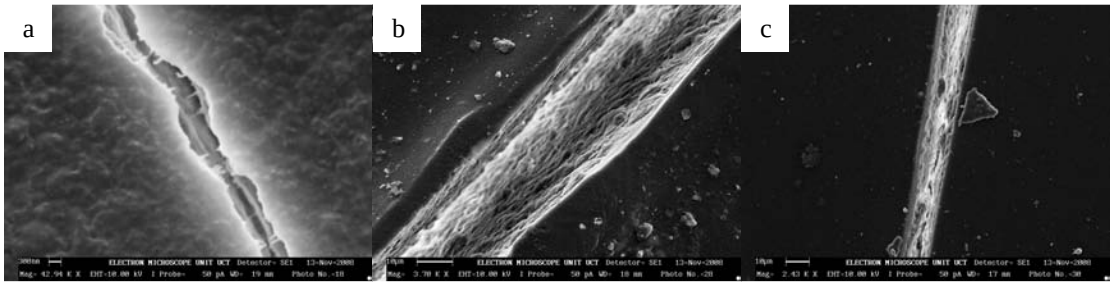

Figure 6.8: SEM images of a styrene-acrylate film (a and b) and pure acrylic film (c) with nanocapsules embedded in the films.

Similar results were obtained as for the composite coatings with nanocapsules embedded in a PMA film as described in Section 6.3.3. Although at some areas in the coatings the cut had a very narrow, shallow appearance, the healing ability of the composite coatings did not seem to be as efficient as the composite coating formulations with microcapsules embedded. One may argue that the cuts show signs of repair, *e.g.* in the styrene-acrylate film (image a) where the cut is very narrow with only 300 nm in diameter, but the signs are not very pronounced. It must also be pointed out that quite a severe cut was introduced in the films, which may have resulted in an insufficient amount of healing agent available. The nanocapsules facilitate in a homogeneous distribution throughout the entire composite coating, which may allow for the incorporation of an increased amount of healing agent in the composite coatings. This may provide the desired self-healing effect as anticipated and prevent the coating from failing, which would lead to the extended protection of the substrate against environmental influences such as corrosion.

6.4 Conclusions

This chapter described the development of a self-healing coating based on the embedding of TetraThiol and DiNorbornene nanocapsules in a composite PMA film. In addition, the self-healing ability of commercial styrene-acrylate and pure acrylic films was investigated with both TetraThiol and DiAcrylate microcapsules and TetraThiol and DiNorbornene nanocapsules embedded in the coatings.

DiNorbornene was encapsulated via miniemulsion homopolymerization of styrene, which resulted in a Z_{avg} diameter of 132 nm with a bimodal distribution. The small particles have a size of about 60–70 nm, whereas the large particles have a size of about 150 nm. Both particle size distributions were in good agreement with TEM analysis. The bimodal distribution may be the result of simultaneous operation of emulsion polymerization and miniemulsion polymerization, due to the fact that DiNorbornene was not sufficiently effective as ultrahydrophobe. This would allow styrene to diffuse from the small droplets to the large droplets, resulting in a distribution in the particle size.

A rhodamine-based fluorescent probe was employed to investigate the rupture of TetraThiol nanocapsules embedded in a composite PMA film upon the introduction of a cut with a razor blade. Fluorescence emission will only be observed if TetraThiol and rhodamine-based fluorescent probe have reacted to form rhodamine. Both reference films, consisting of the probe embedded in a PMA film or TetraThiol nanocapsules embedded in a PMA film, showed hardly any fluorescence emission. The composite PMA film containing both TetraThiol nanocapsules *and* rhodamine-based fluorescent probe on the other hand, showed intense fluorescence emission. This indicated that the TetraThiol nanocapsules do rupture upon the introduction of a cut in the PMA film with a razor blade.

The potential self-healing ability of the composite PMA films containing 10 wt% TetraThiol, ~15 wt% DiNorbornene nanocapsules (with respect to the solid content of the latex) and 0.5 wt% photoinitiator (relative to TetraThiol) was investigated. Visual observation with SEM indicated only partial repair of the coating. The cut introduced in

the composite coating was quite severe with a diameter of about 20 µm and the cut had a shallow appearance. The incomplete recovery of the coating may be explained by the insufficient amount of healing agent present at the cut.

Commercial styrene-acrylate and pure acrylic coatings have been tested for their self-healing ability. The coatings contained either 5 wt% TetraThiol and DiAcrylate microcapsules or 10 wt% TetraThiol and 15 wt% DiNorbornene nanocapsules (relative to the solid content of the latex). In addition, 11 wt% of coalescent (relative to the solid content of the latex) and 0.5 wt% of photoinitiator (relative to TetraThiol) were embedded in the composite coating formulation. SEM images indicate that both styrene-acrylate and pure acrylic composite coatings with microcapsules show only partial repair of the coating after the introduction of a cut with a razor blade. The healing ability does not seem to be as pronounced as for the PMA film, probably due to the more brittle nature of the styrene-acrylate and pure acrylic coatings. The nanocapsules embedded in the styrene-acrylate and pure acrylic coating formulations appear not to be as efficient as self-healing coatings as the coatings with microcapsules. Mainly due to the very brittle nature of the coatings, severe cuts are introduced that require sufficient amounts of healing agent in the cut. Although the amount of healing agent may not be sufficient, the nanocapsules allow for easy, homogeneous distribution throughout the entire coating formulation and therefore the amount of healing agent in the composite coatings can easily be increased. This could lead to the desired self-healing property as anticipated, which would allow for a continued protection of the substrate.

References

1. R.T.C. Ju, C.W. Frank and A.P. Gast, *Langmuir* **1992**, *8*, 2165-2171
2. K. Stubenrauch, C. Moitzi, G. Fritz, O. Glatter, G. Trimmel and F. Stelzer, *Macromolecules* **2006**, *39*, 5865-5874
3. S.J. Bohórquez and J.M. Asua, *J. Polym. Sci., Part A: Polym. Chem.* **2008**, *46*, 6407-6415
4. K. Dören, W. Freitag and D. Stoye, *Water-borne coatings: the environmentally-friendly alternative*, **1994**, ISBN: 1-56990-139-2
5. D. Stoye and W. Freitag, *Paints, coatings and solvents*, Second edition, **1998**, ISBN: 3-527-28863-5

Chapter 7: Epilogue

7.1 General conclusions

The aim of the project, as outlined in Chapter 1, was to introduce a self-healing functionality in a waterborne coating formulation and to investigate its ability to autonomously heal (propagating) microcracks that are formed within the coating. The approach was to synthesize capsules that contain a reactive load and to embed the capsules in a coating formulation. This would potentially lead to rupture of the capsules upon formation of a microcrack within the coating. The healing agent is released and flows via capillary action to the defect where it allows the healing reaction to restore the coating and to supply continued protection to the substrate.

The work described in this dissertation investigated the feasibility of thiol-ene chemistry as a healing mechanism and a two-component healing system was adopted, i.e. the thiol and ene compounds were encapsulated separately. The thiol and ene compounds of choice were pentaerythritol tetrakis(3-mercaptopropionate) (TetraThiol), 1,6-hexanediol diacrylate (DiAcrylate) and 1,6-hexanediol di-(*endo*, *exo*-norborn-2-ene-5-carboxylate) (DiNorbornene). The ability of providing a self-healing functionality to a poly(methyl acrylate) (PMA) film was investigated for both nanocapsules and microcapsules. In addition, commercial styrene-acrylate and pure acrylic coating formulations were adopted as the waterborne coating.

7.1.1 Thiol-ene chemistry

The kinetics of the thiol and ene compounds used as healing agents was assessed as described in Chapter 5. It appeared that both monomer combinations (TetraThiol-DiNorbornene and TetraThiol-DiAcrylate, containing ~1 wt% (photo)initiator with respect to TetraThiol), allowed for rapid network formation at ambient temperature by exposing the solution to UV radiation. More importantly, TetraThiol-DiNorbornene monomer combination proved to rapidly form a network *without* the addition of photoinitiator and/or exposure to UV radiation.

7.1.2 Synthesis of thiol-ene capsules

The synthesis of nanocapsules with TetraThiol content was described in Chapter 4. Miniemulsification was adopted for the synthesis of TetraThiol nanocapsules and various styrene-maleic anhydride (SMA) copolymers were used as surfactant. As was outlined in Chapter 3, Reversible Addition-Fragmentation chain Transfer (RAFT)-mediated polymerization provides good control over radical polymerizations and well-defined (block) copolymers with predetermined molecular weight and narrow molecular weight distribution are obtained. SMA copolymers and block copolymers (chain-extended with styrene P[(Sty-*alt*-MAh)-*b*-Sty]), were synthesized via RAFT-mediated polymerization and successfully used as surfactant for stabilization of the nanocapsules. Well-defined core-shell particles were obtained and the addition of formaldehyde provided steric stabilization to these core-shell particles. It appeared that especially the P[(Sty-*alt*-MAh)-*b*-Sty] block copolymers provided improved stability. DiNorbornene nanocapsules were synthesized via miniemulsion polymerization of styrene. It appeared that DiNorbornene is sufficiently inert towards free-radical polymerization and well-defined particles were obtained. Both TEM and DLS analysis indicated a bimodal distribution, which may be attributed to simultaneous operation of emulsion and miniemulsion polymerization. In addition, DiNorbornene may not have been as effective as the (sole) ultrahydrophobe.

The synthesis of microcapsules proceeded via *in-situ* polymerization of urea and formaldehyde (Chapter 5). Both TetraThiol and DiAcrylate were encapsulated and particles with a very smooth surface were obtained. The particle size of the microcapsules ranged from about one to ten micrometers. These microcapsules were used for the development of a self-healing coating and embedded in various coating formulations.

7.1.3 Investigation into the rupture of TetraThiol capsules

One of the most important criteria for the development of a self-healing coating based on the incorporation of capsules, is that the capsules embedded in the coating do rupture upon the formation of a (micro)crack. The fate of both TetraThiol micro- and nanocapsules was investigated with the aid of a rhodamine-based fluorescent probe. This probe shows practically no fluorescence emission. However, upon reaction with a thiol

compound (TetraThiol), the probe is converted into rhodamine, which shows highly intense fluorescence emission. Thus the embedding of both TetraThiol capsules and rhodamine-based fluorescent probe in a coating and applying a cut with a razor blade, would allow determining if the capsules do rupture. It appeared that reference coatings, containing either TetraThiol capsules or rhodamine-based fluorescent probe, did not show significant fluorescence emission under the fluorescence microscope. The coating containing both TetraThiol capsules *and* rhodamine-based fluorescent probe however, showed significant fluorescence emission, both for the microcapsules and the nanocapsules. This proved that the capsules do rupture upon the formation of a cut with a razor blade, which allows the capsules to be used as reservoir for healing agents and be embedded in a coating formulation for potential use in self-healing coatings.

7.1.4 Self-healing ability of various composite coating formulations

The self-healing ability of coatings was initially investigated for capsules embedded in a PMA film. SEM images indicated that the coatings with microcapsules (5 wt% relative to the solid content of the latex) show only partial recovery of the coatings. This was mainly attributed to the formation of large aggregates of DiAcrylate microcapsules that reduced the efficiency of the self-healing process. The incorporation of nanocapsules (10 wt% TetraThiol and 15 wt% DiNorbornene) also showed partial recovery of the PMA coating, although the healing effect was not as pronounced as for the microcapsules. The main reason given for this was the brittle nature of the DiNorbornene nanocapsules, which were synthesized via miniemulsion polymerization of styrene. This rendered the coating brittle, which affected the introduction of a cut with a razor blade. The incorporation of both microcapsules and nanocapsules in commercial styrene-acrylate and pure acrylic coatings was investigated. Similarly to the results obtained from the PMA coatings, the coatings with microcapsules showed a more pronounced healing effect than the coatings with nanocapsules. This was mainly due to the brittle nature of the DiNorbornene nanocapsules. In addition, the commercial films consisted of an inherently higher glass transition temperature (T_g) than the PMA film, which also affected the healing efficiency. Although Chapters 5 and 6 indicated that the self-healing ability of the coatings is not optimized, there is a lot of space to provide improvements in the self-

healing ability of these coatings. The main point that should be stressed is that the feasibility of thiol-ene chemistry as a healing mechanism was successfully proven in the development of a self-healing coating based on microcapsules or nanocapsules.

7.2 Recommendations

The concept of self-healing coatings has been investigated and the approach adopted was drawn from inspiration from the literature.[1-4] It was outlined that especially microcapsules embedded in a waterborne coating formulation have the potential to provide a self-healing functionality to the coating. In this dissertation, the use of microcapsules has been extended with the use of nanocapsules, and thiol-ene chemistry was chosen as the healing mechanism. This resulted in a two-component healing system that potentially does not require the addition of a photoinitiator in the coating formulation. This is particularly true for the TetraThiol-DiNorbornene monomer system. The rate of network formation is very high, even in the absence of a photoinitiator and/or without exposure to UV radiation. This allows for the development of a self-healing coating with highly reactive healing agents that can potentially rapidly restore the coating and provide protection to the substrate. In addition, thiol-ene chemistry is extremely flexible regarding choice of monomer. In this way, mechanical properties and T_g can easily be tuned to certain (application) requirements.[5]

Although the embedding of microcapsules in various coating formulations indicate that autonomous self-repair of the coatings can be achieved, the use of nanocapsules as reservoir for healing agents should also be considered. The brittle coatings obtained from the incorporation of (DiNorbornene) nanocapsules together with the inherently high(er) T_g of the commercial coatings, only complicates investigation into crack formation and subsequent self-healing. This does not imply that the incorporation of nanocapsules in coatings results in poor performance of the coatings regarding its self-healing ability. As long as the healing agents are encapsulated and the capsules do rupture upon crack formation (which usually occurs within the coating), the coating may still be capable of providing continued protection to the substrate via thiol-ene chemistry as the healing mechanism.

An important aspect before commercialization of a new product is the requirement for extensive testing of the new material. In this respect, the various coating formulations containing both micro- and nanocapsules, as developed and described in this dissertation, are going to be subjected to salt spray tests and additional durability tests in an attempt to simulate exposure to field conditions. It should be mentioned that it has been reported that additives incorporated in a polymer (matrix) could positively affect its intrinsic (mechanical) properties. The addition of liquid-filled microcapsules to an epoxy matrix results in a reinforced effect regarding fracture toughness of the matrix compared to unfilled epoxy.[3,6,7] However, also a decrease in ultimate strength and modulus is observed. Furthermore, the (commercial) incorporation of capsules in a coating formulation requires the capsules to resist the physical impact onto the substrate upon application via *e.g.* a conventional air spray gun. The effect of the capsules on adhesion needs to be assessed as it is believed that the adhesion of certain coating formulations to steel substrates slightly deteriorates.[8] Although a lot of extensive testing precedes the commercial application of self-healing coatings as developed and described in this dissertation, the work described here is an important step forward. The potential of these films to serve as a self-healing coating can provide numerous advantages to highly advanced materials for use in state-of-the-art technological applications, such as in aerospace and automotive finishes.

References

1. S.R. White, N.R. Sottos, P.H. Geubelle, J.S. Moore, M.R. Kessler, S.R. Sriram, E.N. Brown and S. Viswanathan, *Nature* **2001**, *409*, 794-797
2. T. Yin, M.Z. Rong, M.Q. Zhang and G.C. Yang, *Compos. Sci. Tech.* **2007**, *67*, 201-212
3. Y.C. Yuan, M.Z. Rong, M.Q. Zhang, J. Chen, G.C. Yang and X.M. Li, *Macromolecules* **2008**, *41*, 5197-5202
4. A. Skipor, S. Scheifer and B. Olson, **2002**, *WO02/064653*
5. J.A. Carioscia, L. Schneidewind, C. O'Brien, R. Ely, C. Feeser, N. Cramer and C.N. Bowman, *J. Polym. Sci., Part A: Polym. Chem.* **2007**, *45*, 5686-5696
6. E.N. Brown, S.R. White and N.R. Sottos, *Comp. Sci. Tech.* **2005**, *65*, 2466-2473
7. E.N. Brown, S.R. White and N.R. Sottos, *J. Mater. Sci.* **2004**, *39*, 1703-1710
8. A. Kumar, L.D. Stephenson and J.N. Murray, *Progr. Org. Coatings* **2006**, *55*, 244-253

Acknowledgments

On 10 May 2004 I came to South Africa to work as an affiliated student for eight months and since 02 April 2005 I have been working on my PhD project at the University of Stellenbosch. Since then I met many people and each of them needs to be appropriately thanked for their specific, valuable input, in one way or another.

First of all I would like to thank my supervisor Bert Klumperman for all the input that he made during the past six years; not only during my PhD research in Stellenbosch, but already since my graduation project at Eindhoven University of Technology in The Netherlands in 2003, Bert has provided a lot of guidance. I was given the opportunity of doing research abroad at the Institute of Polymer Science at the University of Stellenbosch from May 2004 and I was offered the opportunity of doing my PhD studies at the same Institute from April 2005. I received a lot of guidance during the past years and I really enjoyed the enthusiastic discussions. I will remember Bert for his comments, relaxed attitude and his excellent evaluation of work.

I would like to thank Ron Sanderson, the head of the department and I also acknowledge DPI for funding of both my PhD project and my research project as an affiliated student in 2004. Jaap Renkema (IPecunia B.V., the Netherlands) is thanked for the pleasant collaboration while writing the patent application.

For operation of the various instruments that I used for characterization and the valuable discussions it led to, I like to thank on a special note Ben Loos (fluorescence microscope), Jean McKenzie (NMR spectroscopy), Mohamed Jaffer (TEM) and Miranda Waldron (SEM). Their experience with the instruments and the help that I received was tremendous and is highly appreciated. In addition, I would like to thank Gareth Bailey (SEC), Elsa Malherbe and Trevor (NMR spectroscopy), Jan Gertenbach (DSC, TGA) and Gareth Harding (DSC) for the analyses that they carried out.

Leo van der Ven (Akzo Nobel Car Refinishes BV, Sassenheim, the Netherlands) and James McLeary and Jacques Rinquest (Plascon Research Centre, University of Stellenbosch) are thanked for the various tests carried out on the coatings and for the supply of commercial latexes/coalescents.

In addition, I owe a lot of gratitude to James McLeary, who made me feel home in the free-radical lab and for his guidance during my research. His supervision in 2004 and during one and a half years of my PhD research has been most valuable.

I would like to thank the staff of Polymer Science department for running things as smoothly as they did; in particular my gratitude goes to Hennie Groenewald, Calvin Maart, Deon Koen, Adam Keulder, Jim Motshweni, Aneli Fourie, Erinda Cooper and Margie Hurndall.

On a more personal note, during the past five years I obviously met a lot of people, with many different characters, and some of them need to be mentioned personally. First of all Rueben Pfukwa needs to be mentioned. Mdara, I do not know how to thank you for all your input and guidance. You have been a fantastic friend and always dragged me through difficult times. It was always great to go and watch soccer together and the words Manchester United have a special meaning now. In addition, I thank you for proof-reading of this dissertation. I am glad the shocking English language has been corrected to a decent level. Next I would like to thank m'amie Nathalie Bailly. I am glad I have such a nice friend as you around, who is always in to watch soccer. Good coincidence you and Rueben support the same team, otherwise I had to be a referee all the time. I am thanking you for all your support and nice chats. I am looking forward having more drinks with you guys. I also like to thank Slavi (Svetoslav Todorov) for being around for so long and having such a great input in the fun I had over the past five years. I specifically like to thank you for your calmness, good chats and well-thought considerations, judgements, suggestions and remarks. I am looking forward meeting you again, either in Brazil or in Bulgaria.

Also I would like to thank Gwen Pound for being a good guide and showing me the way to go. Paul Reader is thanked for the work he carried out in the lab. It has been great having you around and you showed a lot of independence and came up with many good thoughts. Ineke Oglivie and Adine Visser are thanked for their help with putting the Afrikaans abstract together. Special thanks for the numerous friendships and people that gave me such a fantastic time during the past five years go to Lebohang Hlalele, Khotso Mpitso, Reda Fleet & Kate, Gareth Harding & Soraya, Patrice Hartmann, Mark Frahn, Matthew Tonge, Niels Akeroyd, Helen Chirowodza, Howard Matahwa, Austin Samakande, JC Stegmann & Angela Bowes, the Libyan guys and the Zimbabwean guys for the great moments at soccer. Also members of the Free Radical Lab are acknowledged for making work in the lab enjoyable.

I should not forget to mention the people with whom I always had good times in The Brazen Head and I would like to specifically mention Brighton, Alec, Jacques, Moses, Amanuel and Maggie & Aman. Also The Brazen Head barmen are thanked for the fun times: Jacques, Hilke, Johan and Pete, and waiter Johan.

I would like to specifically mention people that I know from the time when I was staying in Academia. Lianne Tuijtel and Herlinde van Hooydonck are thanked for their support during the whole of my PhD research and the fantastic times that we had both here in Stellenbosch and during the yearly visits to The Netherlands and Belgium. In this regard Marie-Claire Hermant is also thanked for her good friendship. Last but not least, my parents and brother are thanked for their support over the past five years. I am also very happy that Patrick will be present at my defence in January and that both my parents can be here during the graduation ceremony in March.